Macrophage and T helper dynamics in Classical Hodgkin Lymphoma and their role in PD1 checkpoint blockade

Joseph Taylor

Supervisor: Professor J Gribben

A thesis submitted for the degree of Doctor of Philosophy

January 2020

Barts Cancer Institute

Queen Mary University of London

Statement of Originality

I, Joseph Taylor, confirm that the research included within this thesis is my own work or that where it has been carried out in collaboration with, or supported by others, that this is duly acknowledged below and my contribution indicated. Previously published material is also acknowledged below.

I attest that I have exercised reasonable care to ensure that the work is original, and does not to the best of my knowledge break any UK law, infringe any third party's copyright or other Intellectual Property Right, or contain any confidential material.

I accept that the College has the right to use plagiarism detection software to check the electronic version of the thesis.

I confirm that this thesis has not been previously submitted for the award of a degree by this or any other university.

Signature: Joseph Taylor

Date: 23/01/20

Details of collaboration and publications:

1. Taylor, J. G., Clear, A., Calaminici, M. & Gribben, J. G. Programmed cell death protein-1 (PD1) expression in the microenvironment of classical Hodgkin lymphoma is similar between favorable and adverse outcome and does not enrich over serial relapses with conventional chemotherapy. *Haematologica* **104**, e42–e44 (2019).

Abstract

Classical Hodgkin Lymphoma (CHL) is a germinal centre B cell lymphoma characterised by rare lymphoma cells within a diverse inflammatory infiltrate. It is unusual amongst haematological malignancies in that it responds well to PD1 checkpoint blockade. However, evidence for T cell exhaustion is limited which is surprising given that PD1 checkpoint inhibitors are thought to act via the reversal of exhaustion. This thesis examines the mechanisms by which CHL cells recruit and induce a tolerant myeloid and T cell environment, focussing on the role of the PD1-PDL1 axis and the implications of this for the action of checkpoint inhibitors.

The recruitment and induction of a PDL1 positive macrophage phenotype is modelled in *vitro* and in primary patient samples, confirming the induction of PDL1 by CHL cells. However, no phenotypic or functional evidence of T cell exhaustion is detected above that seen in reactive tissues and no relationship is seen between markers of exhaustion and markers that predict PD1 inhibitor response challenging the current narrative that PD1 inhibitors in CHL work via the reversal of exhaustion. Instead, spatial and *in vitro* modelling identify T helper differentiation as a putative mechanism for PD1 inhibitor action. They highlight CHL major histocompatibility complex II expression as playing a central role in the induction of a T_H1 regulatory cell rich environment but also as a vulnerability for CHL cells once treatment is initiated.

As part of this thesis we focus upon multi-parameter imaging analysis. Multi-parameter imaging enables deep phenotyping whilst retaining spatial relationships between cells. However, whilst advances in phenotyping approaches have been made there remains a need for better tools for spatial analysis. We describe the novel application of spatial point pattern modelling to this task and demonstrate the utility and flexibility of this method in deconstructing spatial relationships and interactions.

Dedication

For Neeta, Asha and Kiran

and in memory of Barbara Crossley

Acknowledgements

Supervisors:

Professor John Gribben
For his supervision, personal and professional support and mentorship

Dr Jeff Davies
For his advice and enthusiasm

Co-workers:

Mr Andrew Clear
For his training and guidance in immunohistochemistry and arraying, development of protocols including the stripping and reprobing method, assistance with staining and micro-arraying and always being willing to discuss ideas.

Dr Jenny Ball
For her training and guidance in flow cytometry and cell culture.

Ms Arantxa Romero Toledo
For her training and guidance in western blotting and for always being willing to help out.

Dr Edward Truelove
For his optimisation and staining of the Imaging Mass Cytometry samples.

Dr Mariagiovanna Caporale and Dr Matthew Poynton
Who spent 6 and 3 months respectively working with me on Erasmus and academic F2 placements and helped with immunohistochemistry and optimisation of the proximal ligation assay.

Funders:

This work was supported by a Wellcome Trust Clinical Research Training Fellowship, Grant No. 200144/Z/15/Z.

The final year was supported by the Baker Foundation and Barts Charity

Table of Contents

Table of Figures

Table of Tables

Abbreviations:

Abbreviation		Notes
+/-/ hi/int/lo	Denotes expression e.g. $PD1^{+}$	
ABVD	Adriamycin, Bleomycin, Vinblastine, Dacarbazine	CHL chemotherapy regimen
ALPS-Fas	Autoimmune Lymphoproliferative Syndrome	Primary immunodeficiency, predispose to CHL
APC	Antigen presenting cell. Also a fluorophore in the context of flow cytometry antibody conjugates	
B2M	Beta 2 Microglobulin	
BCR	B cell receptor	
BTLA	B ant T-lymphocyte attenuator, CD272. Ligand for TNFRSF14	Negatively regulates T cell responses
CCL2	Chemokine of CC family	Macrophage attractant
CCL3	Chemokine of CC family, also known as MIP1α	Macrophage attractant
CCL4	Chemokine of CC family	
CCL5	Chemokine of CC family	
CD3	Cluster of differentiation 3, T cell receptor	T and NKT marker
CD4	Cluster of differentiation 4, T cell receptor co-stimulatory molecule	T_H and macrophage marker
CD8	Cluster of differentiation 8, T cell receptor co-stimulatory molecule	T_C marker
CD25	Cluster of differentiation 25, IL2 receptor alpha	T_{Reg} marker

CD26	Cluster of differentiation 26, surface enzyme DPP4	Low expression on T_{Reg}
CD27	Cluster of differentiation 27, costimulatory molecule, TNFRSF member	T cell expressed, deficiency predisposes to CHL
CD30	Cluster of differentiation 30, TNF receptor superfamily member, co-stimulatory	Expressed on activated but not resting T and B. Highly expressed in CHL
CD38	Cluster of differentiation 38	
CD39	Cluster of differentiation 39, Cell surface nucleotidase	T_{Reg} marker, Converts ATP to AMP.
CD40	Cluster of differentiation 40, TNF receptor superfamily member, co-stimulatory	Expressed on antigen presenting cells. Highly expressed in CHL
CD45RA	Cluster of differentiation 45RA, cell surface enzyme	Naïve and EMRA effector T marker
CD57	Cluster of differentiation 57, cell surface enzyme	T cell senescence and NK marker
CD58	Cluster of differentiation 58, cell adhesion molecule, binds CD2	Important for T_C and NK recognition of tumour cells
CD68	Cluster of differentiation 68, glycoprotein	Expressed in myeloid cells, Note: detected breadth of expression varies by antibody clone
CD73	Cluster of differentiation 73, Cell surface nucleotidase	T_{Reg} marker, Converts AMP to adenosine
CD95	Cluster of differentiation 68, FAS receptor, TNFRSF member	A programmed cell death receptor
CD127	Cluster of differentiation 127, IL7 receptor	Low expression in T_{Reg}

CD154	Cluster of differentiation 154, ligand for CD40	
CD161	Cluster of differentiation 161	Marker of T_H17
CD163	Cluster of differentiation 163	Marker of M2-type macrophages
CD200R	Cluster of differentiation 200 receptor	
CD206	Mannose receptor	
CD273 / PDL2	Programmed cell death ligand 2	Immuno-regulatory, ligand for PD1
CD274 / PDL1	Programmed cell death ligand 1	Immuno-regulatory, ligand for PD1
CD279 / PD1	Programmed cell death 1	Immuno-regulatory molecule, receptor for PDL1, PDL2
cdf	Cumulative distribution function test	
cFLIP	Fas-associated death domain-like IL1-converting enzyme-inhibitory protein	Inhibits CD95-mediated cell death
CFSE	Carboxyfluorescein succinimidyl ester	Cell tracking dye
CSF1/MCSF	Macrophage colony stimulating factor	
CSF1R	Macrophage colony stimulating factor receptor	
CIITA	Class II major histocompatibility complex transactivator	
CHL	Classical Hodgkin Lymphoma	
CHL MHC II	MHC II expressed on CHL cells	
CM	Conditioned media	

CpG	DNA sites where a guanine follows a cytosine	
CXCL9	Chemokine of CXC family	
CXCL10	Chemokine of CXC family	
DAB	3,3'-diaminobenzidine	IHC chromogen
DLBCL	Diffuse Large B-cell Lymphoma	
DMSO	Dimethyl Sulfoxide	
DNA	Deoxyribonucleic acid	
EBERs	Epstein Barr virus-encoded small RNAs	
EBI3	Epstein Barr-Induced gene 3	B subunit of IL6-superfamily cytokine members IL27 and IL35
EBV	Epstein-Barr Virus	Associated with CHL lymphomagenesis
EOMES	Eomesodermin, transcription factor	Associated with exhaustion and T_C
FBS	Fetal Bovine Serum	
FFPE	Formalin-fixed paraffin-embedded	
FOXP3	Forkhead box P3, transcription factor	Master transcription factor of T_{Reg} subset and marker of activation
GATA3	GATA binding protein 3, transcription factor	Expressed in B and T cells. Master transcription factor for T_H2
GMCSF	Granulocyte-Macrophage colony stimulating factor	Cytokine
HLA-DM	Intracellular protein involved in antigen loading on the HLAII complex	
HLA I	Human Leucocyte Antigen complex class I, genes encoding MHC class I	Antigen presentation to T_C

HLA II	Human Leucocyte Antigen complex class II, genes encoding MHC class II	Antigen presentation by professional APC to T_H
HRS	Hodgkin Reed Sternberg Cell	CHL cell
H Score	Histology Score	Semi-quantitative scoring method encompassing both stained area and intensity
IDO1	Indoleamine 2,3-dioxygenase 1, immunoregulatory enzyme converting tryptophan to kynurenines	Expressed by some macrophages as immunoregulatory mechanism
IFNγ	Interferon gamma, pro-inflammatory cytokine	T_H1 are a major source of production
IHC	Immunohistochemistry	
IL2	Interleukin 2, cytokine associated with T activation	Absorbed by T_{Reg} as immunoregulatory mechanism
IL10	Interleukin 10	
IL12	Interleukin 12 – heterodimeric cytokine made up of IL12p35 and IL12p40 subunits	Pro-inflammatory
IL12A/IL12p35	Cytokine subunit	
IL12B/IL12p40	Cytokine subunit	
IL17/IL17A	Interleukin 17A	T_H17 effector cytokine
IL23A/IL23p19	Cytokine subunit	
IL23	Interleukin 23 – heterodimeric cytokine made up of IL23p19 and IL12p40 subunits	Pro-inflammatory
IL27A/IL27p28	Cytokine subunit	

IL27	Interleukin 27 – heterodimeric cytokine made up of IL27p28 and EBI3 subunits	(Anti)-inflammatory
IL35	Interleukin 12 – heterodimeric cytokine made up of IL12p35 and EBI3 subunits	Anti-inflammatory
ITK	IL2-inducible T-cell Kinase	Kinase involved in T cell signalling
IMC	Imaging Mass Cytometry	
IMS	Industrial methylated spirits	
LAG3	Lymphocyte Activating 3	Exhaustion, activation and T_R1 marker
EBV-LMP1	EBV-Latent Membrane Protein 1	Viral protein mimicking CD40 signalling
EBV-LMP2A	EBV-Latent Membrane Protein 2A	Viral protein mimicking BCR signalling
LR-CHL	Lymphocyte rich subtype of CHL	
mIHC	Multiplex immunohistochemistry	
MC-CHL	Mixed cellularity CHL histological subtype	
MCSF/CSF1	Macrophage colony stimulating factor	Cytokine
MHC I	Major Histocompatability complex class I, genes encoded by HLA I	Antigen presentation to T_C
MHC II	Major Histocompatability complex class II, genes encoded by HLA II	Antigen presentation by professional APC to T_H
NFκB	Nuclear factor kappa B	
NK	Natural Killer cell	
NS-CHL	Nodular sclerosing CHL histological subtype	

PD1	Programmed cell death 1	Immuno-regulatory, receptor for PDL1, PDL2
PD1i	PD1 inhibitor e.g. Nivolumab	
PDCD1LG2	Programmed cell death 1 ligand 2 gene, encoding PDL2	
PDL1 / CD274	Programmed cell death ligand 1	Immuno-regulatory, ligand for PD1
PDL2 / CD273	Programmed cell death ligand 2	Immuno-regulatory, ligand for PD1
RIG1	Retinoic acid induced gene 1	
RLN	Reactive Lymph Node	
RNA	Ribonucleic acid	
ROI	Region of interest	Visiopharm software
RORγT	Retinoic Acid Receptor-related orphan receptor gamma T	Master transcription factor for T_H17
RPMI	Roswell Park Memorial Institute 1640 Medium.	Cell culture medium
rpm	Revolutions per minute	
SCS	Single cell suspension	Live cell preparation
TBET	T-box transcription factor TBX21, transcription factor	Master transcription factor of T_H1, associated with exhaustion and T_C
TCR	T cell receptor	
TGFβ	Transforming growth factor beta	
T_H1	T (helper) cell type 1	
T_H17	T (helper) cell type 17	
T_H2	T (helper) cell type 1	
$T_{(H)}$-Ex	Exhausted T (helper) cell	

$T_{(H)}$-EM	Effector memory T (helper) cell	
$T_{(H)}$-EMRA	$CD45RA^+$ effector memory T (helper) cell	
T_C	Cytotoxic $CD8^+$ T cell	
T_{FH}	Follicular helper $CD4^+$ T cell	
T_H	Helper $CD4^+$ T cell	
T_{Reg}	Regulatory T helper cell	$FOXP3^+$
T_R1	T regulatory cell type 1	$FOXP3^-$ $IL10^+$
TIL	Tumour-infiltrating lymphocyte	Used to describe single marker stained cells in IHC
TIM3	T-cell immunoglobulin and mucin-domain containing-3, HAVCR2	Immuno-regulatory molecule, receptor for Gal9
TMA	Tissue micro-array	Array of FFPE samples for IHC
TNFRSF	Tumour necrosis factor receptor super family	Group of related surface cytokine receptors important to costimulation and programmed cell death pathways
V(D)J	Variable, diverse and joining regions of the immunoglobulin gene	
VIP	Vector chromogen trade name	IHC chromogen

CHL cells are also referred to as Hodgkin Reed Sternberg cells, but the term CHL cell will be used in this thesis.

Chapter 1: Introduction

Classical Hodgkin Lymphoma (CHL) is an aggressive lymphoma of germinal centre/post germinal centre B cell origin which is fatal without treatment. CHL is rare with an incidence of 2.7-2.8 per 100,000 per year equating to around 1700 new cases annually in the UK.[1] Treatment is considered a success story in haematology with cure rates of 70-80% with modern chemotherapy regimens.[2] Despite this there are significant unmet needs in CHL. Response to first line treatment is good but associated with significant toxicity and late effects including risk to fertility, cardiac damage and of second malignancy lasting decades after therapy.[3] This is of particular concern given that CHL is the most common lymphoma in young people.[4] Additionally, whilst the initial cure rate is high, cure rates in relapsed/refractory disease are low.[5] For these reasons CHL remains an important area of research.

CHL is a paradigm example of tumour-microenvironmental interaction. The importance of these relationships in CHL are highlighted by the success of immune checkpoint inhibitors.[6,7] The focus of this thesis will be the interactions between CHL and its immune environment with a view to understanding the activity of checkpoint inhibitors. This topic is important as understanding their mechanism of action is essential to accurately predict response and inform the next generation of treatments. The introduction will discuss treatment options followed by the histology and epidemiology relevant to understanding CHL development. We next discuss CHL microenvironmental relationships highlighted by genetic or immune susceptibility to CHL lymphomagenesis. Finally, we discuss current understanding of the roles of the myeloid and T helper (T_H) subsets in CHL and their relevance to immune checkpoint inhibition.

1.1: Therapeutic options and novel treatments

First line therapy for CHL is either radiotherapy, chemotherapy, most commonly ABVD (doxorubicin, bleomycin, vinblastine and dacarbazine) or a combination of the two. Treatment length and the use of radiotherapy is determined by disease stage and the presence of unfavourable features such as B symptoms or bulky disease.[8] Current strategies for the treatment of relapse include the use of high dose chemotherapy or Brentuximab vedotin (an antibody-drug conjugate targeting CD30) and consolidation with autologous stem-cell transplantation.[9–11] In further relapse consideration is given to allogenic stem cell transplant

and novel agents. Amongst novel therapies, immune checkpoint inhibitors targeting Programmed Death 1 (PD1) have shown encouraging responses in heavily pre-treated patients.[6,7] PD1 inhibitors and Brentuximab vedotin are being trialled in combination in the relapsed disease setting and in combination with AVD (ABVD chemotherapy without bleomycin) in the front line setting.[12–14] The activity of PD1 inhibitors in CHL is unusual amongst lymphomas, with more dramatic responses than those observed in other lymphoid malignancies.[15]

Whilst the activity of PD1 inhibitor therapies in CHL is encouraging they do not represent a complete solution for CHL. In the relapsed setting progression free survival to PD1 inhibitors monotherapy is around 60-80% at six months.[6,7,16,17] To date, most data are from single-arm studies with short follow-up and have not yet been confirmed with randomised controlled trials. Used in combination with AVD as first line therapy in advanced stage disease in a randomised controlled trial, progression free survival at 9 months was 92% with 65% achieving CR.[13] Treatment was also not without toxicity: grade 3-4 treatment-related adverse events were recorded in 59% of patients. This combination may be an option to reduce long term therapy-associated toxicity as it allows the omission of bleomycin but further outcome data is needed.

Immune checkpoint inhibitors are notable as a class of drugs because they represent a new approach to cancer therapy, acting by reinvigorating the immune infiltrate as opposed to directly targeting the cancer cell. Early data suggests this novel approach results in fundamental differences in lymphoma cell dynamics under the influence of therapy; investigators observed cycling of clones under PD1 inhibition rather than the outgrowth of individual chemo-resistant clones after conventional chemotherapy.[18] This is likely to be a consequence of PD1 inhibition causing broad T cell activation improving overall immune surveillance as opposed to specific killing of drug-sensitive clones. PD1 inhibitors act by blocking the engagement of PD1 with its ligands. Programmed Death Ligand 1 (PDL1) and Programmed Death Ligand 2 (PDL2), both of which mediate T cell responses.[19] Both PDL1 and PDL2 are overexpressed in CHL due to genetic alteration.[20] PD1 inhibitors are generally considered to act by reinvigorating functionally exhausted T cells, improving the anti-tumour immune response.[9] Responses have been similar with two different PD1 inhibitors, nivolumab and pembrolizumab and the PDL1 inhibitor avelumab (Lugano 2017, JAVELIN HODGKINS study), suggesting that blockade of the PD1-PDL1 interaction is sufficient for the clinical effect.[6,17,21]

PD1 checkpoint blockade represents a novel and interesting approach to cancer therapy and responses in CHL demonstrate that T cell modulation may be a powerful approach in targeting the disease. However, outcome data whilst encouraging does not support the current generation of PD1 inhibitors being a complete solution for CHL. It is therefore important to understand the close relationship between T cell biology and CHL and how and why PD1 inhibitors are acting. A series of features within the microenvironment highlight an important role for T cells and the PDL1 axis but cast doubt as to whether reversal of T cell exhaustion can fully explain PD1 inhibitor activity.[22] These will be discussed in detail in the following sections.

1.2: CHL development: Patterns and links to immune function

CHL is divided into four major histological subtypes; nodular sclerosing (NS-CHL), mixed cellularity (MC-CHL), lymphocyte rich (LR-CHL) and lymphocyte depleted (LD-CHL). A fifth type, nodular lymphocyte predominant Hodgkin Lymphoma, was previously considered to be a subtype of CHL but is now recognised as a different entity with distinct clinical, epidemiological and pathological characterisics.[23] The four CHL subtypes differ histologically but are treated in the same manner and are broadly similar in their clinical response.[24]

Although response to therapy is similar, a series of features suggest different aetiologies for the different CHL subtypes. NS-CHL usually presents with painless cervical or supraclavicular lymphadenopathy and often with mediastinal disease. In contrast MC-CHL is more frequently associated with peripheral or sub-diaphragmatic disease.[8] Additionally, EBV infection within the CHL cell is seen across all histological subtypes but has a stronger association with MC-CHL and LD-CHL (>75% of cases EBV^+) and a weaker association with NS-CHL and LR-CHL (10-40% EBV^+).[1] These differences suggest different modes and locations for lymphomagenesis.

Figure 1.1: Histological Subtypes

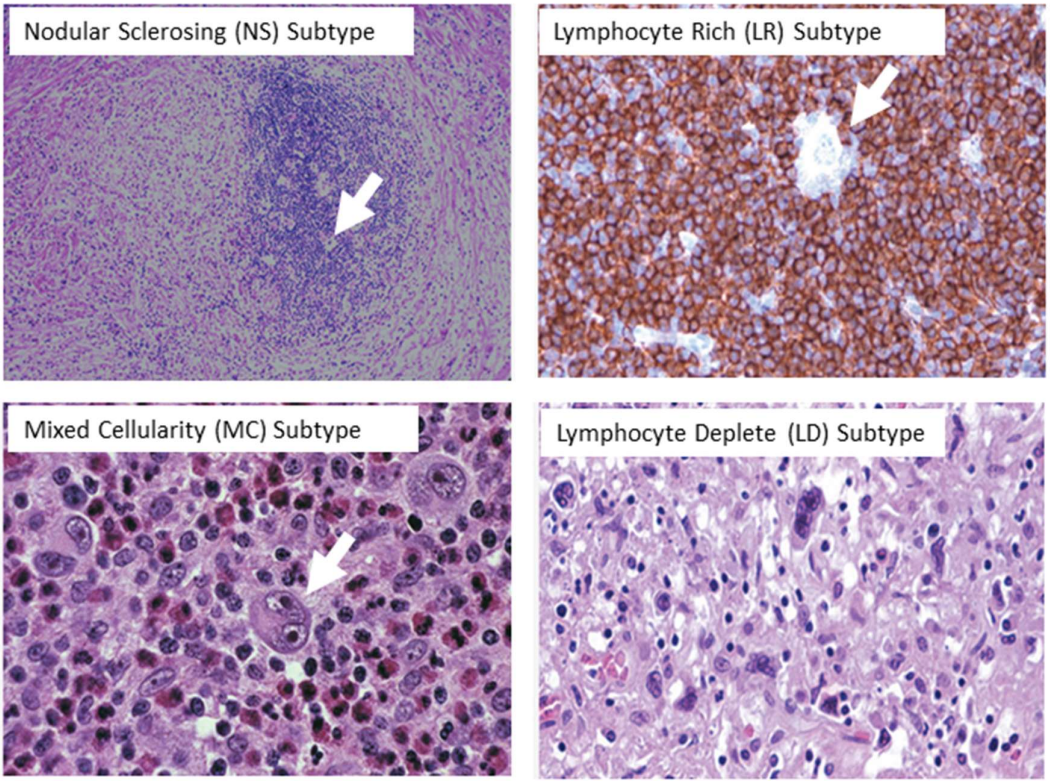

Image source: H.M. Kantarjian, RA Wolff: The MD Anderson Manual of Medical Oncology, 3rd Edition
www.accessmedicine.com © McGraw-Hill Education

Figure 1.1: Rare large multinucleate CHL cells (also referred to as Hodgkin Reed Sternberg cells) are marked with a white arrow. CHL cells exist within a reactive immune infiltrate heavily enriched for T cells. The infiltrate composition varies with the histological subtype. Nodular sclerosing (NS-CHL) subtype is most common accounting for 60-70% of cases. Nodules of lymphoma are surrounded by bands of fibrosis which progressively replaces the tissue. The mixed cellularity (MC-CHL) subtype accounts for 30-40% of cases and has a more varied infiltrate. It is more frequently associated with EBV infection and immunodeficiency. The Lymphocyte Rich and Lymphocyte Deplete subtypes are rare.

There are also epidemiological differences between subtypes: Incidence of CHL overall has a bimodal age distribution with increased incidence in both young and older adults. This pattern is replicated irrespective of racial group and geographical location.[4] However, if cases are categorised by EBV infection status or histological subgroup then distinct patterns emerge. Both EBV negative CHL and nodular sclerosing CHL show a single peak of incidence in the

second to third decade of life in both European and Chinese populations and are associated with higher economic status. In contrast, EBV$^+$CHL and the mixed cellularity and lymphocyte deplete histological subtypes display a bimodal peak, occurring in young adults and older age. Interestingly, the shape of this distribution is similar in both Chinese and European populations but the timing differs, with both peaks occurring around 10 years earlier in Chinese patients.[4] Overall, the EBV$^+$CHL, mixed cellularity and lymphocyte deplete subtypes are associated with lower socio-economic status and are more commonly in the developing world. Finally, cases of CHL associated with immunodeficiency are almost universally associated with EBV and are more likely to be of the mixed cellularity or lymphocyte deplete subtypes.

A series of hypotheses have been proposed to explain these distinctive epidemiological patterns. Host susceptibility and pre-malignant immune function is likely to play an important role as evidenced by an increased CHL incidence in close relatives and monozygotic twins alongside associations with HLA type.[25]

EBV$^+$CHL appears to relate to immune function, either due to immunosuppression or an intrinsic immune defect. This is supported by a series of observations. Firstly, immunodeficiency-associated CHL are almost exclusively EBV$^+$. Additionally, EBV$^+$CHL in general is associated with an elevated incidence of prior infection (particularly sinusitis, encephalitis, herpes simplex virus and tuberculosis), possibly indicating an underlying immune defect or susceptibility.[25–28]. It is proposed that the young adult peak in EBV$^+$CHL may be related to late exposure to EBV, a virus that is normally encountered in early childhood.[29] This supported by the an increased risk of EBV$^+$CHL which is observed for a two year period after a diagnosis of infectious mononucleosis (which is caused by EBV infection).[30] The older peak of EBV$^+$CHL may also be due to immune susceptibility due to the decline in in host immunity seen with age. Similarly, the increase in EBV$^+$CHL and mixed cellularity CHL in the developing world and shift towards EBV$^-$ disease and the nodular sclerosing subtype within countries and institutions over time with improving socioeconomic status may implicate factors such as nutrition which in turn influence immune status.[31,32]

The factors influencing EBV$^-$ disease incidence are less clear. HLA associations are also seen in EBV$^-$ disease as is co-occurrence in monozygotic twins.[25] The young adult peak in EBV negative cases has also been hypothesised be due to late exposure to an as yet undefined childhood infection.[33,34] Patients developing nodular sclerosing CHL (which is usually EBV negative) are of higher socioeconomic status and receive less antibiotics in childhood than their peers suggesting a more protective environment, possibly increasing the risk of late infection exposure.[34] Additionally the predilection for cervical nodes in NS-CHL may suggest an

oropharyngeal link. However, no causative agent has been found despite relationships to a series of candidate infections being investigated.[35–38]

These observations provide insight into the biology of CHL and clues as to factors that may be important in its development and survival. The relationship to EBV infection and prior infections such as herpes simplex, sinusitis and encephalitis is suggestive of a link to cellular anti-viral immunity particularly to the human herpes virus family, suggesting possible defects in T cell function. T cell aging and thymic involution is also a prominent factor in the decline in immune function seen in the elderly, possibly explaining the peak in EBV^{+}CHL seen in older patients.[39] This link to T cell biology is further supported by evidence from CHL arising in immunodeficiency states and associations with HLA type and is explored in detail below.

1.2.1: CHL lymphomagenesis and the immune system

Lymphomagenesis is usually thought of as a genetic event and lymphomas are frequently described by their hallmark translocations. However, cells harbouring lymphoma-associated translocations are frequently detected in the peripheral blood of the normal population, demonstrating that potentially lymphomagenic genetic events are common even in health.[40,41] The survival and outgrowth of a transformed cell after acquiring potentially lymphomagenic mutations is determined by its ability to escape detection and elimination by immune surveillance.[40,42,43] Lymphomagenesis is therefore the combination between the acquisition of lymphomagenic mutations and the failure of immune effectors to control or eliminate the transformed cell, making the immune environment central to this process. The following section explores CHL lymphomagenesis in immune competent and immunodeficiency states with a view to understanding the relationship between CHL and its microenvironment.

1.2.2: The CHL lymphoma cell

CHL is unusual amongst lymphomas due to the rarity of the malignant cell. CHL cells are morphologically and phenotypically distant from their cell of origin and aberrantly express a series of markers from other lineages. As a consequence, the cell of origin of CHL has only recently been established.[44]

CHL is a germinal centre B cell lymphoma. CHL cells are a clonal expansion of cells that are B cell in origin, although rare cases may originate from T cells.[45] They usually have mutated

heavy chain variable genes (the V(D)J region) but do not express activation induced deaminase (AID) or show genetic evidence of ongoing somatic hypermutation, suggesting they have transited the germinal centre but the germinal centre reaction is not ongoing.[46–48] Consistent with this, CHL has only evolved in mammals and its appearance is correlated to the evolution of the germinal centre.[49] CHL cells have lost expression of the B cell receptor due to either crippling mutations or loss of Immunoglobulin gene transcription ability, an event that would lead to programmed cell death under normal circumstances.[50] They express the transcription factors PAX5 and IRF4, indicative of a germinal centre B or plasma cell identity but not further markers suggestive of plasma cell differentiation and gene expression does not reflect a plasma cell-like profile.[51,52] In EBV^+ cases EBV antigens are expressed in a germinal centre-like profile.[53]

The phenotype of CHL cells is unusual even beyond the loss of B cell receptor expression. CHL cells are characterised by high expression of CD30 and CD40, (two TNF receptor superfamily members) and CD15 (a leukocyte adhesion molecule) and the expression of CD30 and CD15 are used diagnostically.[54] Both CD30 and CD40 signalling result in marked NFκB upregulation, which is a hallmark of CHL cells.[55] Their gene expression profile shows similarity to a recently identified $CD30^+$ B cell subset which derive from activated memory B or post GC Bs.[56,57]

Taken together this suggests that CHL cells originate from a B cell that has completed transit of the germinal centre and arrested during transition towards memory B or plasma cell. However, during this process they have lost many of the hallmark features of B cells such as expression of the B cell receptor.

1.2.3: Transformation in the germinal centre

A disproportionate number of malignancies are of B cell origin and these are frequently associated with the germinal centre reaction. The germinal centre reaction is a high risk but important event. The immune system generates antibodies to near infinite variety of un-encountered antigens from a finite genome. This is achieved via genetic reconfiguration of the B cell receptor, firstly by V(D)J recombination during B cell development and later by successive rounds of somatic hypermutation in the germinal centre under the control of the AID enzyme.[58–60] B cells producing high-affinity antigen are selected for survival by supporting T_H and antigen presenting cells. Those that do not receive support (the vast majority) undergo apoptosis.[61] However, the AID enzyme can cause damage outside of the immunoglobulin loci, making this an intrinsically dangerous process.[59,62,63] Almost all breaks or translocations

observed in lymphoma are attributable to either V(D)J recombination or somatic hypermutation, with the remainder attributable to random CpG breaks or random mutations due to reactive oxygen species.[64–66] Amongst these somatic hypermutation is particularly important as even when translocations and mutations occur at an earlier stage further mutations acquired during somatic hypermutation are often required for lymphomagenesis.

These factors highlight the germinal centre reaction as a high-risk event. To compensate for this a series of safety mechanisms protect against malignant transformation. Firstly, when B cell transit the germinal centre they become dependent upon extrinsic support to survive. This creates a checkpoint against transformation as cells that do not receive external support die from neglect.[53] Additionally, if transformation does occur then molecular processes trigger programmed cell death and upregulate markers highlighting the cell to the immune system. [59] This combination of cell-intrinsic and cell-extrinsic devices create a fail-safe device, reducing the probability of a cell surviving in the event of transformation. Finally, if the transformed cell survives, immune surveillance identifies and kills damaged cells, preventing their outgrowth. Key factors influencing lymphomagenesis are therefore those influencing the number of cells entering the germinal centre reaction, those affecting the risk of lymphomagenic mutations, and those affecting the chances of a transformed cell surviving (Figure 1.2).

Figure 1.2: Microenvironmental factors influencing Lymphomagenesis

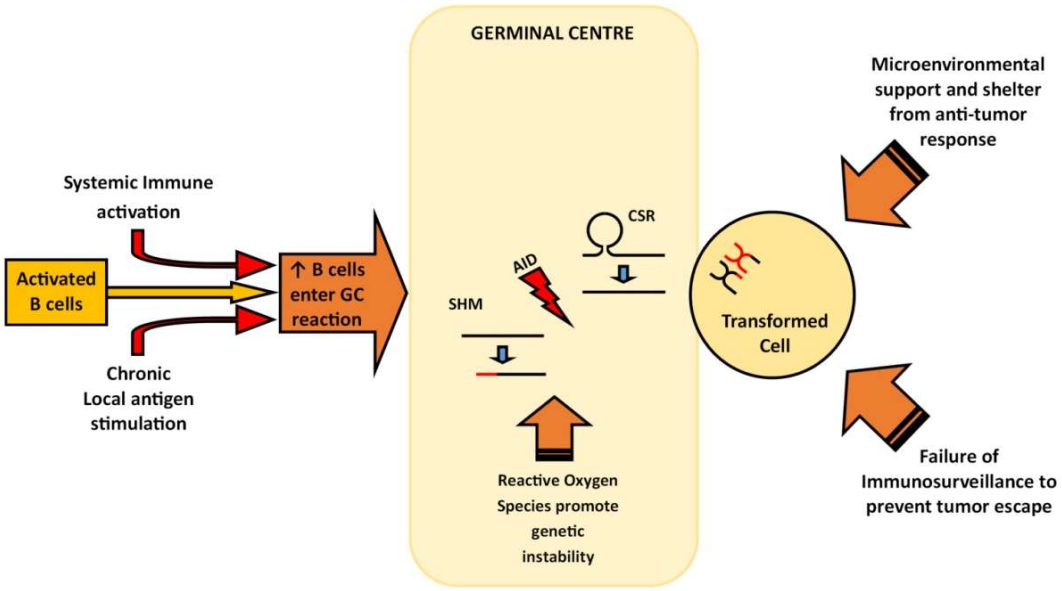

Figure 1.2: 1. Systemic immune activation (e.g. in Human immunodeficiency virus (HIV)) or chronic local antigen stimulation (e.g. from *Helicobacter pylori* in mucosa-associated lymphoid tissue (MALT) lymphoma) increases B cells transiting GC hence the cumulative risk of transformation. 2. Somatic hypermutation (SHM) and Class Switch Recombination (CSR) under the control of Activation Induced Deaminase (AID) and the presence of reactive oxygen species influence the individual risk of a lymphomagenic mutation. 3. Microenvironmental support and immune surveillance influence the chance of a transformed cell surviving.

1.2.4: After transformation: Escape

A cell surviving transformation does not necessarily mean that lymphoma will develop, in fact, potentially lymphomagenic events are common even in health.[40,41] If a cell survives transformation the factors influencing its survival are described by the three E hypothesis; Elimination, Equilibrium and Escape.[67] In this model transformed cells are either eliminated by the immune system, controlled but not eliminated or escape as detectable disease. This theory suggest lymphoma development is dynamic, with a cross-talk between immune surveillance and cancer evasion. This may be determined by fluctuation in immune function, for example lymphoma can develop in the context of a weakened immune system as is seen with falling CD4 counts in HIV, but conversely restoring the immune system can be sufficient to eliminate

the disease.[68,69] Alternatively it may be the result of cancer evolution and immune selection pressure, for example, lymphoma cells may be held in a state of equilibrium (as seen in follicular lymphoma *in situ*) unless or until they develop additional mutations which allow them to escape.[70] Cancer evolution is a combination of the effects of stochastic processes such as mutation rate and genetic drift, alongside deterministic processes such as clonal selection.[71] Cancers vary in the degree of selective pressure they are under, some displaying phylogenies suggestive of selection and others of drift.[71] The adoption of mechanisms minimising immunogenicity and promoting a suppressive microenvironment in CHL suggests that the influence of selective pressure is likely but the inaccessibility of malignant tissue has meant this is yet to be properly assessed.

Selection for evasion mechanisms is driven by pressure from immune surveillance actors and, importantly, the acquisition of one evasion mechanism alters the selective pressures on the malignant cell.[71] This in turn alters the landscape for the acquisition of further evasion mechanisms, promoting selection of those that are complimentary to the first. This principle is exemplified in diffuse large B cell lymphoma (DLBCL) where *B2M* (beta-2 microglobulin) and *CD58* and mutations are co-selected in a large subset of tumours.[72] *B2M* loss leads to downregulation of MHC I molecules allowing evasion of detection by cytotoxic T (T_C) cells. However, the loss of MHC I leads to natural killer (NK) cell killing by missing-self recognition.[73] The concurrent mutation in *CD58* aid NK evasion and therefore assist lymphoma escape. This suggests that immune surveillance might drive the selection not just of individual evasion mechanisms but of packages of complimentary evasion techniques. This principle may have important implications for the shaping of the microenvironment and is discussed in chapter 8.

1.2.5: Compromise to immune surveillance

Within a healthy immune system multiple mechanisms protect against lymphomagenesis. Malignant cells acquire mutations in a stochastic manner and the probability of an advantageous mutations relates to both mutation rate and malignant cell number.[74] This provides the rationale for combination chemotherapy; if the probability of a cell acquiring resistance to chemotherapy agent A is *x* and the probability of acquiring resistance to chemotherapy agent B is *y* then if A and B are used in combination the probability of the same cell acquiring resistance to both drugs is $x*y$. Therefore, by using drugs in combination the probability of resistance is dramatically reduced. Similarly, immune surveillance is achieved by multiple cell types identifying transformed cells by distinct mechanisms. Local or systemic immune dysregulation compromising one or more defence lowers the probability threshold of

a combination of mutations permitting escape occurring. Consistent with this, lymphomas relapsing in the context of immunodeficiency are frequently *de novo* malignancies suggesting a lower threshold for lymphomagenesis.[75] Interestingly, up to 35% of relapses in presumed immunocompetent CHL are clonally unrelated further supporting the possibility of underlying immune defects contributing to lymphomagenesis.[76] A predicted consequence of this is that lymphoma cells developing in immunodeficiency would be intrinsically more susceptible to restoration of the specific defect or actors affected by the immunodeficiency as it will not have adapted to selective pressure from that source. This prediction is difficult to test as response would be confounded by other effects of immune compromise and examples specific defect repair are rare. An example might be the spontaneous resolution of some Kaposi Sarcoma as the immune system is restored by antiviral therapy.[69]

Immune dysregulation might be due to a specific defect or a generalised process and some defects disproportionately affect the risk of specific malignancies. This suggests that certain malignancies might result from a specific type of immune surveillance failure, or conversely, may be uniquely vulnerable to a specific type of immune attack. As discussed below, many of the immune defects disproportionately predisposing to CHL relate to T cell function. Understanding the defects disproportionately predisposing to CHL may provide insight into immune interactions that are of particular importance to CHL biology. Primary and acquired immunodeficiencies and genetic susceptibilities associated with CHL development are discussed in the next section.

1.2.6: CHL lymphomagenesis in primary and acquired immunodeficiency

An increased incidence of lymphomagenesis is seen across a wide variety of both primary and acquired immunodeficiency states.[77] A subset of these predispose disproportionately to CHL. Primary immunodeficiencies states are rare so descriptions of the associated defects are usually incomplete. Additionally, because they result from germ-line mutations every cell in the body is affected. As a result, an association between e.g. a T cell defect caused by an immunodeficiency state and a malignancy and cannot be assumed to be causation. Despite this it is informative to look for recurring themes within primary immunodeficiencies. The increased risk of CHL-specific lymphomagenesis in certain T cell-specific immunodeficiency states discussed below is notable.[78] Equally notable is the absence of non-T cell-specific immunodeficiency states from this list.

Primary immunodeficiencies disproportionately predisposing to CHL include Interleukin-2-inducible T cell Kinase (ITK) deficiency, CD27 or CD70 deficiency, Autoimmune Lymphoproliferative Syndrome (ALPS-Fas) and Ataxic Telangiectasia (Table 1.1). The first four of these conditions affect T cell activation pathways/maturation or T-B interaction pathways. The fifth (Ataxic Telangiectasia) has a weaker association with CHL and is associated with broader immunologic defects including CD4 lymphopenia.[78,79] Acquired immunodeficiencies disproportionately predisposing to CHL also suggest T-cell specificity; in human immunodeficiency virus (HIV) infection T_H cells are specifically depleted but wider immunological dysregulation is also seen.[80] Whilst many lymphomas are seen in HIV, subtleties in the pattern of predisposition to CHL in the context HIV may give further clues as to the role of T cells in this process.[81]

Table 1.1: Immunodeficiencies predisposing to CHL lymphomagenesis

Disorder *Gene*	Role		Defect	Malignancy /All patients	Malignancy
Primary Immunodeficiency					
ITK def. *ITK*	TCR signalling pathway	**T cell specific**	T/NK/NKT cells: T_H and NKT lymphopenia, altered T cell differentiation, T_C/NK levels normal B –hypogamma.	15/20	13x CHL 6x B-LPD 1x NHL
CD27 def. *CD27* CD70 def. *CD70*	CD27-CD70 T cell co-stimulatory pathway		T/NK/NKT – Normal levels. Cytotoxicity impaired, altered T cell differentiation B – mild hypogamma. Impaired NK/T cytotoxicity Mild ↓T_H, ↓memory B – hypogamma.	9/17 4/5 [82,83]	3x CHL B-LPD, BL, NHL 4x CHL
ALPS-FAS *TNFRSF6*	CD95 programmed death pathway and T-B GC help		Expansion CD4/CD8 double-negative T cells	16/150	10x CHL 6x NHL
AT *ATM*	DNA damage repair		Variable T_H lymphopenia, function normal NK normal B – mild hypogamma.	50/279	12x CHL 38x NHL (19 EBV+)
Acquired Immunodeficiency					
HIV-associated	Virus depletes CD4+ T cells and causes immune dysregulation	**T specific**	T_H lymphopenia, NKT lymphopenia, hypergamma., immune dysregulation	20-30x ↑Risk CHL, peak incidence CD4 100-350	

Abbreviations: Deficiency (def.), hypogammaglobulinemia (hypogamma),

Interleukin 2-inducible T cell Kinase (ITK), T cell receptor (TCR), B-cell lymphoproliferative disorder (B-LPD), Non-Hodgkin Lymphoma (NHL), Diffuse Large B cell Lymphoma (DLBCL), Burkitt Lymphoma (BL), Germinal Centre (GC), Autoimmune Lymphoproliferative Syndrome (ALPS-FAS), Ataxic Telangiectasia (AT), T (T cell), T_C (cytotoxic T cell), T_H (T helper cell), B (B cell), NK (natural killer cell), NKT (natural killer T cell)

Table adapted from Palendera *et al.*[78] and Shabani *et al.*[79]

A common feature of immunodeficiency-associated CHL is lymphoma cell infection with the EBV. EBV positivity is reported in close to 100% of HIV-associated, ITK-associated and CD27/70 associated CHL cases.[78,84] This is in contrast to the setting in immune competent patients where only 40% of CHL cases express EBV viral proteins. The strong association between

immunodeficiency and EBV$^+$CHL is likely to be related at least in part to the role T and NKT cells play in EBV control and antitumor immunosurveillance.[85] Loss of EBV control results in increased numbers of EBV-infected B cells transiting the germinal centre, increasing the likelihood of a transformation event. EBV proteins expressed in the CHL cell also increase the likelihood of a transformed cell's survival. Finally, compromised EBV and antitumor immune surveillance increases the likelihood of escape. Transgenic mice expressing EBV-LMP1 and EBV-LMP2A (viral proteins associated with EBV$^+$CHL) rapidly develop lymphoproliferation on T and NK cell depletion highlighting the importance of these cells in this process.[86,87] However, the fact that specific defects predispose to EBV$^+$CHL as opposed to non-specific EBV+ lymphoproliferation as is seen in other immunodeficiencies suggests that these conditions hold clues to important immune interactions between CHL cells and their microenvironment.

EBV exerts its influence in CHL through the expression of a small number of viral proteins. EBV$^+$CHL cells strongly express a limited number of EBV proteins including EBV-LMP1 and EBV-LMP2A in an expression pattern called type II latency.[88,89] This expression pattern is associated with EBV-infected B cells whilst they transit the germinal centre, minimising their detection in a highly immunogenic setting whilst still improving the odds of survival in a process where the vast majority of cells die by apoptosis.[53,90] When healthy B cells transit the germinal centre they become dependent upon T and antigen-derived external signals through the B cell receptor to avoid CD95/Fas-mediated programmed cell death.[53] In EBV infection EBV-LMP1 and EBV-LMP2A supplement the survival signals provided by T_H cells and the B cell receptor respectively, increasing the likelihood of the cell surviving germinal centre selection.[53,91] In CHL these proteins are highly upregulated possibly replacing the need for extrinsic support.

The importance of these pathways to the CHL cell is emphasised by the fact that the same pathways are augmented by distinct mechanisms in EBV negative CHL, suggesting convergent evolution on a central process. Both EBV-LMP1 expression and A20 mutations in EBV$^+$CHL and EBV negative disease respectively result in the upregulation of NFκB. NFκB is the downstream consequence of CD40 signalling and in turn leads to further CD40 upregulation.[92] CD40 engagement by CD154 on is a central mechanism for T_H cell provide survival signals to germinal centre B cells via NFκB activation. Unusually for B cells, germinal centre B's have a pre-formed Fas death-induced signalling complex, creating their requirement for extrinsic support to survive. This complex requires constant inhibition by Fas-associated death domain-like IL1-converting enzyme-inhibitory protein (cFLIP) to avoid programmed cell death.[93] cFLIP is rapidly degraded so constant production is required and cFLIP in turn is maintained by NFκB.[94] This provides a safety mechanism whereby germinal centre B cells should die unless they receive external help from T_H cells.[63] EBV negative and EBV$^+$CHL have independently developed

mechanisms to bypass this requirement that converge on the upregulation of NFκB via CD40-like signalling. At least one of the survival benefits of this mechanism is resistance to CD95/Fas-mediated apoptosis and it is notable that one of the immunodeficiencies that disproportionately predisposes to CHL is ALPS-Fas which is characterised by mutations in the CD95/Fas pathway leading to ineffective CD95/Fas-mediated apoptosis.[95] Importantly resistance to CD95/Fas-mediated apoptosis not only confers protection from death due to lack of support but also from cytotoxic T_H which use the CD95 pathway as an effector mechanism.[96]

The upregulation of NFκB seen in CHL suggests that CHL cells supplement their requirement for extrinsic T cell support. The degree to which this replaces that requirement is unclear. It is hypothesised that these mechanisms are complemented by extrinsic support from environmental T cells via CD40/CD154 ligation. CHL cells do not grow in culture suggesting a requirement for additional support, however, the evidence for a T_H subset that supports CHL cells in this manner originates from allogenic T_H cells expressing CD154 in co-culture with an autonomously growing cell line.[97] Evidence for a T cell subset supporting CHL cells in this manner is therefore weak and needs further evaluation.

The second signal required for germinal centre survival originates from antigen stimulation via the B cell receptor (BCR). However, loss of BCR expression, either due to crippling BCR mutation or loss of immunoglobulin transcription is characteristic of CHL. [50] In normal circumstances this would lead to cell death. In EBV^+CHL the BCR signal is replicated by signalling from EBV-LMP2A. EBV-LMP2A signalling is sufficient to rescue B cells with crippling BCR mutations from programmed cell death and it is notable that most CHL cases with crippling BCR mutations are EBV^+, whereas in EBV negative disease loss of BCR expression is achieved by other mechanisms.[98] In normal circumstances an EBV-infected B cell would transition to a different latency profile on exit of the germinal centre and later to a lytic program for viral reproduction.[53] CHL cells are a dead end for EBV infection as they never enter a lytic program, possibly due to the loss of the BCR pathway components which influence transition to the next phase of the viral life cycle.[99]

HIV-associated CHL provides additional insight into EBV^+CHL. HIV depletes mature T_H as opposed to primary immunodeficiencies which may affect all stages T development. The increased incidence seen in both primary and acquired states therefore suggests that mature T_H dysfunction is important. HIV-associated CHL follows an interesting incidence pattern with a peak of incidence seen at intermediate CD4 counts irrespective of antiretroviral treatment status, viral suppression or whether CD4 counts are falling or recovering.[81] Treatment does not affect disease risk.[100] This suggests that absolute CD4 count is more important to CHL

development than viral control. A moderate fall in CD4 counts is seen in HIV patients for a year prior to a CHL diagnosis, providing insight into the natural history of CHL.[100] Additionally, intra-tumoral CD4 counts do not correlate with peripheral blood CD4 count, although CD4 expression overall is lower in CHL in the context of HIV (our data, unpublished). This is suggestive of a marked recruitment of T_H cells to the lymphoma microenvironment during disease development.

The absence of CHL at very low CD4 counts in HIV is interesting, suggesting a "goldilocks zone" of CD4 counts where T_H levels are low enough but not too low to support lymphoma development. This is in contrast to HIV-associated DLBCL and other Acquired Immunodeficiency Syndrome-defining lymphomas where the highest incidence is seen at very low CD4 counts where immune surveillance is severely compromised.[80] The reasons for this incidence pattern are not well understood. It has been speculated that CHL cannot progress in severe T_H lymphopenia due to a requirement for T_H cell support.[101,102] However, there may be alternative explanations including the possibility that severe compromise to immune surveillance permits aggressive outgrowth of other transformed cells or a change in phenotype in what might otherwise have been a CHL transformation event.

1.2.7: Genetic predispositions in immune competence: HLA associations and familial CHL

Gene association studies have consistently identified associations between specific HLA genes and CHL risk. This has proved robust in both familial and sporadic cases, across European, Chinese and Iranian populations and on meta-analysis.[103–111] Additionally, data suggests a significant number of CHL relapses represent clonally unrelated *de novo* CHL neoplasms.[76] Taken together these data suggest that host constitutional immune function is important to CHL risk. Interestingly, HLA associations differ by CHL cell EBV infection status with HLA I associations predicting EBV^+CHL but HLA II broadly associating with EBV negative, usually NS-CHL (the predominant EBV negative subtype).[112–116] The association between HLA I and EBV^+CHL is likely to relates to variations in the ability of different HLA I subtypes to present EBV-associated antigen and therefore to control EBV infection. Consistent with this, EBV^+CHL patients have higher levels of circulating EBV^+ cells and detectable DNA than those with EBV negative CHL.[117,118] Given that 90% of the population is exposed to EBV which persists as latent infection without detectable circulating DNA this is suggestive of differential EBV control.[119] Within the HLA I alleles, HLA-A*01 is associated with increased risk of EBV^+CHL whereas HLA-

A*02 is protective.[120,121] Infectious mononucleosis infection and specifically late Infectious mononucleosis is associated with an increased risk of EBV$^+$CHL for a window of a few years after infection and this risk is mitigated for by HLA-A*02 status.[30,120,122–126] HLA-A*02 complexes present EBV peptides including EBV-LMP1 and EBV-LMP2A whereas little response to EBV peptides is detected in HLA-A*01 carrying patients.[28,127] Additionally, newly diagnosed HLA-A*02$^+$EBV$^+$CHL patients had higher levels of EBV-LMP2A-specific cytotoxic T (T_C) and EBV-LMP2A-specific T_C from healthy HLA-A*02 heterozygote donors expanded more readily to HLA-A*02-restricted compared to non-restricted cell lines.[28] The strength of this effect was modest but has been validated in subsequent studies.[128] The association between EBV$^+$CHL and HLA I strongly suggests that EBV control by T_C is relevant in determining EBV$^+$CHL risk and the relationship between HLA I alleles and EBV protein presentation make it biologically plausible. This is reinforced by the observation that HLA-A associations are also seen with other EBV-associated malignancies where tumour cells express a similar EBV latency profile such as nasopharyngeal carcinoma, but not in non-EBV associated malignancies such as follicular lymphoma, chronic lymphocytic leukaemia and many solid tumours.[129]

Expression of MHC I (encoded by HLA I) and MHC II (encoded by HLA II) have also been extensively studied in CHL. MHC I or MHC II loss is a common immune evasion mechanism in CHL which has been linked both to response to conventional chemotherapy and, in the case of MHC II, to PD1 inhibitors (PD1i).[130–134] Interestingly, the pattern of MHC complex loss is also dependent upon EBV status but is the inverse of that seen with HLA association studies. MHC I expression is frequently lost in EBV negative CHL whereas EBV$^+$CHL is associated with retention of the MHC I complex and expression of accessory proteins consistent with functional antigen presentation.[135,136] This pattern is robust across European, Chinese and Hispanic populations.[137,138] Similarly, MHC II expression shows the inverse pattern to HLA II association. MHC II expression is more frequently lost in EBV$^+$CHL (either through MHC II molecule loss or HLA-DM loss resulting in retained MHC II CLIP, an invariant chain peptide preventing antigen presentation) and retained in EBV negative cases.[131] Retention of both MHC I and MHC II was most frequent in EBV$^+$CHL and loss of both was most frequent in EBV negative CHL.[131]

Whilst HLA associations and MHC expression have been extensively documented, the inverse relationship between the two patterns has not been widely discussed. Similarly, the increase infiltration of T_C and EBV-LMP2A-specific T_C in EBV$^+$CHL has been noted but this has not been related to the above data.[22,28,139] The differences between HLA/MHC patterns highlight important differences between the disease subtypes but also suggest convergent evolution between EBV$^+$ and EBV negative CHL. Each subtype shows evidence of T_C evasion either through restriction to HLA subtypes with poor EBV antigen recognition or MHC I loss. Increased

T_C infiltration in EBV$^+$CHL is consistent with this as successful cell-intrinsic evasion of T_C recognition reduces the need to evolve evasion mechanisms reducing T_C infiltration. Additionally, the data is suggestive of T_H evasion in both diseases with either MHC II loss or HLA II subtype restriction. In this case however it is harder to connect the HLA II restriction to a functional outcome both because the peptides relevant to anti-tumour cytotoxicity in EBV negative CHL are unknown and because the relationships between T_H cells and their epitope are more complex; T_C cells are activated by and exert their effector mechanism in a MHC I-dependent manner whereas T_H are activated via MHC II but exert either i) local non-specific effector mechanisms, ii) MHC II-dependent T_H-mediated help or iii) MHC II-dependent T_H-mediated cytotoxicity (known to be relevant in EBV control).[96] Of note, loss of MHC II expression would usually be considered as a mechanism of T_H evasion, implying a selective advantage to MHC II loss, however this interpretation is also complicated in some cases by data demonstrating that CIITA is a recurrent fusion partner for PDL1, leading to concurrent MHC II downregulation and marked PDL1 upregulation.[140] This leaves open the possibility that MHC II loss in these cases does not provide selective advantage to the tumour, but that a disadvantage or neutral change is selected for because of a net advantage due to PDL1 upregulation.

Taken together the HLA data strongly imply a central role for T_C evasion in CHL lymphomagenesis and survival. Overall the paucity of MHC I expression in CHL have led to questions as to how T_C could be the effector cells responsible for PD1i activity.[132] The data also implicate a central role for T_H. Interestingly, MHC II expression but not MHC I expression predicts response to PD1 inhibitors in CHL suggesting that T_H relationships may be of particular importance in PD1 checkpoint blockade.[133]

1.2.8: Summary: CHL lymphomagenesis

Taken together, these data suggest the following picture: CHL arises from a B cell that has transited the germinal centre and appears to have arrested in early differentiation towards memory B or plasma cell. During transformation it has lost many hallmarks of B cell identity including expression of the BCR. Within EBV$^+$CHL cells the virus is arrested in a germinal centre-latency state and provides supplementary signals mimicking the signal 1 (BCR stimulation) and 2 (external T cell support) that germinal centre-B cells need to survive. In non-malignant settings these supplement but do not replace external survival signals. In EBV$^+$CHL the proteins providing these signals are upregulated beyond that seen in normal infection so it is unclear if

malignant cells retain an additional need for extrinsic T cell support. In EBV negative CHL other mutations provide similar signals in an example of convergent evolution.

Data from immunodeficiencies disproportionately predisposing to CHL consistently identify an important role for T cells, usually T_H cells in the development of EBV^+CHL. This is likely to also apply to EBV negative disease as they are similarly enriched for T_H. These defects encompass T cell signalling, co-stimulation and resistance to CD95-mediated apoptosis. It is currently unclear whether compromise to overall T cell numbers or deficiencies of specific subsets are responsible for the increased CHL risk. The occurrence of HIV-associated CHL occurs at moderate but not severe levels of T_H lymphopenia (irrespective of viral replication) reinforces the notion of a requirement for T_H presence.

HLA association and MHC expression studies also suggest a central role for T cells: Specific HLA I subtypes predispose to EBV^+CHL, which often retains MHC I expression and loses MHC II whereas HLA II subtypes predispose to EBV negative CHL, which often retains MHC II expression and loses MHC II. This also hints at convergent evolution and suggests important roles for both T_C and T_H irrespective of viral status.

A number of important questions which could prove central to understanding disease risk and optimising treatment remain unresolved. Is the increased risk seen in immunodeficiency attributable to global T_H lymphopenia or specific subset defects? How much of this risk is attributable to failure of EBV immune surveillance? Is there a requirement for T_H support? What is the significance of the differing histological subtypes? How relevant are these findings to the microenvironment of established CHL?

The data discussed above highlights the close relationship between T cells and CHL. T_C evasion is prominent in CHL, with MHC I expression loss in the majority of cases. This raises questions as to whether T_C cells can act as major mediators of immune surveillance in CHL. Additionally, MHC II but not MHC I expression predicts outcome to PD1 checkpoint blockade, with cases retaining MHC II showing an improved response. This suggests that T_H cells play an important role, although does not shed light on the manner in which T_H cells might exert this effect. PDL1 expression is seen in both CHL cells and the myeloid microenvironment and the degree of contribution of each to PD1 blockade is currently unclear. It is likely that CHL PDL1 expression is most important as whilst PDL1 expression overall predicts PD1 inhibitor response one trial has reported that CHL-PDL1 specifically was responsible for the effect.

In light of this, the following sections outline the current literature relevant to PD1 inhibition in CHL, including T cell exhaustion, the T_H compartment and the myeloid compartment (due to its PDL1 expression).

1.3: The role of the microenvironment in established CHL

Lymphomas differ in their degree of dependence on their microenvironment.[141] Lymphomas such as Burkett's lymphoma appear largely autonomous. They grow aggressively, effacing microenvironmental cells and grow readily in culture when removed from it.[141,142] Others such as follicular lymphoma exist within a milieu of cells that resembles the parent tissue whilst lymphomas such as CHL both recruit to their environment and re-educate local cells, resulting in a milieu that is distinct from the parent tissue. The lymphoma cell is rare in CHL, often making up under 1% of the tumour, and is heavily outnumbered by a polyclonal reactive immune infiltrate.[143] CHL cells do not survive in culture suggesting that they depend upon supportive microenvironmental signals to grow. Additionally, treatments targeting the immune infiltrate show activity in CHL.[6] For this reason the microenvironment is considered to play an important role and CHL is frequently cited as a paradigm example of lymphoma-microenvironmental interaction.[143] The tumour microenvironment is a complex network of immune and stromal cells, all of which are likely to be playing important roles in either sheltering or attempting to eliminate the malignant cell. Any model focussing on interactions between one cell type and the tumour is inevitably a gross oversimplification. A challenge in the study of the tumour microenvironment is to move towards multi-cellular models and to identify the broad axes frustrating the anti-tumour response. Data from studies on lymphomagenesis (discussed above), the composition of the immune infiltrate and prognostic biomarker studies (discussed below) have highlighted the myeloid and T cell compartments as of particular importance. These cell types have therefore become the focus of this thesis.

1.3.1: The myeloid compartment

The myeloid compartment and particularly the role of macrophages has been a focus of research in CHL. Globally, a myeloid signature by gene expression analysis is associated with an inferior outcome to therapy.[144] At least fifteen studies have assessed macrophage infiltration by measuring CD68 expression by immunohistochemistry (IHC). The majority have associated high macrophage infiltration with inferior outcomes and these findings have been confirmed

on meta-analysis.[145] Additionally, high levels of CD163, often regarded as an M2 macrophage marker, associates with inferior outcome on meta-analysis.[145] Both markers are more frequently associated with EBV$^+$CHL, increased age and the MC-CHL histological subtype, although marked infiltration can be seen across all tumours.[146,147] Importantly they are independent predictors of outcome and the two markers do not consistently co-localise or even inhabit the same region of the biopsy.[146,148] This suggests important roles for multiple macrophage phenotypes in CHL. The roles of other myeloid cells such as dendritic cells are less well explored, although data suggest that these are less numerous than macrophage and have a weaker association with outcome.[149] Together these studies suggest that CD68$^+$ and CD163$^+$ macrophages play an important role in the CHL microenvironment.

Sufficient data has been reported to comment on the origin of macrophages in CHL. Assessment of sex chromosome expression by fluorescence *in situ* hybridisation in CHL relapses after transplants where the donor was a different sex to the recipient demonstrated that macrophages were bone marrow derived.[150] Xenograft models of CHL cell lines are also highly macrophage-enriched, suggesting recruitment to sites of xenograft injection.[151] Additionally, CHL cells and cell lines express multiple factors involved in monocyte recruitment including CCL2, CCL3, CCL4, CCL5, CXCL9, CX3CL1 and CXCL10.[152,153] Taken together this suggests that macrophages are derived from monocytes which migrate to the microenvironment and originate in the bone marrow. Additionally, it suggests that these cells are at least in part actively recruited by the CHL cell rather than representing an appropriate immune response.

There is also evidence that once recruited the differentiation of macrophages is skewed towards a tolerogenic phenotype in CHL. CSF1/MCSF expression was part of the myeloid signature identified in CHL and expression of its receptor CSF1R on macrophages has been independently associated with inferior outcome.[144,154] MCSF and IL10, both of which are secreted by CHL cells, are thought to promote an M2-like regulatory phenotype with expression of molecules such as IL10, IDO1 and CD163.[155,156] Consistent with this, cases with high CD163 expression were associated with high microenvironmental mRNA expression of IL10 and TGFβ in CHL.[149] Elevated expression of IDO1 by macrophages in CHL is also reported.[157] These data are supported by functional evidence using CHL cell lines. Culture of monocytes or monocyte-derived macrophages with CHL cell line supernatant leads to upregulation of immune tolerance markers CD163 and CD206, and variably HLA-DR (which is more associated with immune activation), particularly in the context of MCSF treatment.[149] Furthermore, CHL-polarised monocyte-derived macrophages reduced the proliferative response of anti-CD19 CAR T cells to an irradiated CD19+ target.[158] Finally, high levels of

$CD163^+PDL1^+CD14^+$ monocytes were detected in the peripheral blood of CHL patients and NK activity increased on monocyte depletion.[153] These data support the concept of a suppressive phenotype for macrophages in CHL.

Expression of PDL1 is also reported by macrophages in the microenvironment of CHL.[159] This may reflect an immunosuppressive phenotype but further evidence is required before this conclusion can be drawn as PDL1 is upregulated in myeloid cells by a wide variety of cytokines, both regulatory and inflammatory.[139] Marked upregulation is seen with IL27 treatment (which may be relevant in CHL, discussed below) and in this context it is associated with immunosuppressive activity.[160] Additionally, PDL1 Fc treatment has been shown to drive differentiation of immunomodulatory macrophages and PD1 blockade can promote an anti-tumour M1 phenotype.[161–163] This raises interesting questions about the effects of PD1 blockade in the myeloid compartment in CHL.

Taken together these data are suggestive of monocytes being actively recruited by CHL cells, differentiating to macrophages and adopting an immune tolerant phenotype. However, these data must be interpreted with caution. As yet no study has phenotyped CHL macrophages in an unsupervised manner leaving results open to selection and confirmation bias due to the markers which were selected. CHL cells also secrete factors such as GMCSF, TNF and IL6, more commonly considered pro-inflammatory.[149,156,164] Elevated TNF mRNA was also associated with increased CD163 expression in CHL.[149] Additionally, the functional data reported is derived from cell lines *in vitro* so is far removed from the tumour microenvironment. There also are a number of unanswered questions. Whilst expression of many of these markers is reported, there is little data regarding marker co-expression. The limited data available suggests that at least two macrophage populations exist and are independently relevant to outcome. It is unclear as to whether these represent a continuum of differentiation, whether they play distinct roles and what roles they play. It is also unclear how these relate to the T cell environment or PDL1 expression which are similarly implicated in chemotherapy response.

1.3.2: The T cell compartment

The epidemiological and lymphomagenesis data discussed above suggests that cellular anti-viral immunity particularly to the human herpes virus family and T cell function are of importance in CHL. T cell functions represent an important arm of the anti-tumour response and to the action of immunotherapies. The immune infiltrate in CHL is markedly enriched for T cells, both T_C and to a greater extent T_H.[22] There is evidence that the CHL cell actively recruits T

cells to the microenvironment and skews their phenotype.[165–167] Finally, T_H cells are observed to form rosettes around the tumour cell leading to speculation of a supportive or protective interaction which would be consistent with CHL's GCB origin.[168–170] These lines of evidence suggest that T cells constitute a functionally important part of the CHL microenvironment. In addition to this, focus on the T cell compartment has increased due to the sensitivity of CHL to PD1 inhibitors, which are thought to act primarily through T cells.

1.3.2.1: T cell exhaustion, anergy and senescence in CHL

The advent of immunotherapy has been heralded as a new era in the treatment of cancer medicine, with checkpoint blockade being central to this revolution. The importance of this advance has been recognised with the awarding of the 2018 Nobel Prize for Medicine to Honjo and Allison.[171,172] The most impressive responses have been seen in solid tumours such as metastatic melanoma. In melanoma T_C infiltration and PD1 expression on T_C are predictive of PD1i response, consistent with exhausted T_C being central to their mechanism of action.[173]

Evaluation of responding T cells in the tumour microenvironment is more complex in the context of lymphoma as compared to solid tumour for a number of reasons. Firstly, because the tumour has developed within a lymphoid structure it is difficult to be certain as to which cells represent an immune response (either anti-tumour or supportive) and which cells represent background noise by virtue of the tumour existing within the lymph node environment. This is illustrated by a paper which used flow to discriminate T_H signatures by chemokine receptor expression in CHL and in colorectal cancer.[174] In colorectal cancer (which exists in a non-lymphoid environment so most sampled T_H will be tumour-infiltrating) the authors detected a effector T_H profile, whereas in CHL they could not separate the receptor profile from that of reactive nodes. It is possible the CHL signature is genuinely comparable to reactive nodes but equally possible that because CHL infiltration of lymph nodes may be incomplete and tumour cell density may be low the T_H sampled represented signal from the parent lymph node environment. Of note Greaves *et al.* performed a flow analysis also using CHL SCS with similar numbers but more detailed phenotyping and did detect differences between CHL and RLN control.[22] Secondly, the majority of lymphoid tumours are derived from professional antigen presenting cells (APC). It is therefore conceivable that the role of the PDL1 axis in this context might be different to that seen with e.g. a stromal cell. The concept of APC-derived tumours interacting differently with their microenvironment is supported by the fact that in lymphomas increased infiltration T_{Reg} are frequently associated with a good response to therapy, whereas in many solid tumours they are associated with adverse outcome.[175,176] This

is significant given that T_{Reg} can be induced both by APC in the tumour microenvironment and by tumour cells with APC function.

PDL1 upregulation is a common mechanism of immune evasion in cancer, and is a prominent feature in CHL.[20,177] CHL cells frequently harbour amplifications of the 9p24.1 region, containing *CD274* and *PDCD1LG2* (encoding PDL1 and PDL2), providing a genetic basis for pathological PDL1 upregulation, further amplified by JAK2 signalling and EBV-LMP1 expression.[20,90] Additionally, fusions between PDL1 and the MHC II transactivator CIITA and PDL1 expression in the microenvironment contribute to upregulation and immune suppression.[140,159] PDL1 expression has consistently been reported to predict response to PD1 inhibitors in CHL trials and in solid malignancies.[6,7,13,178] Tumours including melanoma, NSLCS, RCC are also reported show an association between PD1 and PDL1 expression.[179] However, the association between PDL1 and PD1 inhibitor response was strong whereas the association between PD1 and PD1 inhibitor response was borderline. Of note, geographical assessment associating $PD1^+$ tumour infiltrating lymphocyte (TIL) distribution with PDL1 expression in this study was performed by eye which is unreliable and may be confounded by the distribution of a parent population (see Figure 1.3).

The combination of PD1 inhibitor responsiveness and high PDL1 expression in CHL is often held to be evidence of T cell exhaustion, however this does not necessarily imply the presence of exhaustion. Studies have consistently found low levels of PD1 expression and markers of exhaustion including PD1 do not predict PD1 inhibitor response in CHL.[22,180]

1.3.2.1.1: T cell dysfunction and exhaustion

Various hypo-functional T cell states are described including ignorance, tolerance, anergy, exhaustion and senescence.[181,182] T cell ignorance describes a state where antigen-specific T cells are ineffective because they are restricted from encountering antigen. In T cell tolerance (central or peripheral) antigen-specific T cells are removed or a cell-intrinsic state of hypo-responsiveness is induced or factors promote differentiation towards a regulatory phenotype. Anergy describes a state where sub-optimal co-stimulation at activation leads to hypo-responsiveness, whereas exhaustion occurs when previously activated cells are exposed to persistent antigen exposure without its clearance. Exhausted cells are maintained by ongoing antigen exposure.[183] Blockade of PD1-PDL1 signalling can rescue a subset of exhausted T cells.[184] Similarly blockade of TIM3 restores function in exhausted T cells. These data provide evidence that PD1 and TIM3 play a central role in the maintenance of T cell exhaustion. Finally,

senescent cells have undergone multiple rounds of replication leading to telomere shortening. T cell dysfunction incorporates all of these terms, differentiating them from an appropriate antigen response with functional T cell memory.[182]

Many of these states are of significance to the anti-tumour response.[185] T cell ignorance is relevant because tumours downregulate self-antigen presentation pathways, reducing T cell exposure to antigen.[133] T cell tolerance is also relevant: Centrally it plays an important role because tumour cells are derived from self, clonal deletion due to central tolerance will lead limited numbers of potentially tumour-reactive T cells. Peripherally it is also important because of poor innate immune stimulation, tolerogenic antigen presentation and local suppression mechanisms which are prominent in many cancers.[186] Finally, exhaustion where chronic antigen exposure to effector cells of the tumour without clearance.

Table 1.2: Recognised types of T cell dysfunction

Term		**State**	**Cause**	**Markers**
Ignorance		Antigen-inexperienced, potentially functional	Unexposed to antigen due to physical sequestration or low expression.	Naïve (CCR7, CD45RA)
Tolerance	Central	Deleted	Negative selection of self-reactive in thymus	Nil,
	Peripheral	Antigen-experienced but deleted, suppressed or cell-intrinsic state of unresponsiveness	Peripheral inactivation due to antigen stimulation in tolerogenic context.	↓IL2 prod.
Anergy/ Adaptive tolerance	*in vitro*	Antigen-experienced, dysfunctional	Stimulation in absence of co-stimulation	Nil, PD1, LAG3 ↓IL2 prod.
	in vivo	Antigen-experienced, dysfunctional	Stim. with sub-optimal *in vivo* co-stimulation (adaptive tolerance)	
Exhaustion		Antigen-experienced, Progressive functional hyporesponsiveness	Persistent/repeated antigen exposure	PD1, Tbet, EOMES, TIM3, LAG3
Senescence		Irreversible cell-cycle arrest	(distinct from quiescence which is reversible arrest)	CD57 CD28 loss

Adapted from Schietinger *et al.*[182]

A number of factors have complicated descriptions of exhaustion and anergy in cancer. There are important distinctions between the two states: anergy is induced at first contact whereas exhaustion is progressive and worsens over time and they are molecularly distinct.[183,187] However, there is overlap between identifying markers and functional deficits in each state and their definitions have become blurred.[181,182,188] This has meant that interchangeable use of these terms is common in the literature. Additionally, the hallmark characteristics of exhaustion were described in the setting of chronic viral infection. This raises questions when the concept is translated to the setting of cancer and a number of studies have suggested that exhausted phenotypes and the functional defects in malignancy may differ.[181,189] Lastly, there is no single accepted functional test that allows us to define or separate these conditions, which has led to a wide variety of approaches being used. The lack of a benchmark test is particularly problematic as effector functions are lost progressively in exhaustion and may not correlate with PD1 expression.[181,182,190] Additionally, the order and magnitude of loss may vary between cell type. These factors make comparison across studies difficult.

In addition to the problems in identifying exhaustion there is a lack of clarity as to which subset of exhausted cells are targeted by PD1 inhibition. Data from mouse models suggests that exhausted T cells are differentially responsive to reversal by PD1 inhibitors depending upon their PD1 expression, with $PD1^{int}$ cells being most responsive.[191] This has been suggested as an explanation for the low expression of PD1 in CHL despite PD1i clinical efficacy.[6] Data confirming this relationship in human samples is sparse and data looking specifically at T_H cells is sometimes conflicting.[192]

Tissue expression of PDL1 inhibits T cell function and maintains T cells in an exhausted state, but it does not necessarily follow that PDL1 induces exhaustion *per se* and therefore that if PDL1 expression is seen then exhaustion is present. The concept of PD1 expression acting as a rheostat, controlling and maintaining an exhausted state rather than inducing it, is consistent with its roles in other settings such as in activation where it is upregulated irrespective of the presence of PDL1, and also in T follicular helper (T_{FH}) cells which are $PD1^{hi}$ and whose maintenance is restrained by the presence of PD1-PDL1 signal.[193,194] There is further evidence suggesting that a direct line cannot be drawn between PDL1 expression and exhaustion. PD1 and PDL1 expression varies by tissue type, with some areas, including bone marrow, representing $PDL1^{lo}$ niches. However, these tissues contained high levels of exhausted $PD1^{hi}$ CD8 lymphocytes during chronic viral infection, suggesting $PDL1^{lo}$ areas could represent niches for survival.[195] PDL1 expression may however induce anergy.[196,197] The induction of anergy by PDL1 is consistent with the concept of PD1 as a rheostat dampening T cell receptor (TCR) signal

strength and the effects of co-stimulation, increasing the possibility of a cell receiving sub-optimal costimulatory signals at activation.

There are multiple features of the CHL microenvironment which appear conducive to the development and maintenance of T cell dysfunction. High PDL1 expression on CHL cells and microenvironmental APC may be conducive to the development of both anergy and the maintenance of exhaustion.[181] Similarly, galectin-9 (a principal ligand of TIM3) is expressed and was first identified in CHL and may also maintain exhausted cells.[198] Conversely, other features seem inconsistent. For example, IL21 is reported to rescue cells from exhaustion and is secreted by CHL cells.[199,200] Robust experimental evidence for the presence of exhausted cells in CHL is currently lacking.

1.3.2.1.2: Studies quantifying PD1 as a single marker in CHL

Multiple studies have quantified PD1 expression by IHC, usually as part of an assessment of prognostic impact. Eleven have quantified PD1 as a single marker. The studies vary in antibody clone and positivity cut-off but all studies have reported low PD1 expression or positivity in a minority of cases. [22,201–210] Four of small to medium size have detected no association with outcome.[204–207] Five, including those with the largest cohorts, detected a survival association and all of these reported high PD1 expression to associate with poorer prognosis.[22,201–203,211] Two studies assessed PD1 and PDL1 side by side. In the first, neither PD1 expression nor microenvironmental PDL1 expression individually associated with survival but expression of both together associated with adverse prognosis.[211] In the second, both markers individually and independently associated with adverse outcome.[203] One study by Muenst *et al.* assessed a large cohort and reported a negative correlation between PD1 expression and 9p24 gains (the amplification implicated in PDL1 upregulation).[201] This inverse correlation does not support model whereby $PDL1^{+}$ cells are inducing a $PD1^{hi}$ exhausted T_H population. One study quantified PD1 alongside other exhaustion markers by proteomics but made comparison to DLBCL as opposed to reactive tissue controls. They found no enrichment of PD1 and TIM3 in CHL relative to DLBCL, although CHL was associated with a higher proportion of $LAG3^{+}$ cells and T_H.[212] DLBCL is less responsive to PD1 inhibition than CHL.[15] If PD1 was a direct reflection of exhaustion and PD1 inhibitors functioned by reversal of exhaustion this might be considered a negative control for exhaustion. One might therefore predict low PD1 expression in DLBCL in line with little exhaustion and high in CHL in line with marked exhaustion, however no difference was observed.

Only a small number of studies have reported PD1 expression in the context of PD1 inhibitor therapy. A small study examined PD1 expression in paired pre-treatment/relapse samples before and during PD1 inhibition.[213] They noted increased in PD1 positivity in cases relapsing after PD1 inhibitor therapy, but this did not reach significance. Samples on PD1 therapy are rare given that biopsies are only taken in persistent disease or progression and the limited indications for biopsy make this a biased group. Sample quality was also variable and comparisons were made across tissue type (e.g. lymph node to bone marrow) and histological type, both of which are biasing as expected T cell numbers and PD1 expression differs by compartment and histological subtype.[195,214] Interpretation of PD1 expression is challenging as PD1 expression may represent multiple phenotypes including exhaustion, activation and subset variation as seen in T_{FH} cells. Interpretation of expression under PD1i therapy is even more challenging due to the further possibilities of PD1 inhibitor-mediated hyper-activation or increased exhaustion due to PD1i resistance.[215] These factors make this study hard to interpret. PD1 expression has not been reported of predictive of response in any trial to date, in contrast to PDL1 which has been consistently predictive.[13,133] One trial reported PD1 expression but found no association with response.[6]

In summary, multiple studies to date have quantified PD1 expression in CHL. All studies reported either no difference or a decrease in PD1 expression compared to RLN, low PD1 expression or PD1 expression in a minority of cases. No study has reported correlation between PD1 and PDL1 expression.

1.3.2.1.3: Studies phenotyping PD1 expressing cells in CHL

Few studies have phenotyped $PD1^+$ T cells in CHL. Most are limited by sample size due to low numbers of CHL single cell suspensions available for analysis. Greaves *et al.* performed immunophenotyping of the T_H compartment with a panel focussed on senescence and immunosuppression.[22] They found lower PD1 expression in CHL than RLN. Additionally, CD57 expression (associated with senescence) and the T_H-EMRA subset were significantly reduced in CHL. Of note, three samples overlap between the fifteen SCS used in the Greaves study and the fifteen presented in the data below.

A recent study performed deep phenotyping of T_H cells in seven CHL cases compared to ten RLN controls. They observed a relative expansion of cells in CHL with T helper 1 effector memory (T_H1-EM), T helper 1 effector memory RA (T_H1-EMRA) and T helper 1 regulatory (T_H1_{Reg}) phenotypes based upon CD3, CD4, TBET, CD25, FOXP3, CCR7, CD45RA, CD57 and

EOMES expression. They noted higher PD1 expression in T_H1-EM, T_H1-EMRA populations and concluded that this identified an exhausted T_H1 population.[216] An expansion of T_H-EM was also described by Greaves *et al.* but they noted the absence of T_H-EMRA.[22] This paper adds depth to our understanding of phenotypes in CHL but does not provide functional data to support its conclusions. They identify immune sub-populations that are not well understood or defined. Defining an exhausted $PD1^+T_H1$-EMRA is difficult. In contrast to T_C-EMRA, the concept of T_H-EMRA is not well established and frequencies vary dramatically within the healthy population.[217,218] Similarly T_H exhaustion is distinct from T_H-EMRA, but the markers used to define each population overlap.[218,219] Finally, the use of TBET to define T_H1 alongside T_H-EMRA and T_H exhaustion is problematic given that it is a marker of all three populations. The addition of chemokine receptor markers to TBET to define T_H1 alongside T_H-EMRA led some to conclude that $TBET^+$ T_H-EMRA are distinct from T_H1.[219] T_H1 in other settings are observed to enrich in memory but not exhausted populations.[217] Further possibilities also exist: cytotoxic T_H also been express markers consistent with the T_H-TEMRA $CCR7^{lo}CD45RA^{lo}$ phenotype and express TBET and EOMES.[220] Cytotoxic T_H population have also been described to differentiate on co-culture with CHL cell lines.[221] it has also been noted that basal expression levels of PD1 vary by T_H subset, with the highest expression in T_{FH} and T_H1.[222] Importantly, whilst the T_H1-EMRA population size differs between CHL and RLN in their study, PD1 intensity is similar, raising the possibility that this represents basal expression not exhaustion. Taken together, the increased PD1 expression on T_H1-EM and T_H1-EMRA may represent exhaustion, but could equally be attributed to a cytotoxic T_H identity or to higher basal PD1 expression in T_H1. The concept of T_H1_{Reg} is also a novel one and the functional differences between T_H1_{Reg} versus e.g. T_H17_{Reg} subpopulations are not yet clear. It has been suggested that T_H1_{Reg} might specialise in suppressing a T_H1 response, with data supporting this concept for T_H2_{Reg} and T_H17_{Reg}.[223,224] It is also possible that these represent plasticity and intermediate stages in a transition either to or from T_{Reg} to T_H1.[225] In conclusion, whilst this data is interesting, the author's conclusion that they have defined an exhausted T_H1-EMRA population without functional validation is too bold a statement.

1.3.2.1.4: Studies assessing spatial distribution of PD1 expressing cells

Spatial analysis has been performed in CHL in one study which observed that the CHL microenvironment was enriched for macrophages expressing PDL1.[159] 20 CHL cases were assessed by immunofluorescence multiplex imaging and in all cases macrophages were deemed to be $PDL1^+$ and enriched around CHL cells. The authors then assessed distribution of

PD1$^+$ T_H and T_C relative to either macrophages or CHL cells. The paper found that average nearest neighbour distance from PD1$^+$ T_H to PDL1$^+$ macrophages or was reduced compared to distance from PDL1$^-$ macrophages. They next compared T_H in proximity to CHL cells or macrophages and found enrichment for T_H contact. They repeated this analysis for PD1$^+$$T_H$ and found the same relationship, although less marked. The headline conclusion that PDL1$^+$ macrophages were enriched for T cell contact, and PD-L1$^+$ CHL cells were enriched T_H contact, a subset of which are PD1$^+$, is correct and supports CHL associating with a PDL1$^+$ microenvironmental niche. However, the conclusion that PD1$^+$ T_H proximal to PDL1$^+$ macrophages represent a locally enriched population are incorrect and illustrates a pitfall in spatial analysis as their finding is confounded by the distribution of the parent T_H population.

Figure 1.3: A pitfall in spatial analysis

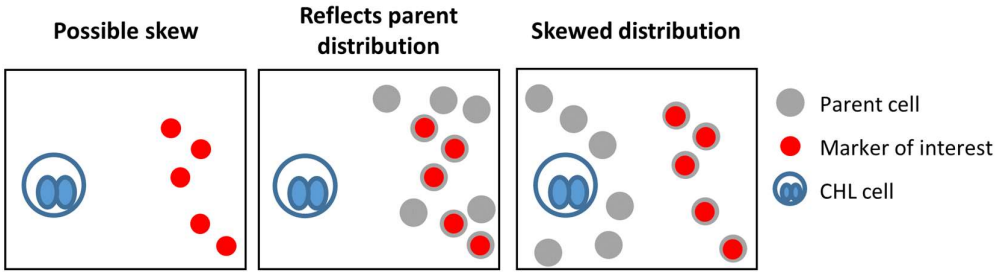

Figure 1.3: 1. Possible skew: Marker of interest (e.g. PD1) appears to have a non-random distribution relative to tumour cell. 2. Reflects parent distribution: The apparent skew is attributable to random distribution of the marker of interest within a skewed distribution of the parent cell (e.g. T_H) so conclusion cannot be drawn about the marker of interest specifically. 3. Skewed distribution: There is discrepancy between the distribution of the parent population and the marker of interest.

i.e. Conclusions should only be drawn if comparison is made to a biologically meaningful parent or control population, the choice of which will vary according to the question.

After accounting for parent T_H and macrophage distribution, the reported PD1 distribution appears either random within the T_H subset or skewed away from the CHL cell, although this cannot be properly tested without access to their data. The correct statistical approach would have been to assess distribution of PD1$^+$$T_H$ within the parent T_H population and test if this deviated from a pattern expected with random labelling. Comment that PD1 positivity was in low abundance, that the frequently attributed exhausted phenotype of PD1$^+$ T cells in CHL is

incompletely described was also made in a response to this paper by Steidl.[180] In summary, this paper confirms the presence of a $PDL1^+$ myeloid niche but does not identify any relationship to $PD1^+$ T cells.

A second study by Ma *et al.* noted that cells in proximity to CHL cells were $CD26^-$ while cells at greater distance from CHL cells were $CD26^+$.[226] No formal spatial analysis was performed to assess how faithfully CD26 expression discriminates proximity to CHL cells however it is a previously reported phenomenon.[227] The major finding of the study was that the $CD26^-$ fraction displayed a regulatory profile and CD26 has since been described as a marker for T_{Reg}.[228] This finding was validated in a later study that phenotyped CHL SCS T cells by CD26 expression and noted enrichment for T_{Reg} markers in the $CD26^-$ group.[229] We also observe $FOXP3^+$ T_{Reg} to be enriched around CHL cells, consistent with this finding. Targeted gene expression from $CD26^+$ and $CD26^-$ T cell subsets in RLN and CHL was performed. *PDCD1* (encoding PD1) was the only exhaustion marker included in the panel and comparable intermediate *PDCD1* expression was seen across all subsets in both CHL and RLN.

1.3.2.1.5: Studies functionally testing T cells with reference to exhaustion and anergy

The study by Ma *et al.* discussed in the last section also performed functional testing, stimulating the $CD26^-$ and $CD26^+$ sorted T cell fractions with PMA ionomycin.[226] They found that the $CD26^-$ (putative T_{Reg}) population which was enriched locally to CHL cells was cytokine unresponsive (as measured by mRNA levels). This was in contrast to the equivalent $CD26^-$ population in RLN and the $CD26^+$ (putative non-T_{Reg}) population in both CHL and RLN. The lack of cytokine responsiveness is referred to as an anergic profile, however given that they provide no phenotypic evidence of an anergic profile so cannot attribute a cause this can only really be referred to as hyporesponsiveness and is consistent with a T_{Reg} phenotype. The $CD26^+$ subset (non-T_{Reg}) reported to be locally depleted around CHL cells upregulated IL8, IL21, IL17 and TBET mRNA at 6 hours on PMA ionomycin stimulation. Low level upregulation of IL2 and IFNγ, IL4 and IL12p40 was also seen. On comparison between CHL and RLN, upregulation of cytokine mRNA was universally more pronounced in the RLN group. The RLN control group provides valuable information as to the expression patterns expected in the CHL subsets but care must be taken when comparing amplitude of response between CHL and RLN: In our hands viability of CHL SCS are usually low as compared to RLN and this will be amplified once cells are subjected to sorting. Taken together these data support a local enrichment for T_{Reg} but are insufficient to conclude that T cells in CHL are anergic compared to RLN.

A second paper assessed the influence of PD1 signalling on T_H cells in CHL more directly and adopted an innovative approach.[230] An RNA fingerprint of PD1 signalling was generated by stimulating healthy donor T_H cells with CD3/28/MHC-1 bound artificial APCs with or without a bound antagonistic PD1 antibody and filtering for differentially expressed genes. The choice of an antagonistic PD1 antibody rather than an agonistic antibody or recombinant PDL1 makes it harder to interpret this fingerprint as it is harder to draw a direct comparison to PDL1-expressing APCs in the CHL microenvironment. Despite these drawbacks the authors were able to separated T_H cells of CHL from RLN with the resultant fingerprint. This was not the case for T_H from follicular lymphoma or using other control signatures. We can conclude from these data that the influence of the PD1 signalling pathway differs in CHL T_H when compared to RLN. The authors conclude that PD1 signalling is more prominent in CHL although it is unclear if this conclusion can be drawn definitively as the "PD1 signal" fingerprint was constructed from both upregulated and downregulated differentially expressed genes in the context of using an antagonistic antibody. However, given the high PDL1 expression in CHL it seems likely that PD1 signalling is indeed more prominent. Importantly, this is not equivalent to concluding that cells are exhausted, only that CHL T_H are influenced by PD1-PDL1 signalling, which is also relevant in other settings such as during activation.

Greaves *et al.* provide the strongest evidence to date against the presence of an exhausted T_H population. They assessed PD1 expression in a cohort of 122 patients by IHC and found low PD1 expression. They additionally noted low PD1 expression in CHL SCS and prolonged survival in culture to 60 days with ongoing cytokine secretory capacity, comparable to RLN and far exceeding that seen in tonsil-derived cultures.[22] Limitations of this analysis include the use of the NAT105 clone which we demonstrate to have weaker sensitivity than other commercial clones. Additionally, the high expression of PD1 in T_{FH} could skew comparisons to RLN. Prolonged survival in culture supports the presence of a T_H population with long term growth capacity but is less robust to exclude the presence of an exhausted population as it allows for the possibility of selection in culture for long lived T clones that bear little resemblance to the parent population. Output measurement by phenotyping and measuring population doubling times at 30 and 60 days could be criticised for the same reason.

1.3.2.1.6: Conclusions on exhaustion, anergy and senescence

The strongest evidence for exhaustion comes from observations that CHL is responsive to PD1 inhibitors alongside data suggesting that PD1 inhibitors in solid tumours act via reversal of exhaustion. However, as outlined above there is currently little published evidence supporting

the presence of an exhausted T cell population. Repeated studies have reported little expression of PD1 in CHL. Studies phenotyping $PD1^+$ cells in CHL are sparse with one finding no evidence of exhaustion and a second finding increased PD1 expression in a T_H1 subset but providing no functional evidence that this represents exhaustion. Spatial studies find a $PDL1^{hi}$ microenvironment but do not demonstrate enrichment of PD1 expression. Furthermore, the fact that PDL1 but not PD1 expression predicts PD1 inhibitor response and that PD1 and PDL1 are independent prognostic factors suggests that their expression patterns are driven by independent processes.

Taken together these data suggest a need for a more thorough assessment of exhaustion in CHL and for an open mind to alternative mechanisms of actions of PD1 inhibitors in this context. The default null hypothesis in this situation should be the absence of exhaustion in CHL, however, the strength of the narrative of exhaustion in CHL is such that proof that exhaustion is not present will be required to change opinion.

1.3.2.2: Roles of the major T_H subsets in established CHL

A significant amount of data is available describing the T cell composition and phenotypes of the CHL microenvironment, although none without significant limitation. CHL lymphoma cells are rare within a large inflammatory infiltrate. Nodal involvement may be uneven, so factors such as spatial distribution are likely to be important and means that in low-infiltration cases an element of background noise is expected from cells that may be too distant to be under the direct influence of the CHL cell. As regards functional assessment, the inability to maintain primary CHL cells *in vitro* and the lack of a representative animal model makes testing difficult. Cell lines are available but most were isolated from CHL-involved effusions which differ significantly from CHL cells from the primary lymph node environment. Many statements regarding functional roles are therefore subject to severe limitations. They are often extrapolated from observational data obtained from immunohistochemistry (usually using single-marker cell identification) or flow cytometry analysis (where spatial information is lost and sample sizes are limited). Alternatively, they are inferred from other disease states or *in vitro* interactions either with CHL cell lines or in the absence of the primary CHL cell.

1.3.2.2.1: T_H subsets with a purported anti-tumour role

T_H2

The CHL microenvironment has frequently been described as enriched for T helper 2 (T_H2) cells, although the evidence supporting this statement is limited.[167] A T_H2-dominated infiltrate is hypothesised to protect the HRS cell by creating a misdirected immune response, with ineffective effector functions unsuited to an anti-tumour response. Early small studies suggested a dominance of a T_H2-like profile but these were based upon immunological markers that subsequent data suggests may simply indicate antigen experience.[165,231]

IHC analysis of T_H2 master transcription factors CMAF and GATA3 to date have been limited by poor antibody quality.[165] Flow cytometry studies have not detected evidence of a T_H2-polarised response, finding either a T_H1-dominant pattern, or being unable to separate a T_H1/T_H2 immune profile from reactive nodal tissue.[22,174,229] Flow cytometry-based studies allow more rigorous assessment of a T_H2 profile than classical IHC but do not provide spatial information so cannot assess for a local skewing effect, leading to the possibility of background noise from T cells distant from the tumour. Sample size also limits interpretation of flow cytometry studies as IHC data reveals a marked heterogeneity of cellular phenotypes across CHL cases.[165] One study, albeit with small sample size, performed global gene expression analysis of CHL-infiltrating T_H cells and compared to global T_H signatures from tonsil.[232] Their analysis separated CHL T_{Reg} and non-T_{Reg} from the corresponding tonsil signature by unsupervised clustering, but these differences did not reach significance when using supervised clustering to evaluate subsets. Gene signature enrichment analysis revealed increased T_H2 polarisation in CHL relative to naivety, but also revealed increased T_H1 polarisation in relative to naivety and overall activation. This therefore supports that CHL is enriched for activated and differentiated T_H cells of both types but does not demonstrate that one infiltrate dominates. A second study separated $CD26^-T$ (thought to be enriched around CHL cells) from $CD26^+T$. They found increased T_{Reg} markers in the $CD26^-T$ and detected T_H2 markers in the $CD26^+T$ subset, although these were at a lower frequency than seen in $CD26^+T$ RLN control.[226] Evidence exists that CHL cells secrete factors capable of attracting or skewing towards a T_H2 phenotype but the functional impact of this is not known.[166,233,234] Overall it is likely that T_H2 cells are represented but there is no strong evidence to support a dominance of a T_H2 phenotype, although this does not exclude local skewing proximal to the HRS cell.

T_{Reg}

More convincing evidence is available for the enrichment of T_{Reg} in CHL. FOXP3 is a master transcription factor for a subset of T_{Reg} cells. [235] $FOXP3^+$ cells are seen at a higher concentration in the CHL microenvironment when compared to reactive lymph node, as are other T_{Reg}

markers.[229,233] Gene expression data of $CD26^-$ lymphocytes, a subset shown to be enriched around the tumour cell, is consistent with a regulatory phenotype.[226,236] Flow cytometry of the $FOXP3^+$ subset is similarly supportive and the largest flow-based study to date (comparing 108 CHL SCS to 43 RLN) noted enrichment for a $CD4^+CD26^-CD38^+$ subset across all subtypes of CHL hypothesised to be activated T_{Reg}.[22,236] Additionally, CHL infiltrating lymphocytes suppress proliferation of autologous PBMCs by CTLA4 and IL10 dependent mechanisms, suggesting the presence of functional $FOXP3^+T_{Reg}$ and possibly T regulatory 1 (T_R1, a $FOXP3^-T_{Reg}$ expressing the effector cytokine IL10).[237] Further evidence suggests that CHL cells both attract T_{Reg} and T_R1 and promote their local differentiation. Allo-culture with CHL cell lines promotes $FOXP3^+$ cell differentiation and IL10 expression and CHL cell line-primed T_H suppress proliferation and T_H1 cytokine production *in vitro*.[221,232] Furthermore, CHL cells express chemokines promoting T_{Reg} migration and differentiation.[88,166,233,238,239] This data is supportive of a T_{Reg}-enriched CHL microenvironment. Furthermore, CHL-associated T_{Reg} differ phenotypically from those seen in tonsil, with higher CD200R, BTLA, CD38 and lower CD26 expression.[232] Counterintuitively, higher numbers of $FOXP3^+$ cells in the CHL microenvironment have been associated with improved outcome after chemotherapy.[176] This has been interpreted by some as indicating that T_{Reg} have an anti-tumour role, supressing CHL cell growth.[221] This is theoretically possible as T_{Reg} can suppress proliferation of both T cells and B cells.[240] However, this seems unlikely given that T_{Reg} appear actively induced by the CHL cell and if these processes limited CHL cell growth their expression would be selected out by clonal selection. The connection between cell number within a microenvironment and outcome post chemotherapy is so complex that no mechanistic conclusions can be made from this observation, although the finding hints at a biologically important role.

A putative CHL-supporting T_H cell

T_H cells are seen to rosette around CHL cells, although this only occurs in a small subset of cases. The biological role of rosetting T_H cells, which are polyclonal, is unknown but it is hypothesised that they provide B cell support.[169,170,241] This hypothesis makes sense given that GC B cells rely on external support for survival.[53] The degree to which this requirement is replaced by EBV proteins or other mechanisms is, however, unclear. IHC data suggests that cells express CD154 (the ligand to CD40), a central molecule to the T_H-B support interaction, although flow cytometry data is less clear.[22,242] *In vitro* T cells express CD154 on co-culture with CHL cell lines.[97] CHL cells in turn strongly express CD40 and NFκB (a factor which is downstream of CD40).[168] CD40 expression further correlates with Ki67 (a marker of proliferation) and CHL cell lines proliferate in response to CD154.[243–245] However, rosetting cells

do not express markers of a T_{FH} cell and their phenotype is poorly defined. CHL cells do express the costimulatory molecules CD80 and CD86 which are involved in the T-B help interaction, although they downregulate MHC II molecules in at least a subset of cases, which would make a conventional T-B help interaction less likely. [28,134,140,246–248] Finally, the expression of CD154 *in vitro* on co-culture with CHL cell lines is in the context of an allogenic reaction and CD154-CD40 interaction is also reported to be an effector mechanism of cytotoxic CD4 cells perhaps providing an alternative explanation for this observation.[249] Overall, the function and biological significance of rosetting cells is unclear and the evidence supporting the presence of a T_H subset providing support to the CHL cells is limited.

1.3.2.2.2: T_H subsets with a purported anti-tumour role

The T_H1 subset is generally considered to have anti-tumour activity in the context of lymphoma through the release of cytokines augmenting cellular immunity. The role of the T_H17 cell is less clearly defined in the context of lymphoma, although its function in the context of autoimmunity and secretion of similar effector cytokines by NKT and CD8+ T cells (key effectors of immune surveillance) suggests an antitumor role. However, data from solid tumours is inconsistent.[250]

T_H1

There is limited evidence supporting the traditional view of a T_H1-suppressed microenvironment. IHC studies reveal massive heterogeneity between cases and often large numbers of $TBET^+$ cells. TBET is a master transcription factor for T_H1 which is also expressed in subsets of cytotoxic cells (among others).[165] Flow cytometry studies and gene expression data has revealed either a T_H1-dominated pattern in CHL-involved lymph nodes, or no consistent pattern of T_H1 or T_H2 dominance.[22,174,206,229] CHL cells also express chemokines capable of recruiting T_H1 polarised cells. [251–256] IHC data is supportive of a globally T_H1-rich microenvironment. An inability to separate T_H subsets by chemokine profile in CHL from RLN by flow cytometry may imply that the global T_H pattern is due to a dominant secondary lymphoid organ recruitment effect rather that local tumour effect. However, although other phenotypic differences in CHL microenvironmental T_H populations point to their being a distinct population. Overall there is no convincing evidence of the CHL microenvironment being T_H1-suppressed, or consensus to suggest that it is T_H1 dominated although IHC data suggests a strong presence. The variability among findings by flow cytometry may be explained by sample size and heterogeneity. It is assumed from other contexts that their role is anti-tumour, although functional data to demonstrate this is lacking.

T_H17

T_H17 cells are infrequent but evidence points to them playing important roles, including data implicating the in autoimmune disease, being long-lived, exhibiting phenotypic plasticity and possessing stem-like properties.[181]

The role of T_H17 cells in CHL is poorly defined. A study examining gene expression in CHL-infiltrating lymphocytes HLIL found increased IL17 mRNA in both $CD26^-$ putative T_{Reg} and $CD26^+$ T cells.[226] A small study measured CD161+ (a marker of IL17-producing cells) in relapsed CHL pre and post Brentuximab with donor lymphocyte infusion and noted a low CD161+ count which recovered post treatment.[257] A recent study noted IL17 staining in 40% of cases within the CHL microenvironment.[258] Finally, a small study defining T_H17 as CD4+/IL17+ by flow cytometry did not detect a significant difference in T_H17 number to healthy controls in peripheral blood.[259] There is currently little published data assessing T_H17 number by IHC in CHL. IHC studies assessing T_H17 in the literature have done so by enumerating cells positive for IL17A, an effector cytokine for T_H17 cells, or by quantifying cells positive for RORγT.[260] RORγT is a master transcription factor for T_H17 cells which is critical to the expression of T_H17 effector cytokines.[261–263] RORγT expression is also seen in other IL17A-expressing cells including type 3 innate lymphoid cells, some NKT cells and $_{\gamma\delta}$T cells.[264]

T_H17 differentiation is closely related to T_{Reg} development and cells undergo a common development pathway before skewing towards a tolerogenic T_{Reg} or inflammatory T_H17 phenotype. In some senses the CHL microenvironment might be expected to be conducive to T_H17 differentiation. CHL cells secrete CCL20, which promotes chemotaxis of $CCR6^+$ cells, a marker that is strongly expressed by T_H17.[258] CHL also secrete IL6, TGFβ, IL21, soluble CD30 and PGE2, all of which are reportedly conducive to T_H17 differentiation.[199,226,258] However, all of these factors have concurrent alternative effects: TGFβ and CCL20 also attract and promote T_{Reg} differentiation which are prominent in CHL suggesting potential T_H17 cells may be diverted down a different pathway. PGE2 is associated with a broad range of effects on the T cell compartment, including the suppression of IL10 production which is highly expressed in CHL, suggesting its effects may be outweighed by other factors.[226,265,266] Multiple factors are also secreted that are reported to skewing T_H17 differentiation towards T_{Reg}. These include expression or secretion of Galectin 1, EBI3 and PDL1 by CHL cells and expression of PDL1 and IDO1 in the microenvironment.[140,157,166,208,230,238,267–273]. Additionally, in the presence of viral RNA (such as EBERs produced in EBV^+CHL) RIG1 skews from T_{Reg} to T_H17 and *DDX58* polymorphisms associated with increased RIG1 expression are seen at reduced frequency in patients with EBV^+CHL.[274–277] Of note, in HIV infection (which is associated with CHL

lymphomagenesis) a similar pattern T_H17/T_{Reg} dysregulation is seen to that observed in CHL and IDO1 and PDL1 expression is upregulated.[278–280] Overall there is limited data examining the role of T_H17 in CHL but multiple factors secreted by CHL cells suggest skewing of the T_H17/T_{Reg} axis.

Figure 1.4: Differentiation of TH subsets in CHL

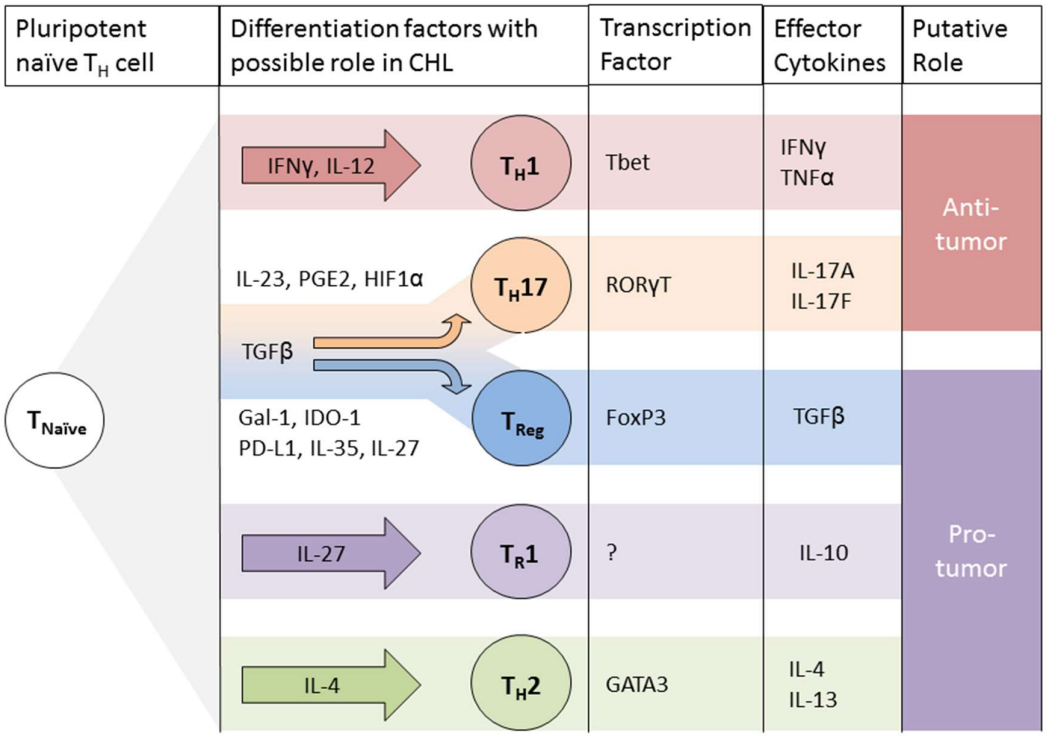

Figure 1.4: Naïve T_H recruited to the CHL microenvironment may be skewed to different T_H effector phenotypes with anti- and pro-tumour roles. Despite apparently opposing roles T_H17 and FOXP3$^+$ T_{Reg} share a common differentiation pathway and microenvironmental factors may push cells between regulatory and inflammatory effector phenotypes.

1.4: Summary and Hypothesis

Multiple factors including HLA associations, epidemiological patterns, CHL lymphomagenesis in T cell-specific immunodeficiency, T cell recruitment, CHL-T interactions, MHC expression patterns and prognostic power of T cell subsets suggest an important role for T cells, and particularly T_H cells in CHL biology. Furthermore, the activity of PD1 inhibitors highlights he

value of T cells as a therapeutic target. Additionally, the prognostic power and recruitment of macrophages and PDL1 expression emphasises the importance of the myeloid compartment.

Currently, the major goals in CHL treatment are to improve responses in relapsed or refractory disease and reduce toxicity of front line treatments. The encouraging responses seen with novel immunotherapies such as PD1 inhibitors have led to excitement in the field, but many questions remain; responses may not be durable, we cannot accurately predict who will respond and there is limited experimental evidence of cell exhaustion (the population that PD1 inhibitors are thought to act on) raising questions as to their mechanism of action. PD1 inhibitors therefore represent an advance in therapy for CHL but not a solution. Answering these questions should improve our understanding of CHL biology, help identify likely responders in advance and improve the next generation of immunotherapy.

Specific conclusions regarding CHL biology from the literature to date include:

- CHL develops from a post-GCB cell that retains a GC-associated viral transcription profile (in EBV^+ disease) but has lost expression of B cell hallmarks including the BCR.
- EBV^+CHL is associated with HLA I polymorphisms and cells frequently lose MHC II but retain MHC I. Conversely EBV negative CHL is associated with HLA II polymorphisms and cells frequently lose MHC I but retain MHC II.
- T cell-specific immunodeficiencies predispose to CHL and CHL cells recruit T_H.
- The CHL microenvironment is enriched for effector T_H including T_{Reg}, T_H1 and T_H2 and PDL1-expressing macrophages but there is little evidence of PD1 expression and this does not correlate to PDL1.
- CHL cells may retain a need for T_H support but evidence for this population is scant.
- Predictors of PD1 inhibitor response in CHL to date include PDL1 and CHL MHC II expression but not PD1.

The difficulty in establishing a representative *in vitro* or murine model makes it difficult to move past observational findings in CHL.

1.4.1: Hypothesis

T cells play an important role in the biology of CHL with evidence of both T_C and T_H evasion and represent an important therapeutic target. The balance of T_H phenotypes reflects both the effectiveness of CHL T_H manipulation towards a tolerant phenotype and the effectiveness of

the anti-tumour response. The CHL T_H microenvironment is not exhausted, despite a PDL1^{hi} myeloid environment, suggesting that PD1 inhibitors may act by an alternative mechanism. The predictive power of CHL MHC II expression suggests that CHL manipulation of T_H is central to this.

Chapter 2: Materials and Methods

2.1: Human Samples and Cell Lines

2.1.1: Ethics statement

Human tissue was accessed as part of a study approved by the local Regional Ethics Committee (REC ref: 05/Q0605/140). Single cell suspensions were obtained via the Barts Tissue Bank and were obtained with informed consent. Healthy donor PBMCs were separated from leukocyte cones produced as a by-product of apheresis during platelet donation. Cones were obtained in anonymised form through National Health Service Blood and Transplant with informed consent. FFPE tissues were accessed from the Royal London Hospital diagnostic archive under the terms of the Human Tissue Act 2008. Follow-up data was obtained from Barts Haematology Clinical Database.

2.1.2: Formalin-fixed Paraffin-Embedded Tissues

Patients were identified by cross-referenced searches of the Barts Haematology Clinical Database and the Barts pathology database. Inclusion criteria were age >18, lymph node or mediastinal biopsy site, adequate biopsy size and availability of clinical data for confirmation that represented pre-treatment presentation samples.

CHL cohorts appearing on TMAs:

- Cohort 1: 169 patients (80 ABVD treated) – Arrayed 2008
- Cohort 2 ABVD treated: 151 patients (including 80 from Cohort 1) – Arrayed 2016
- Cohort 3 HIV^{+}CHL: 17 patients – Arrayed 2015
- Cohort 4 Paired Presentation-Relapse: 35 patients – Arrayed 2015

2.1.3: Frozen Single Cell Suspensions

15 CHL samples were chosen to overlap with the TMA cohort for cross comparison. Samples included 12 NS-CHL (3 EBV^{+}) and 3 MC-CHL (all EBV^{+}). 5 RLN samples were selected at random.

2.1.4: Cell Lines

KMH2 (DSMZ Cat# ACC-8, RRID: CVCL_1330) and L428 (DSMZ Cat# ACC-197, RRID: CVCL_1361) CHL cell lines were used in this study. KMH2 and L428, like most CHL cell lines, were derived from pleural effusions. Both lines were obtained directly from the supplier.

DSMZ reported cell line characteristics:

- KMH2: HLA type A*24:02; B*15:01,52:01; C*04:01,12:02; DPB1*02:01,05:01; DQA1*03:01,05:05; DQB1*03:01,03:02; DRB1*04:65,11:01; DRB3*02:02; DRB4*01:03 (IMGT/HLA; 15116). Microsatellite instability: Stable (MSS) (Sanger).
- L428: Microsatellite instability: Instable (MSI-low) (Sanger)

2.2: Immunohistochemistry

2.2.1: Contribution acknowledgements

Classical IHC staining and stripping protocols and were developed and optimised by A Clear. Progressive Multiplexing protocol was developed by J Taylor with A Clear. Stripping validation protocol was developed with A Clear, J Taylor and J Ball. Some staining was performed by M Caporale and M Poynton under supervision of J Taylor. Older TMAs were arrayed by A Clear and A Owen. Newer TMAs (HDA, HDB, HDC, HDC2, HDD, HDD2, HDE, 1cV2) were arrayed by J Taylor.

2.2.2: Staining method for Classical Immunohistochemistry

Three micrometre sections of FFPE tissue were cut and placed overnight in a 60°C oven. Slides were moved through two changes of de-waxing xylene and one change of industrial methylated spirits (IMS) with two minute incubations followed by two five minute incubations in IMS with 2% H_2O_2 and a final incubation of two minutes in IMS before transferring to running tap water. All antibodies used demonstrated good signal with heat induced epitope retrieval using a pressure cooker. Slides were incubated for ten minutes at full pressure in Citric Acid based antigen unmasking solution before returning to running tap water. Slides were washed with tris-buffered saline with tween, marked with a hydrophobic barrier pen and incubated for forty minutes at room temperature in primary antibody at the optimised dilution in antibody diluent. Detection was performed using the SuperSensitive™ Polymer-HRP Kit as

per manufacturer instructions (twenty-minute incubation with super-enhancer and thirty-minute incubation with SS-label separated by tris-buffered saline with tween washes). Signal was then detected by applying either DAB or VIP substrates for 10 minutes. Slides were transferred to running water before regressive haematoxylin counterstaining (five minutes in Gill's II followed by five rapid dips in acid alcohol), bluing with Scott's Solution for three minutes, dehydration with three changes of IMS, clearing with three changes of xylene, all with two minute incubations, and mounting in DPX. Once dried slides were scanned using a digital slide scanner (Pannoramic 250 Flash, 3DHISTECH). Staining was performed in batches using the DAKO Autostainer.

Table 2.1: Reagents

REAGENT	MANUFACTURER	ITEM CODE	DILUTION
ANTIGEN UNMASKING SOLUTION	Vector	H3300	1:100
ANTIBODY DILUENT	Zytomed	ZUC025-500	1:1
SUPERSENSITIVE™ POLYMER-HRP	Biogenex	QD440-XAKE	neat
DAB SUBSTRATE	Biogenex	QD440-XAKE	As per kit
VIP PEROXIDASE (HRP)	Vector	SK-4600	As per kit
HAEMOTOXYLIN SOLUTION GILL II	Sigma	GH216	
SCOTT'S SOLUTION	Sigma	S5134-6X	1:10
DPX MOUNTANT	Sigma	06522	neat

2.2.3: IHC Antibodies

Application-specific validation is essential as data suggests under half of commercially available research-grade antibodies pass quality assurance and specificity tests.[281–283] Antibodies give non-specific signal for a reasons including epitope cross-reactivity, batch variability and differences between applications.[284] This is particularly true in FFPE tissue where fixation-induced crosslinking affects antibody binding. This leads to wasting of charitable resources, unnecessary sacrificing of animals and unreproducible misleading data.[285] Of note, legal responsibility for proof of specificity for research antibodies lies with the purchaser not the vendor and there is no responsibility to inform other purchasers or publishing journals of an identified issue.[284] The periodic replacement with improved clones makes it impossible to

validate published data with the same experimental conditions. Published data using clones that are no longer commercially available should therefore be treated with caution.

Direct confirmation of antibody specificity requires either knockdown, orthogonal comparison to an antibody-independent method, comparison to an independent antibody to a different epitope on the same target, concurrent use of tagged proteins or confirmation with immunocapture.[286,287] In practice this is rarely performed. More frequently reported isotype, omission and absorption controls are of little value as they do not demonstrate specificity or accurately estimate background.[288,289] Histochemical Society validation recommendations include a western blot of target in a cellular lysate, positive and negative anatomical controls and the use of a genetically confirmed knockdown and positive control.[288]

Of note, confirmation of specificity should be a requirement for IHC, but alone it is insufficient as proper optimisation is also essential for reliable data. Most antibodies will see increasing background if concentrations are sufficiently high and loss of signal if concentrations are too low. This is problematic where antibodies are reactive to secreted proteins as separation of background from true signal is hard. Superior optimisation can be achieved with stripping/phenotyping methods where marker titrations can be plotted against biological positive and negative controls assess sensitivity and background.

Antibodies were appraised by comparison to published or manufacturer validation data. Orthogonal comparison to RNA data is performed by the Human Protein Atlas project and cell line knockdown is performed during validation by Cell Signaling Technology.[283] Staining was compared to anatomical positive and negative controls noting appearance and subcellular location. For extended validation, stripping experiments confirmed co-expression of lineage markers. Optimisation was performed by comparing serial dilutions. Antibody optimisation and validation is reported in Table 2.2.

Table 2.2: Validated IHC Antibodies

TARGET	CLONE	VENDOR	CODE	DILUTION	VALIDATION		STRIP
CD68	KP1	Dako	GA609	1:8000	D iA T+	✓✓	✓
CD3	LN10	TFS		1:500	D iA T+	✓✓	✓
CD4	4B12	Leica	368-L-CE	1:500	D iA T+	✓✓	✓
CD8	C8/144B	Dako	M7103	1:400	D iA T+	✓✓	×
CD15	LeuM1	BD		1:50	T+	✓	×
CD30	BerH2	Dako	M0751	1:200	D iA T+	✓✓	✓

CD40	11E9	Leica	NCL-CD40	1:50	T+ O*	✓✓	?
CD154	R poly	Atlas	HPA045827	1:500	T O*	✓✓	?
CD161	R poly	Atlas	HPA039113	1:75	T+ O	✓	?
CD163	10D6	Leica	NCLLCD136	1:250	D W*	✓✓	?
EOMES	R poly	Atlas	HPA028896	1:200	T+ (O)	(✓)	✓
EBI3	R poly	Atlas	HPA046635	1:200	T+ O* ~~iA~~	✓	✓
EBI3	15k8D10	Novus	NBP227362	1:100	(T) ~~iA~~	(×)	?
EBI3	42N12F7	Novus	discontinued	1:100	T ~~iA~~	(?)	?
FOXP3	263A/E7	Abcam	ab20034	1:500	T+	✓	✓
GATA3	D13C9	CST	5852	1:50	T+ K* W*	✓✓	?
IDO1	R poly	Atlas	HPA023149	1:250	T O* W*	✓	?
IL12A	R poly	Atlas	HPA001886	1:350	(T) W*	×	?
IL12B	R poly	Atlas	HPA040970	1:100	T (O)	(✓)	?
IL23A	R poly	Atlas	HPA001554	1:500	T (O) W*	(✓)	?
IL27A	R poly	Abcam	ab118910	1:500	T	(✓)	?
IRF4	MUM1p	Dako	GA644	1:400	T+ W*	✓	×
LAG3	R poly	Atlas	HPA013967	1:200	T+ O*	✓✓	✓
LMP1	CS.1-4	Dako	M0897	1:12000	D T+	✓✓	×
MHC II	CR3/43	Dako	M0775	1:500	D, T+	✓✓	✓
PD1	NAT105	Abcam	ab52587	1:25-50	D iA T+	✓✓	✓
PD1	EH33	CST	43248	1:50	K* iA T+	✓✓	✓
PD1	D4W2J	CST	86163	1:50	K* iA T+	✓✓	✓
PDL1	E1L3N	CST	13684	1:200	K* iA T+	✓✓	✓
PDL1	SP142	Spring B	M4420	1:200	iA T	✓✓	?
TBET	4B10	SC	sc21749	1:500	T+ O*	✓	✓
TIM3	G poly	R&D	AF2365	1:200	T+ O*	✓	✓
RORγT	6F3.1	Merck	MABF81	1:1000	T+	✓	✓

Table Key:

Validation = Validation methods used. Abbreviations: K = Cell line knockdown, iA = Independent antibody, T = Positive and negative tissue control, T+ = Tissue controls and coexpression, W = Western to lysate, O = Orthogonal comparison, * = literature/by manufacturer, D = Diagnostic use, T = passed T, (T) = uncertain T, ~~T~~ = failed T, × = failed validation, ? = unable to assess, (✓) = passed, limited data or concern in one validation domain, ✓ = passed, ✓✓ = passed with high confidence in specificity

Strip = passed stripping validation (see section 2.2.6). × = fail, ? = unassessed, ✓ = passed

Other abbreviations: R = rabbit, G = goat, poly = polyclonal CST = Cell Signaling Technology, TFS = Thermo-fisher Scientific, SC = Santa Cruz, R&D = R&D systems

2.2.4: Tissue Microarrays

Sample selection for TMAs is discussed in 2.1.2. Eligible biopsies were reviewed by a Consultant Histopathologist (Prof Maria Calaminici) and CHL-involved areas were marked. 1mm cores were arrayed in triplicate. Patients were assigned to TMA blocks randomly. A single RLN control was included across all TMAs to allow assessment for batch effect. TMAs were validated by CD30 immunostaining to confirm the presence of CHL cells.

Figure 2.1: Tissue Microarraying

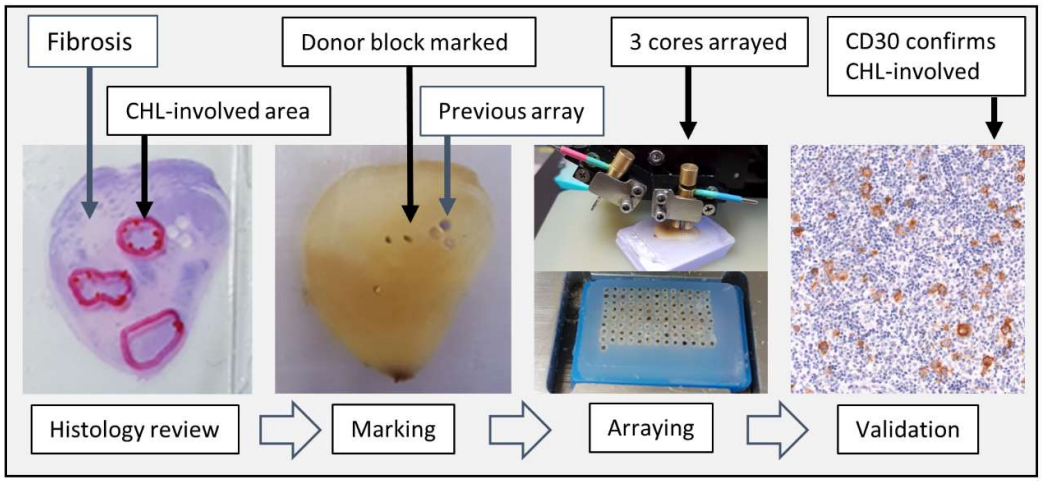

Figure 2.1: Lymphoma-involved areas of eligible blocks are marked. Fragmented blocks, thin blocks and core biopsies are rejected due to insufficient tissue depth for array. Haematoxylin and Eosin stained sections are reviewed and CHL-involved areas identified. Donor blocks are marked and cores are taken. Cores are inserted into the recipient block in triplicate to ensure representative sampling and allow for core drop-out during cutting of the TMA. Immunostaining of the cut TMA for lymphoma markers ensures lymphoma-involved areas are sampled.

2.2.5: Technical considerations

2.2.5.1: Sampling, TMA design and batch effects

TMAs were validated for effects of technical variables and batch effects and study design was adapted to minimise these. The consequences of batch effect and TMA burnout may dramatically affect results (section 3.1.1). Non-biological effects that might affect IHC staining quality include:

i. Fixation time
ii. Block storage
iii. Sample age
iv. TMA burnout
v. TMA section age[290]
vi. Batch effect

Effects of fixation time within the cohort could not be assessed but is likely to be randomly distributed across biopsies. Block storage conditions were uniform. H-score (encompassing area stained and stain intensity) was calculated for EBI3 staining (a CHL marker).[291] Sections were freshly cut. Effect of biopsy age was assessed by comparison within individual TMAs to control for batch effect. No relationship between EBI3 H-score and biopsy age was detected. TMA burnout was assessed by comparing matched biopsies appearing on TMAs arrayed in 2008, 2010 and 2016. A significant effect was detected with loss of signal proportional to TMA age ($p<0.0001$, Figure 2.2). Additionally, when assessing background intensity of CD154 staining performed by hand significant batch effect by TMA was detected. (Figure 2.3).

TMAs have been validated as a robust method of sampling tumours to study large patient numbers.[292] However, validations were performed in breast cancer which may have more uniform tissue involvement. CHL TMAs are susceptible to burnout due to variable node involvement and rare tumour cells and cellularity loss due to fibrosis. With CHL TMAs this creates a risk that with serial sectioning you will move out of the validated tumour area into an area less representative of the tumour. This effect might also be explained by TMA cores degrading within the TMA block. Overall cellularity within paired biopsies did not change with older TMAs, excluding the possibility that the effect was due to over-representation of fibrosis on multiply sectioned TMAs.

These effects could bias results in studies where samples are not randomly distributed across TMAs, which is often the case with ad hoc retrospective analyses. It highlights the need for revalidation of older TMAs, particularly in conditions were involvement is patchy. To minimise batch effects all staining was performed as single batches using an automated stainer. When

designing the 2016 TMAs matched control biopsies were included across all arrays to allow cross-comparison. Samples were randomly allocated across TMAs and all data was reported from patient cohorts represented on TMAs created within the same year.

To further characterise this effect samples should be reanalysed, assessing area stained and stain intensity separately as this would allow us to separate the effects of TMA burnout due to repeated sectioning (leading to loss of area stained but not intensity) from TMA degradation (leading loss of intensity alone).

Figure 2.2: TMA Burnout

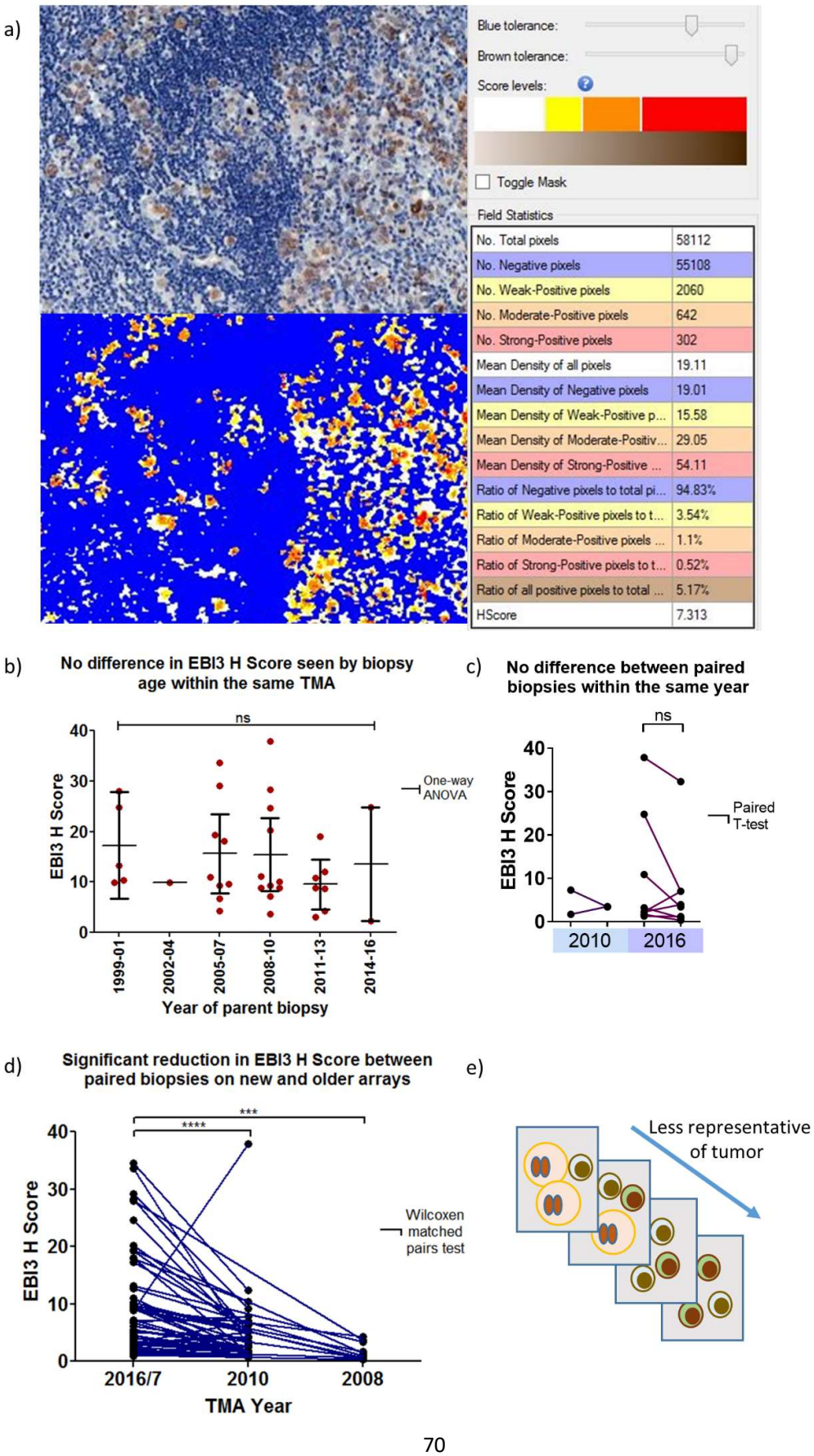

Figure 2.2: a) Sample case of EBI3 staining by IHC marking CHL cells and paired mask of negative, weak, moderate and strong pixels alongside H score calculation (which accounts for both stained area and intensity) within the Pannoramic Viewer software. b) Comparisons between unpaired samples by IHC on a single TMA by year of donor block (i.e. diagnosis). c) Comparison between paired samples appearing on different TMAs made in the same year. Compared by paired t-test. d) Comparison between paired samples arrayed in different years demonstrating a loss of signal in older TMAs. Compared by Wilcoxon paired rank test. e) Graphical illustration of TMA burnout - TMAs may initially reflect CHL-rich areas but because of patchy infiltration CHL content decreases with repeated sectioning.

Figure 2.3: TMAs and batch effects

a) Analysis by histological subtype suggests differences by HIV status

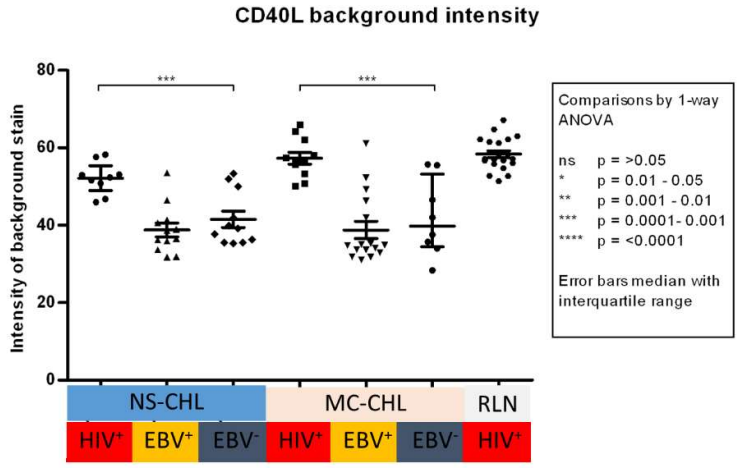

b) Analysis by TMA suggests confounding by TMA batch effect

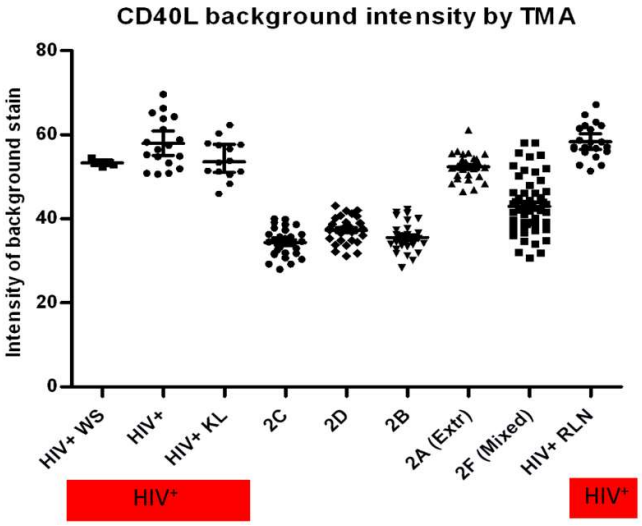

Figure 2.3: a) IHC analysis of CD40L background intensity by disease subtype suggests a difference by HIV status. b) Reanalysis by TMA (for batch shows clear effect by TMA. HIV-WS (HIV whole sections), HIV, HIV-RLN and HIV-KS TMAs batch all HIV$^+$ cases together creating confounding. Similarly, 2A TMA includes only cases at the extremes of CHL survival and shows a different pattern to 2B, 2C, 2D and 2F which were randomly arrayed. 2F contains some HIV$^+$ cases. This data may represent a genuine biological difference but it is hard to be confident due to batch effect.

2.2.6: Progressive Multiplex Immunohistochemistry

Slides were stained with DAB chromogen as per classical staining method (section 2.2.1). After scanning slides were placed in xylene for coverslip removal. Depending upon the period the coverslip has been in place this can take hours-days. The classical staining protocol was repeated unaltered including antigen retrieval step but VIP was substituted for DAB. VIP chromogen was reconstituted as per manufacturer instruction (Table 2.2.1) and incubated for 10 minutes. VIP stains were added to previously stained sections upwards of six months after the initial DAB stain with good results.

DAB is heat stable and not removed by repeated heat induced epitope retrieval.[293] This method has advantages over protocols incorporating staining of both antibodies within a single run. The progressive addition of stains enables imaging of the counterstain only, DAB only and dual stain, which assists colour deconvolution during analysis. Staining clarity with progressively stained DAB/VIP was superior to other multiplex combinations tested (Vector Slate Grey/Vector AEC) and had less background when compared to DAB/VIP applied during a single run, likely due to additional wash steps. Of note, it is preferable to use VIP for markers where intensity readings are required due to the non-linear relationship between DAB staining and light absorbance.[294]

2.2.7: Antibody stripping and reprobing

Slides were stained using the same protocol as for progressive multiplex IHC, but VIP chromogen was selected for stains that were subsequently removed.

The majority of IHC antibodies tested proved suitable for stripping. However, rarely antibodies fail to strip leading to the detection of residual signal. Antibodies that fail to strip were placed at the end of a stripping panel to avoid false signal in future staining rounds. Validation for stripping was performed by staining using the above protocol before repeating the complete protocol including amplification and detection steps but omitting the addition of primary antibody and counterstain. Successful stripping was confirmed by the absence of residual signal (Figure 2.4). In antibodies with residual signal successful stripping was achieved with the addition of pronase for 1 minute, however further validation is required to ensure this does not compromise further antibody staining. A tonsil stripping control and concurrently performing single stain tonsil controls were included to assess signal loss due to the stripping process (Figure 2.5).

Figure 2.4: Antibody stripping validation

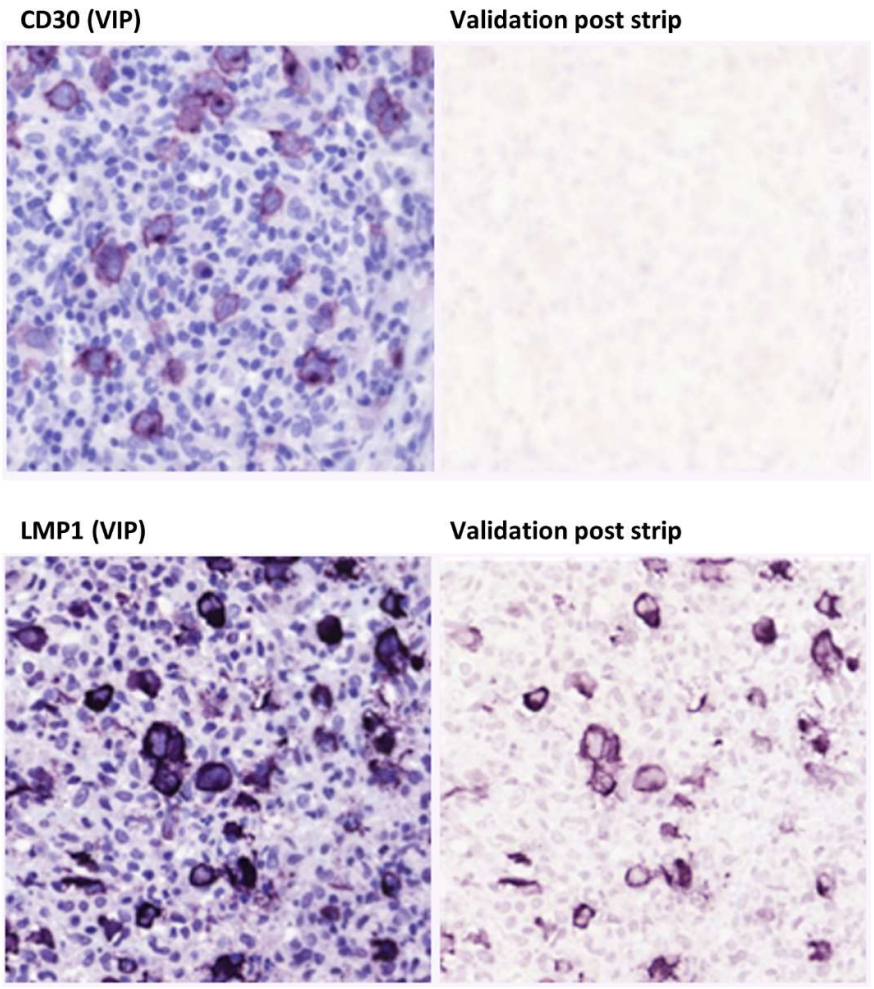

Figure 2.4: Stripping of IHC stain of CD30 and subsequent detection for residual antibody demonstrates complete antibody removal validating it for use in stripping experiments. Stripping of IHC stain of LMP1 and subsequent detection shows residual staining demonstrating that the antibody has not been removed by the stripping process so should not be used for stripping experiments or should be placed at the end of a stripping panel.

Figure 2.5: Antibody stripping signal validation

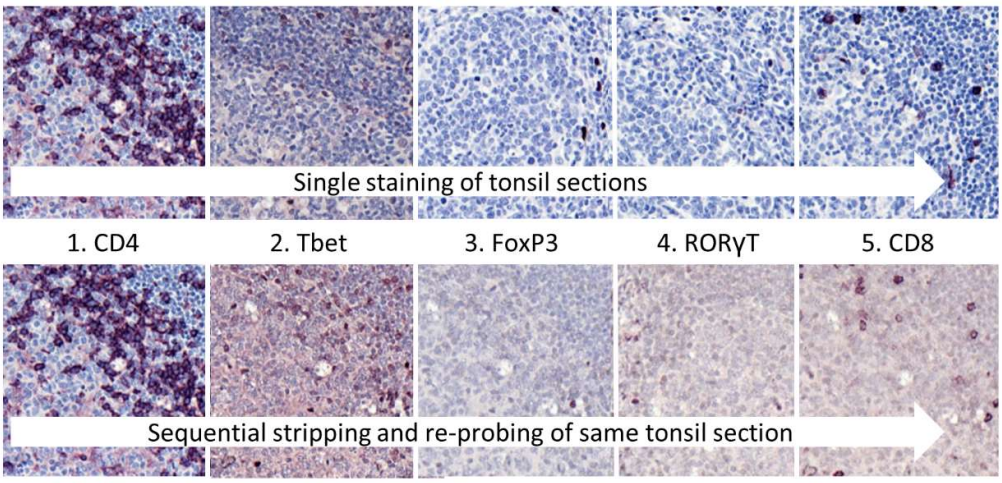

Figure 2.5: Comparison of serially IHC stained and stripped tonsil to sections of the same tonsil stained with a single marker by conventional IHC and not subjected to the stripping process. Demonstrates some signal loss in FOXP3, RORγT and CD8 which are placed later in the stripping panel, although not sufficient to limit detection, and some increase in background in RORγT and CD8. This should inform panel design with highly expressed of phenotyping antibodies being placed later in the panel.

This method builds on published stripping techniques but the use of VIP chromogen over AEC improves sensitivity and permits non-aqueous mounting giving brighter and more durable signal.[295,296] VIP is not heat stable and heat induced epitope retrieval removes the chromogen and denatures bound antibody. Denaturing has the additional advantage that same-species interaction is not a concern, so consecutive antibodies of the same species can be used and the detection method does not need to be varied.[297] Stripping panels of up to six round of heat induced epitope retrieval were performed with good results however some loss of staining intensity was seen with gradual increase in background.

2.2.8: Proximal ligation assay

IHC antibodies derived from different host species (one mouse, one rabbit) were selected to target individual halves of heterodimeric cytokines and revalidated for 12 hour staining at +4. Assay performed as per manufacturer instructions with following modifications: Antibodies were used at 30-50% higher concentrations than validated concentrations for IHC with Biogenix kit. Wash steps were performed in large volume on rocker. Manufacturer

recommends biological positive and negative controls plus omission of one antibody as technical negative control. Addition of second technical negative control: replacement of one antibody with another target expressed in the tissue but proximal ligation not expected (e.g. to detect IL27 requires IL27A (α subunit, rabbit) and EBI3 (β subunit, mouse) – for control replace IL27A with CCL5 (also CHL-secreted and rabbit host)). Kit: Duolink In Situ (Brightfield reagents, DPX mountant), Sigma-Aldrich, anti-Rabbit MINUS, DUO92005 and anti-Mouse PLUS, DUO92001 probes.

1 x 1cm TMA of recent (<10 year) biopsy specimens was arrayed, including positive (placenta), and negative (heart) control tissue to minimise reagent use. Fresh sections were cut and circled with hydrophobic barrier pen. 40 µL of Hydrogen Peroxide Solution was applied and incubated at room temperature for 5 minutes followed by two washes in wash buffer A, blocking for 60 minutes (double reagent volume due to drying) and heat induced epitope retrieval. Primary antibodies incubated overnight at 4°C. Subsequent incubations were performed at 37°C in a humidity chamber and separated by wash steps. Note: increased reagent added for amplification step due to drying. Samples were incubated in ligation-ligase solution for 30 minutes then amplification-polymerase solution for 120 minutes. Brightfield detection solution was then applied for 60 minutes at room temperature followed by substrate solution for 10 minutes. Slides were then progressively counterstained with haematoxylin, before taking through deionized water, ethanol and xylene and mounting in DPX.

Table 2.3: Re-validated IHC antibodies for proximal ligation assay

TARGET	CLONE	HOST	VENDOR	CODE	DILUTION	VALIDATION	
CCL5	poly	Rabbit	Abcam	ab9679	1:650	T	(✓)
EBI3	15k8D10	Mouse	Novus	NBP227362	1:75	(T) ~~iA~~	(×)
EBI3	42N12F7	Mouse	Novus	discontinued	1:50	T ~~iA~~	(?)
IL12A	poly	Rabbit	Atlas	HPA001886	1:50	(T) W*	×
IL23A	poly	Rabbit	Atlas	HPA001554	1:500	T (O) W*	(✓)
IL27A	poly	Rabbit	Abcam	ab118910	1:350	T	(✓)

2.3: Flow Cytometry

2.3.1: Antibody optimisation

Antibodies were validated by assessment of marker co-expression with biological positive and negative controls. Transcription factors were validated by co-expression of lineage-defining cytokines. RORγT failed validation due to high background compared against Fluorescence minus one control with no distinct positive population after multiple validation runs. RORγT was not co-expressed with CD161 and IL17A. CD161 and CD73 required further validation as they showed clear positive populations but CD161 did not co-express with IL17A and unlike IL17A did not enrich in PBMCs stimulated with CD3/CD28/IL6/IL1β. CD73 did not enrich in $CD25^{hi}CD127^{lo}FoxP3^{+}$ T_{Reg} as reported in the literature.[298]

Table 2.4: Optimised antibody list for flow cytometry

ANTIGEN	VENDOR	FLUORO	CAT #	CLONE	DIL/TEST	VALID.
DAPI	BD Bio	*live/dead*	564907	-	1:2000	✓
CFSE	Thermo	*proliferation*	C34554	-		✓
CD3	Biolegend	BV421	300434	UCHT1	2.5 µl	✓
CD3	BD Bio	FITC	561806	UCHT1	2.5 µl	✓
CD3	Biolegend	PercP-Cy5.5	300430	UCHT1	2.5 µl	✓
CD4	Biolegend	APC-Fire 750	344638	SK3	2.5 µl	✓
CD4	Biolegend	APC-Cy7	300518	RPA-T4	1 µl	✓
CD4	Biolegend	PE-Cy7	317414	OKT4	1 µl	✓
CD25	Thermo	APC-efl780	47-0251-82	CD25-4E3	1µl	✓
CD73	eBioscience	PerCP-efl710	46-0739-42	AD2	1 µl	?
CD127	Biolegend	FITC	351312	A019D5	1µl	✓
CD161	Biolegend	PE-Cy7	339917	HP-3G10	1µl	?
CD183	BD	PE-Cy5	551128	1C6/CXCR3	2µl	✓
CD194	Biolegend	BV604	359418	L291H4	1µl	✓
CCR10	BD	PercP-Cy5.5	564772	1B5	1µl	✓
FOXP3	Biolegend	PE-Daz 594	320126	206D	5µl	✓
IFNγ	eBioscience	APC	17-7319-41	4S.B3	2.5µl	✓
IL2	BD Bio	PE	554566	MQ1-17H12	2.5µl	✓
IL17A	eBioscience	PE	12-7178-42	64CAP17		✓
KI67	Biolegend	BV711	350516	Ki-67	2.5µl	✓
PD1	BD Bio	BB515	564494	EH12.1	2.5µl	✓

PD1	eBioscience	PE	12-2799-42	eBioJ105	2.5µl	✓
RORγT	BD Bio	BV421	563282	Q21-559	5µl	✗
TBET	BD Bio	BV711	563320	O4-46	5µl	✓
ZY	Biolegend	*live/dead*	423104	-	1:1000	✓

Table 2.5: Reagents

REAGENT	DETAILS
ACRIDINE ORANGE/PROPIDIUM IODIDE	Logosbio (cat. F23001)
BD BRILLIANT STAIN BUFFER	BD Bio (cat. 563794), 50ul/test
CELL STIMULATION COCKTAIL	eBioscience (cat. 00-4970-93), 1:500
COMPENSATION BEADS	UltraComp eBeads (cat. 01-2222-41), 1 drop/test
DNASE	Sigma (cat. D4263)
FACS BUFFER	PBS with 1% FBS
FETAL BOVINE SERUM (FBS)	Gibco
IC FIX & PERM BUFFER SET	eBioscience (cat. 88-8824-00)
PENICILLIN STREPTOMYCIN (P/S)	Sigma
PHOSPHATE BUFFERED SALINE (PBS)	Sigma
PROTEIN TRANSPORT INHIBITORS	eBioscience (cat. 00-4980-03), 1:500
RPMI 1640	Complete = with 10% FBS, 1% P/S. Gibco
TRANSCRIPTION FACTOR BUFFER SET	BD Bioscience (cat. 562574)
TRYPAN BLUE	Logosbio (cat. T13001)

Table 2.6: Functional Antibodies

ANTIGEN	VENDOR	FLUORO	CAT #	CLONE	DIL/TEST	PASS
CD28	Biolegend	*functional*	302934	CD28.2	1 µg/ml	1 µg/ml
CD3	Biolegend	*functional*	300438	UCHT1	10 µg/ml	10 µg/ml

Unless stated otherwise wash steps were performed by centrifugation at 300g for 5 minutes. Media was poured off or if using 96 well plates removed by a single inversion of the plate.

2.3.2: Cell resuscitation

Vials were transferred from liquid nitrogen storage on dry ice until resuscitation. All reagents were warmed to 37°C prior to defrosting. PBMC vials were briefly thawed in waterbath until pellet started to defrost. 1ml FBS was added dropwise to the cryovial and cells were transferred to 15ml falcons containing 8ml of RPMI media supplemented with 5% FBS and 1% penicillin-streptomycin. The cryovial was rinsed with media to maximise cell retrieval. Cells were washed twice with RPMI.

For SCS 1mg/ml DNAse reconstituted in PBS and 0.5ml was added to 9.5ml complete RPMI to make a 0.1mg/ml solution. Cryovials were briefly thawed in waterbath until pellet started to defrost before 0.1mg/ml DNAse RPMI solution was added dropwise to the vial and transferred to a falcon containing the DNAse RPMI solution. Cells were washed twice with complete RPMI by centrifugation at 300g for 5 minutes. After the second wash 0.5ml of 1mg/ml DNAse in PBS was added to the cell pellet and it was resuspended in a further 1ml of complete RPMI. Cells were passed once through a 40μm cell strainer and washed once more in RPMI before proceeding to counting. All counting was performed using a Luna fluorescent cell counter using Acridine Orange/Propidium Iodide stain to mark live and dead stain unless cells were marked with CFSE when brightfield counting was used with Trypan blue due to CFSE fluorescence.

2.3.3: Surface staining Protocol

Fluorescence minus one controls were included for all experiments and compensation was performed for each acquisition with the flow cytometer. Cells were transferred to 96 well v-bottom plates and washed once with FACS buffer. Master mix staining cocktails of antibodies were created to minimise batch effect. 50μl per test of Brilliant Stain Buffer was used when two or more Brilliant Violet™ or Brilliant Blue™ antibodies were added to the same staining cocktail. Master mixes were prepared a maximum of 24 hours in advance. After the wash cells were resuspended with surface master mixes in the residual FACS buffer and incubated for twenty minutes in the dark at room temperature. Cells were then washed twice in FACS buffer before resuspending in 200μl of FACS buffer with DAPI for live-dead discrimination and transferred to FACS microtubes for acquisition.

2.3.4: Intracellular staining Protocol – Cytokines

Surface staining was completed as per 2.3.3 with minor modification. Prior to surface staining cells were washed twice with PBS (without FBS). Cells were stained in 100 μl of 1:1000 Zombie Yellow diluted in PBS. Live/dead staining was usually included in the surface antibody master mix unless brilliant stain buffer was used. If brilliant stain buffer was included or if efluor 780 viability dye was used live/dead staining was performed for 15 minutes at room temperature prior to surface antibody staining. DAPI was omitted. After surface staining cells were fixed for 40 minutes at room temperature with 200 μl 1x IC fix buffer (IC Fixation & permeabilization kit). Cells were then washed twice with 1x Perm wash buffer with 600g centrifugation and 5 minute incubations. Cells were resuspended in master mix staining cocktails of intracellular antibodies and incubated for 40 minutes at room temperature. After staining cells were then washed twice with 1x Perm wash buffer and 600g centrifugation before resuspension in 200 μl PBS and transferred to FACS microtubes for acquisition.

2.3.5: Intracellular staining Protocol – Transcription Factors

Intracellular staining was completed as per 2.3.5 with minor modification. After surface staining cells were fixed for 40 minutes at room temperature with 200 μl 1x Fix/Perm solution (Transcription factor buffer set). Cells were then washed once with 1x Perm/Wash buffer before incubating for 30 minutes at room temperature in Perm/Wash buffer. Cells were resuspended in master mix staining cocktails of intracellular antibodies and incubated for 40 minutes at room temperature. After staining cells were then washed twice with Perm/Wash buffer and 600g centrifugation before resuspension in 200 μl PBS and transferred to FACS microtubes for acquisition.

2.3.6: Acquisition and gating

Data were acquired on a BD LSR Fortessa flow cytometer. Voltages were optimised by using NxN plots comparing individual single stains. Compensation was performed and Fluorescence minus one controls were included at every run. Compensation was reassessed and data analysed using FlowJo software. Gating was performed in the following sequence:

- FSC-A/SSC-A (population identification) →
- Live-dead/SSC-A (dead cell discrimination) →

- FSC-A/FSC-H (doublet discrimination) →
- SSC-A/SSC-W (doublet discrimination) →
- SSC-A/CD3 (T cell) →
- SSC-A/CD4 (T_H cell)

2.3.7: CFSE staining

Cells were washed twice with PBS (without FBS). CFSE was reconstituted from stock with 18µl DMSO and diluted at 1:500 in PBS. Cells were resuspended in 500µl CFSE solution and mixed well. Mixing is essential for even staining. Cells were incubated for eight minutes in the dark at room temperature and vortexed every ninety seconds. 1.5ml (3 times volume) of cold FBS was added to quench the reaction and incubated in the dark at room temperature for three minutes. Cells were washed a further two times in complete RPMI with three minute incubations before proceeding to plating.

2.3.8: Cell stimulation for functional assays

Cell stimulation was performed in a 200 µl volume within a 96 well plate. For PMA/Ionomycin stimulation a mastermix 100 µl per well of RPMI and 0.4 µl per well of 500x PMA/Ionomycin was created. If intracellular cytokine staining was required a further 0.4 µl per well of 500x protein transport inhibitor was added. For CD3/CD28 stimulation a mastermix 100 µl per well of RPMI and 2 µl per well of 10 µg/ml CD3 (UCHT1) and 0.2 µl per well of 1 µg/ml CD28 (CD28.2) was added. For small pipetting volumes a 1:10 dilution was made. For unstimulated wells RPMI alone was added. Each well was then primed with 100 µl of RPMI/stimulation mastermix. Finally, 100 µl of 2 x 10^6/ml cells was added to each well for a final cell concentration of 1 x 10^6/ml. PMA/Ionomycin stimulation was performed with a 4-hour incubation. CD3/CD28 stimulation was performed with a 4-day incubation.

2.4: Cell Culture

2.4.1: Maintenance of Cell Lines

KMH2 and L428 cell lines were maintained in complete RPMI, KMH2 at concentrations of 0.8-1 x 10^6 per ml and L428 at 5 x 10^5 per ml with media change every 2-3 days. Cells grow in suspension but tend to cluster and precipitate in culture and grow more readily with the culture vessel placed on its side.

2.4.2: Conditioned media

Conditioned media were collected from KMH2 cells with high viability. Cells were resuspended at 1 x 10^6 per ml and cultured for 24 hours in complete RPMI. Cells were centrifuged at 1400 revolutions per minute (rpm) for 5 minutes. Supernatant was aspirated and centrifuged a second time at 1400 rpm for 5 minutes. Supernatant was aspirated and passed through a 22 μl filter before being divided into aliquots and stored at -80°C.

2.4.3: Separation of Peripheral Blood Mononuclear Cells

Cones are opened by cutting the tube running into the base at a length of 1 cm and cutting at the apex before inverting over a 50 ml falcon tube and allowing the blood to run out. Residual blood is removed from the cone by injecting air through the base tube with a 19-gauge needle and syringe then rinsing gently 2-3 times with PBS. PBS is added to the falcon to a final volume of 50 ml. 5 ml of lymphoprep (Stemcell Technologies, Cat# 07801) is added to a 15 ml falcon. The 15ml falcon is held at 45 degrees and 10 ml of blood is slowly added at a rate that maintains a clear separate layer of blood on the lymphoprep. Tubes are centrifuged at 1500 rpm for 30 minutes without braking on centrifuge deceleration. Buffy coat is aspirated with a Pasteur pipette without disturbing other layers and transferred to a 50ml falcon. The buffy coat aspirate is made up to 40ml with PBS and centrifuged at 130 rpm for 10 minutes. PBMCs are washed once more in PBS before incubation in 10ml of 1x Red Cell Lysis Buffer (Biolegend, Cat# 420301) for 5-7 minutes. Cells are washed twice more in PBS before freezing or further applications.

2.4.4: Cell Freezing

A freeze mix of 20% DMSO and 80% FBS was prepared. Cells were washed and resuspended in complete RPMI at twice the desired freeze concentration. 0.5 ml of cells and 0.5 ml of freeze

mix was added to each cryovial for a final concentration of 10% DMSO. Cells were placed in a Mr Frosty (Nalgene/Thermoi) primed with 100% isopropyl alcohol and stored at -80°C for a minimum of 24 hours before transferring to liquid nitrogen storage. Cell lines were frozen at early passage at 4 x 10^6 per vial. PBMC or $CD3^+$ or $CD14^+$ sorted PBMC fractions were stored at 30-100 x 10^6 per vial.

2.4.5: Cell separation by MACS sorting

Cells separation was performed by hand according to manufacturer protocol. CD14 selection was performed using positive selection (Miltenyi CD14 microbeads human cat. 130-050-201). Protocol was performed on ice. PBMCs were centrifuged at 300g for 10 minutes. Supernatant was aspirated before resuspending in 80 µl/10^7 cells of MACS buffer (PBS with 0.5% Bovine serum albumin and 2mM EDTA) and adding 20 µl/10^7 cells of CD14 microbeads. Cells were mixed and incubated for 15 minutes at +4°C before washing with 1-2ml MACS buffer. Cells were then centrifuged at 300g for a further 10 minutes, the supernatant was aspirated and up 10^8 cells were resuspended in 500 µl of buffer. Cells were passed through a primed LS column on a MACS column separator and washed twice with 3ml of MACS buffer before using the plunger to collect the CD14 positive fraction. T cell separation was performed using negative selection (Stemcell EasySep cat. 17555). Cells were resuspended at 5x10^7/ml in MACS buffer in a polystyrene round bottomed tube before adding 50 µl/ml isolation cocktail and incubating at room temperature for 5 minutes. RapidSpheres were then vortexed and added at 50 µl/ml before topping up to 2.5 ml with MACS buffer, incubating for 3 minutes in magnet, pouring to a fresh tube, repeating the magnet incubation step and collecting the untouched cell fraction.

2.4.6: *In vitro* differentiation of macrophages

$CD14^+$ cells were seeded at 5x10^5/ml in 6 well plates in 2ml RPMI with the addition of either MCSF 100ng/ml or MCSF 50ng/ml with GMCSF 1ng/ml. After seven days, cells were checked for morphology change and the growth of a macrophage lawn. On day 7 the supernatant was aspirated and discarded. For priming, macrophages were treated with either RPMI alone or RPMI with 50% conditioned media from CHL cell lines (KMH2) for 24 hours. After 24 hours conditioned media was removed.

2.5: Western Blotting

Western blots were performed in non-reducing conditions. Supernatants were aspirated stored at -80°C. Harvested cells were centrifuged at 1500 rpm for 10 minutes before aspiration. Cells were lysed for 20 minutes with agitation in the presence of protease and phosphatase inhibitors (Cellytic solution (Sigma, cat. C2978), protease inhibitors (Sigma, cat. P8340-1ML), phosphatase inhibitors (Sigma, cat. P5726)) before centrifuging at 13000 rpm for 15 minutes at 4°C before snap freezing on dry ice and -80°C storage. Protein concentration was determined by Bradford assay (BioRad, cat. 5000001). For blot samples were diluted in lysis buffer to equal protein concentration and 20 µg per well was diluted at 4:1 with loading buffer (Invitrogen, cat. NP0007), heated at 95°C for 10 minutes and loaded to wells. Gels were run by SDS-PAGE at 200V before semi-dry transfer to a methanol-wetted PVDF membrane at 20V for 1 hour (MOPS/MES Invitrogen running buffer, 10x Transfer buffer (0.25M Tris BASE/1.92M Glycine)). Membranes were blocked under agitation for 1 hour in polyvinylpyrolidine (Sigma, cat. P5288-500g) with 5% FBS and 1% sodium azide before addition of primary antibodies (1:3000 dilution) to blocking solution and incubation for 1 hour at room temperature. Membranes were washed in TBST before incubation with secondary antibody for 1 hour (species appropriate, 1:5000 dilution), washed again in TBST, developed with ECL (GE Healthcare) and visualised using a Fujifilm LAS 4000 developer.

2.6: Extraction of protein from formalin-fixed paraffin embedded (FFPE) tissue

Protein was extracted using QProteome FFPE Tissue Kit (cat. 37623) as per manufacturer instructions. Briefly, sections were deparaffinised and dehydrated using xylene and ethanol, extraction buffer with β-mercaptoethanol was added before heating to 100°C and incubating at 80°C under agitation. Supernatants were collected and stored at -80°C. protein content was determined using the Bradford Protein Assay (BioRad 5000001) at 1:10 dilution due to interaction between assay and QProteome buffer. Standard curves were spiked with equivalent concentration of QProteome buffer. The use of FFPE tissue protein extracts for cytokine assessment by array has not previously been published. For validation, fresh tonsil was bisected and half was snap frozen at -80°C, whilst the other half was fixed in formalin and paraffin embedded before comparison after 5 days using Abcam $T_H1/T_H2/T_H17$ 34 target membrane array (ab169809). Protein was extracted from the fresh frozen sample using cell lysis buffer (Abcam ab169809 array kit) and protease inhibitor (cOmplete ULTRA, Roche cat.

05892791001) before homogenisation using gentleMACS, incubation on ice and high velocity centrifugation. Arrays were incubated in blocking buffer before incubation with 200µg of protein, biotin-conjugated anti-cytokines then HRP-conjugated streptavidin. Membranes were transferred to blotting paper and incubated with detection buffers before detection using a CCD camera. Analysis was performed using ImageJ (Protein Array Analyzer plugin). Results were normalised as per manufacturer instruction to an arbitrary reference array.

Two technical replicates of each sample were compared. Due to drying artefact 7 points were excluded (6 from FFPE extract replicate 1 and 1 from FF extract replicate 1). Excluded points were identified due to poor concordance between spots arrayed in duplicate on the membrane. A high level of agreement was seen between paired tissues in 27 out of 34 target cytokines. For 6 cytokines results were inconsistent but no difference was seen between the 2 approaches. For 1 cytokine (CCL20) marked discordance was seen between the FF and FFPE method. Results highlight the need for individual validation of proteins before adopting this approach as inconsistency, whilst uncommon, was observed. (Figure) For validation of the detection of heterodimeric cytokines sandwich ELISA was used according to manufacturer instruction (Human anti-IL27 Ready-SET-go Kit, eBioscience, 15511097). IL27 was not detectable by this method in FFPE protein extracts.

Figure 2.6: Validation of cytokine analysis from FFPE protein extracts; Comparison of yield on cytokine array from paired fresh frozen and FFPE tonsil

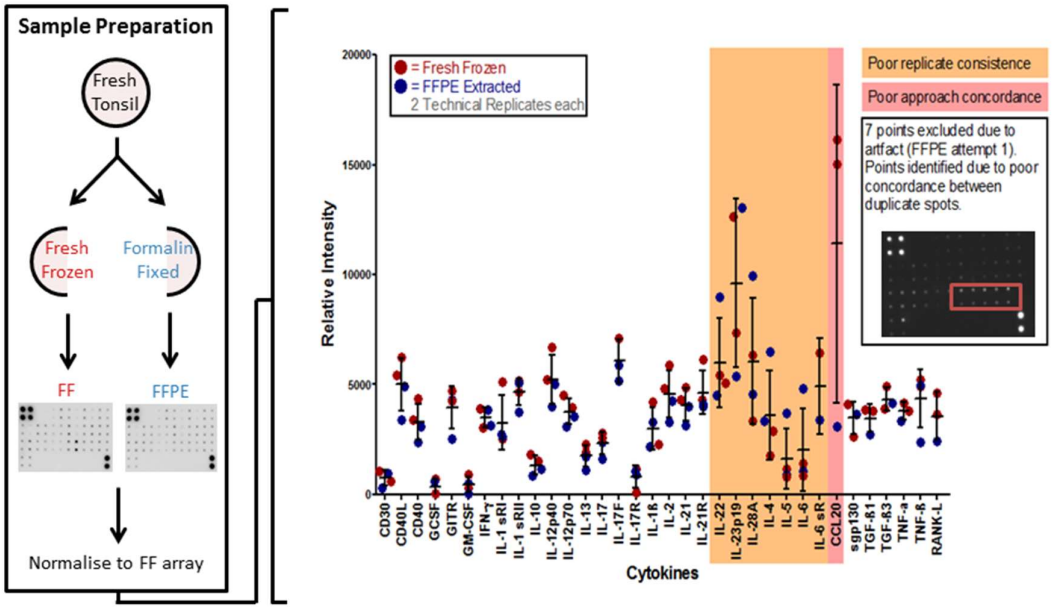

Figure 2.6: Fresh tonsil was bisected, half was fresh frozen (FF), half formalin fixed and paraffin embedded (FFPE) before processing of tissue from each source and analysis by cytokine array. Results are shown for comparison between methods. Seven data points were excluded due to drying artefact on one array. Points for exclusion were identified due to poor concordance of duplicate spots on the same array. 26 cytokines showed consistency between both fixation method and replicates. 6 cytokines (orange) showed poor consistency between replicates (either FF or FFPE), 1 cytokine (red) showed poor consistency between fixation methods.

2.7: Imaging Mass Cytometry

Imaging Mass Cytometry (IMC) staining and acquisition was performed by E. Truelove.

2.8: Statistical Analysis

Data was processed in Microsoft Excel and R. Statistical comparison was performed in GraphPad Prism and R. Data was assessed for normal distribution using histograms and Shapiro-Wilk normality test. Where data sets were normally distributed paired T test was performed. Where one data set was not normally distributed by Shapiro-Wilk paired analysis was performed using the Mann-Whitney test. Where multiple groups were compared distribution at least one set was not normally distributed in all cases. Kruskal Wallis test was performed and for post-test analysis of selected pairs Dunn multiple comparison test was used. For correlations data sets were not normally distributed and Spearman's rank test was used. Survival analysis was performed in IBM SPSS Statistics version 24. Kaplan Meier curves were generated and the log rank test was used to assess significance. Multiple cut point analysis was performed using X-Tile (https://medicine.yale.edu/lab/rimm/research/software/).

Chapter 3: Extended Methods: Advanced Image Analysis

Classical Hodgkin Lymphoma (CHL) is a paradigm example of tumour-microenvironmental interaction, with rare tumour cells depending on an inflammatory immune microenvironment. However, a series of challenges make the CHL microenvironment difficult to study; Firstly, primary tumour cells do not survive *in vitro* and are frequently undetectable in tumour-derived single cell suspensions (SCS) due to their scarcity and fragility. Secondly, when working with SCSs it is impossible to tell which immune cells were in proximity to the tumour and difficult to estimate the effect of disproportionate cell death among cell types. Finally, there is no representative mouse model and CHL cell lines are genetically distant from primary disease and survive independently of their microenvironment. As a result, formalin-fixed paraffin-embedded (FFPE) tissues are both the most representative and readily available samples to study. For these reasons methods that maximise the information obtained from FFPE samples is valuable. These factors make image and specifically spatial analysis a valuable tool in the study of CHL biology.

3.1: Technical issues in image analysis

The aim of most IHC-based studies is to compare absolute counts of cells expressing a single marker. More complex studies incorporate multiplexing and the addition of spatial data. Tissue-based approaches bring a series of advantages. Firstly, they permit the testing of primary diagnostic samples. This unlocks the pathological archive for study bringing with it access to large numbers of samples, the ability to link to clinical data and access to rare samples where collection of any quantity of live tissue is not possible. Secondly, key spatial information is preserved. This is important as it controls for a limitation of studies of dissociated tissue were it is difficult to distinguish whether an identified population is biologically relevant or so distant to the tumour that there can be no meaningful interaction. This is of particular concern in conditions like CHL where the malignant cell is rare and is exemplified by flow studies that have been unable to separate the signature of CHL-involved nodes to that of RLN – most likely due to the background noise created by cells distant to the tumour.[174] Finally, because biopsies are fixed immediately on removal they are likely to represent a more accurate description of the tissue *in vivo.* In contrast, SCS are created by mechanical dissociation and freezing, usually subjecting the biopsy to hours of hypoxia and freeze-thaw. This results in differential cell death leading to better preservation of robust cell types such as T cells but disproportionate loss of cells such as macrophages and in the case of

CHL, tumour cells, rendering them frequently being undetectable in CHL SCS.[165] This also likely leads to unknown phenotypic changes and even within the T cell compartment disproportionate loss of senescent and terminally differentiated cells.

The major limitation of FFPE tissue is that cells are fixed so it is not possible to perform true functional testing of live samples. Spatial analysis methods can mitigate this. A tissue image represents a snapshot of a dynamic tumour in time and each image captures thousands of individual cell-cell interactions.

3.1.1: Accuracy across biological replicates

Given that high replicate numbers are a key strength of IHC single marker studies, accurate cell quantification that is robust between biological replicates is important. Unfortunately, this represents a challenge as variations in staining quality between samples is common and affects the accuracy of the count. Factors such as staining protocol, antibody choice and optimisation affect sensitivity and background but provided batch staining is performed are uniform across replicates. However, some factors including tissue type, section age and tissue fixation vary by biological replicate and affect background and stain intensity. Finally, for many markers intra-sample biological variability is seen with varying intensity of expression between cells, likely representing different biological functions or differentiation states. Selection of a threshold for positivity has traditionally been arbitrary and reflects a compromise between these factors. This inevitably leads to under-estimation of counts in weak-staining tissue and/or over-estimation in high background tissue. The effects of this decision must be considered. The bias effect is likely to be small provided that sample size is large enough and variation in tissue fixation time etc. is randomly distributed amongst comparison groups.

Figure 3.1: Technical variation leading to variability in staining quality

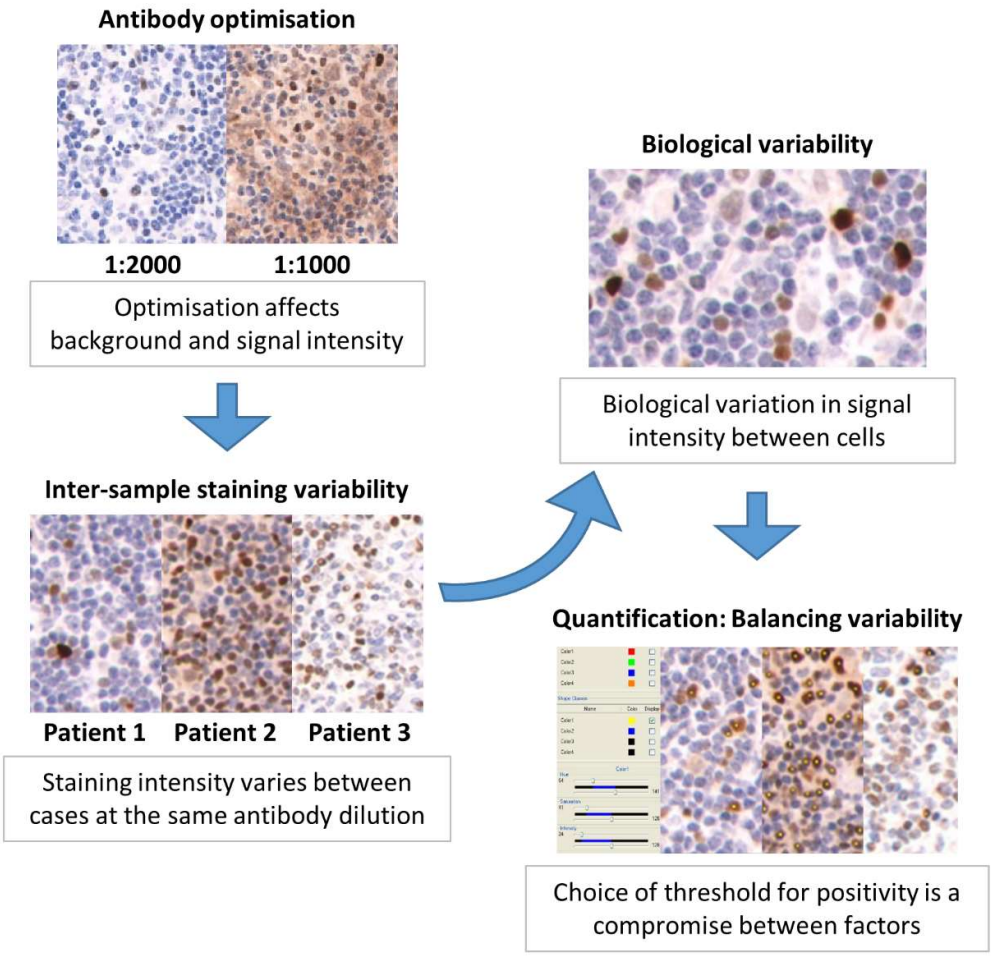

Figure 3.1: a) IHC Antibody optimisation represents a compromise between positive staining intensity and level of background. Optimal antibody concentration is protocol-specific and decided by eye, risking either true signal loss or false positivity. b) Fixation, tissue differences and artefact lead to inter-sample variation in staining quality with the same antibody concentration. c) Intra-sample expression variability of marker expression creates a gradient of positivity rather than binary groups. d) Choice of cut-off for positivity is arbitrary and represents a compromise between these factors.

There is no consensus as to how approach this problem. It is usually resolved by applying a single threshold to the study (accepting that variability will occur but assuming it is randomly distributed). The alternative is to manually calibrate thresholds for each tissue, providing greater accuracy but time consuming and open to investigator bias. Advances in image analysis provide novel solutions to this problem including algorithms such as rescaling, normalising to background or k-means clustering classification. When applying these it is essential that the

investigator understands the principles of the algorithm or there is a risk of unexpected results. For example, both rescaling and k-means clustering rely on examples of a true positive and true negative signal existing within every field. If this is applied to an entirely negative field the most intense of the negative pixels will be scaled up and appear positive. A more robust approach that has been developed but not finalised during this PhD would be to dynamically identify positivity within each sample using deviations from the normal distribution. By this method "positive" would be defined as any cell where the mean signal intensity fell above the bell curve of intensity in all cells. This would therefore account for the possibility that "negative" cell intensity would shift with variations in background. An assumption in this approach is that a minority of cells would be positive. Theoretically this approach could also identify bimodal populations providing rationale for multiple cut-points, or be extended to perform cell cytometry against features such as cell size or a second marker. The identification of bimodal populations in practice is challenging as it requires a high level of accuracy on cell segmentation.

Figure 3.2: Dynamic classification of positivity

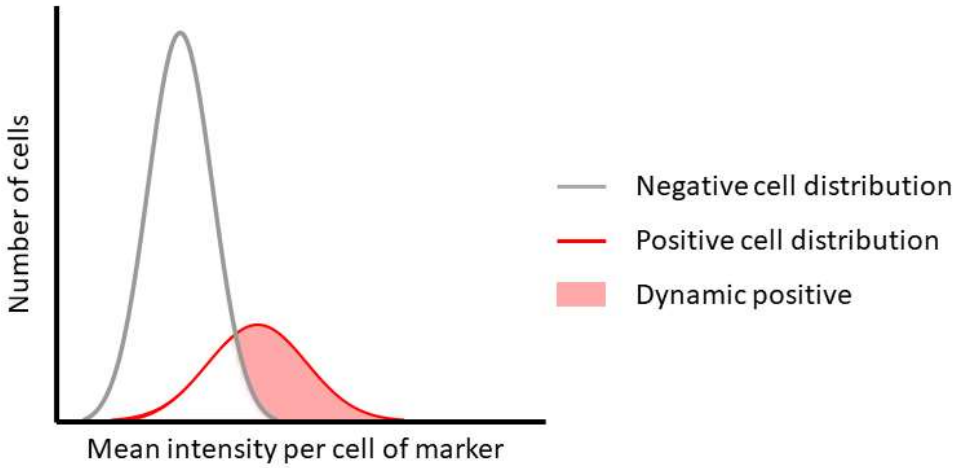

Figure 3.2: In IHC staining a degree of background signal is expected even in negative cells. In practice, histogram distributions of individual cell intensities rarely separate into binary populations, likely due to inaccuracies in segmentation. The optimal threshold for "positive" is where the negative and positive cell distributions intersect. Establishing this by eye is difficult and shifts in stain intensity between cases will lead to negative cells being classified as positive in high background cases and failure to identify positive cells in weak intensity cases. Mapping Gaussian distribution of negative cells to intensity histograms as below (similar to proliferation assay algorithms) provides a method to automatically calibrate the threshold in each tissue in an unbiased manner.

3.1.2: Impact on reproducibility

The impact of small variations in staining or protocol can be significant. IHC based biomarker studies suffer from poor reproducibility, demonstrating that results are sensitive to small changes in approach.[299] This reinforces the need for protocol standardisation if markers are to adopted for clinical use. This issue was exemplified in the assessment of RORγT (a T_H17 marker) as a prognostic biomarker in CHL as part of this study. RORγT proved to be highly predictive of outcome (overall survival and freedom from treatment failure) in a large test cohort ($p < 0.001$). This effect was robust to multiple cutpoints and showed a smooth cutpoint-risk relationship on multiple cutpoint analysis with X-Tile. The test cohort was comprised of patients treated in the pre-ABVD era and those treated in the ABVD era and the effect was independently detectable in each subcohort.

As validation a larger uniformly treated cohort was arrayed, partially overlapping with the test cohort. These were batch stained with a higher antibody concentration. The effect of re-arraying and alteration to the protocol led to the effect being completely lost, even in the subcohort that was present in the initial group despite the earlier high degree of statistical confidence. It is unclear if this is due to sampling differences during arraying or sensitivity in count. It is also unclear as to which result is more reliable. This should therefore be repeated in a further validation cohort.

Figure 3.3: Biomarker reproducibility

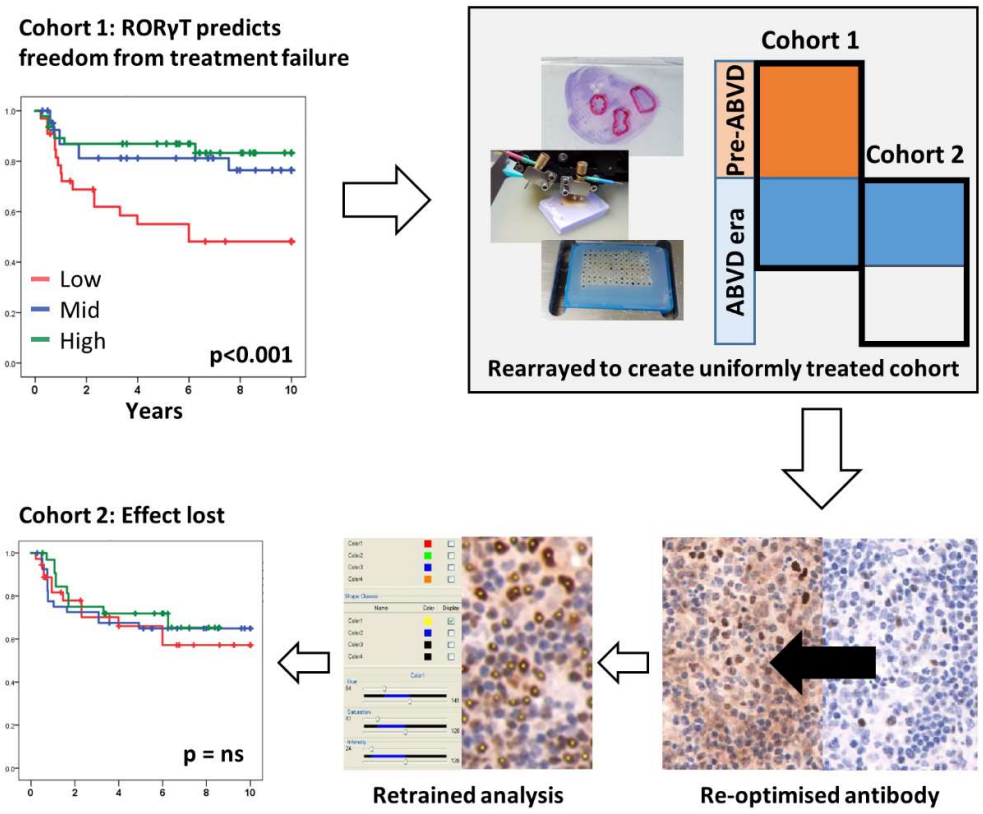

Figure 3.3: Effects of small changes of analysis or sampling on biomarker reproducibility in IHC cell classification. 1) Percentage of RORγT^{+} lymphocytes predicts overall survival and freedom from treatment failure with a high statistical confidence. Effect is robust to change of cut points and displays a dose-response relationship and remains significant in the ABVD treated sub-cohort of cohort 1. 2) Samples re-arrayed and cohort expanded to create a uniformly ABVD treated validation cohort. 3) Antibody re-optimised and analysis software retrained. 4) Effect lost in Cohort 2, including in the sub-cohort where a significant effect had previously been detected.

3.1.3: Area targeting and exclusions from analysis

Tissue damage, crush artefact and necrosis are a recurrent problem within tissue studies which lead to inaccurate cell identification and false positivity on IHC. These areas were excluded from analysis. Fibrosis in CHL is directly related to the disease process so it is potentially biasing to exclude on this basis. However, most tissue studies use TMAs and when biopsies are marked for arraying cellular tumour-rich areas are usually selected, avoiding fibrotic bands. Choosing the most "representative" tumour region is therefore already a subjective decision, albeit an informed one made by a Haematopathologist. The TMA is therefore focussed on tumour-rich areas but does not necessarily capture heterogeneity or the most relevant areas with respect to the microenvironment. To minimise subjectivity, after TMA validation the following rules were applied: To account for variation in fibrosis content wherever possible counts are reported as a percentage of total nucleated cells as opposed to cells by unit area. Large areas of acellular fibrosis were excluded from analysis due to overestimation of the negative nucleated cell count. Cores with marked fibrosis such that over 50% of the core was replaced were excluded.

In CHL further complexity is introduced due to patchy and variable infiltration with CHL cells between cases. This can lead to cores from CHL biopsies without any CHL cells and others that are heavily infiltrated. This variability is a feature of the disease but means in cases with low infiltration cells within the core may not be under the direct influence of CHL cells. Studies have either disregarded this problem or excluded from analysis cores with insufficient CHL cells.[300] Both approaches are open to criticism as one risks quantifying cells unrelated to the tumour creating background noise whereas the other is open to subjective assessment of what constitutes sufficient CHL cell numbers, potentially biasing against some subtypes.[301] This problem is most effectively addressed with spatial analysis where cellular infiltrate can be directly related to tumour cell density or distance.

3.2: Image segmentation and analysis software

3.2.1: Ariol and Pannoramic analysis systems

Single marker IHC quantification was analysed using the Leica Ariol Digital Pathology scanner and image analysis software. Ariol is a legacy system that quantifies pixel regions by size and intensity. An intensity threshold and nuclear size range is selected and Ariol quantifies the

number of objects meeting that criteria. No cell segmentation is performed so it is most effective at counting nuclear spots of uniform size. This is an effective method of quantifying provided cells are of uniform size (e.g. small lymphocytes) and markers are nuclear. Quantification of membrane markers is challenging as the system tends to count junctions between cells. Quantification of histiocytes is difficult as cells may have projections making the cell appear to be multiple distinct objects. Single marker quantification of T cells and macrophage markers was performed by this method. Macrophages were quantified as total area stained without segmentation.

The Pannoramic system is also a legacy system that performs basic analysis including manual cell counting and calculation of the histology score (H score). This score aims to account for both area stained and expression intensity in a single value by weighting pixel staining by intensity.

3.2.2: Visiopharm analysis system

Visiopharm is a proprietary software for image analysis. It is sold in a modular form with basic licences for image viewing (Viewer), analysis app design (Author) and analysis (Engine). Further licences are required for TMA analysis (Tissuearray), linking of tissue sections for virtual multiplexing (TissueAlign and Viewer+) and Imaging Mass Cytometry (IMC) analysis (Phenomap). The interface is based on the construction of analysis “apps” which flexibly phenotype, measure and quantify cells or objects identified within the image according to the programming of the app.

The apps described below require the Viewer, Author and Engine packages. Multiplexing for spatial analysis is also described using the TissueAlign and Viewer+ packages which add significant functionality for multiplex IHC (mIHC). These are required for any phenotyping analysis that uses one marker to identify cells and seeks to measure the co-expression of a second marker within the same cell. They also add flexibility to mIHC based spatial analysis, however, if the TissueAlign and Viewer+ packages are not available then the need for image alignment can be bypassed by combining the stripping and progressive multiplex IHC techniques described in 2.2.5/6. The approaches below permit TMA analysis without the need for the Tissuearray module and analysis of IMC data without the need for the Phenomap module.

3.2.3: Fundamentals of analysis

Accurate cell segmentation is essential for deep phenotyping and spatial analysis. The most common initial step is identification of cells by their nuclei. A challenge is that cells within a section do not sit on a single plane so parts of cells and overlapping nuclei are captured. Additionally, nuclei vary dramatically in size and uniformity. Haematoxylin binds DNA and RNA and is the most common counterstain used in IHC. Nuclear counterstains do not identify cell membranes so their location is usually inferred by the watershed point between cells. Due to the IHC amplification process and the fact that cells are not sectioned in a perfect plane membrane and cytoplasmic stains do not cleanly follow this pattern leading to signal bleed between neighbouring cells with these markers. Additionally, cytoplasmic or membrane stains may also obscure the nuclear border making segmentation difficult.

3.2.3.1: A TMA division app pipeline

TMA analysis is an essential part of most IHC studies but the Visiopharm license to integrate TMA processing is expensive so was not purchased as part of the investment in software at Queen Mary University of London. I have developed a simple app sequence to bypass this problem which I outline below as it is a problem that will frequently be faced by future users of the program. The purpose is to assign each core with an ID reliably defining its position on the TMA. This is essential to data analysis where the data from cores arrayed in triplicate are aggregated and results are connected to patient data.

Visiopharm analyses fields of view from the top left corner and moves left to right in rows. If asked to enumerate Regions of Interest (ROI) it assign numbers sequentially as it meets a new ROI. This does not result in predictable core numbering unless the TMA sits precisely horizontal and cores are exactly the same size, which is never the case. The app series first identifies all cores then sequential apps identify each row by enumerating from top to bottom, then each core within the row by enumerating from left to right. This is robust to all but large variations in TMA placement on the slide. If the TMA is inverted or flipped on the slide the app sequence can be corrected to account for this.

Sequence:

1 App: 1 TMA Tissue Detection - outlines cores with green “default/Core marker” ROI
2 Manual step: Missing cores are manually drawn with green “default/Core marker” ROI so that a green identifier is present for every core that was arrayed on the original TMA

3 Row apps: Identifies each row in turn by enumerating the first e.g. 10 cores from the top then enumerating the cores horizontally. A sequence of row apps is run, one for each row in the TMA.

4 The End Process app finalises the process.

5 After running each TMA core will appear in a different colour ROI. Hover over each ROI to ensure they are correctly identified.

6 Troubleshooting: The app will enumerate every ROI in the field. If the app has misidentified regions it is usually because small additional ROIs are present in the field that must be deleted, or the app settings do not correspond to the TMA size or orientation. To correct this, see notes below.

7 Once each core is surrounded by an ROI with a name corresponding to the TMA core ID press “crop image” on the Tools bar and an individual file will be created for each core with a name corresponding to the core ID. These can be analysed as a batch and data will export with the core ID associated to it.

Note: Apps are specific for the number of rows and columns in a TMA. To customise the app to a new TMA size each of the row apps must be amended. Apps are opened in App Author and Post Processing is selected. The “Change ROI” steps are then selected so that the change steps correspond to the number of cores in the row:

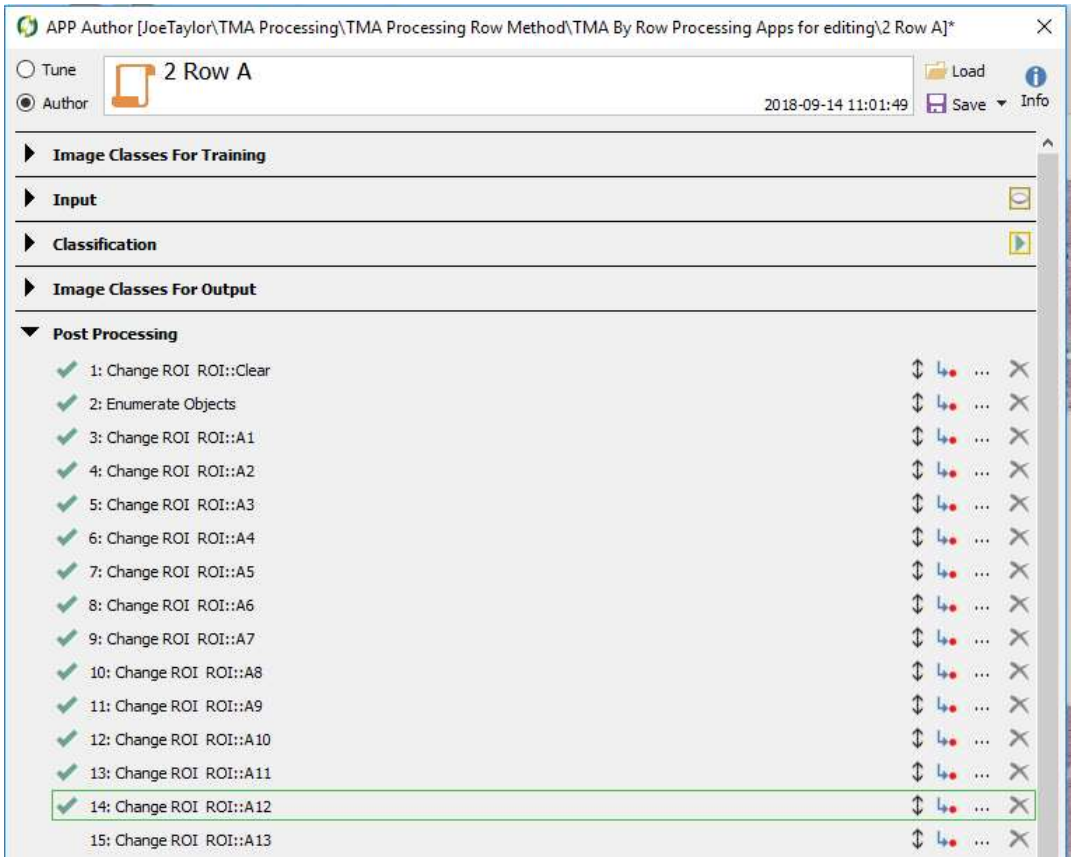

(Pictured: Settings for TMAs where there are 12 cores in row A)

Occasionally TMAs are inverted or flipped on the slide. If this happens the direction that the app enumerates in will no longer be correct. To correct the app the enumerate object steps direction must be altered with step two changed from Left->Right to Right->Left and step 23 changed from Top->Bottom to Bottom->Top or vice versa. Step 24 must not be unchecked. This must be performed for every row app in the sequence. After this has been done for a new TMA it can be saved and run as an app sequence and will work for all TMAs of that size and orientation in the future.

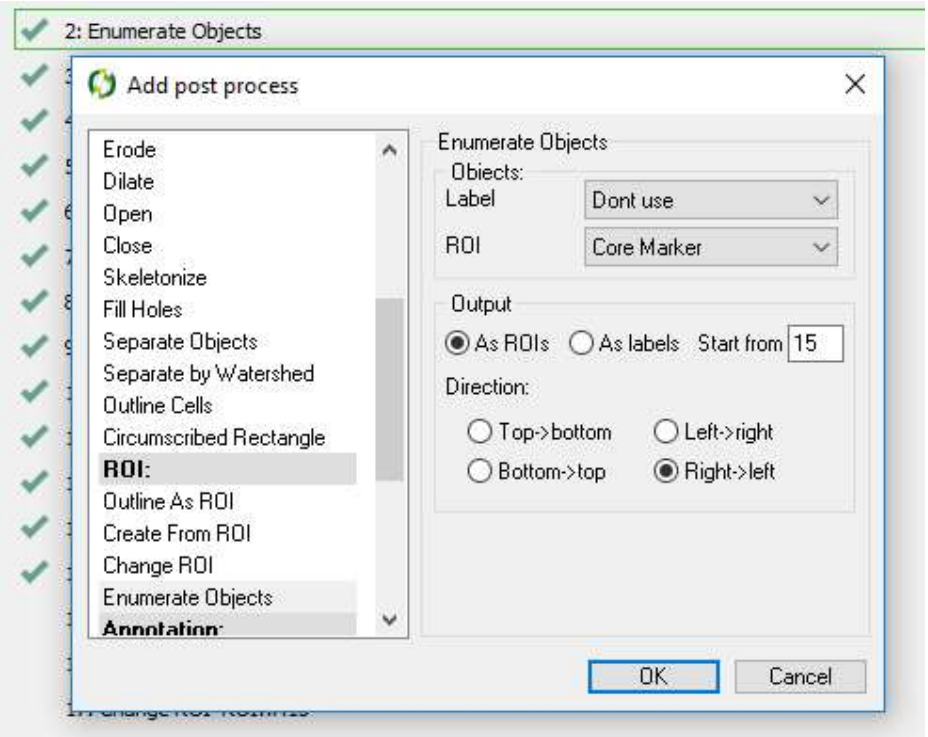

3.2.4: Cell Segmentation and Post processing

App design follows a pattern of classification (identification of different areas by colour band and pixel intensity) followed by post-processing where identified objects are sequentially expanded, altered or separated to best identify cell areas. Finally, output steps can be configured to give overall or per-cell information as required including location, shape, eccentricity and marker intensity metrics as required.

App design approach depends on the marker and question. Cells are usually identified within an image by identification of nuclei, either using a nuclear marker, a nuclear counterstain (e.g. haematoxylin) for IHC or DNA signal for IMC. For nuclear markers in single marker studies cell

identification is straight-forward either for total counts or per-cell. For cytoplasmic markers where individual cell readouts are required app design is more complex, requiring the identification of nuclei, which may be partially obscured by the membrane stain, then segmentation by watershed between nuclei. Data quality is lower than with nuclear markers due to the problem of signal bleed into neighbouring cells. For phenotyping panels nuclear markers are recommended where possible and for heavy membrane stains an initial counterstain-only slide for segmentation can solve a lot of analysis difficulty if image alignment software is available. A strong counterstain and time spent on antibody optimisation/selection to ensure strong clean staining is preferable for image analysis particularly in per-cell phenotyping panels. Most challenging are apps requiring per-cell comparison of nucleus and cytoplasm and phenotyping panels for macrophages as they can have a spindle-like morphology and appear to be multiple cells due to the angle of the section cut. Macrophage phenotyping panels are particularly difficult when trying to compare nuclear and cytoplasmic markers due to the difficulty of identifying which processes belong to which cell in a robust automated manner. We have developed apps to deal with these problems but data quality is improved with good study design and planning to anticipate these issues.

3.2.4.1: An app for robust unsupervised multiplexing

Imaging Mass Cytometry (IMC) images are usually segmented based upon nuclei identification via DNA signal channels before using the watershed point between nuclei to estimate membrane borders. This approach is effective for small cells with compact nuclei such as lymphocytes but leads to poor identification and over-segmentation of cells with loose nuclei such as histiocytes and CHL cells. This also assumes that membranes run at the midpoint between nuclei which is not necessarily correct and leads to signal bleed of cytoplasmic and membrane markers into neighbouring cells. An additional problem is of overlapping nuclei which are classified as a single cell and the failure to detect cells with small nuclear fragments due to the angle of the section.

As part of this thesis we develop an approach that robustly identifies and segments multiplex by building composite features. It is easily adaptable so can be changed to accommodate a new panel with minimal understanding of the program.

App principles:

1 Create composite nuclear feature by the addition of the signals of all nuclear markers

2 Create composite membrane/cytoplasmic feature by the addition of the signals of all membrane and cytoplasmic markers
3 Subtract composite membrane feature from composite nuclear feature to separate overlapping nuclei
4 Use new nuclear-membrane channel to identify nuclei
5 Second nuclei separation step using standard deviation channel
6 Estimate membrane boundaries by watershed between nuclei, defining watershed points using the composite membrane channel

Composite features ensure that all markers are represented in the cell segmentation process, reducing the risk of over or under-segmentation. The creation of a composite nuclear feature ensures that cells nuclei are identified even in the case of histiocytes and CHL cells where loose nuclei leads to failure using DNA alone. The standard deviation transformation of the nuclear feature identifies nuclear edges by highlighting areas of rapid colour change within the image and is used to separate overlapping nuclei. The subtraction of the composite membrane feature from the composite nuclear feature ensures that true cell boundaries are emphasised in the nuclear image. Finally, the use of the composite membrane feature to define the watershed points between nuclei ensures that segmentation follows true cell boundaries.

Adaptation of this app to a new panel requires the user firstly to identify classify channels as nuclear or membrane markers and add them to the appropriate channel within the “Features” section of the App using the Author module. Finally, because outputs are named manually within the app the new user must check that the output names correspond to the appropriate channel (e.g. that the output from the TBET signal channel is labelled as “TBET”) in the “Output” section of the App.

Figure 3.4: Cell Segmentation for IMC

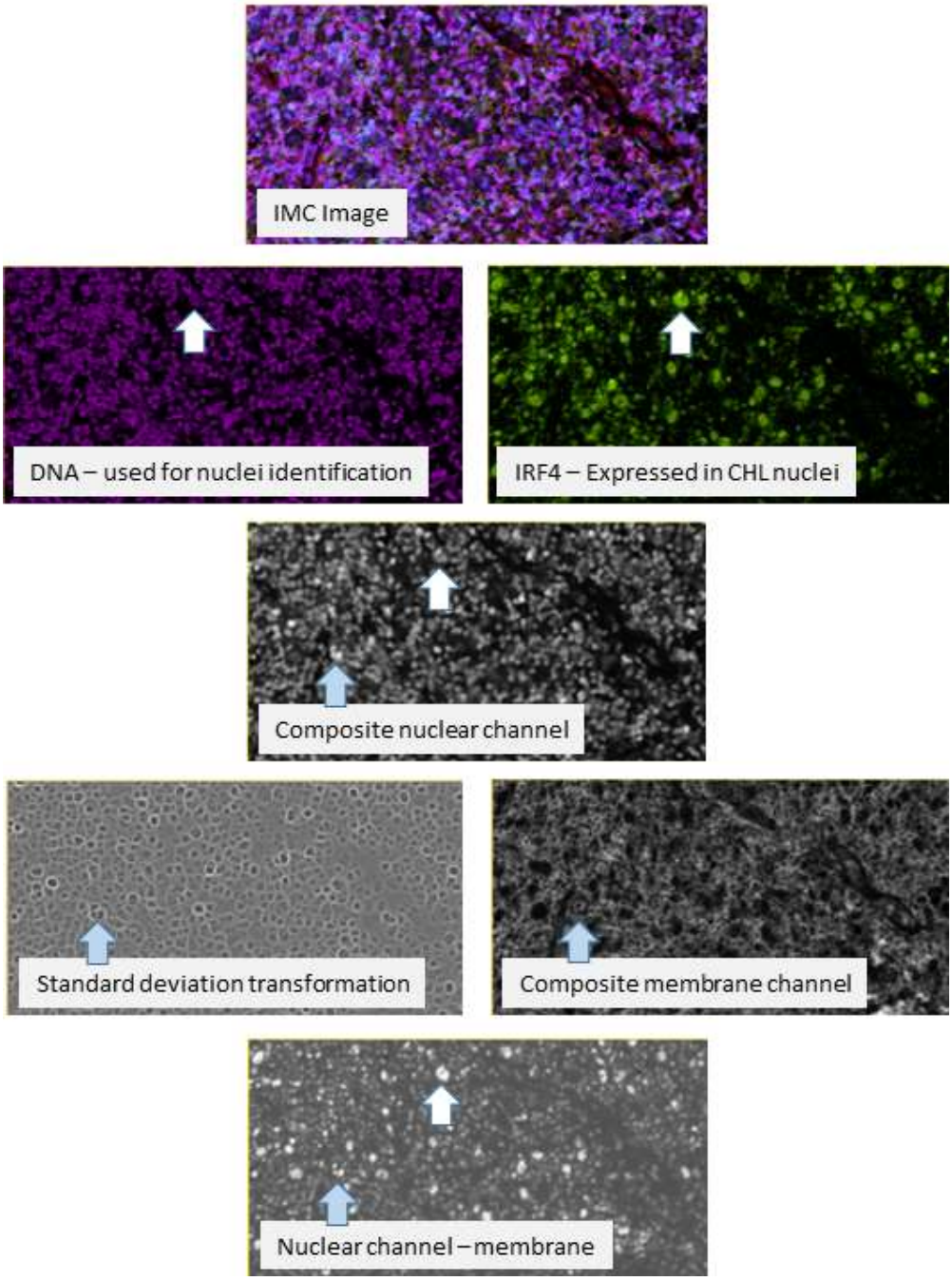

Figure 3.4: Screenshots from Visiopharm – improved IMC cell segmentation using additive channels. i) IMC image – virtual image of CHL case with all channels/markers. ii) DNA channel –identifies compact nuclei but large loose nuclei (e.g. CHL cells) are poorly identified (white arrows) leading to misclassification. iii) IRF4 channel –identifying large CHL nuclei. iv) Composite nuclear channel (addition of all nuclear markers). Small and large nuclei are now identifiable. v) Standard deviation of nuclear channel – identifies cell outlines improving separation of overlapping nuclei (blue arrows). vi) Composite membrane channel (addition of membrane/cytoplasm markers) – Identifies cell boundaries. vii) Nuclear-membrane – subtraction of the composite membrane channel improves clarity and separation of nuclei. Cell segmentation is performed on the Nuclear-membrane channel, using the composite cytoplasm and standard deviation channels for

3.3: Further analysis – Clustering and Spatial Analysis

Further analysis was performed in R and all aspects are open-source. Starting data structure for the following analysis is a table containing a row for each cell and a column containing mean intensity values for each marker of interest and x and y locations for the cell. This is sufficient for point pattern analysis. For larger structures where reducing to a single point in space risks inaccuracy then linear patterns are required. Starting data for this analysis is a list of x and y coordinates marking the boundary of the structure. Visiopharm software was used to generate starting data in this study but it could be achieved with other proprietary (e.g. HALO, Definiens) or open source software (e.g. CellProfiler).

R packages used in analysis:

- Package management: pacman, here, devtools, conflicted, BiocManager[302–306]
- Data processing: tidyverse, reshape2, scales, XML[307–310]
- Clustering: Rphenograph, FlowSOM, flowCore, Rtsne, cytofkit, largeVIS[311–316]
- Spatial analysis: spatstat, sp[317,318]
- Plotting: ggthemes, ggpubr, cowplot, GGally, ggrepel, RColorBrewer, pheatmap[319–325]

3.3.1: Cell cytometry

The ability to extract per-cell marker intensity data enables us to use cell cytometry plots similar to those used in flow analysis. These can be used for manual gating of populations and also for validation purposes and the assessment of background and signal bleed. Intensity signals were plotted using asinh transformation in the same manner as are applied to mass cytometry data. This is similar to applying a log transformation. A log transformation cannot be applied to data containing zeros. The asinh (or inverse hyperbolic sine) function is adapted from the cytofkit package:[315]

```
cytofAsinh <- function(value, cofactor = 2) {
    value <- value - 1
    loID <- which(value < 0)
    if(length(loID) > 0)
      value[loID] <- rnorm(length(loID), mean = 0, sd = 0.01)
    value <- value / cofactor
    value <- asinh(value) # value <- log(value + sqrt(value^2 + 1))
  return(value)}
```

3.3.2: t-SNE, clustering and data summaries

t-Distributed Stochastic Neighbor Embedding (t-SNE) is a data visualisation method that creates a map with cells placed close to each other based upon phenotypic similarity. It is most effective as a visualisation method rather than to define clusters. t-SNE was implemented with the Rtsne package using the Barnes-Hut algorithm.[314]

Identification of cell clusters using an unsupervised clustering algorithm has advantages over traditional gating and can be performed within subsets of within the entire identified cell population. Multiple clustering algorithms have been used and this pipeline is compatible with all of them. Hierarchical and phenograph clustering algorithms were used.

3.3.3: Spatial Modelling

Many multiplexing papers to date have focussed upon methods of analysis of deep phenotyping data, largely imported from the mass cytometry field. A major strength of multiplex imaging data is the connection between phenotype and spatial relationships. Most papers to date are restricted to nearest neighbour-style analyses.[159] A more complex approach is available in the HistoCat neighbourhood analysis which performs an NxN assessment of cell-cell interactions by performing permutation testing (equivalent to Monte Carlo tests or spatial

tests of random labelling). These are then filtered by significance. Analysis can be run for direct contact or enrichment within a specified distance. Bi-clustering then identifies frequent neighbour clusters by tissue type.[326] This is a powerful approach which has the advantage of being unsupervised. Its limitations are that it only considers cell-cell contact or a fixed arbitrary distance. A fixed distance leads to the problem of what distance to select, which is difficult as e.g. diffusion of soluble factors varies by tissue type. This method is well-suited for modelling contact-dependent cellular interaction such as T cell activation but is less so for soluble factor effects such as are seen with macrophage polarisation. In Chapter 8 we develop an adaptation of this analysis to account for these issues. Generally, methods used to date are limited in the complexity of question that can be asked and further analysis tools are needed. This will become more pressing with the advent of *in situ* sequencing data.

In this thesis we apply tools and spatial modelling techniques adopted from other scientific disciplines such as geography and species biology to expand the toolkit of currently used spatial analysis techniques. These techniques enable improved assessment of cytokine effects, allow the building of models for multivariate effect comparison and assessment of hidden features. Most of the approaches and techniques described below are drawn from work by Baddeley *et al.* (authors of the spatstat) and their book which contains detailed information as to how to use the program and statistical guidance for analysis.[317] The following tests and approaches with the exception of distance index graphing are performed within spatstat.

3.3.3.1: Edge corrections and hidden features

Edge correction is an important consideration in spatial analysis but is overlooked in recent publications within the cell biology field.[327] The window is the field of view in which the spatial analysis is performed. If all the boundaries of the window are a biological boundary (such as the capsule of a lymph node) then edge correction is not required. However, more frequently the window is a sample of the area. In this scenario if a point is close to the edge of the window its true nearest neighbour may fall outside. Edge correction adjusts for this. A series of edge correction methods have been proposed.[317] In this study we apply Ripley's edge correction using the spatstat program.[317]

A valid criticism of spatial analysis in tissue sections is that it assumes a two dimensional structure whereas tissue is three dimensional. All spatial analysis methods described (including nearest neighbour analysis) are designed to perform analysis on a 2D plane. More complex 3D approaches exist but the challenge lies in data acquisition as this would require analysis of up

to one hundred serial sections to cover a 300 µm cube of tissue. The three dimensional structure of tissue means that closest neighbours are likely to be found in a different plane to that in the section and that "hidden features" such as islands of tumour cells below or above the plane may affect results. These features are invisible to the analysis but are likely to have a normalising effect – increasing the possibility of a type II (false negative) result. If tumour cells were evenly distributed within the tissue this may be problematic as hidden feature effects would then be frequent. In CHL malignant cells are dispersed but usually occur in islands of higher tumour cell density. Hidden features are difficult to control for in simple nearest neighbour analyses but can be detected with point pattern modelling by analysis of the residuals after a model is fitted.

Figure 3.5: Edge correction and hidden features

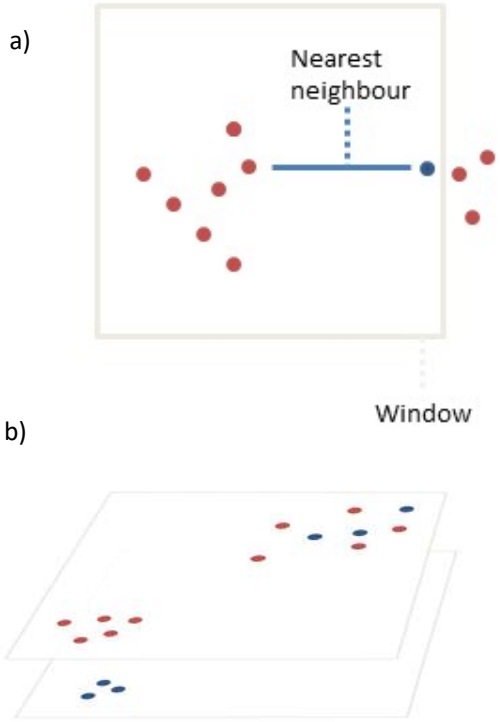

Figure 3.5: a) Spatial analysis of cell distributions is performed within a 2 dimensional window (or field of view). Unless the window edge is the edge of the structure then analysis might be confounded by the fact that the true closest neighbour of a point near the edge may fall outside the window. Edge correction mathematically adjusts for this.

b) Because tissue is 3 dimensional but the window is 2 dimensional other neighbours may be closer but not visible due to lying in a different plane (a hidden feature)

3.3.3.2: Nearest Neighbour analysis and distance indexes

The simplest form of spatial analysis involves calculating individual nearest neighbour comparisons across cell types, reporting either individual or mean distances.

In the cancer biology literature these are the most commonly reported statistics. However, it is common to see two mean nearest neighbour distances compared by t test with the statement that one is statistically smaller than the other.[328] The high numbers of nearest neighbour measurements within a tissue section field makes a significant difference relatively easy to detect by t-test. However, to put context to the analysis the correct comparison account for the distribution expected in complete spatial randomness. The mean nearest neighbour index calculates mean minimum nearest neighbour distance and compare to the *expected* minimum nearest neighbour distance in complete spatial randomness. Significance can be tested with the Clark-Evans test.[329] This assumes a stationary process and can give spurious significance in a non-stationary process.[317] The Hopkins-Skellam index performs a similar calculation that is less sensitive to a non-stationary pattern and edge effects.[317]

Limitations of the use of nearest neighbour distances include the problem of edge effects and non-independence of points due to frequent reflexive nearest neighbours (where pairs are each the other's nearest neighbour), inflating the variance of the result.[330]

Distance index was used as a method of comparison of nearest neighbour distance between two objects. Distance index was calculated using the formula:

Distance Index = -0.5 + nnA / (nnA + nnB)

Where: nnA = nearest neighbour distance to structure A, nnB = nearest neighbour distance to structure B

3.3.3.3: Spatial summary functions

The following functions can be calculated within a cell type (distribution of cell type A relative to other members of cell type A), across cell types (distribution of cell type A relative to cell type B) or to any cell type (distribution of cell type A relative to any cell irrespective of type). If measured between cell types they are called cross functions in the spatstat program, if they measure to any cell they are called dot functions. These functions are based upon the assumption that the point pattern is a Poisson process (see section 3.4.3.4.1) with different algorithms for stationary and non-stationary/inhomogeneous processes.

- G (cross) function: the distribution of cell type "B" nearest neighbour distances from an arbitrary cell "A". This compares observed nearest neighbour distances to that

expected with complete spatial randomness by creating a confidence envelope using Monte Carlo simulations. If the observed line falls above the envelope cells of type B are more frequent clustered, within the envelope is consistent with a random pattern and below is consistent with being more regular or dispersed. Function is most powerful at detecting deviation from randomness towards regularity.[330]

- F (cross) function: Similar to G but measures from a sample of points in empty space. Deviations from randomness are the opposite of those seen in G function (clustering is seen if the line falls below the confidence envelope). This function is most powerful in the detection of clustering.[330]

A limitation of the G function is that it only takes into account the nearest neighbour. The K function measures more points so gives a broader estimate of spatial dependence, although with large datasets is computationally demanding.

- Ripley's (cross) K function: the number of "B" within every given distance of each cell A and compares with complete spatial randomness. This is a second order statistic, measuring tendency to be clustered, dispersed or regularly spaced. The result is a curve displaying the pattern expected with regular spacing and a second curve displaying the observed pattern. If the line deviates above the regularity line at a point we can conclude that at distance X from cell-type A, cell-type B is more clustered than expected. Conversely if it deviates below then at distance X cell-type A, cell-type B is more dispersed than expected. Edge corrections are included within the calculation. Variations on this function include the L function which provides the same information but the curve of "expected" distribution is transformed to a straight line making deviations from expected easier to identify. Importantly this is cumulative so the reading at distance X is calculated using all distances from zero to X. Hence the expected line for cell type B seen in complete spatial randomness is always rising. A final variation on the K function is the pair correlation function which is not cumulative so the expected line is flat.

Significance envelopes are applied to these functions. These are calculated using Monte Carlo simulations. If a point-wise envelope is calculated it provides a 95% confidence interval that would be correct if the analysis has *only* been performed at that given distance. It is therefore incorrect to conclude that if observed line crosses the confidence envelope at point X that the deviation is statistically significant due to the problems of multiple testing. This confidence envelope is therefore informative to give context to the magnitude of deviations or if the point to measure at has been pre-determined.[317] Alternatively, a global envelope calculates whilst correcting for multiple testing.

3.3.3.4: Evaluation of dependence on a covariate

The above tests compare a distribution to complete spatial randomness. Other tests are required to evaluate the dependence of a distribution of a covariate.[317] The simplest way is to divide the area into quadrats based upon the intensity of the covariate, then perform quadrat testing comparing numbers of the cell-type of interest within the regions. Alternative methods which capture the exact values of covariates at specific points include cumulative distribution functions with the Kolmogorov-Smirnov statistic and the Berman-Lawson-Waller test. These tests essentially compare the value of a covariate at the points associated with the cell type of interest and tests whether this represents a random sample of the value seen at all locations.[317]

3.3.3.5: Spatial point pattern modelling

Fundamentally, this method models the degree to which the distribution of cell type or structure "B" can explain the distribution or phenotype of cell type "A" and is a detailed and flexible form of spatial correlation. It carries multiple advantages over more basic spatial comparisons, most importantly the ability to build of multivariate models testing the relative effects of multiple factors on a cell type simultaneously, quantify the strength of individual relationships and identify factors that best predict the distribution of the cell type. This provides a versatile and powerful method to interrogate spatial interaction between cells, permitting us to ask functional questions within primary tissue and validate observations made *in vitro*.

Figure 3.6: Spatial point pattern modelling overview

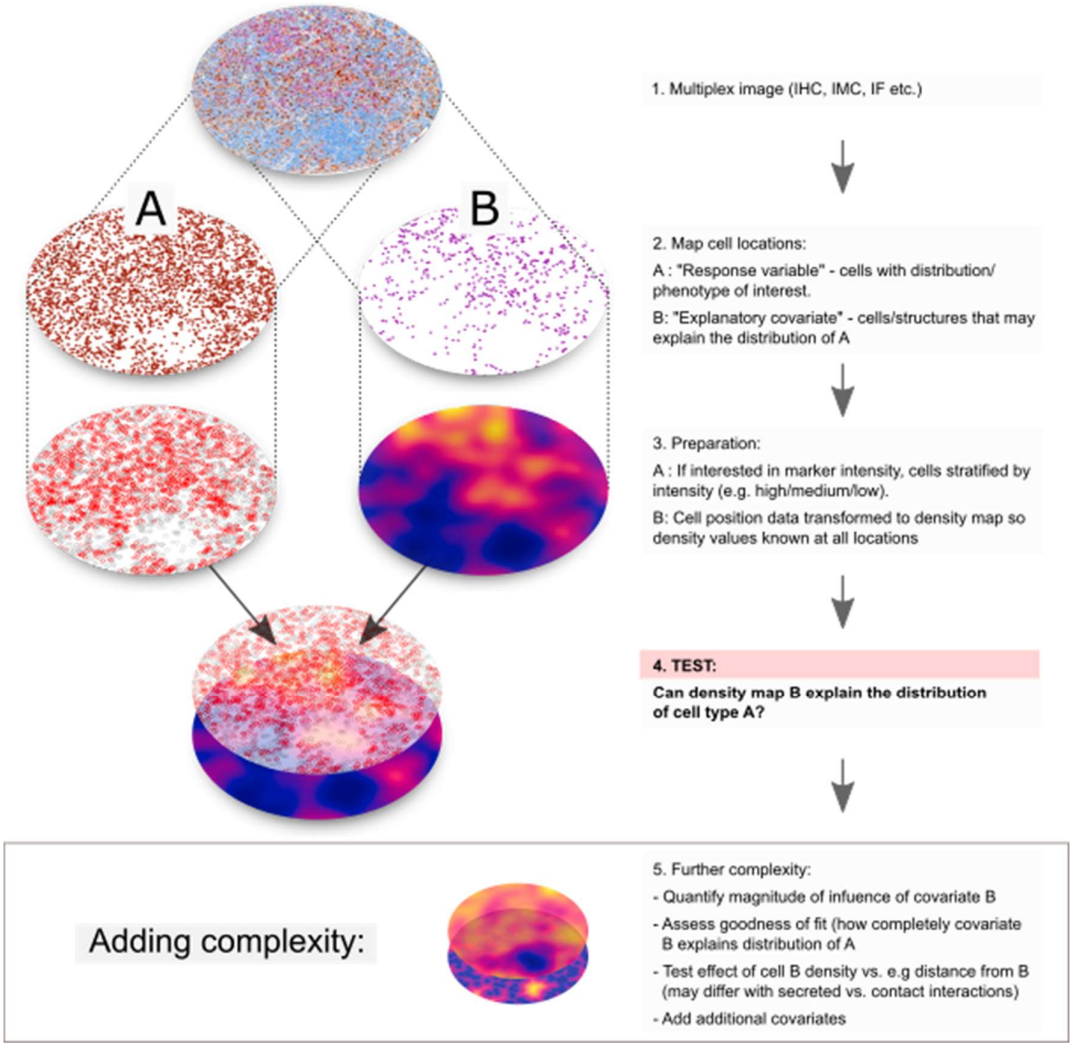

The principal of this method is that the cell type of interest is analysed as a point pattern distribution, but the covariate (which could be expression of a marker such as PDL1, distribution of a second cell type such as tumour, distribution of structures such as vessels, marker expression intensity on a specific cell type etc.) is converted to an image where intensity values are available for every point within the window. This is akin to building maps to describe the niche that the cell of interest exists within and can be compared to an example from species biology which builds maps to assess the influence of factors such as gradient, soil type and elevation on the distribution of *Beilschmiedia* tree growth.[317] A key strength is that images can be varied to test different aspects of the influence of individual factors. For example, the influence of the distribution of CHL cells may vary depending upon the manner in which they are interacting with the cell type of interest: If their influence is contact-dependent then distance to the nearest CHL cell might be the most relevant measurement, whereas if it is

cytokine-dependent then CHL cell density may be more relevant, finally if it is related to the expression of a particular marker then relative marker expression on CHL cells can be measured. Images describing each of these scenarios can be generated and tested against cell of interest distribution.

3.3.3.6: Pitfalls

As with any statistical technique, using a model based upon incorrect starting assumptions could lead to misleading results. Many models are based upon the assumption that the point process has a Poisson distribution, i.e. that points are randomly distributed and independent from each other. A second assumption determining which models to use is whether the process is stationary (has uniform intensity) or non-stationary (has varying intensity). Many cellular point processes, such as that created by microenvironmental cells within a tumour, can be regarded as Poisson (often non-stationary). However, some patterns would not meet criteria for a Poisson process. Examples would include tumour cells growing by division from each other, cellular patterns analysed by pixel rather than segmented as cells or macrophages if over-segmented (where processes extending from a cell might be treated as a different cell). None of these examples are Poisson as they do not meet criteria for independence of points – the location of a point is related to its neighbour either as part of the same cell or as a daughter cell. This does not preclude analysis using models with different assumptions or their distribution being incorporated in a model as an explanatory variable.

A second pitfall is relevant if all cells within a histological field are analysed as a process simultaneously. Spatial point pattern modelling considers cell locations as single points in space rather than a tessellation of objects. Cells are identified by the coordinates of the cell centre. If cell size and spacing is regular then cytoplasmic volume therefore means that a tessellation of cells violates the assumption of random and independent points required to use a Poisson-based model as spacing is more regular than random and nuclei can never be closer than a certain distance.[317] In practice this is more of a problem within a tissue monolayer as in 3D tissue cells vary in size and overlap so pass tests for Poisson.

Even if an all-cells analysis was acceptable from a mathematical perspective it comes with other complications so should be performed with caution. One is an issue that occurs at high spatial scale when comparing the distributions of cells that vary in size due to differences in lineage – if you were to compare the distribution of (large) macrophages to (small) lymphocytes within the same point process it would be possible to conclude that lymphocytes

were disproportionately clustered by virtue of lymphocytes having a smaller cell volume rather than a true difference in distribution. If this analysis needs to be performed these issues can be circumvented with careful design of the question and test. Related to this is the choice of an appropriate comparator to the distribution of cell of interest. If the distribution of a marker is compared to the distribution of all cells it is possible that the result will be confounded by the distribution of a parent population (a T_H1 marker appearing clustered by virtue of clustering distribution of all T_H cells or all T cells). The result must therefore be interpreted in comparison to the distribution of the parent lineage. The choice of parent marker will vary with the question being asked. This error is made in two recent publications in the CHL field. This first is discussed in section 1.3.2.1.4. The second, in abstract form, compares distribution of $TIM3^+CD4^+$ and $LAG3^+CD4^+$ T_H from $PDL1^+CD30^+$ CHL cells and $PDL1^-CD30^+$ CHL cells, where both phenotypes are significantly closer to $PDL1^+CD30^+$ CHL cells.[328] This approach is drawn from my own 2018 abstract which compared *relative* distribution of $TBET^+CD8^-$, $GATA3^+CD8^-$, $FOXP3^+CD8^-$ and $ROR\gamma T^+CD8^-$ T_H from $PDL1^+CD30^+$ vs. $PDL1^-CD30^+$ CHL cells.[331] The comparison of the effect of PDL1 expression on CHL cells in this manner within a single biopsy is appealing in that it is internally controlled. The Colombo abstract has strengths over my own, including superior identification of the T_H population by using CD4 instead of CD8. However, by making individual comparisons between $TIM3^+CD4^+$ or $LAG3^+CD4^+$ and each CHL subtype as opposed to a relative assessment within the $CD4^+$ population their data might be confounded if the $CD4^+$ population as a whole is more enriched around $PDL1^+CD30^+$ CHL cells.

Figure 3.7: Comparison to parent distribution

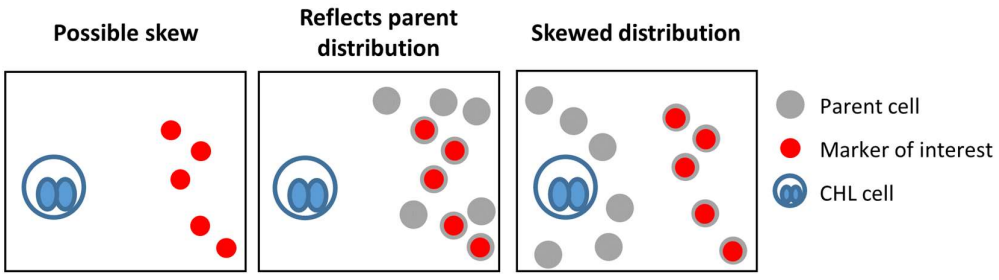

Figure 3.7: 1. Possible skew: Cells expressing the marker of interest (e.g. PD1) appears to have a non-random distribution relative to tumour cell. 2. Reflects parent distribution: The apparent skew is attributable to random distribution of the marker of interest within a skewed distribution of the parent cell (e.g. T_H) so conclusion cannot be drawn about the marker of interest specifically. 3. Skewed distribution: There is discrepancy between the distribution of the parent population and the marker of interest.

i.e. Conclusions should only be drawn if comparison is made to a biologically meaningful parent or control population, the choice of which will vary according to the question.

Detailed explanations of mathematical approaches and many pitfalls are published by the authors of the spatstat program and the methods and some examples described here are drawn from their work.[317] Other examples (such as the need for a parent population marker) given stem from my interpretation of the principles they describe to the specific challenges faced applying these techniques to tissue sections and immunobiology.

3.3.3.7: Robust experimental design

This approach is flexible but a series of experimental design principles should be considered when planning to maximise the chances of detecting an effect if present. Firstly, the analysis area should capture some variation in tissue (areas of high and low expression or areas or high and low infiltration) and be of sufficient size to capture a range of events. This might be a tumour margin if tumour infiltration is uniform. One larger region is preferable to multiple smaller due to the need for edge corrections. Secondly, most questions require the measurement of the location of the cell of interest (plus phenotyping information if relevant) and an explanatory variable. As discussed above, I also advocate the measurement of a parent lineage marker to avoid the distribution of a parent lineage confounding data regarding the distribution of the marker of interest (see 2.4.3.3.1 and 1.3.2.1.4). Additionally, from a technical perspective, clean and well validated antibodies for robust starting data. Finally, it is important to recognise that this is in essence a detailed form of spatial correlation, so whilst it can detect and describe a relationship in detail (and provide a rare opportunity to test hypotheses in primary tissue) it cannot prove causation.

3.3.3.8: Choice of test and null hypothesis

The choice of statistical test and null hypothesis varies with question and study design. In some settings the appropriate null is that of complete spatial randomness. However, in other situations e.g. where the locations of a parent and a subpopulation are being compared a null of random labelling or independence of components is more appropriate. A null hypothesis of random labelling can be tested with permutation testing. Strength of association can be quantified using area under a receiver operator curve.

Results overview:

Chapter 4: A PDL1^{hi} myeloid microenvironment

PD1 inhibitor response in CHL is predicted by PDL1 expression.[6] PDL1 expression in CHL is seen on the CHL cell and in the myeloid microenvironment. Myeloid recruitment and the induction of PDL1 by CHL cells is assessed. We confirm that CHL cells recruit and induce PDL1 expression in the myeloid environment. However, we find evidence of inter-case heterogeneity between PDL1-expressing myeloid subsets, correlation of myeloid PDL1 expression to both regulatory and pro-inflammatory markers and functional assessment of macrophages did not demonstrate a skew to regulatory T cell priming. These data support the presence of a PDL1^{+} myeloid microenvironment induced by PDL1-expressing CHL cells, but highlight that the functional implications of myeloid PDL1 expression are unclear.

Chapter 5: EBI3 and IL27: A putative mechanism for CHL immune evasion and microenvironmental PDL1 upregulation

PDL1 upregulation by CHL cells is well described and frequently has a genetic basis.[140] However, the mechanisms of PDL1 induction within the microenvironment are poorly understood. We assess evidence for IL27-induced induction of PDL1 expression. We find evidence of upregulation of the components of IL27 and indirect evidence of the influence of IL27 on the CHL microenvironment but are unable to demonstrate the presence of formed IL27, with assessment limited by technical considerations. We are therefore unable to demonstrate or exclude a link between PDL1 and IL27 and find indirect evidence of its influence as an evasion mechanism.

Chapter 6: T cell exhaustion in the CHL microenvironment

PD1 expression in CHL is low despite the expression of PDL1, raising questions as to how PD1 inhibitors can act by the reversal of exhaustion.[22] We perform a detailed assessment of exhaustion and find no phenotypic or functional evidence of exhaustion above levels seen in non-malignant controls. Furthermore, we find no relationship between PD1 expression and PDL1 or CHL MHC II expression, known predictors of PD1 inhibitor response. These data do not support reversal of exhaustion as the primary mechanism of PD1 inhibitor response.

Chapter 7: Skewing of T cell differentiation and its relationship to PDL1 and CHL-MHC II expression

Another major role for the PD1-PDL1 axis in T cell biology is in effector differentiation and plasticity.[332] We find that the T_H environment in CHL is skewed to a regulatory phenotype, and that skewing associates with both PDL1 and CHL-MHC II expression. We show that PDL1 associates with CHL-MHC II expression, suggesting that a role in antigen presenting function. We further demonstrate functional evidence of skewing *in vitro*. These data suggest that PDL1 and CHL-MHC II shapes the T_H infiltrate without necessarily inducing exhaustion. Reversal of exhaustion may therefore be too narrow a lens through which to view PD1 inhibitor activity in CHL and broader effects on the T cell environment may play a more dominant role.

Chapter 4: A PDL1^{hi} myeloid microenvironment

4.1: Introduction

The myeloid compartment has been a focus of interest due to a series of pivotal studies identifying a myeloid signature as predictive of poor outcome in CHL (See section 1.3).[144,145] The CHL myeloid environment is described as macrophage-enriched with high levels of CD68 expression, CD163 expression and immunosuppressive markers such as IDO1, Galectin 1 and PDL1.[145] Whilst it is clear that macrophages play an important role in CHL, the nature of their role is less well defined with most studies only describing their presence. CD68 and CD163 are independent predictors of outcome and the two markers do not consistently co-localise or even inhabit the same region of the biopsy, suggesting heterogeneity amongst myeloid subpopulations.[146,148] Recently there has been renewed interest in the myeloid compartment due to the success of PD1 inhibitors in CHL and the high expression of PDL1 on CHL associated macrophages.[6,159] Data suggest that PDL1 expression predicts response to PD1 inhibitors whereas PD1 infiltration does not.[6] This led us to focus on the nature of PDL1 expressing macrophages in CHL.

Published data suggest that macrophages are recruited by CHL cells and that their differentiation is skewed towards a tolerogenic phenotype. Notably, CHL cell lines secrete factors promoting an M2-like regulatory phenotype with expression of markers such as CD163 and IDO1 and microenvironmental mRNA of these secreted factors are associated with CD163 expression in primary CHL.[149,155,156] Furthermore, CHL-polarised monocyte-derived macrophages reduced the proliferative response of anti-CD19 CAR T cells to an irradiated CD19+ target.[158] High PDL1 expression is also seen in the CHL microenvironment, as is the secretion of soluble PDL1 which drives the differentiation of an immunosuppressive macrophage phenotype.[159–161,163,333]

These data suggest a suppressive myeloid environment, however, there are a number of unanswered questions and reasons to treat this conclusion with caution. As yet no study has phenotyped CHL-associated macrophages in an unsupervised manner. Additionally, some studies also identify markers more associated with an inflammatory M1 phenotype such as IL23p19 and CSF1R, with one study in paediatric CHL suggesting that EBV^{+} paediatric CHL associates with an M1 phenotype whereas EBV^{-} paediatric CHL associates with M2.[139,154,334] Overall studies investigating immunosuppressive markers are well represented whereas studies focussing on pro-inflammatory markers are rare, despite evidence of their expression.

The lack of studies providing deeper phenotyping data also means it is unclear as to whether studies to date are describing a single population or multiple populations with distinct roles. The available functional data does support the induction of an immunosuppressive phenotype but is derived from cell lines so is far removed from the tumour microenvironment. High expression of PDL1 is assumed to induce exhaustion and is generally referred to in the context of an immunosuppressive phenotype.[159] However, elevated PDL1 expression is not a robust marker for either an inflammatory M1 or regulatory M2 phenotypes. PDL1 upregulation is seen in response to both pro and anti-inflammatory cytokines and role of PDL1 on macrophages is not clear with some studies suggesting its principal role is to protect macrophages from destruction by T cells.[139,335,336] Additionally, an immune tolerant phenotype and induction of exhaustion are distinct concepts (relating to activation of naïve cells and stimulation of effectors respectively) and it is not clear that they are necessarily connected, or even that PDL1 expression does induce exhaustion as opposed to maintain it. (see section 1.2.3.1)

Taken together these data are suggestive of monocytes being actively recruited by CHL cells, differentiating to macrophages and broadly adopting an immune tolerant phenotype, although the possibility of confirmation bias exists. Reports of PDL1 expression within the microenvironment are consistent but its role within the microenvironment is not entirely clear, although it is thought to reflect a tolerant phenotype.

The myeloid environment in CHL plays an important role and the relevance of PDL1 expression is of particular interest given that it is predictive of PD1 inhibitor response. We therefore sought to investigate the expression and role of PDL1 in macrophages in the CHL microenvironment.

4.2: Aims and Objectives

4.2.1: Aims

To test the hypothesis that CHL cells recruit and induce a $PDL1^{+}$ immunosuppressive myeloid microenvironment.

4.2.2: Objectives

1 To quantify expression of immunosuppressive markers in the CHL myeloid microenvironment in comparison to RLN.

2 To assess spatial distribution of immunosuppressive markers within the CHL myeloid microenvironment and its relationship to the CHL cell

3 To functionally assess whether CHL cells induce upregulation of immunosuppressive markers.

4 To functionally assess whether this confers an immunosuppressive phenotype.

4.3: Materials and Methods

4.3.1: Spatial Analysis

4.3.1.1: Spatial relationship to PDL1

Macrophage PDL1 expression was assessed in 51 CHL patients by multiplex IHC (mIHC) represented on a single TMA. Sections were stained for PDL1 (VIP chromogen) before stripping and reprobing with a dual stain identifying $CD68^+$ macrophages and $CD30^+$ CHL cells (DAB and VIP respectively). Images were linked and mapped with Visiopharm software. Cell segmentation was performed on the dual stained image. Per-cell mean PDL1 intensity was read from the corresponding mapped region of the PDL1 stain. Pixel outputs assign a value of 0 to black and 255 to white. PDL1 intensity was therefore corrected with the formula 255-x. Cell locations and mean PDL1 intensity figures were exported and analysed using the spatstat package in R.[317] Other packages used included extrafont, pacman, ggthemes, ggpubr, XML, tidyverse, here, export, future and conflicted.[302–304,307,308,319,320,337,338]

Figure 4.1: Mapping macrophage PDL1 intensity by mIHC

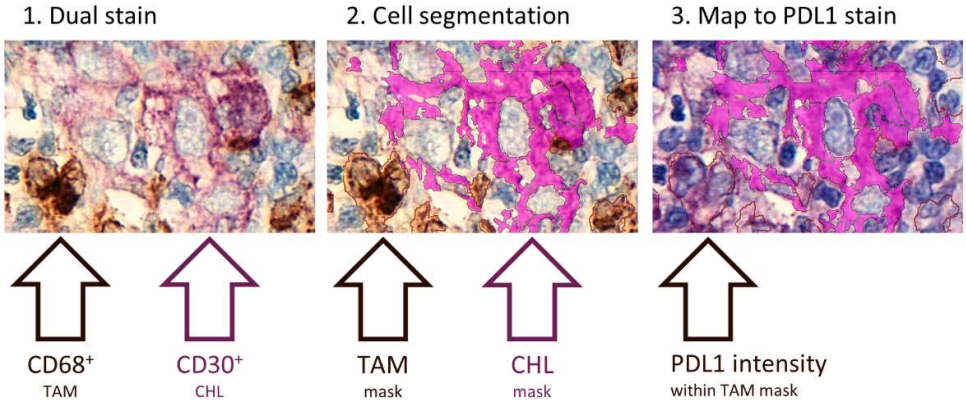

Statistical assessment of macrophage enrichment was performed using quadrat and chi-squared testing. Quadrat regions were defined by CHL cell density, stratifying into high, high-

intermediate, low-intermediate and low density regions. To assess PDL1 expression, macrophages were stratified into high, intermediate, low and negative expression groups. Negative expression was defined as below the upper quartile of expression of all non-macrophage non-CHL nucleated cells. Because these cells are predominantly small lymphocytes that do not express PDL1 this represents an estimate of background signal intensity. High, intermediate and low expression groups were defined by splitting at the upper quartile and median of macrophage PDL1 expression within the core. Segregation testing assessed whether macrophage groups were interspersed or segregated from each other. Quadrat and chi-squared testing as described above was used to assess whether PDL1 high or low macrophages disproportionately associated with CHL-rich regions relative to the overall macrophage population. Nearest neighbour distances between CHL cells and macrophages were calculated and adjusted for edge effects using Ripley's edge correction. Cumulative distribution testing and correlation of PDL1 intensity to distance to nearest CHL cell were performed. Area under the receiver-operator curve was calculated to quantify effect magnitude. Data analysis approach was informed by Baddeley *et al.* Section 14.2.6. and followed a marginal and conditional distribution approach.[317] Response variables were PDL1-stratified $CD68^+$ macrophages. CHL location data was treated as an explanatory covariate.

4.3.2: *In vitro* modelling of PDL1 induction

$CD14^+$ Monocytes were isolated from healthy donor PBMCs by positive selection and differentiated *in vitro* to monocyte-derived macrophages in the presence of MCSF and GMCSF. Flow cytometry confirmed upregulation of HLA-DR, CD11b and CD16 and downregulation of CD14 as compared to the parent $CD14^+$ monocyte population. After 7 days MDM were treated with CM harvested from the KMH2 CHL cell line for 24 hours before harvest. See section 2.3.

4.3.3: IMC myeloid subset spatial point pattern modelling

Myeloid subset modelling was performed on a test case of CHL by Imaging Mass Cytometry (IMC) with the following panel. Panel design, optimisation and data acquisition was performed by E. Truelove.

Table 4.1: IMC Panel

ANTIGEN	METAL	CLONE	DILUTION	CONJUGATION	VENDOR
ALPHA-SMA	141 Pr	1A4	1:200	Company	Fluidigm
BCL2	143 Nd	124	1:100	Self	Cell Signaling
CD14	144 Nd	EPR3653	1:100	Company	Fluidigm
TBET	145 Nd	D6N8B	1:50	Company	Fluidigm
CD16	146 Nd	EPR16784	1:100	Company	Fluidigm
CD163	147 Sm	EDHu-1	1:100	Company	Fluidigm
CD30	148 Nd	E4L4I	1:30	Self	Cell Signaling
CD11B	149 Sm	EPR1344	1:100	Company	Fluidigm
CD10	150 Nd	polyclonal	1:25	Company	R&D Systems
CD31	151 Eu	EPR3094	1:100	Company	Fluidigm
CD45	152 Sm	CD45-2B11	1:100	Company	Fluidigm
CD11C	154 Sm	D3V1E	1:25	Self	Cell Signaling
FOXP3	155 Gd	236A/E7	1:50	Company	Fluidigm
CD4	156 Gd	EPR6855	1:200	Company	Fluidigm
IRF4	158 Gd	polyclonal	1:30	Self	R&D Systems
CD68	159 Tb	KP1	1:50	Company	Fluidigm
CD20	161 Dy	H1	1:400	Company	Fluidigm
CD8	162 Dy	C8/144B	1:100	Company	Fluidigm
PDL1	165 Ho	E1L3N	1:50	Self	Cell Signaling
B7H2	166 Er	H74	1:50	Company	Fluidigm
GRANZYME B	167 Er	EPR20129-21	1:100	Company	Fluidigm
KI67	168 Er	B56	1:50	Company	Fluidigm
COLLAGEN 1	169 Tm	polyclonal	1:300	Company	Fluidigm
CD3	170 Er	polyclonal	1:100	Company	Fluidigm
CX3CR1	171 Yb	8E10.D9	1:15	Self	Biolegend
PD1	172 Yb	D4W2J	1:50	Self	Cell Signaling
CD45RA	173 Yb	HI100	1:30	Self	Biolegend
SIRP ALPHA	174 Yb	D613M	1:15	Self	Cell Signaling
CD25	175 Lu	EPR6452	1:50	Company	Fluidigm
HISTONE H3	176 Yb	D1H2	1:300	Company	Fluidigm

Cell segmentation was performed in Visiopharm and designed to identify cells in an unbiased manner. Briefly, IMC channels were divided into nuclear and membrane/cytoplasmic markers. Signals from nuclear marker channels including DNA and histone markers were added together to form a composite nuclear channel. This approach allows superior identification of larger (including malignant) cells where DNA signals may be more fragmented and ensures all markers are represented within the segmentation process. A second composite channel was created by the addition of all membrane and cytoplasmic markers. This channel was used to define cell boundaries during nuclear segmentation and as a watershed marker when identifying cell membranes. Once cells were identified location and per-cell mean marker intensities were exported for analysis. Cells were visualised by t-SNE and clustered using the Rphenograph algorithm before arc-sinh transformation. Mean marker expressions per cluster confirmed that markers followed biologically plausible patterns. An element of signal bleed

from neighbouring cells is expected, particularly with membrane markers due to overlapping cells and the image resolution, although these would be expected at low signal intensity. Consistent bleed signal is informative as it indicates common cell neighbours.

A semi-supervised spatial analysis pipeline was designed. Briefly, a cell cluster of interest was identified. Kernel-smoothed density maps of individual markers and of identified cell clusters were created and an additive model was built with all elements. Unsupervised subtraction of elements from the model was then performed to identify marker and cluster distributions that were most predictive of the distribution of the cluster of interest.

4.3.4: *In vitro* modelling of CHL-primed macrophage induction of T cell responses

$CD14^+$ Monocytes were isolated from healthy donor PBMCs by positive selection and differentiated *in vitro* to monocyte-derived macrophages in the presence of MCSF and GMCSF. After 7 days MDM were treated with CM harvested from the KMH2 CHL cell line for 24 hours. CM was then removed and autologous T cells or naïve T_H cells were added and co-cultured for 8 days before T cell phenotyping to assess differentiation. Differentiation was assessed by flow.

Table 4.2: Flow Panel

ANTIGEN	FLUOROCHROME	CLONE	CAT NO	DILUTION	VENDOR
DAPI	N/A	N/A	1:2000	1:2000	BD
CD4	PE-Cy7	OKT4	317414	0.5 µl	Biolegend
CD25	APC-eFl780	CD25-4E3	47-0251-82	0.5 µl	Thermo
CD127	FITC	A019D5	351312	0.5 µl	Biolegend
CXCR3	PE-Cy5	1C6/CXCR3	551128	1 µl	BD
CCR4	BV605	L291H4	359417	0.5 µl	Biolegend
CCR6	Afl647	G034E3	353404	0.5 µl	Biolegend
CCR10	PerCP-Cy5.5	1B5	564772	0.5 µl	BD

Table 4.3: Gating Strategy

CELL	GATING
T_H	$DAPI^- CD4^+$
T_{REG}	As $T_H \rightarrow CD127^{lo} CD25^{hi}$

T_H1	As $T_H \rightarrow CXCR3^+ CCR4^- CCR6^- CCR10^-$
T_H1_{REG}	As $T_{REG} \rightarrow CXCR3^+ CCR4^- CCR6^- CCR10^-$
T_H2	As $T_H \rightarrow CXCR3^- CCR4^+ CCR6^- CCR10^-$
T_H2_{REG}	As $T_{REG} \rightarrow CXCR3^- CCR4^+ CCR6^- CCR10^-$
$T_H1/17$	As $T_H \rightarrow CXCR3^+ CCR4^- CCR6^+ CCR10^-$
$T_H1/17_{REG}$	As $T_{REG} \rightarrow CXCR3^+ CCR4^- CCR6^+ CCR10^-$
T_H17	As $T_H \rightarrow CXCR3^- CCR4^+ CCR6^+ CCR10^-$
T_H17_{REG}	As $T_{REG} \rightarrow CXCR3^- CCR4^+ CCR6^+ CCR10^-$

Table 4.4: In vitro macrophage-T priming model

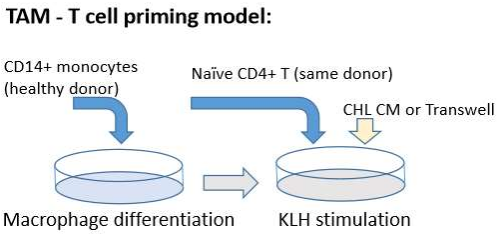

Figure 4.4: Monocyte-derived macrophages are cultured from healthy donor PBMCs before priming with CHL cell line conditioned media. Media is removed and autologous naïve T_H are added to test the functional effects of priming.

4.4: Results

4.4.1: Quantification of immunosuppressive macrophage markers in the CHL myeloid environment

4.4.1.1: Single marker IHC

We first assessed expression of immunosuppressive myeloid markers in the CHL microenvironment by single marker IHC. TMAs were stained for CD68, CD163, Gal1, IDO1 and PDL1. We also assessed IL27p28, a novel myeloid cytokine which signals as a monomer but can form the heterodimeric immunoregulatory cytokine IL27 in combination with EBI3 (a cytokine secreted by CHL cells). IL27 is discussed further in chapter 5.

PDL1 was significantly elevated in CHL compared to reactive nodes ($p<0.0001$). Amongst CHL cases PDL1 expression was significantly higher in EBV^+ cases and the mixed cellularity subtype. The same pattern was observed with CD68, IDO1 and IL27p28 staining ($p<0.001$ respectively). Similarly, CD163 staining was higher in the mixed cellularity subtype but did not reach

statistical significance on comparison by EBV status. In contrast, Gal1 staining was enriched in CHL but expression did not differ significantly by histological subtype or EBV status.

These data validate the increased expression of immunosuppressive markers in the myeloid environment of CHL. They also suggest elevated expression of immunoregulatory markers in the EBV^{+} and mixed cellularity subtypes, however it is unclear how much is confounded by elevated CD68 expression and therefore a higher frequency of macrophages rather than a "more immunosuppressive" phenotype. (Figure)

Figure 4.2: Immunosuppressive macrophage markers in the CHL myeloid

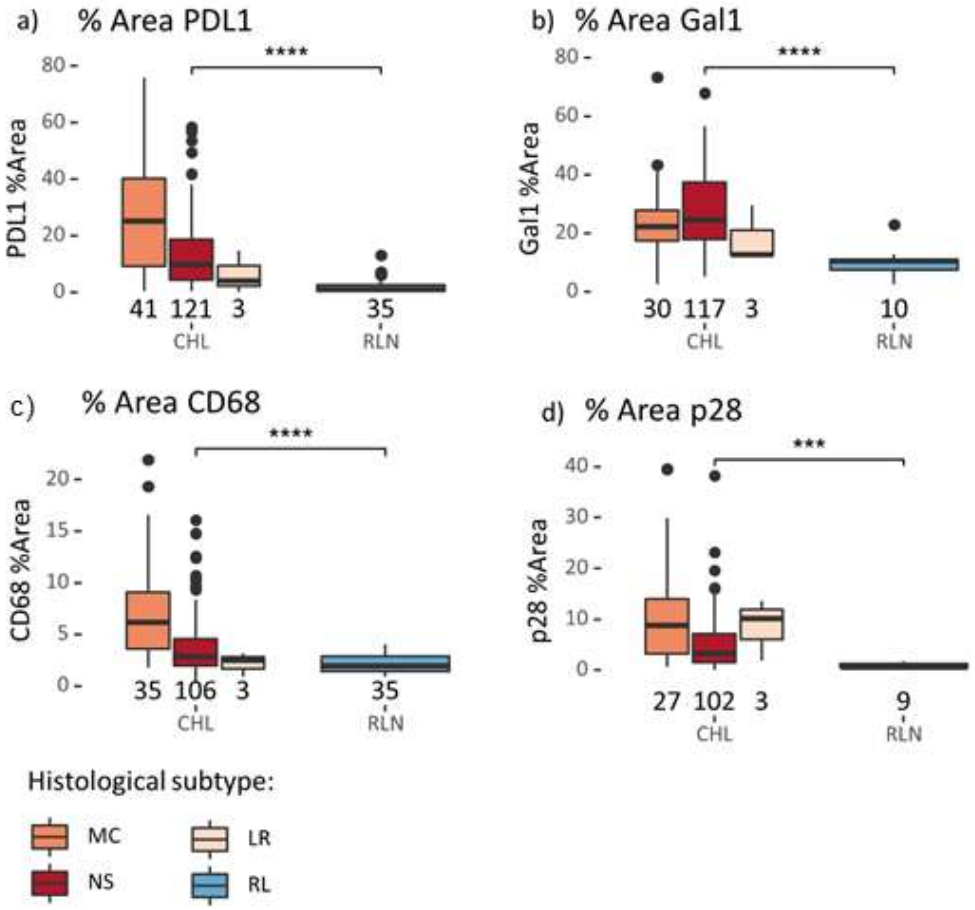

Figure 4.2: Expression of PDL1, Galectin 1, CD68 and IL27p28 in CHL and reactive lymph node (RLN) by histological subtype.

(MC = Mixed Cellularity, NS = Nodular Sclerosing, LR = Lymphocyte Rich, RL = Reactive Lymph node. Analysis by IHC on TMA. Number on x axis represents biological replicates per group. Statistical comparison by Kruskal-Wallis)

4.4.1.2: Clustering of IHC data

Given the similar expression patterns of immunoregulatory markers across histological and EBV subtypes we sought to establish whether PDL1^{+} cases clustered with other immunosuppressive markers consistent with it representing a regulatory macrophage phenotype. To avoid the biasing effect of only quantifying immunosuppressive markers we evaluated Gal1 and CD163 (reported to associate with an M2 phenotype), CD40, IL23p19 (reported to associated with an M1 phenotype), IL27p28 (variably described as pro-inflammatory) and PDL1.[339,340] IL23p19 is considered a marker of M1 macrophages due to its frequent secretion as a heterodimer with IL12p40 making the cytokine IL23. However, as discussed in chapter 5, IL12p40 staining revealed minimal expression in CHL suggesting that these are secreted as monomers or in complex with other subunits forming different cytokines. It is therefore unclear if they represent true M1 markers in CHL. Microenvironmental PDL1 staining was manually scored due to its concurrent expression in CHL cells. Of note CD40 is also expressed on B cells and CHL cells but this was not adjusted for in this analysis.

Figure 4.3: Unsupervised clustering of macrophage markers

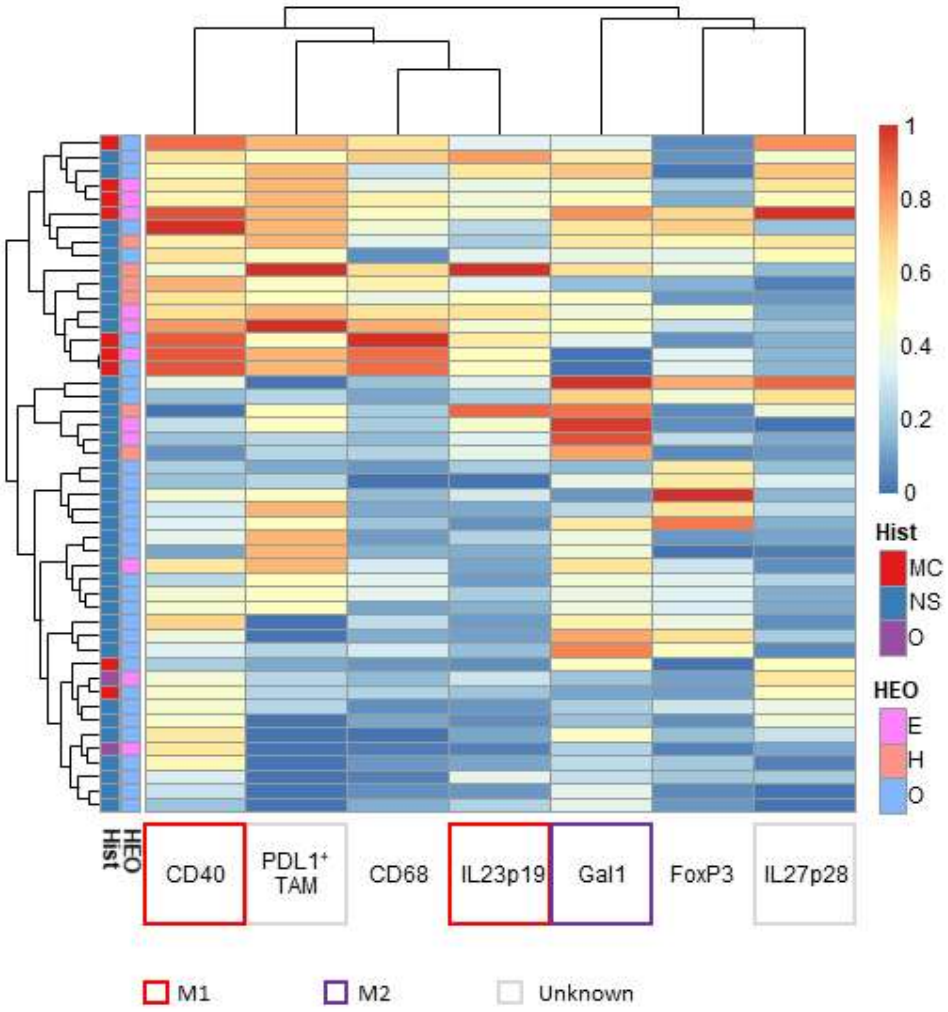

Figure 4.3: Unsupervised clustering of macrophage markers by IHC on tissue microarray associates PDL1 with CD40 and IL23p19 over Gal1 and IL27p28. EBV^+ and HIV^+ cases overrepresented in this group. FoxP3 included as T_{Reg} marker (surrogate for inducing regulatory T_H environment).

M1 = M1 macrophage marker, M2 = M2 macrophage marker, Unknown = mixed or insufficient data. HEO = Viral status: H = HIV^+EBV^+, E = EBV^+, O = EBV^-, Hist = Histological

These data associate PDL1 expression on macrophages with EBV^+ CHL (and HIV^+ which are universally also EBV^+, but also with the M1 markers CD40 and IL23p19. M1 macrophage phenotype is reportedly associated with EBV positivity in paediatric CHL.[334] IL23 receptor

upregulation has conversely been associated with EBV negative CHL.[139] As noted above IL23p19 represents an M1 marker in the context of co-secretion with IL12p40 which we did not detect in CHL. Additionally CD40 is also expressed on CHL cells and B cells. A strong positive correlation was seen between PDL1 on macrophages and CD40 (R0.75. $p<0.0001$, $n = 72$) and between PDL1 on macrophages and IL23p19 ($R = 0.54$, $p = 0.0002$, $n = 50$). The association to CD40 remained significant irrespective of viral status or histological subtype. The association to IL23p19 remained significant across histological subtypes. However, CD68, CD163 and IDO1 were similarly positively correlated to PDL1 raising the possibility that this is confounding due to macrophage frequency.

These data cast doubt as to whether PDL1 expression identifies immunosuppressive macrophages in CHL, but do not exclude the possibility. As noted above crude correlation of marker expression may be confounded by variation in macrophage frequency so marker expression intensity would be better in this regard. Additionally, it is impossible to assess whether these observations represent measurements of a single phenotype or a heterogeneous myeloid compartment. From these data we can conclude that upregulation of immunosuppressive, but also pro-inflammatory markers, is seen in the CHL myeloid environment and that marker expression appears heterogeneous between cases.

In light of these findings we next sought to characterise the spatial relationship between $PDL1^+$ macrophages and the CHL and look for evidence that macrophages are recruited and PDL1 induced by CHL cells as this would support a pro-tumour role.

4.4.2: Spatial relationships between $PDL1^+$ macrophages and CHL cells

We assessed the spatial relationship between CHL cells and overall macrophage distribution expression by multiplex IHC. A pooled distribution analysis of all samples found that macrophages were non-randomly distributed and enriched in regions of high CHL cell density (Berman test $p = <0.0001$). A uniform random sample was taken from each case to avoid over-sampling of macrophage-rich cases skewing the analysis. When examined by individual biopsy, significant enrichment was detected in 22/47 cases. Spatial enrichment was not related to EBV status, histological subtype, CHL MHC II expression, total CD68 infiltration or overall PDL1 expression. A trend towards lower $PD1^+$ lymphocyte infiltration was detected in cases with spatial macrophage enrichment ($p = 0.07$).

Figure 4.4: Spatial relationships between macrophages and CHL cells

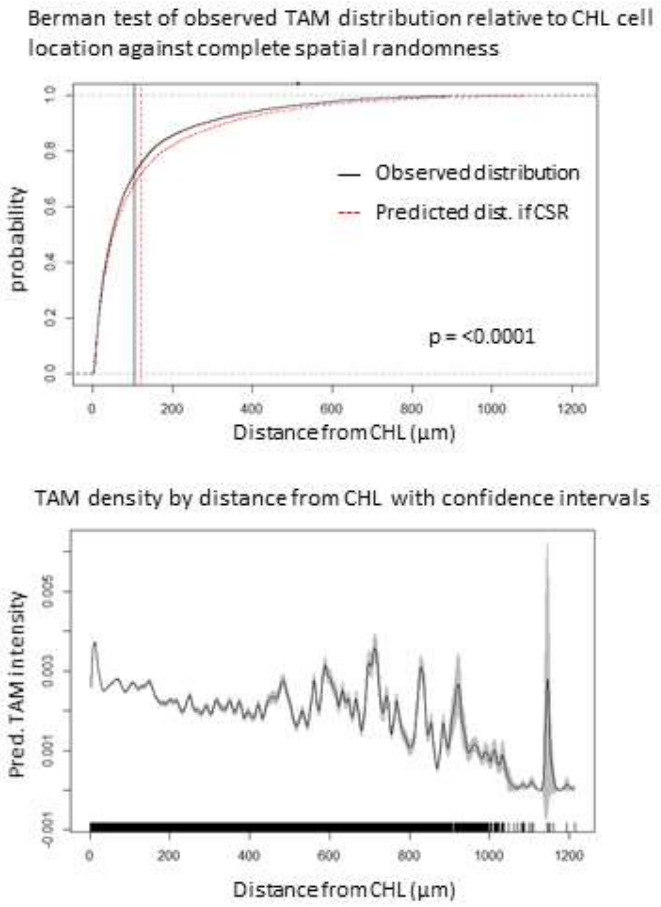

Figure 4.4: a) Berman test of spatial mIHC data in a single sample evaluating the cumulative probability of tumour associated macrophages (TAM) being located close to CHL cells as compared to the predicted distribution if their location was due to complete spatial randomness (CSR). b) rhohat model of the same sample estimating the density of TAM by distance from the CHL cell in the same sample. Variations seen at higher distances may be attributable to hidden features such as CHL cells in a different plane.

From these data we conclude that in a large proportion of cases macrophages enrich in proximity to tumour. The lack of relationship to overall CD68 infiltration is surprising but might be attributable to the tissue area used for analysis (1mm TMA cores). To perform spatial analysis both CHL rich and poor areas must be captured for comparison. It therefore possible that uniformly involved cores may not capture sufficient variation across the tumour so spatial analysis would not detect enrichment.

We next assessed the relationship between CHL cells and macrophage PDL1 expression. Macrophages were stratified by PDL1 intensity. Populations of $PDL1^{hi}$, $PDL1^{int}$, $PDL1^{lo}$ and $PDL1^{-}$ macrophages were spatially segregated from each other within the biopsy (segregation test, p = <0.05 47/47 cases). The $PDL1^{hi}$ macrophage subset was positively associated with both CHL cell density and distance from CHL cells (cumulative distribution function (cdf) test, p = <0.0001). Conversely, the $PDL1^{-}$ macrophage subset was negatively associated with CHL cell density and distance (cdf test, p = <0.0001). These findings were validated by quadrat testing:

cores were divided into equal quadrats by tumour cell density, distributions of macrophages by PDL1 expression were then compared to random labelling using permutation testing. A biological gradient was detected with PDL1 expression falling as CHL density reduced.

From these data we concluded that macrophages overall were enriched proximal to CHL regions and that within the macrophage population PDL1^{+} macrophages are enriched in areas with high CHL density and close CHL proximity. This suggests that PDL1^{+} macrophages are actively recruited and induced by CHL cells. Furthermore, the gradient of expression intensity is suggestive of induction by a secreted factor as opposed to a cell-contact based mechanism.

Figure 4.5: Quadrat testing to evaluate biological gradient of macrophage PDL1 expression

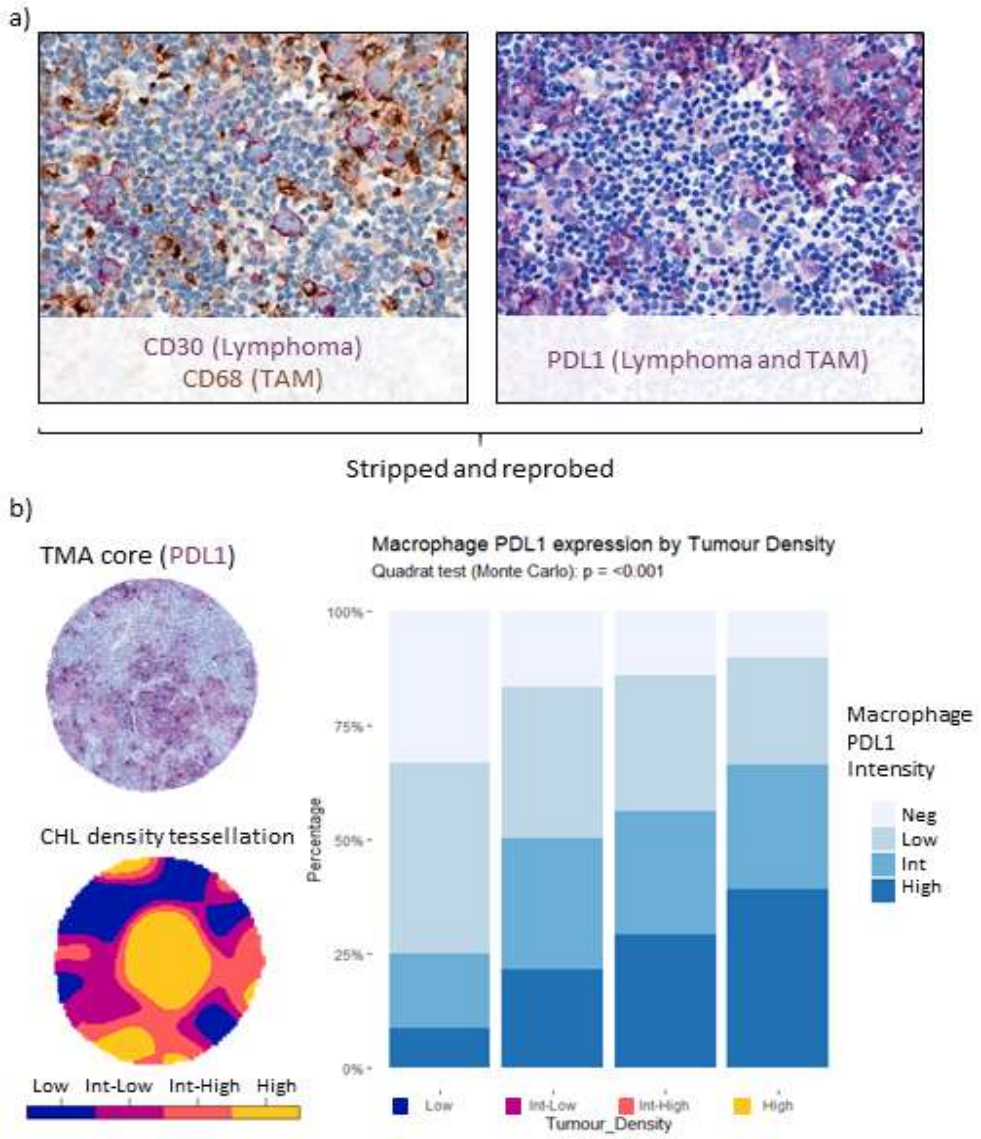

Figure 4.5: a) Dual IHC staining identified $CD68^+$ macrophages (TAM) and $CD30^+$ CHL. PDL1 intensity was measured within identified cell types by IHC stripping and reprobing. b) Tissue was divided into quadrats based upon $CD30^+$ CHL cell kernel-smoothed density (low to high). Macrophages were then classified by PDL1 expression into high (> upper quartile (UQ)), Intermediate (> median), low (> UQ of non-CHL non-macrophages), or negative (< UQ of non-CHL non-macrophages (non-CHL non-macrophage nucleated cells were PDL1 negative so the UQ of PDL1 intensity represents an internal control for background staining intensity)). Frequency of different macrophage classes were then measured within CHL quadrats. Monte Carlo permutation tests were used to assess observed macrophage distribution against random labelling. Graph demonstrates a biological gradient of reducing macrophage PDL1 intensity with lower CHL density in a single case.

4.4.3: Monocyte PDL1/PDL2 and IDO1

To confirm our hypothesis that PDL1 was directly induced in macrophages by CHL cells via a secreted factor we tested the effects of CHL cell line conditioned media on monocyte derived macrophages. PDL1 was significantly upregulated in the presence of conditioned media (three independent experiments, $p < 0.01$). In a single experiment IDO1 and PDL2 were also measured: Concurrent upregulation of PDL2 but not IDO1 was detected, however further replicates are required to test the significance of this result.

Figure 4.6: Monocyte derived macrophages upregulate PDL1 on CM treatment

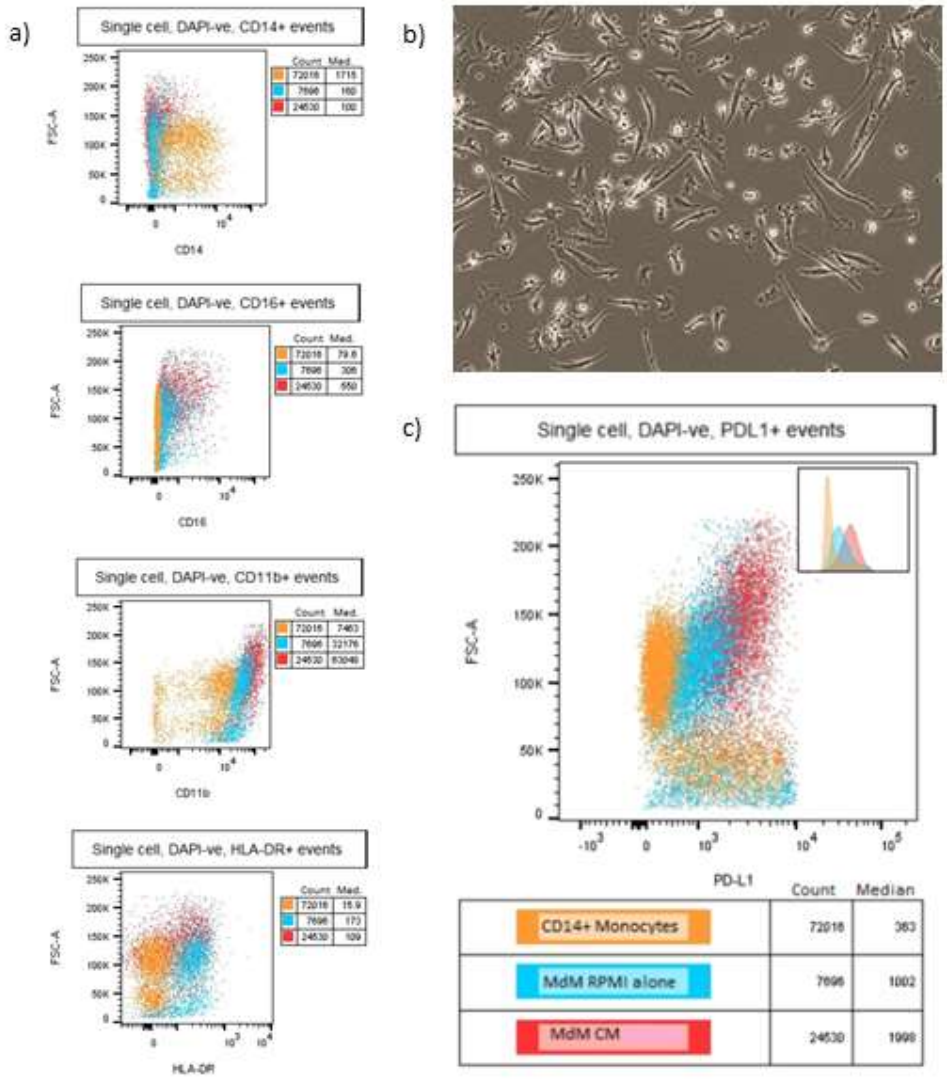

Figure 4.6: a) CD14+ monocytes downregulated CD14 and upregulate CD16, CD11b and HLA-DR on differentiation to monocyte derived macrophages (MDM) and express similar levels of these markers in the CHL cell line conditioned media (CM)-treated and control groups measured by flow cytometry. b) MDM change morphologically on differentiation *in vitro*. Image day 6 of differentiation with MCSF and GMCSF. c) PDL1 is upregulated in MDM compared to $CD14^{+}$ monocytes and further upregulated in the presence of CM

Taken together, these data suggest that macrophages are recruited to the CHL microenvironment and differentiate into a PDL1-expressing phenotype in response to factors

secreted by the CHL cell. These findings suggest that a PDL1-rich myeloid microenvironment is conducive to CHL growth. However, the association between PDL1 expression and M1 markers and correlation to both M1 and M2 markers raises questions about heterogeneity within the myeloid environment and whether PDL1 expression corresponds to an immunosuppressive macrophage phenotype in CHL.

4.4.4: Modelling the spatial distribution of myeloid subsets within a single tumour biopsy

To assess heterogeneity within myeloid subsets deep phenotyping and spatial analysis was performed on a randomly selected CHL test case analysed with a restricted Imaging Mass Cytometry (IMC) marker panel (CD14, CD16, CD163, CD68, PDL1, CD30). This represents a pilot analysis in preparation for a larger study.

Unsupervised clustering of cells across four regions of interest across the tumour identified three major myeloid phenotypes characterised by the differential expression of key markers. (Figure 4.7 section b) Clustering on individual sub-regions confirmed that the major clusters were independently identifiable across the biopsy:

- Cluster 1:
    - Phenotype: $CD14^{hi}CD16^{-}CD68^{-}CD163^{-}PDL1^{int}$
- Cluster 2:
    - Phenotype: $CD14^{+}CD16^{-}CD68^{+}CD163^{-}PDL1^{+}$
- Cluster 3:
    - Phenotype: $CD14^{+}CD16^{+}CD68^{+}CD163^{+}PDL1^{-}$

We hypothesised that myeloid cells were recruited by CHL cells from the vasculature. We therefore predicted that myeloid subtypes would vary in distribution within the tumour with differentiated macrophages localising to CHL cells and newly immigrant monocytes proximal to vessels. Given that the identified clusters mirrored phenotypes of monocyte and macrophage populations by CD14 and CD16 expression we gated by these markers into four categories (Figure 4.7 section c):

- $CD14^{+}CD16^{-}$ Classical monocytes (Cl)
- $CD14^{+}CD16^{+}$ Intermediate monocytes (I)
- $CD14^{-}CD16^{+}$ Non-classical monocytes (nC)

- $CD14^{-}CD16^{-}$ Other myeloid/macrophages (O) (expressing CD68)

The marker subsets differed by CD68 expression (upregulated in the Other myeloid (O) group), CD163 expression (upregulated in the Intermediate monocyte (I) group) and PDL1 expression (upregulated in the Classical monocytes (Cl) group and to a lesser extent the Other myeloid (O) group). (Figure 4.7 section d)

Figure 4.7: Myeloid marker and cellular distribution in a CHL case by IMC

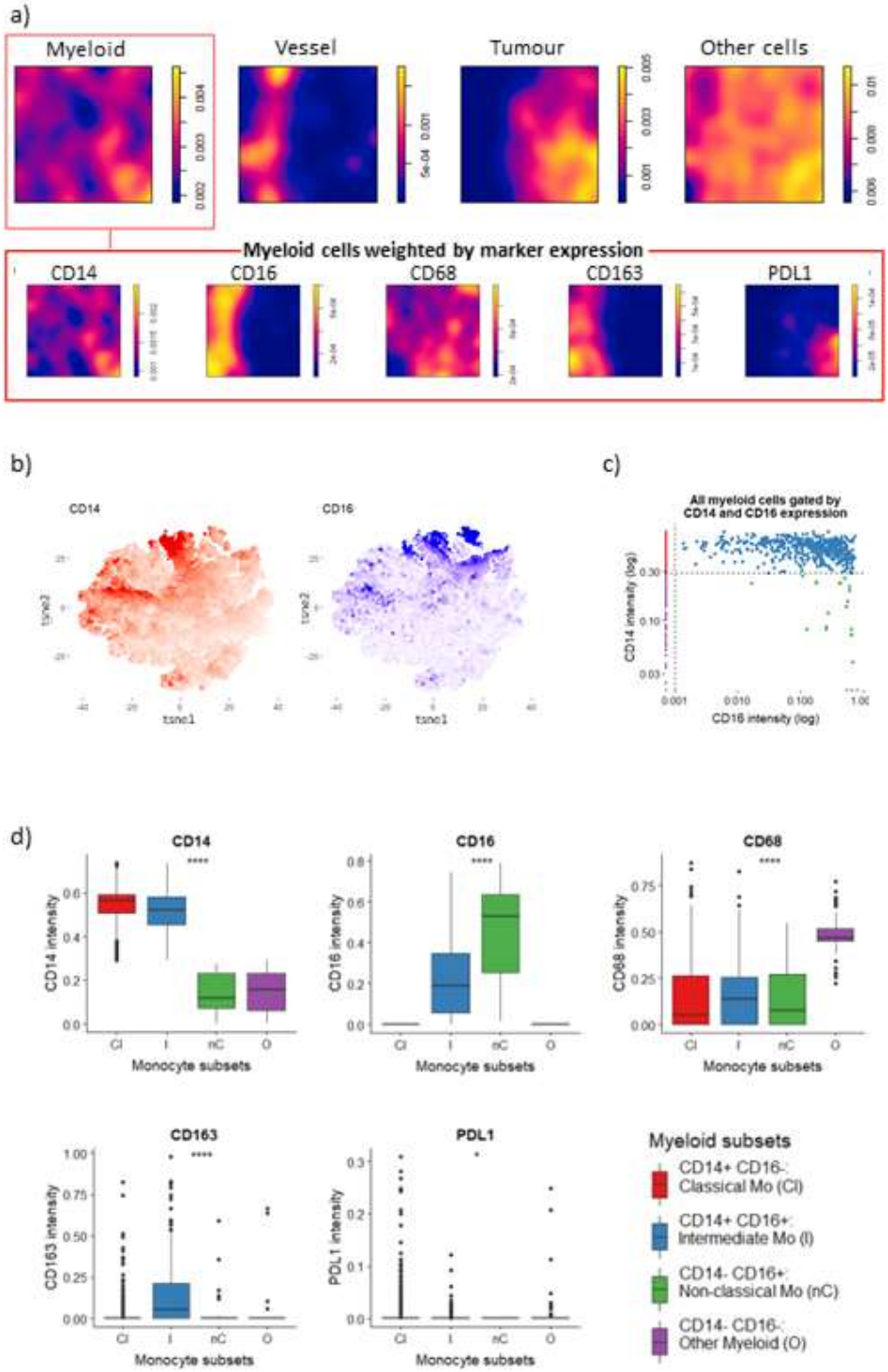

Figure 4.7: a) Cells were segmented within a single case of CHL by IMC. Individual cell intensities were calculated and cell x y locations were calculated. Cells were classified into tumour, myeloid, vessels and other. Kernel-smoothed density distribution maps were calculated of cell types within the tumour. Red box: Within myeloid cells, marker-weighted kernel-smoothed density distributions were calculated to reflect varying myeloid marker expression. b) t-SNE identification of classified cells demonstrates distinct marker expression and subpopulations within myeloid subsets. c) Cell cytometry gating of myeloid subtypes by CD14 and CD16 expression was used to separate the myeloid population into 4 biologically meaningful subsets. D) Marker intensities varied significantly within subsets gated by CD14 and CD16 expression. * = significant difference between groups by One-way ANOVA

We used edge corrected nearest neighbour analysis to assess cellular distribution. We found enrichment of the classical monocyte group and other/macrophages group in the peritumoural environment and enrichment of intermediate and non-classical monocyte groups in the perivascular region (cdf test, $p = <0.0001$ Figure 4.8 section c). We next used a distance index to evaluate whether cells were found closest to tumour, vessel or equidistant and plotted relative subset distribution, identifying a transition in myeloid subtype between regions (Figure 4.8 section a).

Figure 4.8: Myeloid subset spatial distribution

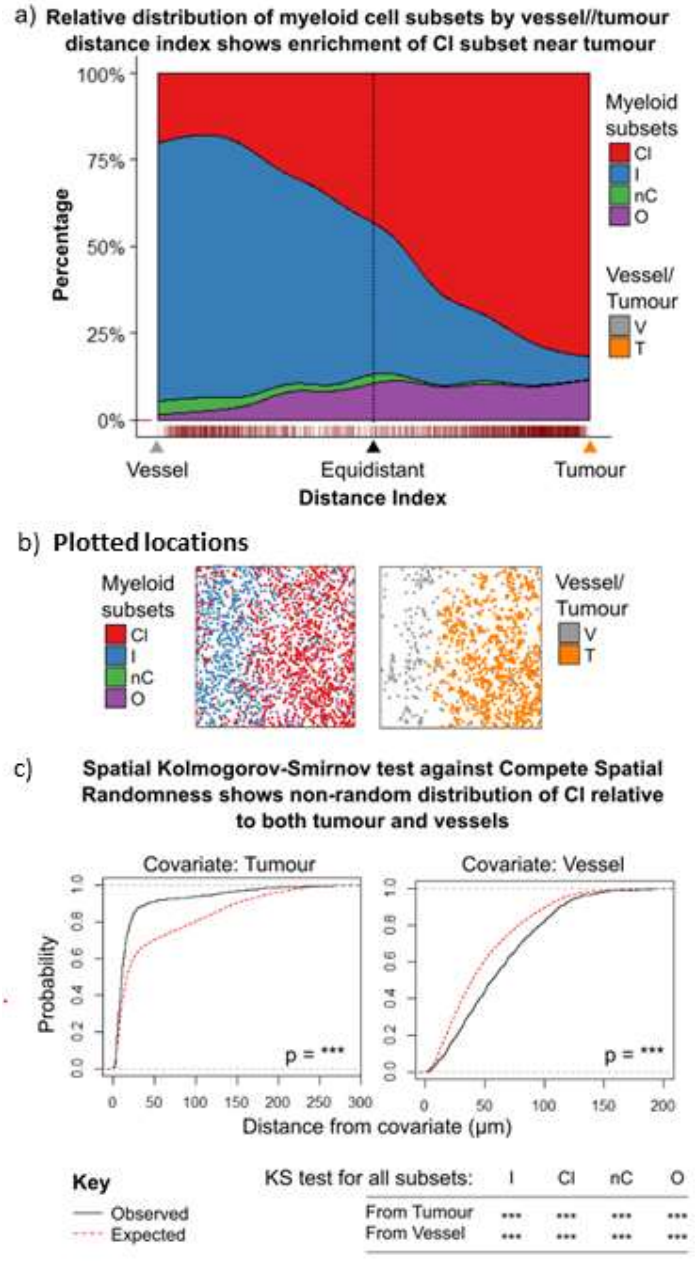

Figure 4.8: a) Relative frequency of CD14/CD16 gated myeloid subsets by distance index of relative proximity to tumour, vessel or equidistance between the two. Cl = Classical monocyte ($CD14^{+}CD16^{-}$), I = Intermediate monocyte ($CD14^{+}CD16^{+}$), nC = non-classical ($CD14^{-}CD16^{+}$), O = Other ($CD14^{-}CD16^{-}$), V = vessel ($CD31^{+}$), T = Tumour (CHL, $CD30^{+}$). b) plotted locations of myeloid subsets, vessels and tumour cells. c) Test of influence of tumour and vessel location on Cl distribution (graphed) and other subsets (table) demonstrating non-random distribution of against both vessel and tumour locations.

These data support our hypothesis of segregation of myeloid subtypes by distribution relative to the CHL cell and suggest either differential migration to the tumour by subtype (due to CHL recruitment or an immune response) or distinct differentiation of cells by proximity to the tumour. The cumulative distribution function testing described above demonstrated that both vessel and tumour location predicted subset distribution and the distance index suggests this effect may be driven by both factors, however, these tests do not assess the relative influence of each factor and cannot exclude the fact that e.g. the predictive effect of vessel location is an

artefact of vessels being found more frequently outside the tumour. To evaluate the relative contribution of each component and assess whether they are independently predictive we therefore proceeded to model myeloid cell distribution as a function of either vessel distance, CHL cell distance or both. Next, the intensity model was used to predict the expected distribution of myeloid cells based on knowledge of intensity of e.g. CHL cells alone and this was compared to the true distribution. By this approach it is possible to assess the degree to which the cellular distribution can be predicted by knowledge of the factor (e.g. CHL location). This enables the predictive power of e.g. vessel location to be quantified and compared to other factors, determining which is dominant. Furthermore, by combining the two in a composite model it is possible to determine whether a factor is redundant or adds predictive power. (Figure 4.9)

Figure 4.9: Intensity modelling of the predictive power of vessel and tumour location on myeloid subset distribution

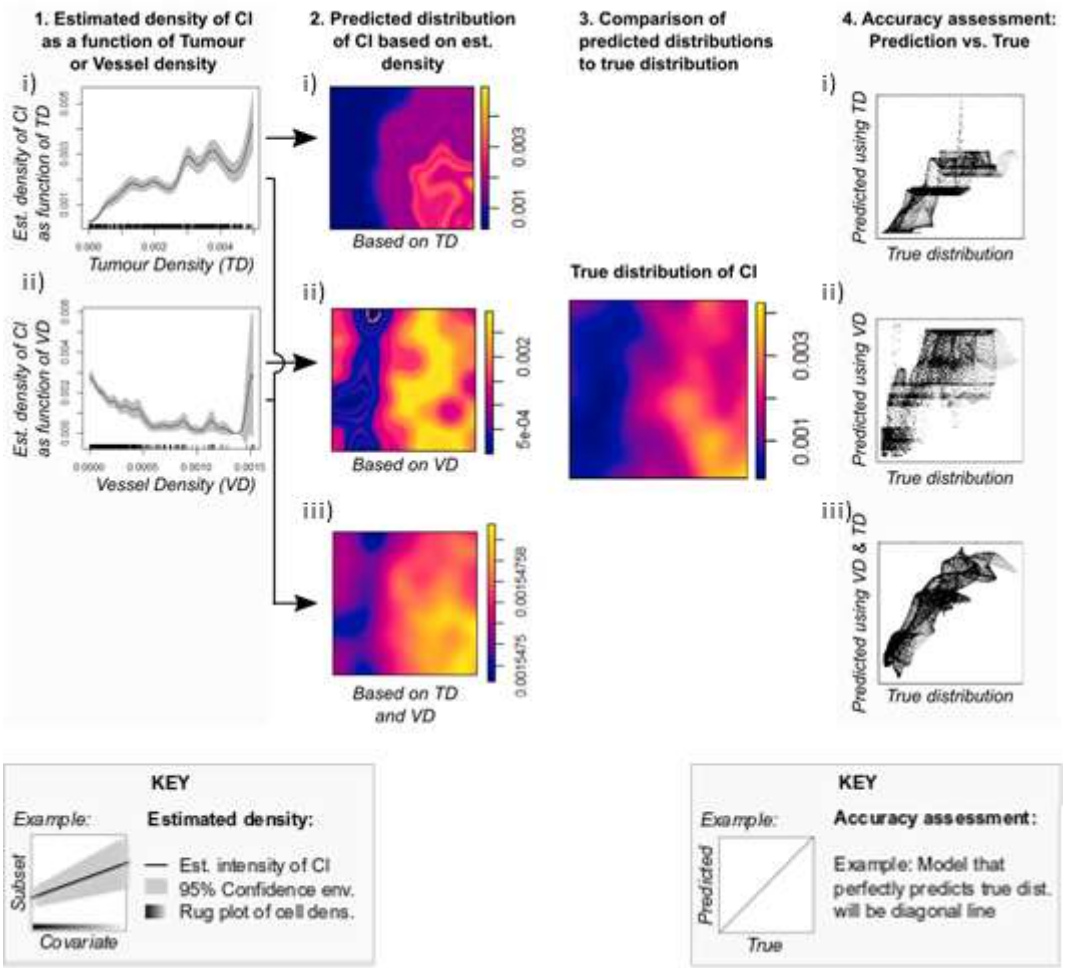

Figure 4.9: Testing the degree to which vessel and tumour distribution can explain the distribution of the Cl myeloid subset ($CD14^{+}CD16^{-}$, classical monocyte). 1. Density function of Cl against i) tumour density or ii) vessel density. Explanation of key: x axis - covariate density, y axis - predicted subset density. Line represents estimated intensity of subset by covariate density. Rug plot indicates density of cells by covariate density. This determines the grey confidence interval band which widens at low cell density (leading to the apparent prediction of high Cl numbers at high vessel density in graph 1 ii. 2. Predicted distributions of Cl subset based only on knowledge of i) tumour density, ii) vessel density or iii) both. 3. Kernel-smoothed density map of true Cl subset distribution for comparison. 4. Plots of predicted distribution against observed distribution evaluating accuracy of prediction based upon tumour or vessel density alone. Explanation of key: True distribution on x axis, predicted on y. A perfect model/prediction would be a diagonal line. Graphs demonstrate that i) CHL cell density is a relatively good predictor of Cl location at low CHL cell density but is less accurate at high density. ii) Vessel density is a generally inaccurate predictor, but does have predictive power. iii) The combination of both is superior across the range of densities but has a bias to over-prediction.

These data demonstrate that both vessel and CHL location alone have predictive power and suggest that the combination of both factors is superior to either factor alone. This suggests either differential migration by recruited myeloid subsets from vessel to tumour or changes in differentiation of recruited cells depending on their proximity to tumour.

We considered whether it was possible to assess differentiation and migration within primary tissue using spatial analysis. We hypothesised that if sufficient numbers of cells were migrating then cells should be observed upon a path between the origin point (the vessel) and the destination (the tumour) at a frequency greater than that expected by chance. We recognise that the tissue biopsy represents a three dimensional object and cells may be on a path between objects in another plane which will cause background noise and may dilute the observed effect. However, tumour infiltration is patchy and CHL cells frequently cluster which should mitigate for this. This problem would theoretically increase the chances that a true effect would not be detected but would be unlikely to lead to false positive results. We developed a trajectory path analysis which uses trigonometry to assess the proportion of cells that fall on a path between

which tests the hypothesis that if cells are being differentially recruited from one point to another within the tissue they should be found on a path between the two points on at a frequency greater than that expected at random. This also corrects a weakness of the distance index – the distance index divides a cell's distance from point A by its distance from point B to determine which point it is nearest to. However, if a cell has left point A in the opposite direction to point B it will be assigned a score similar to a cell near point A. The frequency of these cells is visible within the trajectory analysis. (Figure 4.10)

Figure 4.10: Cellular distribution relative to nearest vessel and tumour cell for individual cells

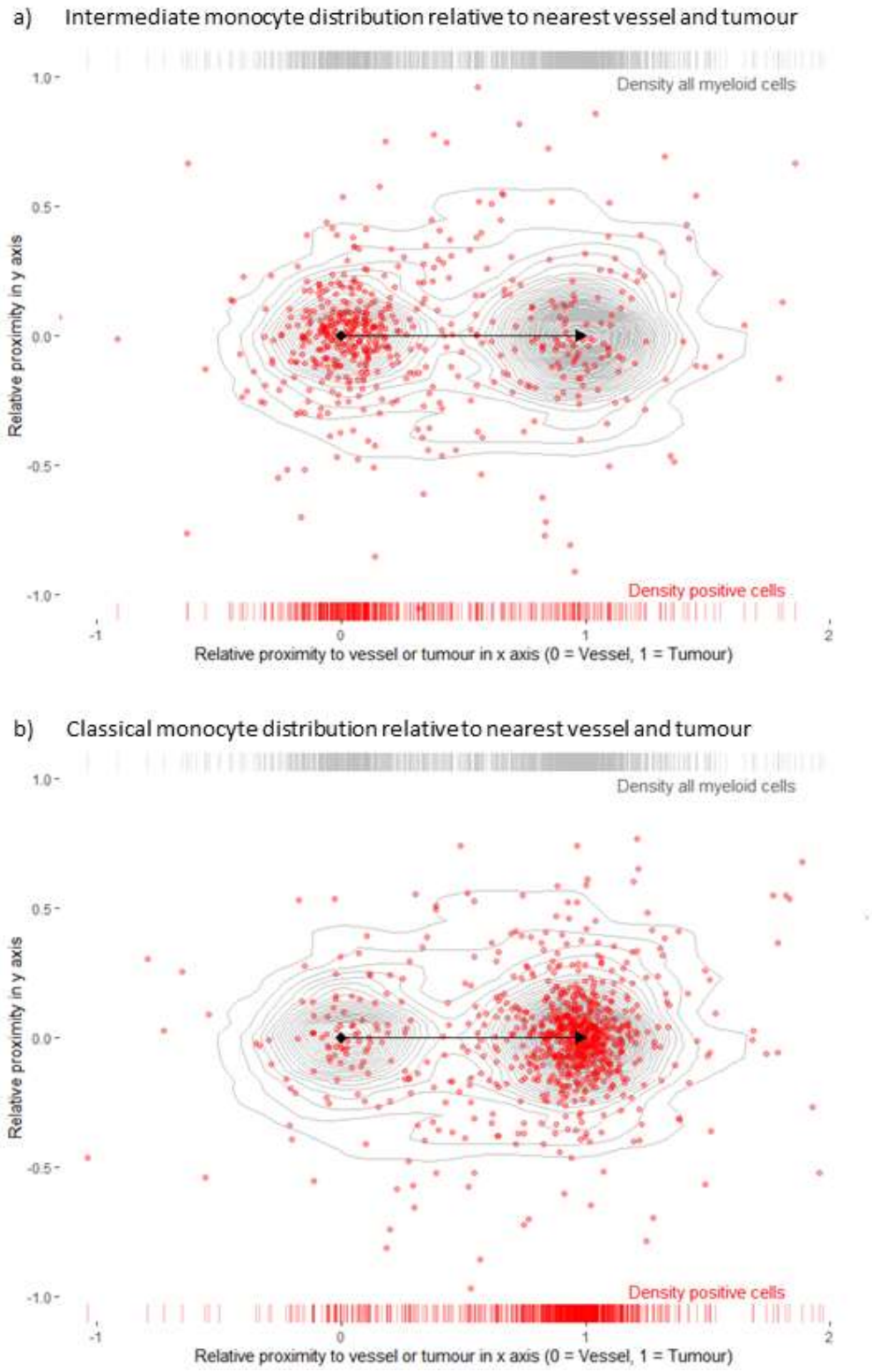

Figure 4.10: a) Distribution of intermediate monocytes relative to each cells nearest vessel and tumour cell. Cell point locations in red are determined by first calculating the triangle created by each cell and its nearest vessel and tumour cell. The triangle is then scaled and translated onto fixed vessel (0,0) and tumour (1,0) coordinates, allowing the relative cell coordinates to be calculated and plotted. This graph therefore creates a summary of the nearest neighbour relationships across the whole biopsy. The resulting distribution is compared to the distribution of all myeloid cells plotted as a density map in grey. This enables visual assessment and assessment of migration trajectory as if cells were migrating between the two points would be predicted to fall near the black arrow between origin (black dot) and destination (arrow tip) at a frequency above that expected by chance. b) Distribution of classical monocytes relative to each cells nearest vessel and tumour cell.

Graphs represent analysis by Imaging Mass Cytometry and plot individual cell locations within a single tumour biopsy.

This analysis is novel and requires further development. The data demonstrates clear clustering of intermediate monocytes by vessel and classical monocytes by tumour. There is not clear evidence of an excess of cells on a trajectory between the origin (vessel) and destination (tumour) points. To apply a statistical test requires permutation testing, comparing the observed distribution against all other possible cellular locations. We are incorporating this code. Additionally, given that cells migrate along a chemokine gradient, an adaptation to assess cell distribution against tumour density as opposed to nearest neighbour may be more appropriate as multiple cells are likely to produce greater concentrations of cytokine.

In order to assess differentiation, we combined the trajectory path analysis with assessment of individual marker intensity. We hypothesised that if fully differentiated cell types are recruited to a tumour environment no difference in lineage marker intensity would be observed in immigrant cells moving from vessel to tumour, whereas if naïve or precursor cells such as monocytes were recruited and then developed into macrophages then lineage marker intensity should change as cells immigrate to the microenvironment. This pattern would be predicted for cell types such as macrophages, where differentiation is driven by soluble factors alone, but less suitable for cells where differentiation is driven by contact-dependent mechanisms such as T cells. We predicted that we would observe a fall in CD14 expression and concurrent rise in CD68 as cells differentiated from classical monocyte to macrophage on entering the tumour microenvironment.

Amongst $CD163^+$ cells we observed a significant fall in CD163 intensity in cells proximal to tumour as compared to vessel. The same pattern was observed for cells expressing CD16. We observed a significant increase in CD68 intensity in $CD68^+$ cells proximal to the tumour. The same pattern was observed in cells expressing PDL1, but no change was seen in CD14 expression intensity amongst $CD14^+$ cells. In cells co-expressing CD14 and CD68 we observed a significant rise in CD68 expression and fall in CD14 expression consistent with our hypothesis. (Figure 4.11)

These data suggest that $CD16^+$ and $CD163^+$ cells are both less numerous in the tumour and that expression intensity of these markers falls with tumour proximity, consistent with a shift away from that phenotype. Additionally, $CD68^+$, $PDL1^+$ and $CD68^+CD14^+$ cells are both more numerous within the tumour, that CD68 and PDL1 expression intensity significantly increases with proximity and that $CD68^+CD14^+$ significantly increase CD68 expression and lose CD14 expression with proximity. In contrast $CD14^+$ cells overall are significantly more numerous but CD14 expression intensity does not change. This observation can be explained by the fact that $CD14^+$ cells are far more numerous in this biopsy than $CD14^+CD68^+$ and suggests that both groups preferentially localise to tumour but only a minority differentiate to macrophages in this case. Importantly, we conclude that intensity differs by location from this analysis, but that these cells are more numerous within the tumour due to the previous cumulative distribution testing (Figure 4.8). Whilst the graphs in Figure 4.11 do show greater numbers in the tumour region they do not account for the fact that tumour and vessel regions may make up different proportions of the biopsy.

Figure 4.11: Comparison of marker intensity against relative cellular proximity to vessel or tumour to assess changes in marker expression due to differentiation

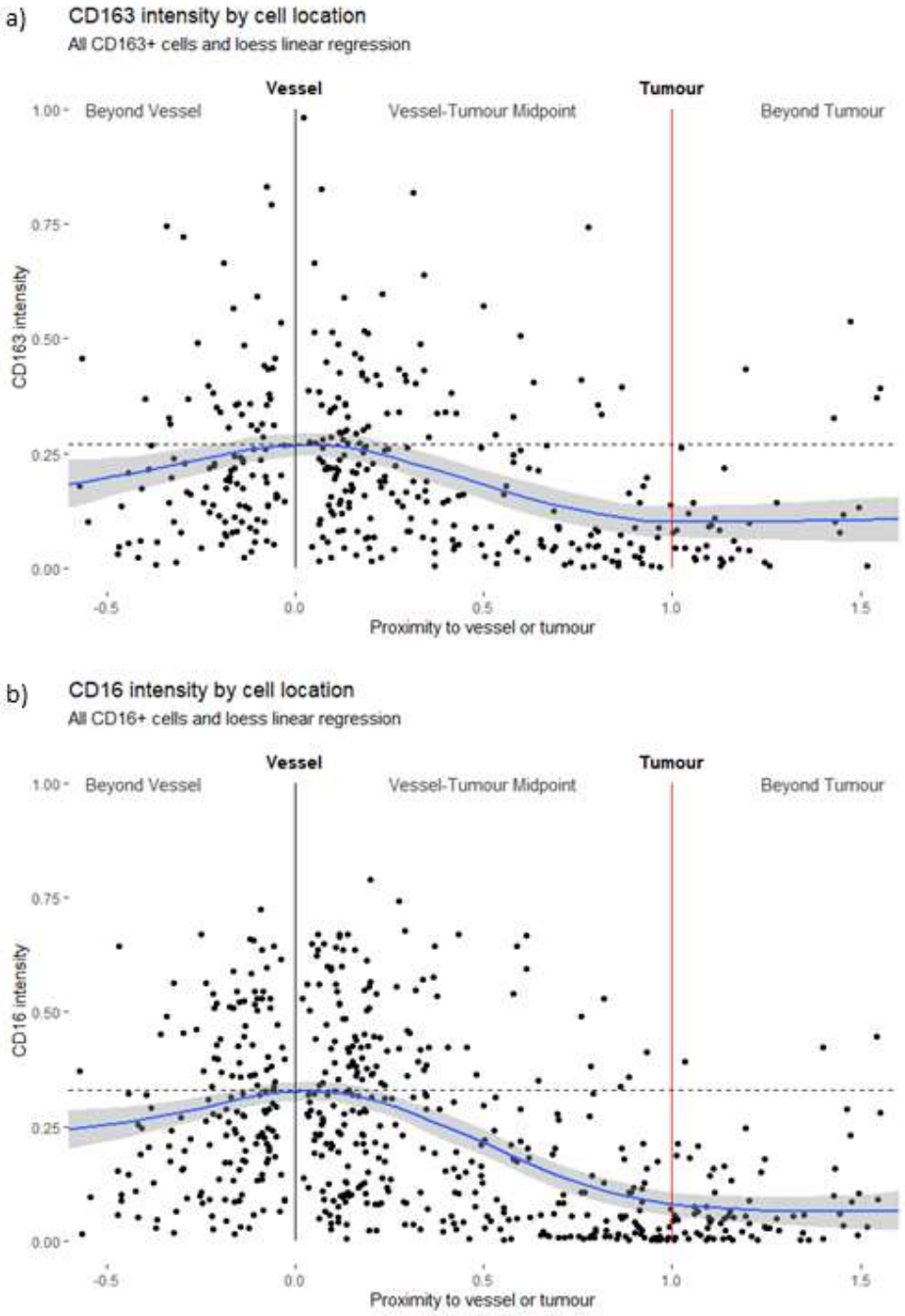

c) CD68 intensity by cell location

All CD68+ cells and loess linear regression

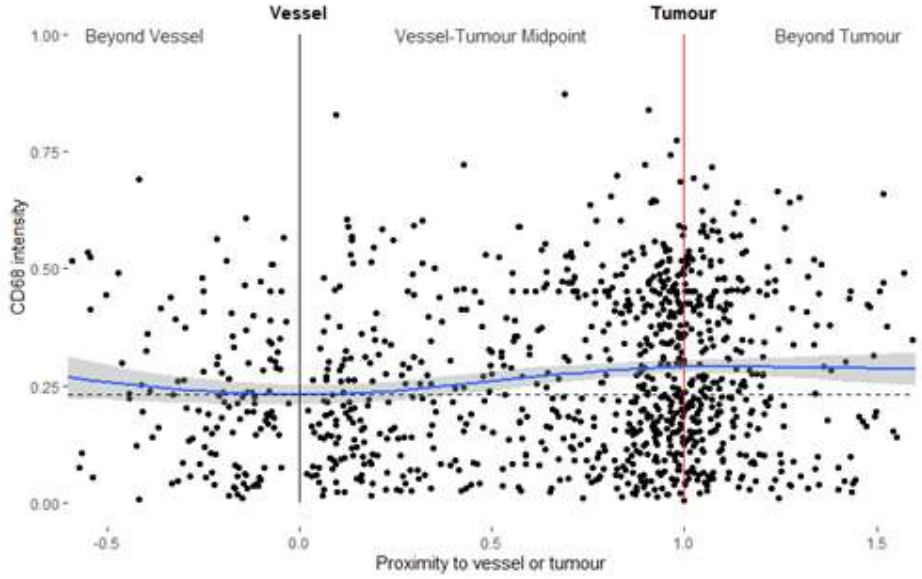

d) CD14 intensity by cell location

All CD14+ cells and loess linear regression

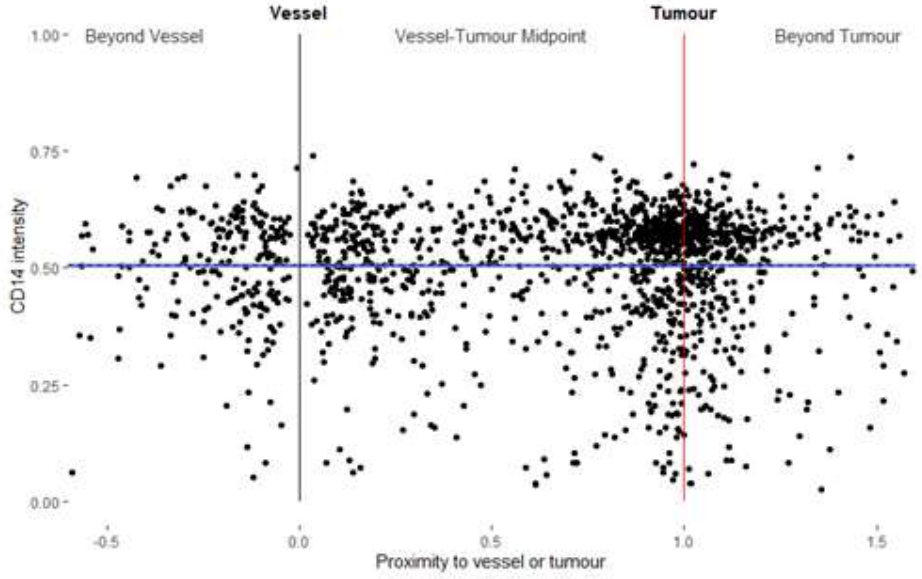

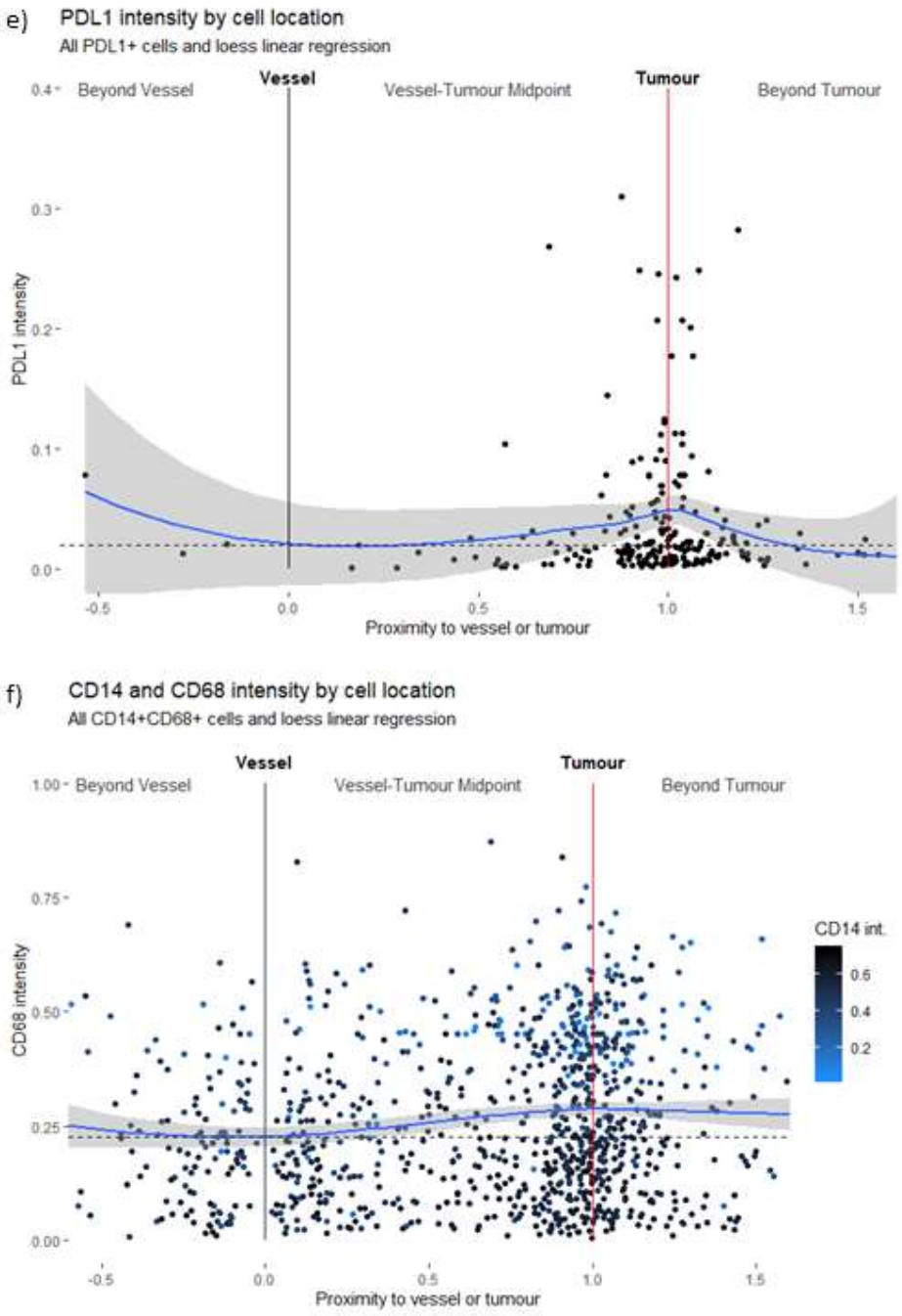

Figure 4.11: a) Individual CD163^{+} cells plotted by relative proximity to vessel or tumour against intensity of CD163 expression. Black line (0) indicates location of nearest vessel. Red line (1) indicates location of nearest tumour cell. Mid-point (0.5) indicates cell is equally close to both vessel and tumour and on a path between them. Beyond vessel (<0) or tumour (>1) indicates that a cell does not lie on a path between vessel and tumour. Blue line and confidence interval indicates loess linear regression of CD163 intensity. Black dotted line marks the intersection between the linear regression and the vessel and is provided for reference to aid comparison between regression at the vessel and tumour.

b-e) Equivalent analysis for CD16, CD68, CD14 and PDL1 respectively. f) Individual $CD14^{+}CD68^{+}$ cells plotted by relative proximity to vessel or tumour against intensity of CD68 expression and coloured by CD14 expression. Demonstrates significant increase in CD68 expression with proximity to tumour. Analysis of $CD14^{+}CD68^{+}$ cells against intensity of CD14 also confirms significant fall in CD14 expression (not shown).

All graphs represent analysis by Imaging Mass Cytometry and plot individual cell locations within a single tumour biopsy.

To improve and extend upon this analysis approach we are currently working on combining trajectory evaluation with the PHATE (Potential of Heat-diffusion for Affinity-based Transition Embedding) algorithm.[341] This algorithm can identify for transitions in phenotype by assessing multiple markers simultaneously, giving a more detailed assessment of differentiation.

In conclusion we demonstrate that within this test case several distinct myeloid phenotypes are observed that differentially associate with vessel regions and tumour. This case is characterised by $PDL1^{+}$ macrophages and $PDL1^{hi}$ CHL cells, but PDL1 expression in the microenvironment is not prominent, unlike in some other cases. Here $CD14^{hi}CD16^{lo}CD163^{-}$ classical monocytes and $CD68^{+}CD163^{-}$ macrophages are associated with both PDL1 expression and tumour proximity. In contrast, $CD14^{hi}CD16^{lo}CD163^{-}$ intermediate monocytes were PDL1 negative and excluded from tumour areas, being found proximal to vessels. Point pattern modelling demonstrated that both vessel and tumour location were predictive of myeloid subset location and that the combination of both factors was more predictive than either alone, suggesting that both play independently important roles. The trajectory analysis confirmed the findings of the spatial dependency analysis showing enrichment by subtype around vessel or tumour. This analysis did not clearly demonstrate a pattern supporting migration from vessel to tumour although this was not tested statistically as the code to perform this is still being developed. Assessment of differentiation by analysis of marker intensity by location demonstrated a fall in CD163 intensity amongst $CD163^{+}$ cells and a similar fall in CD16 intensity amongst $CD16^{+}$ cells on transition from vessel to tumour regions. Conversely on $CD14^{+}CD68^{+}$ cells CD14 intensity fell and CD68 intensity rose on transition to tumour regions consistent with monocyte to macrophage differentiation. Similarly, on $PDL1^{+}$ cells PDL1 intensity rose on transition to tumour regions. These data suggest heterogeneity and spatial segregation of myeloid subsets in CHL. Interestingly in this case PDL1 expression does not co-localise with CD163, an M2 marker, suggesting that myeloid PDL1 expression in CHL does not necessarily imply a tolerogenic or M2 phenotype. In contrast, preliminary

analysis of a second case does show co-localisation with CD163 suggesting that PDL1^{+} subsets in the CHL microenvironment may be heterogeneous across cases making conclusive statements of the role of PDL1 in the CHL microenvironment more difficult to make.

4.4.5: Functional evidence for CHL induction of immunosuppressive markers

To assess the functional impact of PDL1-expressing macrophages within the microenvironment we developed a model of macrophage priming. Monocyte-derived macrophages were differentiated from CD14^{+} donor monocytes and primed for 24 hours with CHL conditioned media. After priming monocyte-derived macrophages upregulated PDL1 ($p<0.0001$, see section 5.4.5). Conditioned media was then removed and macrophages were then co-cultured for 8 days with autologous naïve T_H in RPMI to assess the difference in antigen presentation and T cell priming. After optimisation a pilot experiment was performed across technical replicates but with only a single biological replicate. No significant differences in T_H effector differentiation were observed, although effect trends were seen. T_{Reg} overall (defined as CD4^{+}CD127^{lo}CD25^{hi}) levels were similar between CHL primed and unprimed groups. A trend to increased T_H17 cells (CD4^{+}CXCR3^{-}CCR4^{+}CCR6^{+}CCR10^{-}), fall in T_H17_{Reg} cells (CXCR3^{-} CCR4^{+}CCR6^{+}CCR10^{-}CD127^{lo}CD25^{hi}) and fall in T helper 1 regulatory (T_H1_{Reg}) cells (CXCR3^{+}CCR4^{-} CCR6^{-}CCR10^{-}CD127^{lo}CD25^{hi}) was observed in the CHL-primed group. No difference was noted in the T_H1 group. Although none of these reached statistical significance it is interesting to note given that in each case this is the opposite of what would be predicted if CHL-associated macrophages were priming T_H cells in a tolerogenic manner and suggest the inverse pattern to that seen when T_H are directly stimulated with CD3/CD28 in the presence of CHL conditioned media (see Chapter 7). These experiments deserve repeating with further biological replicates as if these trends were replicated it would go against our current understanding of the role of macrophages in T cell priming in the microenvironment.

Figure 4.12: T helper cell differentiation on co-culture with CHL conditioned media primed monocyte derived macrophages

Figure 4.12: Monocyte derived macrophages were differentiated *in vitro* before priming for 24 hours with CHL conditioned media or RPMI control. Macrophages were then washed and co-cultured with naïve T_H for 8 days before differentiation was assessed by flow. After gating to T_H cells T_{Reg} were defined as $CD127^{lo}CD25^{hi}$ and T_H1, T_H2, $T_H1/17$ and T_H17 were defined by expression of chemokine receptors CXCR3, CCR4, CCR6 and CCR10. See methods for gating

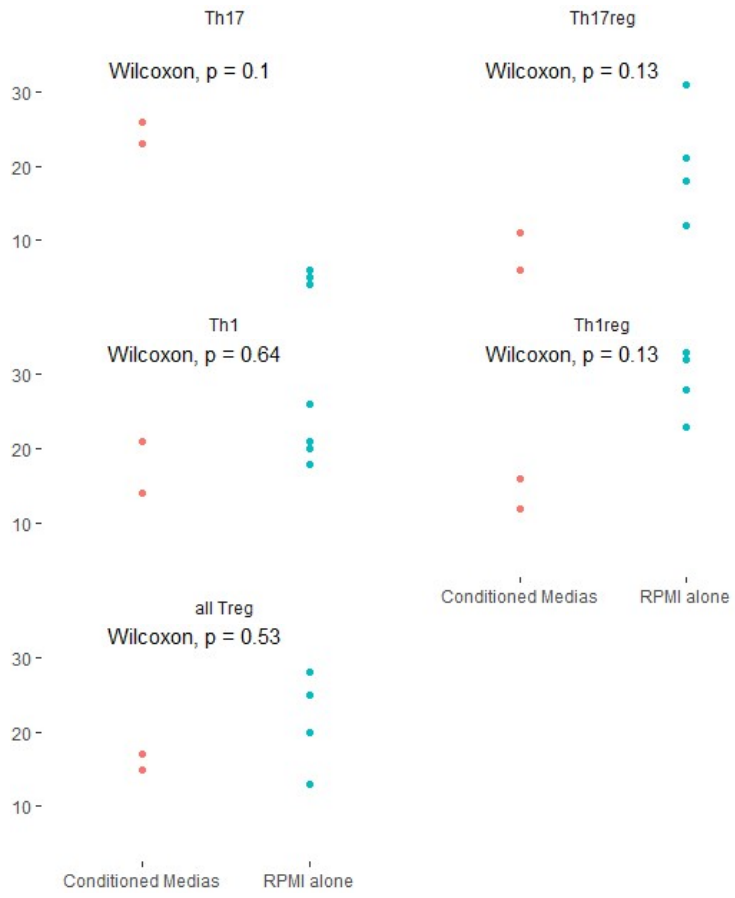

4.5: Discussion

Our spatial analysis of CD68 and PDL1 expression revealed enrichment of macrophages around CHL cells and elevated PDL1 expression on proximal macrophages. Additionally, we identified a gradient of PDL1 expression intensity with increase distance from the CHL cell suggesting induction by a CHL-secreted factor, an observation confirmed by the induction of PDL1 on monocyte-derived macrophages by CHL cell line supernatant *in vitro*. These data validate and extend the findings of Carey *et al* who reported that $PDL1^+$ macrophages were enriched around CHL cells.[159] Our findings suggest that a PDL1-rich myeloid microenvironment is conducive to CHL growth, given that $PDL1^+$ macrophages appear to be actively recruited and induced by CHL cells. An alternative explanation might be that PDL1-expressing macrophages are an anti-tumour population responding to the presence of CHL, however, this seems less

likely as if this were the case evolutionary pressure on the tumour should select for the down-regulation of mechanisms recruiting and inducing PDL1.

PDL1 expression in the myeloid environment is often regarded as identifying tolerogenic and exhaustion-inducing phenotypes. Our IHC data validate reports of high expression of immunosuppressive markers in the myeloid environment in CHL including PDL1.[157,159,166] However, they do not demonstrate clustering of PDL1 expression with other immunosuppressive markers and even demonstrate elevated expression of some myeloid pro-inflammatory markers which correlated with macrophage PDL1. This raises questions as to whether PDL1 identifies an immunosuppressive macrophage population in CHL. Similarly, deep phenotyping and spatial analysis within a randomly selected test case revealed several distinct myeloid phenotypes which differentially associated with vessel regions and tumour and interestingly in this case PDL1 expression and tumour proximity did not associate with CD163, an M2 marker. The CD163 expression seen in this case (co-expressed with CD14, CD16 and CXR3CR1 but CD68 negative) may identify intermediate monocytes as opposed to M2 macrophages.[342] This analysis was performed in a single case and, interestingly, on initial analysis of a second case PDL1 expression is again seen but the phenotype of the monocytes/macrophages differs with PDL1 positivity now seen on the $CD14^{+}CD16^{+}CXR3CR1^{+}$ subset of monocytes.

In vitro we were unable to demonstrate a clear pattern of T cell differentiation with conditioned-media priming of monocyte-derived macrophages, or in a single experiment using conditioned-media primed dendritic cells. Macrophage priming of naïve T_H cells with cytokines produces detectable differences in T_H differentiation in other contexts, validating the model concept and positive controls with T_H17-differentiation cytokines and LPS showed modest changes consistent with their expected effects.[343] It is possible that the conditioned media was not sufficient to prime the macrophages, although when testing the effects of conditioned media alongside CD3/28 stimulation it was sufficient to promote T_{Reg} differentiation (see chapter 7). Additionally, the media promoted PDL1 upregulation on macrophages suggesting phenotypic differences. Alternatively, it is possible that PDL1 expression in this context is not related to immunoregulatory T cell priming but serves another function such as a “don’t eat me“ signal.[336]

Together these data highlight that whilst PDL1 expression may be a common feature of the CHL myeloid environment the functional implications of microenvironmental PDL1 expression are not yet clear and may vary between cases. It is difficult to interpret this in the context of CHL, which is further complicated by the expression of PDL1 both in the microenvironment and on the malignant cell, which itself expresses proteins consistent with antigen presenting

capacity. One study suggests that despite the fact that the majority of PDL1 expression in CHL is microenvironmental, it is CHL PDL1 expression that is most predictive of PD1 inhibitor response.[133] The functional impacts of CHL PDL1 vs microenvironmental expression are hard to separate but are further assessed in chapter 7.

4.5.1: Further work

The functional macrophage priming model did not demonstrate a clear effect of CHL supernatant on T cell priming despite leading to PDL1 upregulation. The first experimental iteration did demonstrate both T_H17 suppression and increased T_{Reg} differentiation. Further experiments used a different batch of conditioned media. To exclude the possibility that batch differences have affected the results it should be repeated using a single batch of media across all replicates or in transwell. Additionally, further phenotyping of primed monocyte-derived macrophages for changes consistent with an M1 or M1 phenotype would be of benefit. Finally, it must be recognised that cell lines are related to a single biological replicate and there is significant intra-disease heterogeneity. It is also therefore important to expand the imaging mass cytometry cohort to assess inter-case heterogeneity amongst PDL1-expressing myeloid cells.

The next chapters will assess IL27, a putative mechanism of microenvironmental PDL1 upregulation in CHL followed by evidence for PDL1 inducing exhaustion in CHL and other possible influences of the PD1/PDL1 axis.

4.5.2: Spatial analysis methods

The spatial analysis approaches used in this chapter represent novel applications of techniques to multiplex imaging data. Additionally, the approaches used in 4.4.2.2b (a), 4.4.2.2d and 4.4.2.2e, alongside the spatial dependency analysis in 7.4.4.2 are entirely novel and developed as part of this PhD. These approaches lend statistical strength and flexibility to current commonly used techniques. Publications to date frequently use comparison of average nearest neighbour distance above or below an arbitrary distance (e.g. 75 µm) from the tumour cell.[159] Some extend these techniques to include random labelling testing for cell-cell contact.[344] The approaches outlined here have a series of strengths over more commonly used approaches. These include assessment of effect gradient over distance and adjustment for cellular density other factors such as distribution of a parent population. They also make the separation of

spatial and phenotypic effects more straight forward and can identify subtler distribution relationships that may not be obvious by eye. Furthermore, it enables the testing of the relative influence of multiple factors simultaneously through the building of mathematical models and assessment for hidden features.

These tools are particularly suited to the assessment of secreted factors where effect gradients rather than cell-cell contact are relevant. Predicting the influence of a secreted factor is complex in tissue and this is a novel way of approaching the problem. Cytokine diffusion distance is a function of a number of factors including cytokine molecular weight, tightness of cell-cell junctions, cellular consumption and whether the cytokine is broadly secreted or released in a directional manner within an immunological synapse.[345,346] The effects of cytokines can be modelled *in vitro* but there is no current system that effectively capture the dynamics of cytokines within human tissue at a cellular level. The ability to assess the strength and radius of effect is important in assessing whether an observation is not just detectable *in vitro* but biologically relevant in primary tissue. This approach can therefore provide valuable additional information to inform *in vitro* cytokine studies.

Chapter 5: EBI3 and IL27: A putative mechanism for CHL immune evasion and microenvironmental PDL1 upregulation

5.1: Introduction

Multiple mechanisms have been identified to explain the upregulation of PDL1 in CHL cells.[20,140,269] However, much of the observed PDL1 expression is within the microenvironment on tumour associated macrophages and our understanding of the factors inducing PDL1 expression are limited. A candidate mechanism is via secretion of the cytokine subunit EBI3, which is recognised to be markedly upregulated and secreted in the majority of CHL cases but its biological role in this context is currently poorly defined.[270,347]

The IL6/IL12 superfamily cytokine are predominantly produced by antigen presenting cells and play a prominent role in T_H cell biology with different members promoting differentiation to different effector subtypes (see figure 1.3.2.4.2). Furthermore, once differentiate T_H17 in particular display plasticity and the ability to shift to either T_H1 or T_{Reg} depending on the cytokine environment.[223,225] Here again the IL6/12 family and particularly IL27, IL23 and IL35 are central. Some cytokines have a pro-inflammatory role. IL12 promotes differentiation towards T_H1 whereas IL6 and IL23 promote differentiation towards T_H17 cells.[348,349] Others such as IL35 are anti-inflammatory, skewing T_H development from T_H17 to T_{Reg}. IL27 is an interesting cytokine with mixed anti and pro-inflammatory roles. It has anti-inflammatory effects in the myeloid compartment, promotes the differentiation of T regulatory 1 (T_R1) cells (a $FOXP3^-$ T_{Reg} with IL10 as its major effector cytokine) and suppresses differentiation of T_H17.[350–352] However, unusually, it suppresses T_H17 by promoting a skew towards the T_H1 phenotype and increasing T_C activity which has led some to regard it as pro-inflammatory.[353] Novel cytokine family members such as IL39 are recently described and their roles poorly defined and still further theoretical subunit pairings have activity *in vitro* but are yet to be detected in humans.[354–357]

Each cytokine is a heterodimer, made up of an α and a β subunit. In reports to date single cells produce both an α and a β subunit and secrete as a heterodimer, but interestingly the subunits are independently regulated at a transcriptional level.[358] The α subunits are relatively broadly transcribed whereas the β subunits are more tightly controlled. Additionally, it is binding to the two major β subunits identified to date (IL12p40 and EBI3) which appears to determine whether the resulting heterodimer has pro or anti-inflammatory action. This promiscuous

sharing of subunits between family members makes the deciphering the global activity of individual cytokines *in vivo* difficult as a knock-out model will inevitably affect more than one cytokine. This is further complicated by the cytokines engaging heterodimeric receptors which also share subunits.

Figure 5.1: The IL6/IL12 cytokine superfamily

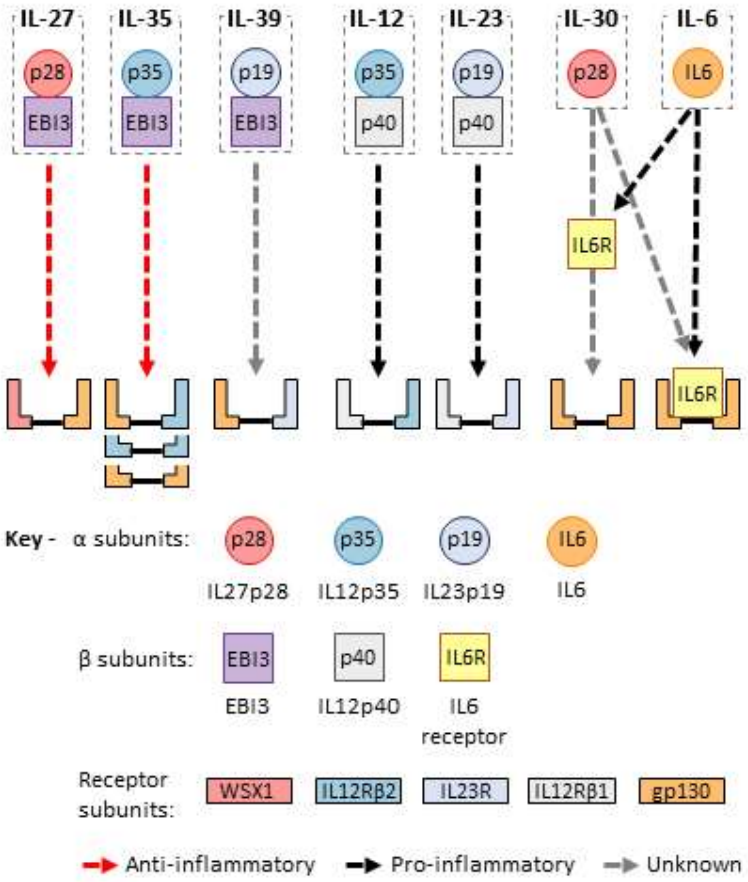

Figure 5.1: Multiple cytokine family members are formed from the promiscuous partnering of a series of alpha and beta subunits. Similar promiscuous partnering is seen among receptor heterodimers. Subunits can form pro or anti-inflammatory cytokines depending upon their partners. Transcriptional regulation of subunits is independent of each other.

EBI3 is interesting cytokine in the context of CHL as it provides a mechanism of T_H17 suppression, T_{Reg} induction and PDL1 upregulation that is directly linked to the CHL cell. EBI3 expression is a consequence of CD30 and CD40/EBV-LMP1 signalling via the upregulation of NFκB, a central survival pathway for CHL cells.[359,360] EBI3 expression is identified in CHL and CHL cell lines by ELISA, western blot and IHC and is consistently identified by gene expression

of microdissected tissue.[270,361] Evidence points to monomeric EBI3 secretion in CHL unlike in normal tissue where it is usually secreted as a heterodimer.[359] The biological function of monomeric EBI3 secretion is not well understood although it has now been reported in a number of cancers. [350,362] Unlike IL12p40, EBI3 does not bind to its subunits covalently making its association weaker.[359,363,364] It is capable of associating with its α subunit in solution and a recent study in DLBCL demonstrated the induction of IL27p28 in monocyte derived macrophages leading to IL27 formation, which in turn led to PDL1 upregulation in a STAT3-dependant manner.[350] Cytokine subunits can be independently secreted and whilst active secretion of p35 monomer is not reported it is constitutively expressed at low levels across a wide range of cell types and can be released on cell death where it forms active heterodimers in solution.[365,366] This is reported in the context of recombination with IL12-p40 to form the pro-inflammatory IL12. Monomeric EBI3 secretion might therefore allow the lymphoma cell to subvert an otherwise pro-inflammatory stimulus to create IL27 and IL35. Skewing of a cytokine environment in solution in this manner would represent a novel category of immune evasion mechanism and an interesting way in which a malignant cell could reshape an anti-tumour myeloid response into one that was conducive to tumour growth. Additionally, EBI3 inhibition might be attractive as a therapeutic target given that monomeric secretion is currently only reported in malignancy.

Figure 5.2: Proposed disease model

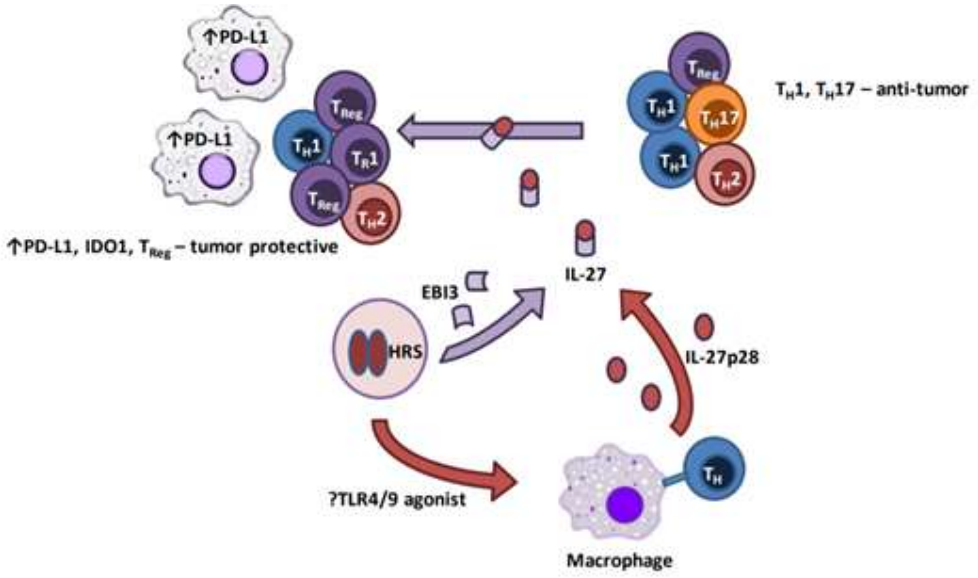

Figure 5.2: Proposed mechanism of CHL immune evasion by production of EBI3. Tumour associated macrophages produce IL27p28 due to an unknown factor produced by CHL cells. In isolation this has an anti-tumour role. Monomeric EBI3 secreted by CHL cells associates with IL27p28 in the microenvironment to form pro-tumour IL27, promoting the conversion of T_H17 to T_H1 and T_R1 (IL10 producing T_{Reg}) and the upregulation of PDL1 and IDO1 microenvironmental macrophages, which in turn promote T_{Reg}. This model is consistent with high levels of PDL1, T_H1 and IL10 but low levels of T_H17 observed in CHL.

5.2: Aims and Objectives

5.2.1: Aims

To evaluate evidence for the formation of IL27 from CHL-derived EBI3 within the microenvironment.

5.2.2: Objectives

1 Confirm the expression and secretion of EBI3 by CHL cells.
2 Evaluate the expression of α subunit partners to EBI3 in CHL cells and within the microenvironment.
3 Confirm the presence of formed heterodimeric cytokines and evidence for their effects.
4 Functionally validate findings within an *in vitro* system.

5.3: Materials and Methods

5.3.1: Immunohistochemistry

For validation approach summary and assessment of confidence in individual antibody specificity see section 2.2.2.

Due to limited availability of antibodies to the targets in this chapter antibodies with less robust validation data were used. Of note, three EBI3 antibodies were validated with notable differences in staining pattern (Figure 5.3). It is unclear if the signal one of these antibodies represents clean but off-target staining or whether they bind EBI3 in different configurations (e.g. bound/unbound forms). No clear difference is evident as regards to choice of immunogen and the company was unable to provide an explanation. All antibodies gave positive signal in placental trophoblast tissue (a biological positive control). Antibody 1 (Atlas) was selected for study due to data consistency with published studies using other modalities.[270,347] Antibody 2 (Novus) was published by multiple studies, none providing validation and all describing in novel tissues or settings for EBI3. A third antibody was validated that gave an overlapping staining pattern. Antibodies to IL27p28, IL12p40 and IL12p35 were validated. IL27p28 and IL12p40 gave clean and specific signal but extended validation data was not available. IL12p35 failed validation.

Figure 5.3: EBI3 Antibody specificity

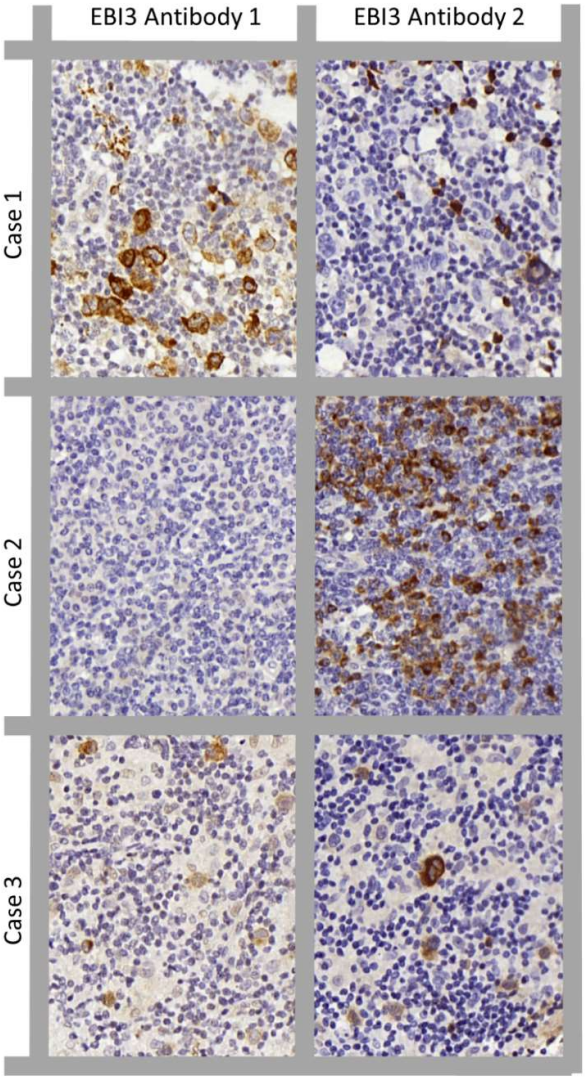

Figure 5.3: Case by case comparison of two EBI3 antibodies by IHC with clean but inconsistent signals. In case 1 antibody 1 marks CHL cells (documented to express EBI3) whilst antibody 2 marks only background cells. In case 2 antibody 2 strongly identifies background cells but antibody 1 shows only weak signal. Both mark CHL in case 3. This may represent off-target signal by one antibody or different conformations of EBI3 e.g. monomeric EBI3 vs hetero-dimerised.

Antibody 1 = Atlas EBI3 1:500 (extensive validation data, consistent with literature, 0 publications)

Antibody 2 = Novus EBI3 15k8D10 1:100 (No validation data, 7 publications)

5.3.2: Proximal Ligation assay

For method see 2.2.7. The proximal ligation assay requires antibodies raised in different species (i.e. one mouse and one rabbit). The antibodies to EBI3 and IL27p28 used in the IHC single marker studies were both raised in rabbit. As a result, the Novus EBI3 antibody raised in mouse was used.

5.3.3: *In vitro* model

Figure 5.4: Overview of in vitro model

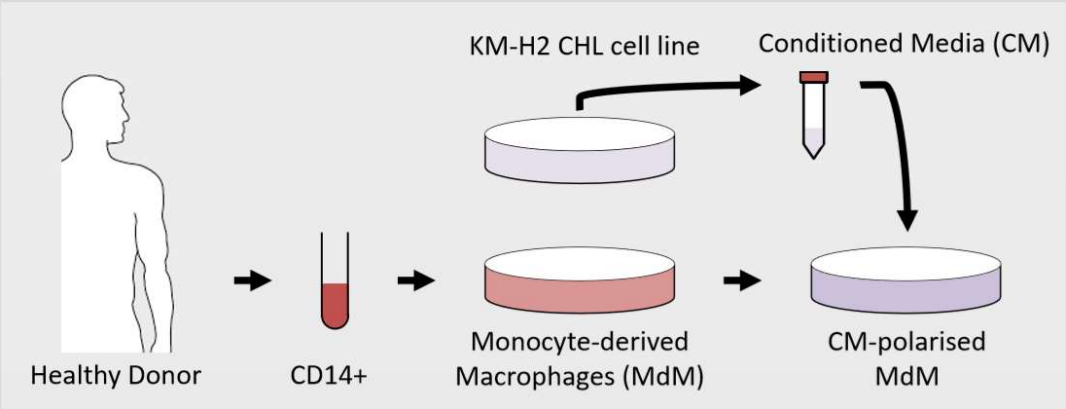

Healthy donor PMBC were positively enriched for monocytes with CD14 bead and differentiated to macrophages *in vitro* with MCSF and GMCSF (see 2.4.6). Monocyte derived macrophages were treated for 24 hours with CHL cell line conditioned media with or without the addition of inhibitors before harvest. TLR4 inhibitor (LPS-RS ultrapure, Invivogen, cat. tlrl-prslps), TLR9 inhibitor (ODN TTAGGG, invivogen, cat. tlrl-ttag151), RIG1/TLR3 inhibitor (0.1uM, BX795, sigma), MYD88 inhibitor (50 uM, Pepinh-MYD, Invivogen, cat. tlrl-pimyd). PDL1 expression was measured by flow cytometry.

5.4: Results

To functionally test the hypothesis that IL27 (formed in solution by CHL-secreted EBI3 and macrophage-secreted IL27p28) induced PDL1 upregulation we evaluated expression in tissue and sought to model the interaction *in vitro*.

5.4.1: Single marker IHC assessment of IL27 cytokine components

IHC staining confirmed EBI3 staining of CHL cells in the majority of cases. IL27p28 and IL23p19 (forming anti-inflammatory IL27 and novel cytokine IL39 with EBI3) stained positive in microenvironmental macrophages at levels above that seen in RLN ($p<0.001$) and in CHL cells in a small minority of cases and stained positive in the microenvironment. EBI3 H score correlated positively with IL27p28 intensity but not with IL27p28 area stained. The other potential cytokine subunit partners of IL12p35 (forming anti-inflammatory IL35 with EBI3) was

not assessed due to poor antibody quality. IL12p40, the alternate β subunit partner of IL12p35 and IL23p19 (forming pro-inflammatory IL12 and IL23) was identified in rare cells in CHL tissue but was absent in macrophages and CHL cells.

Stripping and reprobing of EBI3/IL27p28 and IL12p40/IL23p19 in CHL and RLN tissue confirmed infrequent dual expressing cells in RLN tissue but dissociation of expression in CHL cells and macrophages in CHL. These data are consistent with a hypothesis whereby EBI3 is secreted by CHL cells and a further unidentified factor stimulates the secretion of IL27p28 by macrophages within the microenvironment. IL27 is then formed in solution within the microenvironment, skewing the potentially anti-tumour effects of IL27p28 monomer secretion to pro-tumour IL27 and contributing to PDL1 upregulation. Because of promiscuous subunit partnering it is not possible to establish the presence of IL27 by demonstrating the presence of its constituent parts, only by demonstrating the presence of the formed heterodimer.

Figure 5.5: EBI3 and IL27p28 expression by IHC

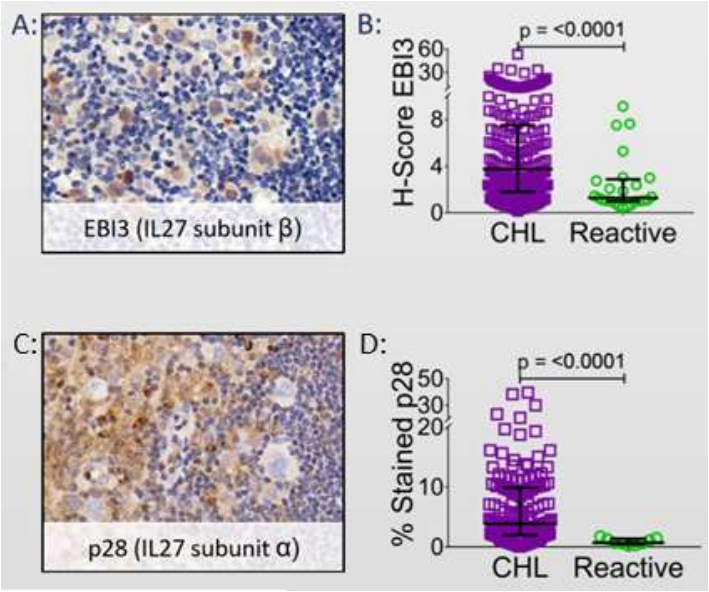

Figure 5.5: A + B) IL27 β subunit EBI3 is expressed in CHL cells but not the microenvironment above levels seen in RLN. C + D) IL27 α subunit IL27p28 is expressed in microenvironmental cells but rarely in CHL cells at levels above that seen in RLN tissue. Analysis by IHC on TMA. Comparison by Mann-Whitney

5.4.2: Assessment of IL27 heterodimer by sandwich ELISA from FFPE-extracted protein

Protein was extracted from tissue rolls of FFPE biopsy sections. Measurement of cytokine concentrations from FFPE protein extracts by ELISA based methods is novel. The method was validated against paired fresh frozen tissue as described in section 2.6. Heterodimeric IL27 was not detectable by ELISA from FFPE extracts, or in biological controls (placenta). This could be

due to crosslinking during fixation, loss of secreted proteins during fixation or insufficient concentrations recovered in starting material. Additionally, the bonding in the IL27 heterodimer are non-covalent leading to a higher risk of dissociation in tissue or during the extraction process. This may represent true absence of the cytokine but it is hard to be confident of this without signal in positive controls.

5.4.3: Assessment of IL27 heterodimer by proximal ligation assay in FFPE tissue

The proximal ligation assay gives signal when two antibodies of different species mark a target in close proximity to each other, therefore theoretically giving signal when EBI3 and IL27p28 are present as a heterodimer but not as individual subunits.

Figure 5.6: Proximal ligation assay

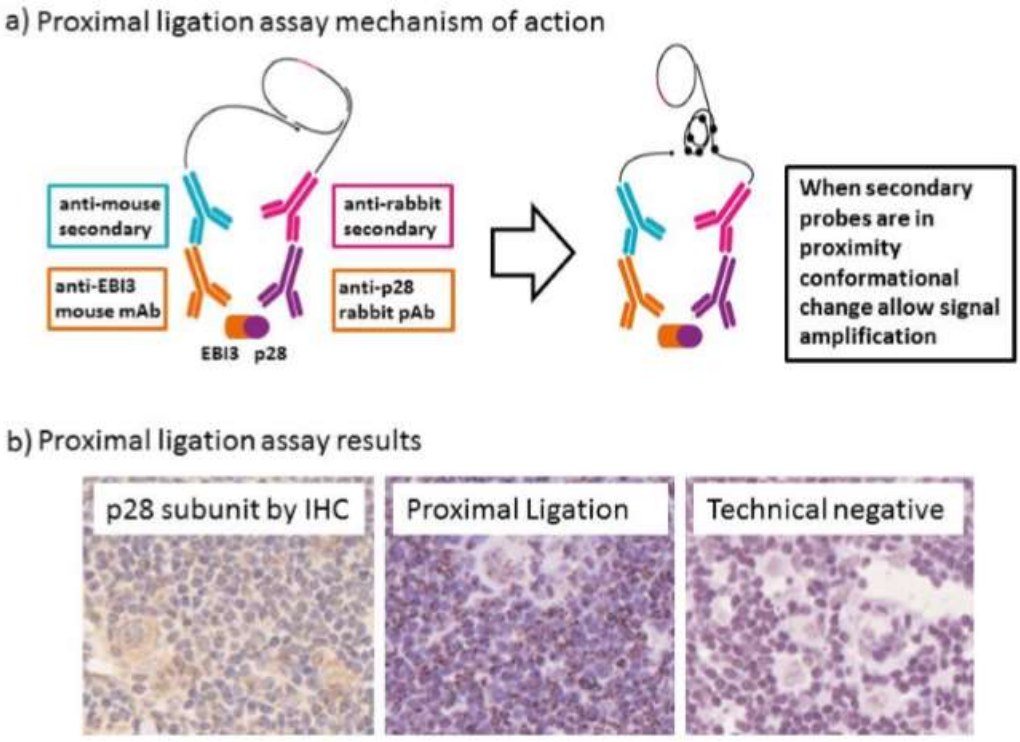

Figure 5.6: a) Primary antibodies to targets (EBI3 and IL27p28 – α and β subunits of IL27) from different host species (mouse and rabbit) bind to target. Hybridisation reaction occurs when species-specific secondaries bind in close proximity to each other, giving signal. b) Positive signal for IL27 in CHL tissue. No signal in the same tissue technical negative control.

Signal was detected in some but not all CHL tissue and was absent from the manufacturer-advised technical negative control (omission of one primary antibody). However, low level signal was also detected in heart tissue (a biological negative control) and signal was not consistently detected in placental tissue (a biological positive control). No correlation was observed between levels of proximal ligation assay signal and either EBI3 or IL27p28 subunit expression. These data led us to add a further control – pairing anti-mouse EBI3 with anti-rabbit CCL5. These two cytokines are both produced at high levels by CHL cells but do not associate with each other. This control also gave signal and despite multiple validation experiments we were unable to optimise the assay in a manner where we were confident of signal specificity. No conclusion could therefore be made on the presence of IL27, and the need for additional controls over and above those recommended by the manufacturer was highlighted.

5.4.4: Assessment of IL27 subunits in an *in vitro* model by western blot

We confirmed the presence of EBI3 in CM by western blot. Western blotting also detected a band consistent with IL27p28 induction in MDM lysates, although in lysates signal strength was weak so can only be regarded as tentative confirmation and this was not validated in a second experiment using a second CM batch. The detection of EBI3 by western blot was validated over three independent experiments. Western blots were performed in non-reducing conditions.

Figure 5.7: EBI3 and IL27p28 by western blot

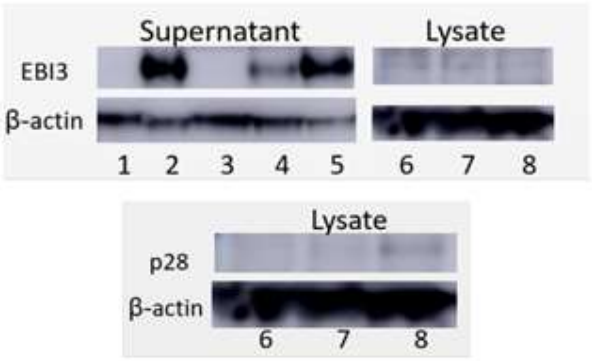

Figure 5.7: A) IL27 β subunit EBI3 in supernatants (sup.) and lysates of Monocyte-derived macrophages (MdM) treated for 24 hours with CHL cell line conditioned media (CM), B) IL27 α subunit IL27p28 in CM-treated MdM lysates. Key: 1. Control: RPMI, 2. CM, 3. RPMI-treated MdM sup., 4. 50% CM-treated MdM sup., 5. 100% CM-treated MdM sup., 6. RPMI-treated MdM lysate, 7. 50% CM-treated MdM lysate, 8. 100% CM-treated MdM

5.4.5: Assessment of IL27 induction of PDL1 in an *in vitro* model

PDL1 was upregulated on monocyte derived macrophages with the addition of CM (see 4.4.3.1). Magnitude of PDL1 upregulation was noted to vary with plate use, with more marked upregulation seen on standard culture plated and less marked on ultra-low adhesion plates. We attempted to inhibit the upregulation of PDL1 on monocyte derived macrophages by CM *in vitro* via multiple mechanisms:

1. Inhibition of putative signalling pathways for IL27p28 induction identified by literature review (TLR4, TLR9, RIG1, MyD88)
2. Direct inhibition of IL27 signalling via anti-IL27 antibody
3. Removal of EBI3 from CM by absorption and pull-down

If the hypothesis was correct TLR4, TLR9 or RIG1 would reduce the expression of IL27p28 depending upon the signalling pathway used. MYD88 would be a common inhibitor of TLR4 and TLR9 pathways. Cleaning of EBI3 from conditioned media by pull-down should abrogate the effect due to limiting the formation of IL27. IL27p28 pull-down should represent a negative control.

Figure 5.8: Knockdown of CM-induced PDL1 expression on monocyte derived macrophages

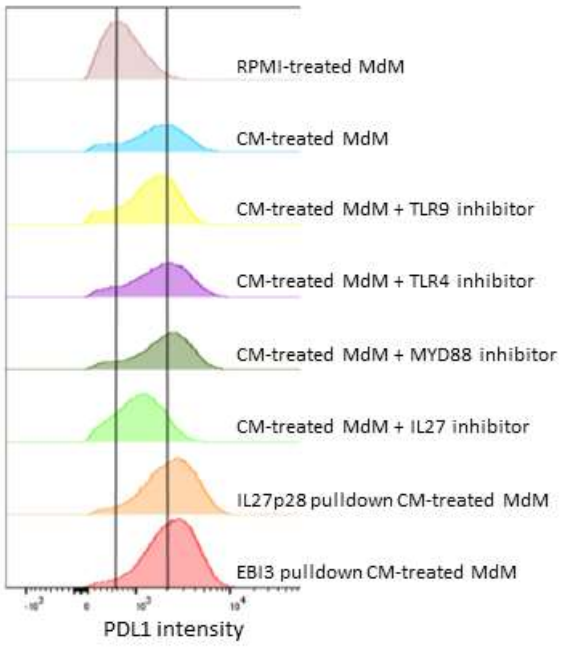

Figure 5.8: PDL1 upregulation on monocyte-derived macrophages by CHL cell line conditioned media (CM) is partially abrogated by competitive IL27 inhibition but not by TLR4, TLR9 or MYD88 inhibition and not by pulldown of IL27p28 or EBI3 from CM.

Note: Single experiment. IL27 knockdown not replicated. Analysis by flow cytometry

None of these approaches resulted in consistent down-regulation of PDL1 in CM-treated MDM as measured by flow cytometry, although partial downregulation was observed with direct inhibition of IL27. Batch variability was noted with conditioned media. The failure to observe PDL1 downregulation with TLR4, TLR9, RIG1 and MYD88 inhibition is evidence against the induction of IL27p28 by this mechanism, however these experiments lacked an appropriate positive control of inhibitor activity and IL27p28 expression was not measured which would have provided a more direct experimental endpoint. IL27p28 expression in MDM lysates was measured but poor detection of IL27p28 expression by western blot due to antibody quality combined with batch effects prevented interpretation. Similarly, the failure of EBI3 pulldown to reduce PDL1 expression goes against our hypothesis, however, adequacy of pulldown was not assessed and this data conflicts with the partial abrogation seen with IL27 inhibition. The inconsistency of PDL1 abrogation with IL27 inhibition with CM batches is a further concern.

5.4.6: Indirect evidence of the effects of IL27 signalling in the CHL microenvironment

5.4.6.1: PDL1 upregulation within the microenvironment

Marked upregulation is seen in the myeloid microenvironment in CHL. In section 4.4.2.2 we demonstrate that PDL1 intensity is inversely related to distance from CHL cell, consistent with induction by a factor secreted by the CHL cell. This is validated in 4.4.3 *in vitro*. PDL1 expression is positively correlated with EBI3 H score (rho = 0.44, p <0.0001) but inversely correlated with IL27p28 intensity (R-0.33, p = 0.0003). No relationship is seen to IL27p28 area stained.

Figure 5.9: PDL1 upregulation in CHL

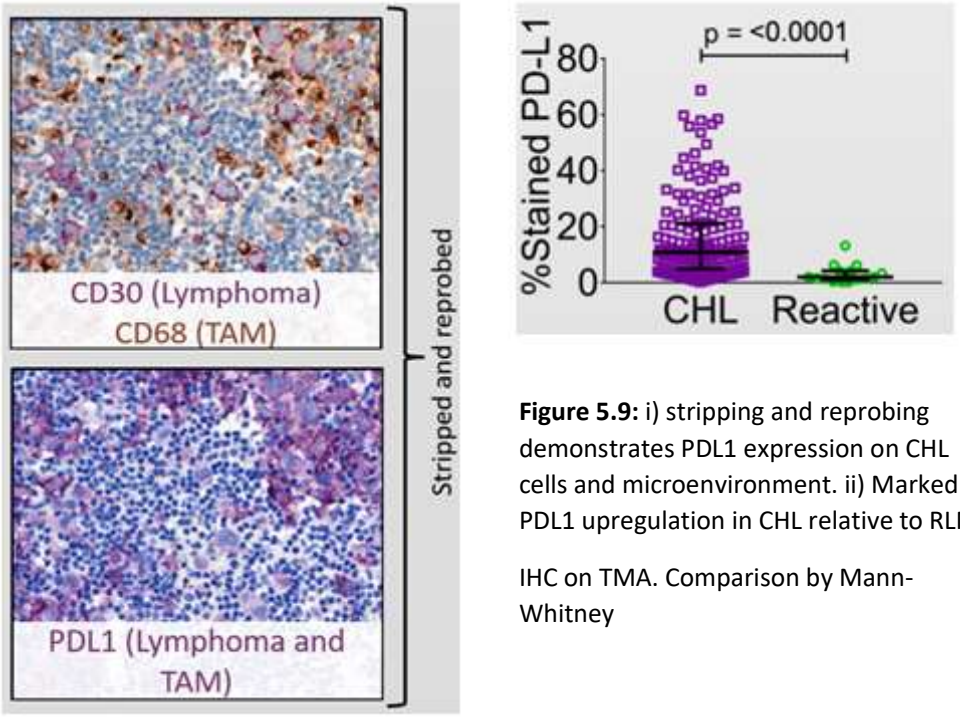

Figure 5.9: i) stripping and reprobing demonstrates PDL1 expression on CHL cells and microenvironment. ii) Marked PDL1 upregulation in CHL relative to RLN.

IHC on TMA. Comparison by Mann-Whitney

5.4.6.2: T_H17 suppression and T_H17 to T_H1 differentiation skew

$ROR\gamma T^+$ (T_H17 transcription factor) cells are significantly reduced in CHL biopsies relative to RLN, (IHC p <0.001) whereas $TBET^+$ (T_H1 transcription factor) cells and $FOXP3^+$ (T_{Reg} transcription factor) cells. By multiplex IHC $CD4^+ROR\gamma T^+$ T_H17 cells were suppressed in CHL relative to RLN, as were $CD4^+FOXP3^+ROR\gamma T^+$ T_H17_{Reg}, $CD4^+ROR\gamma T^+TBET^+$ $T_H1/17$ and

$CD4^+FOXP3^+$ T_{Reg}. In contrast $CD4^+TBET^+$ T_H1 and $CD4^+TBET^+FOXP3^+$ T_H1 regulatory (T_H1_{Reg}) were over-represented. When assessing relative proportions T_H17_{Reg}:T_H17 ratios were equivalent between CHL and RLN whereas T_H17:$T_H1/17$ ratios were significantly elevated in CHL ratio (median 1.59 in CHL vs 0.68 in RLN, p <0.001), suggesting skewing of differentiation towards T_H1 as opposed to T_{Reg}. This is consistent with the reported effects of IL27. These observations are further strengthened by significant inverse correlations between IL27p28 and RORγT (R -0.4, p = 0.0006) and positive correlations between IL27p28 and TBET (R 0.4, p = <0.0001)

Figure 5.10: Fold change of median cell frequency in CHL biopsies compared to median frequency in reactive lymph node

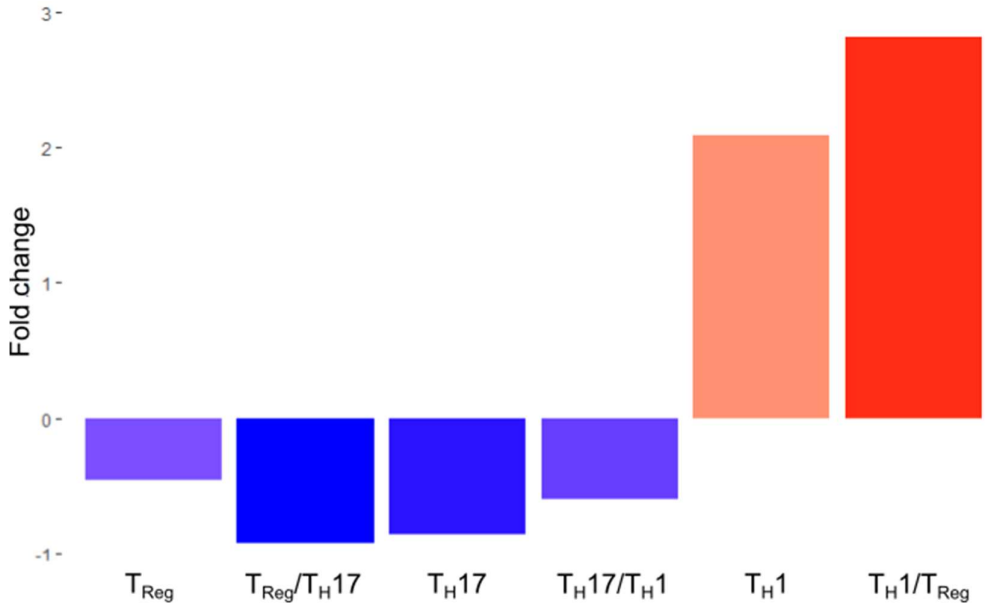

Figure 5.10: Fold change of median cell frequency in 47 CHL presenting biopsies and 25 RLN controls on TMA. Analysed by IHC with a CD4/TBET/RORγT/FOXP3/CD8 multiplex panel. Reduction in T_{Reg} ($CD4^+FOXP3^+$), T_{Reg}/T_H17 ($CD4^+FOXP3^+ROR\gamma T^+$), T_H17 ($CD4^+ROR\gamma T^+$) and T_H17/T_H1 ($CD4^+ROR\gamma T^+TBET^+$) relative to reactive lymph nodes. T_H1 ($CD4^+TBET^+$) and T_H1/T_{Reg} ($CD4^+TBET^+FOXP3^+$).

5.5: Discussion

We demonstrated high EBI3 expression in CHL cells and EBI3 production by CHL cell lines. Additionally, we identified IL27p28 upregulation within the microenvironment and rarely in CHL cells and demonstrated that neither EBI3 nor IL12p40 (potential subunit partners) were expressed within these cells. We were unable to demonstrate IL27 heterodimer formation in FFPE tissue by ELISA on protein extracts or by proximal ligation assay although technical issues limit the interpretation of data from both of these methods. We also identified the expression of IL23p19 within the microenvironment but not co-expression of the corresponding IL12p40 subunit required to form IL23.

In vitro we demonstrated the upregulation of PDL1 on monocyte derived macrophages on treatment with CHL cell line conditioned media but noted variability on the strength of PDL1 upregulation dependent upon the batch of conditioned media and less PDL1 upregulation when using ultra low attachment plates to aid macrophage harvest. We achieved a partial reduction in PDL1 expression with a competitive IL27 inhibitor but this effect could not be replicated on repeating the experiment with a new batch of conditioned media. We observed no reduction in PDL1 expression with TLR4, TLR9, RIG1 and MyD88 inhibitor treatment (potential mechanisms of isolated IL27p28 induction in macrophages) or with absorption of EBI3 or IL27p28 from conditioned media (although absorption efficiency was not confirmed).

Assessment of the effects of the IL6 superfamily cytokines is challenging due to the promiscuous partnering of subunits forming multiple cytokines with different effects, compounded by equally promiscuous partnering of their corresponding receptor subunits.[348,367] We validate previous reports of marked upregulation and secretion of EBI3 in CHL cells without expression of IL27p28 or IL12p35.[270,347,368] We provide evidence of the dissociated expression of individual subunits, validating and extending previous findings but were unable to demonstrate the presence of formed heterodimeric cytokines.[347] The absence of expression of IL12p40 and the co-expression of EBI3 and IL27p28 is notable as recent studies have identified upregulation of IL27p28 and IL23p19 in CHL by gene expression and concluded that this represents the presence of IL27 and IL23 respectively.[139] Our data suggests IL27 would only be formed if there was cytokine combination in the microenvironment and that formed IL23 is unlikely to be present. This is relevant given that IL27p28 is active as a monomer with different biological functions.[366] IL23p19 does not have biological functions described in isolation but it is conceivable given the behaviour of closely related cytokines. Our experimental evidence is not strong enough to conclude that EBI3/IL27 is playing a role in CHL immune evasion but technical limitations at each stage made us unable to reject it.

We did identify a series of features of the CHL microenvironment that would be consistent with the effects of IL27. These include high microenvironmental PDL1 expression, elevated IL10, induction of STAT3 signalling, suppression of T_H17, skewing to T_H17 towards T_H1, prominence of T_H1 regulatory (T_H1_{Reg}) and of T regulatory 1 (T_R1).[139,369,370] The upregulation of PDL1 is characteristic of the effects of IL27 but not specific to it.[139] The positive correlation with EBI3 H-score supports the hypothesis that this is IL27-related. IL10 upregulation has long been noted in CHL and has also been recently linked to the presence of T_R1 cells which have recently been reported to be prominent in CHL (a $FOXP3^-$ T_{Reg} expressing IL10 and LAG3).[344] This is interesting as induction of T_R1 is a well-recognised effect of IL27, as is the suppression of T_H17 and skewing to T_H1.[371] Finally IL27 is also noted to promote the development of T_H1_{Reg}.[372] Individually each of these observations represent weak evidence but taken together they reflect many of the reported effects of IL27 signalling.

These findings, combined with a recent publication suggesting that the same mechanism is active in $EBI3^+$ DLBCL suggest that further assessment may be worthwhile, albeit with a revised approach.[350] The mechanism is potentially of greater interest in CHL because EBI3 upregulation is both marked and consistent. Additionally, monomeric EBI3 secretion is to date primarily reported in the context of cancer, with formed heterodimer secretion being more usual in other settings.[364,373] This is attractive as it suggests that a competitive EBI3 inhibitor may confer greater tumour specificity than e.g. a STAT inhibitor which might have broad off-target effects.

5.5.1: Future work

Before improved *in vitro* modelling, western blotting and validation is attempted more robust basic hypothesis supporting data is required. Initially multiplex ELISA of the key IL6 superfamily cytokines associated with EBI3, comparing levels in CHL patients to healthy controls. These include IL27 (EBI3/IL27p28), IL35 (EBI3/IL12p35), IL39 (EBI3/IL23p19). Given that this is a simple experiment to perform this at least would be worthwhile before closing this line of investigation.

IHC data can be extended if and when more reliable antibody clones for EBI3, IL12p35 and IL10 or a specific T_R1 marker become available. This would improve single marker studies and the combination of IL10 or a more specific T_R1 marker (a factor induced by IL27 signalling) and RORγT (a factor suppressed by IL27 signalling) would make robust spatial analysis more feasible.

If increased IL27 is detected by ELISA then *in vitro* modelling should be reattempted with a more robust approach which minimises some of the factors compromising the data discussed above. Firstly, the model should be performed in trans-well plates as opposed to using conditioned media to reduce the variability with batch effects. Secondly, better model validation to prove the presence of formed IL27 within the system before proceeding to functional work. Finally, the use of PDL1 expression as a functional endpoint for TLR and MYD88 knockdown whilst not incorrect introduces too many variables. Given that we hypothesised that these pathways were involved in the upregulation of IL27p28 in macrophages before its secretion to form IL27 then measurement of IL27p28 expression would be a more reliable output for this question.

Chapter 6: T cell exhaustion in the CHL microenvironment

6.1: Introduction

Prominent PDL1 is seen in CHL cells due to 9p24.1 amplification and *PDL1/CIITA* fusions and is induced in the local microenvironment.[20,140,159,177] PDL1 expression predicts response to PD1 inhibitors in CHL trials and in solid malignancies.[6,7,13,178] The combination of PD1 inhibitor responsiveness and high PDL1 expression in CHL is held to be evidence of T cell exhaustion, however this does not necessarily imply the presence of exhaustion as the PD1-PDL1 axis has a range of other important roles in immune regulation.

11 studies have quantified PD1 in CHL, most for prognostic assessment. All have reported either low expression or positivity in a minority of cases, associating PD1 with either adverse prognosis or not detecting an effect. [22,201–210] Few studies perform deeper phenotyping of PD1 expressing cells; one found no evidence of exhaustion, a second identified elevated PD1 expression in a T_H1 subset.[22,216] Functional studies support signalling via the PD1-PDL1 axis but do not show convincing evidence of exhaustion.[176,230]

Data also cast doubt on whether a direct line can be drawn between PD1 and PDL1 expression. Like PD1, PDL1 is reported to be an adverse prognostic marker but studies assessing PD1 and PDL1 side by side found them to be independently prognostic.[203] Additionally a negative correlation was observed between 9p24 gains and PD1 expression.[201] Spatial studies support a PDL1-enriched microenvironment but conclusions suggesting preferential interaction with $PD1^+$ cells are statistically flawed.[159] PDL1 expression has consistently been reported as a predictor of response to PD1 inhibition in CHL, whereas PD1 is not predictive.[6,13,133] These data suggest that the expression patterns of PDL1 and PD1 may be driven by independent processes in CHL.

Taken together, despite a $PDL1^{hi}$ microenvironment, there is currently little published evidence supporting the presence and none providing direct evidence of an exhausted T cell population. That said, data is sufficiently limited that its presence cannot be excluded. Secondly even if a level of exhaustion were present there is currently limited evidence connecting this to PD1 inhibitor activity or known markers of PD1 inhibitor response (PDL1 and CHL expression of MHC II).[133] The strengths of these data is discussed in section 1.3.2.

In light of this, this chapter represents an assessment of exhaustion in CHL and the relationships between markers of exhaustion an PDL1 and CHL-MHC II, factors which predict

response to PD1 inhibition in CHL. The null hypothesis should be the absence of exhaustion, however, the strength of the narrative in the literature demands that evidence for the absence of exhaustion will be required to change opinion.

6.2: Aims and Objectives

6.2.1: Aims

To test the hypothesis that T cells in the CHL microenvironment are exhausted due to high expression of PDL1 by the CHL cell.

6.2.2: Objectives

1. To assess whether PD1 is overexpressed in the CHL microenvironment by quantifying PD1 expression in CHL compared to non-malignant controls.
2. To assess the degree to which PD1 positivity represents exhaustion by evaluating PD1 co-expression with other exhaustion markers.
3. To functionally assess whether CHL-infiltrating T cells are exhausted compared to non-malignant controls

6.3: Materials and Methods

6.3.1: Conventional IHC

Analysis was performed on 149 CHL patients and compared to RLN controls. Patient characteristics are discussed in Material and Methods 2.1. Three commercially available PD1 antibody clones were validated (Table 6.1). All marked small lymphocytes in the expected distribution, with $PD1^{hi}$ lymphocytes visible in germinal centres, consistent with T follicular helper (T_{FH}). Clone NAT105 showed lower sensitivity than the other two clones.

Analysis was performed using clones D4W2J and NAT105 in parallel. NAT105 was used due to its current use in diagnostic laboratories. Clone D4W2J was selected due to its higher signal at validation and superior cross-platform validation data. Of note, clone D4W2J showed comparable signal to EH33, the clone used in the paper by Carey *et al.* reporting proximity of $PD1^{+}$ tumour infiltrating lymphocyte (TIL) to $PDL1^{+}$ macrophages.[159] NAT105 was used in the

study by Greaves *et al.* reporting low PD1 expression in CHL.[22,374] Unless clone is specified, results of clone D4W2J are reported.

Table 6.1: Comparison of PD1 Clones

PD1 CLONE	MANUFACTURER	ITEM CODE	DILUTION	EPITOPE RETRIEVAL
NAT105	Abcam	ab52587	1:50	Heat Induced
EH33	Cell Signalling Technology	43248S	1:50	Heat Induced
D4W2J	Cell Signalling Technology	86163S	1:50	Heat Induced

Figure 6.1: Validation of commercially available PD1 clones in tonsil (serial sections)

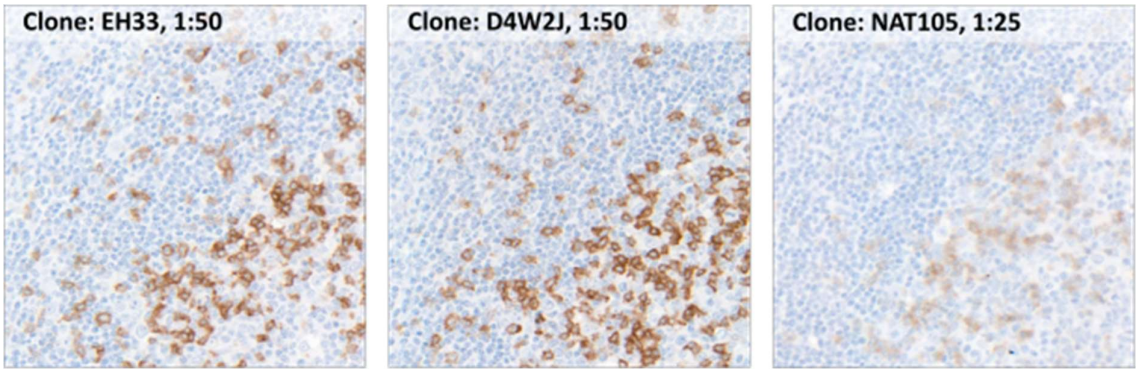

6.3.2: Virtual multiplex IHC

Multiplex IHC (mIHC) was performed on 47 patients arrayed on a single TMA and compared to RLN controls. mIHC was selected over flow cytometry as it allowed the testing of a greater number of biological replicates and preserved single cell suspensions (SCS) for functional studies. All antibodies stripped on validation with the exception of CD8 which was placed last. Stripping method is discussed in Material and Methods 2.2.6. EOMES, TBET, LAG3 and TIM3 were selected for phenotyping of PD1+ T cells as markers of exhaustion. The phenotype of T_H-Ex cells is less clearly defined than T_C-Ex but these markers are reported to associate with exhaustion in both subsets.[219]

Table 6.2: mIHC stripping panels

	DAY 1	DAY 2	DAY 3	DAY 4	DAY 5	DAY 6	DAY 7
PANEL 1	CD4	PD1	LAG3				
PANEL 2	PD1*	CD30	PDL1	MHC II	TBET	EOMES	CD8
PANEL 3	PD1	LAG3	TIM3**	CD8			

*DAB chromogen, **Goat polyclonal – ABC detection method

6.3.3: Flow Cytometry and functional assays

CFSE-based proliferation assays were performed with CD3/28 stimulation over 5 days. 2 µg/ml of pembrolizumab (PD1 inhibitor) or 2 µg/ml of isotype control was tested. Dosage was based upon published studies and functional data contributing to the European Medicines Authority Assessment report.[375,376] SCS were randomly assigned to batches with RLN SCS represented across all experiments.

Cytokine production capacity was assessed in response to PMA/Ionomycin with a 4-hour assay duration. Cytokine production capacity loss in exhaustion is recognised but data is less consistent than with proliferation loss with one article noting two distinct populations of ExT_H; the first induced by strong T cell receptor (TCR) stimulus which downregulated TCR expression but produced cytokine in response to PMA/Ionomycin and a second induced by prolonged weak TCR stimulus that was hypo-responsive to PMA/Ionomycin.[377] Baseline PD1 expression was measured from unstimulated controls.

Table 6.3: Antibody cocktail for proliferation assay

ANTIGEN	MANUFACTURER	FLUOROCHROME	ITEM CODE	CLONE	DIL/TEST
DAPI	BD Bioscience	-	564907	-	1:2000
CFSE	Thermo Fisher	-	C34554	-	
CD3	Biolegend	PercP-Cy5.5	300430	UCHT1	2.5µl
PD1	eBioscience	PE	12-2799-42	eBioJ105	2.5µl
CD4	Biolegend	APC-Fire 750	344638	SK3	2.5µl

Table 6.4: Stimulation reagents for proliferation assay

REAGENT	MANUFACTURER	CODE	CLONE	DETAILS	CONCN
CD3	Biolegend	300438	UCHT1	Mouse mIgG1k	10μg/ml
CD28	Biolegend	302934	CD28.2	Mouse mIgG1k	1μg/ml
PEMBROLIZUMAB	BioVision	A1306	-	Human mIgG4k	2μg/ml
ISOTYPE	Biolegend	403701	-	Human mIgG4k	2μg/ml

Table 6.5: Antibody cocktail for intracellular cytokine assay

ANTIGEN	VENDOR	FLUOROCHROME	ITEM CODE	CLONE	DIL/TEST
CD3	Biolegend	BV421	300434	UCHT1	2.5μl
ZY	Biolegend	-	423104	-	1:1000
KI67	Biolegend	BV711	350516	Ki-67	2.5μl
PD1	BD Bioscience	BB515	564494	EH12.1	2.5μl
IL2	BD Bioscience	PE	554566	MQ1-17H12	2.5μl
IFNγ	eBioscience	APC	17-7319-41	4S.B3	2.5μl
CD4	Biolegend	APC-Fire 750	344638	SK3	2.5μl

*ZY = Zombie Yellow

6.4: Results

6.4.1: Quantification of PD1 expression in the CHL microenvironment by single marker IHC

6.4.1.1: Quantification of PD1

We first quantified expression of PD1 in the CHL microenvironment. We observed low levels of $PD1^+$ TIL despite marked T_H and T_C infiltration and high expression of PDL1. Additionally, on comparison between CHL and RLN tissue significant enrichment of CD4, CD8, CD3 and PDL1 expression was seen ($p<0.001$ for each) but PD1 expression was significantly lower than that seen in reactive tissue ($p<0.001$. We considered that this might be related to the presence of $PD1^+T_{FH}$ cells in germinal centres in RLN which are rarely seen in CHL. We therefore repeated the analysis excluding germinal centre regions and stratifying the analysis to PD1 strong and PD1 weak TIL. Total PD1, PD1 strong an PD1 weak cells were seen at significantly lower frequencies in CHL tissue before and after germinal centre exclusion ($p < 0.001$). PD1 weak cell frequency correlated inversely with PDL1 expression ($p < 0.001$). Assessment of PD1 expression by CHL EBV status and histological subtype demonstrated significant enrichment of PD1 expression in the rare LR-CHL subtype, consistent with previous reports but no significant difference between other groups. ($p < 0.0001$).

Figure 6.2: T cell frequencies in CHL and PD1 expression

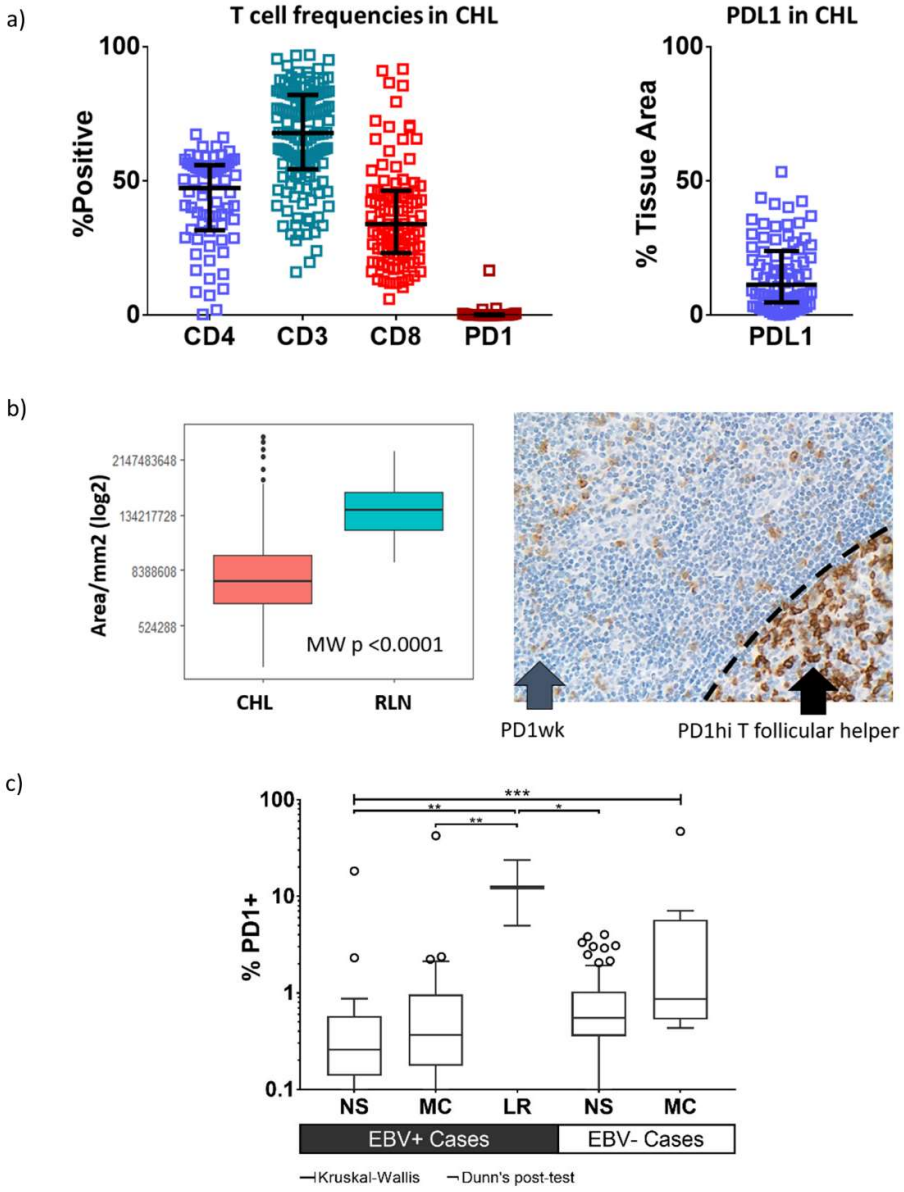

Figure 6.2: a) Quantification of CD4, CD3, CD8, PD1 and PDL1 expression by IHC on TMA. n = 160. b) Comparison of PD1 weak cells between CHL and RLN in the same cohort after exclusion of germinal centres. c) Comparison between CHL cases by EBV status and histological subtype (NS = nodular sclerosing, MC = mixed cellularity, LR = lymphocyte rich). Comparison: Kruskal-Wallis (p = 0.006) with Dunn's post-test demonstrates significant enrichment in lymphocyte rich cases but not between other subgroups. EBV+NS n=20, EBV+MC n=22, EBV+LR n=3, EBV-NS n=87, EBV-MC n=8. EBV: Epstein-Barr virus. (* = $p < 0.05$, ** = $p < 0.01$, *** = $p < 0.001$). Panel c reproduced from Haematologica publication, (see Chapter 9: Original Manuscripts).

6.4.1.2: Assessment over serial relapses

Whilst PD1 inhibitors are being explored in the first line setting, trials showing activity to date have been in the multiply relapsed setting. An alternative hypothesis that might explain the apparent absence of PD1 expression whilst still allowing for PD1 inhibitors acting through the reversal of exhaustion would be an increased frequency of cases with exhaustion in the relapse setting. This could either be due to selection of exhausted cases due to poor response to first line chemotherapy or increasing exhaustion within each case due to tumour evolution under chemotherapy. To address the first possibility, we looked for enrichment of PD1 expression among the diagnostic biopsies of patients who went on to relapse but detected no difference between groups. (Figure 5.4.2a, p = 0.49). Enrichment of PD1 positive cases might have been anticipated given that PD1 expression is associated with an increased risk of relapse.[22,202,203] The apparent discrepancy may be dues to these studies associating rare $PD1^{hi}$ cases with poor outcome, hence although $PD1^{hi}$ cases may be preferentially enriched this does not necessarily imply a difference in overall PD1 expression between groups. PD1 enrichment in LR-CHL does not explain the increased relapse rate in $PD1^{hi}$ cases as this entity is associated with improved outcome.[378]

Given this finding we considered the alternative possibility of increasing exhaustion within each case due to tumour evolution under chemotherapy. To assess this, we compared PD1 and PDL1 expression in biopsy-site matched paired presentations and relapse biopsies but found no evidence of a shift in expression of either marker (Wilcoxon paired, two-tailed, p=0.84 and p=0.6 respectively, n = 35). Marked changes were observed in some cases but these did not occur in a consistent pattern. We further assessed 9 cases where serial relapses were available, but again no enrichment or depletion of PD1 or PDL1 expression was observed (one-way ANOVA p = 0.47 and p = 0.68 respectively). This finding is reassuring for the incorporation of PD1 inhibitors into front line therapy for CHL. The data discussed in this section was published in Haematologica (see Chapter 9: Original Manuscripts).[214]

Figure 6.3: Assessment over serial relapses

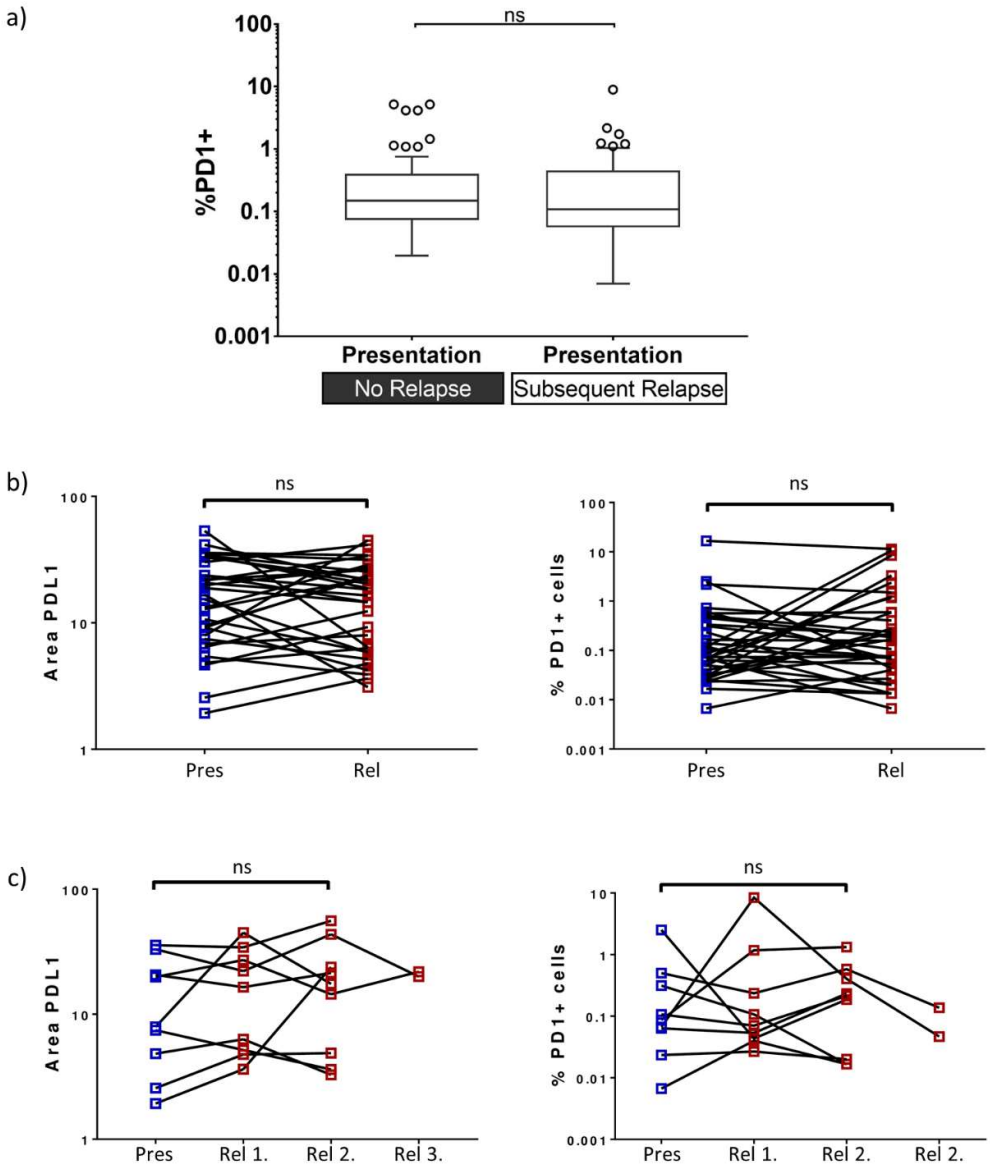

Figure 6.3: a) Frequency of PD1⁺ TIL on presentation biopsies by subsequent relapse status. No significant enrichment of PD1⁺ lymphocytes between presentation biopsies comparing patients who subsequently relapsed (n=43) to those who remained in remission (n=80). Box and whiskers in Tukey style, log 10 scale. Mann-Whitney test *P*=0.49. ns: non-significant. b) PDL1 expression and PD1⁺ lymphocyte frequency does not significantly enrich between presentation and first relapse (n = 35, comparison: paired Wilcoxon rank). c) No enrichment is seen over serial relapses (n = 9, comparison: Friedman test). Pres = Presentation biopsy (pre-therapy), Rel = Relapse biopsy, ns = non-significant

Figure reproduced from Haematologica publication, (see Chapter 9: Original Manuscripts).

6.4.1.3: Summary of single marker IHC data

In summary we find under-representation of $PD1^+$ TIL in CHL despite marked infiltration of both T_C and T_H cells. And high PDL1 expression The same pattern is seen when restricting analysis to $PD1^{hi}$ or $PD1^{lo}$ cells and when germinal centres are excluded from analysis. This finding was replicated with two different commercially available anti-PD1 antibodies. An inverse correlation was seen between $PD1^{lo}$ cells and PDL1 expression, the opposite of what would be expected if PD1 expression reflected exhaustion induced or maintained by PDL1. Additionally, we find no evidence that $PD1^+$ TIL enrich over serial relapses, which would have provided an alternative explanation for the efficacy of PD1 inhibitors in multiply relapsed disease.

These findings are in agreement with previously published data that quantifies PD1 expression, but run counter to the prevailing narrative of an exhausted T cell population in CHL. To investigate how closely the observed $PD1^+$ TIL population represents exhaustion we next assessed co-expression of other exhaustion markers by multiples IHC (mIHC).

6.4.2: Co-expression of exhaustion markers

Co-expression of PD1, LAG3, TIM3 and CD8 were assessed by mIHC in 50 CHL cases and compared to 28 RLN. Germinal centre regions were excluded. T_C were defined by expression of CD8. PD1, LAG3 and TIM3 are broadly T cell restricted and T_H are prominent in CHL and RLN tissue so cells expression exhaustion markers in the absence of CD8 were classified as T_H. T_H and T_C cells singly expressing LAG3, expressing both LAG3 and TIM3 or expressing all exhaustion markers (PD1, LAG3 and TIM3) were significantly less numerous in CHL as compared to RLN after correction for multiple comparisons ($p < 0.001$). Similarly, T_H cells expressing both PD1 and TIM3 were significantly less numerous in CHL as compared to RLN. None of the exhaustion phenotypes were found to be more numerous in CHL as compared to RLN.

Because CHL-MHC II expression and PDL1 have been connected to response to PD1 inhibition we next assessed their relationship to exhaustion marker expression within CHL cases. No significant relationship was observed between any exhaustion marker, or combination of markers to PDL1 or CHL-MHC II expression in the T_C or T_H subsets.

Figure 6.4: Co-expression of PD1, LAG3 and TIM3 in CHL and RLN

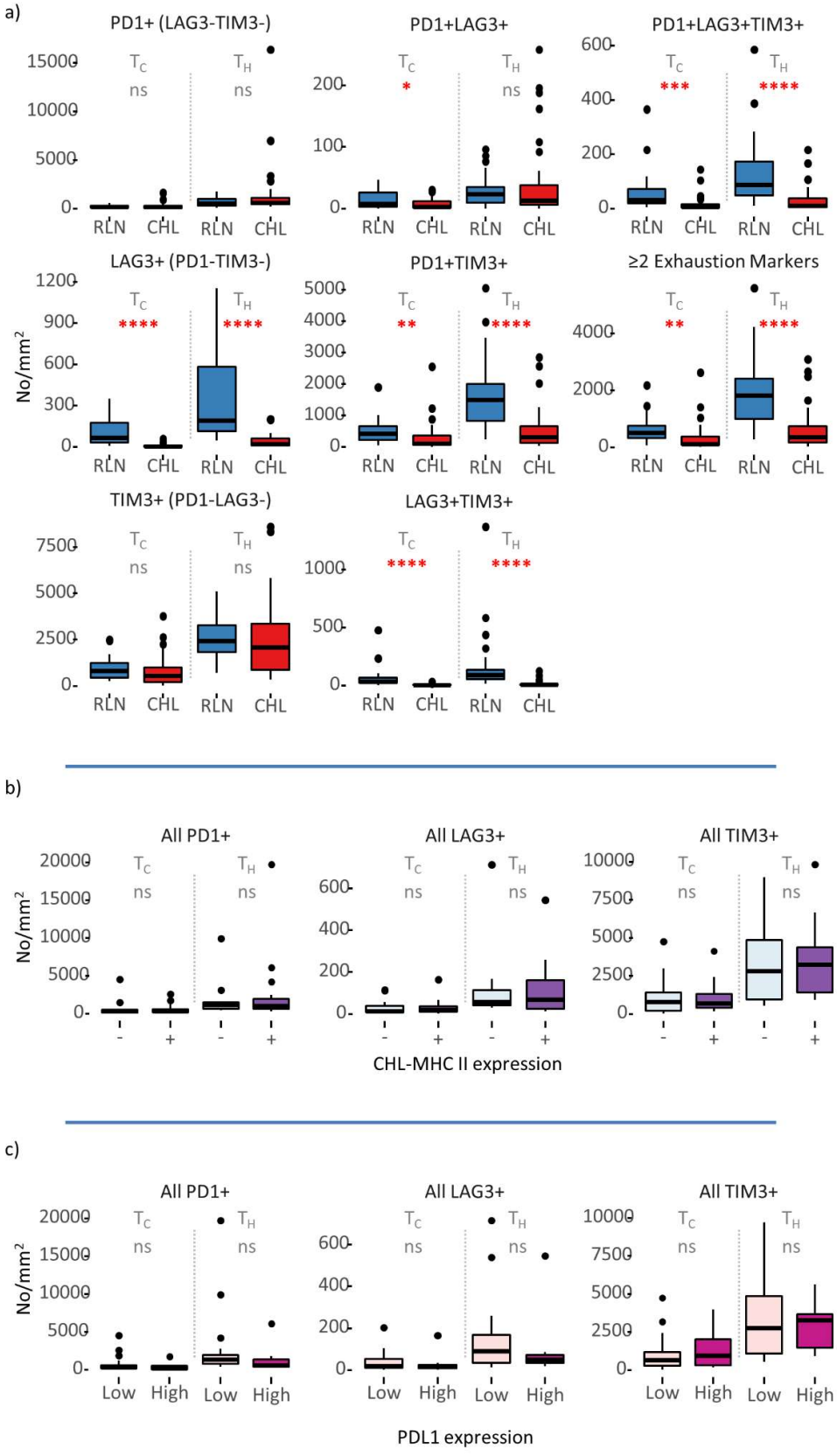

Figure 6.4: a) Comparison of exhaustion marker expression in RLN and CHL by mIHC demonstrates significantly lower numbers of infiltrating cells expressing exhaustion markers in CHL as compared to RLN tissues. c) Comparison of CHL cohort by CHL cell expression (a marker of response to PD1 inhibitors) of MHC II detects no relationship to individual markers or subsets. c) Comparison of CHL cohort by PDL1 expression (a second marker of response to PD1 inhibitors) detects no relationship to individual markers or subsets.

T_C = Cytotoxic T cell, T_H = T helper cell, T_C cells defined as CD8 positive. T_H cells defined as exhaustion marker positive but CD8 negative. CHL n = 50, RLN n = 28 on TMA. Statistics: Wilcoxon unpaired. p values corrected for multiple comparison by Holm-Bonferroni method

Given this finding we performed a second independent experiment within the same cohort of patients, measuring co-expression of PD1, EOMES, TBET and CD8. And performed the same comparison to PDL1 and CHL-MHC II expression. No relationship was seen between exhaustion markers and any T_H subset. Increased EOMES expression was detected in the T_C compartment in CHL when compared to RLN. In contrast to the LAG3 and TIM3 analysis, within the T_C compartment enrichment for co-expression of TBET and EOMES with PD1 was seen. No significant relationship between PDL1 expression or CHL-MHC II expression was detected.

Figure 6.5: Co-expression of PD1, EOMES and TBET in CHL and RLN

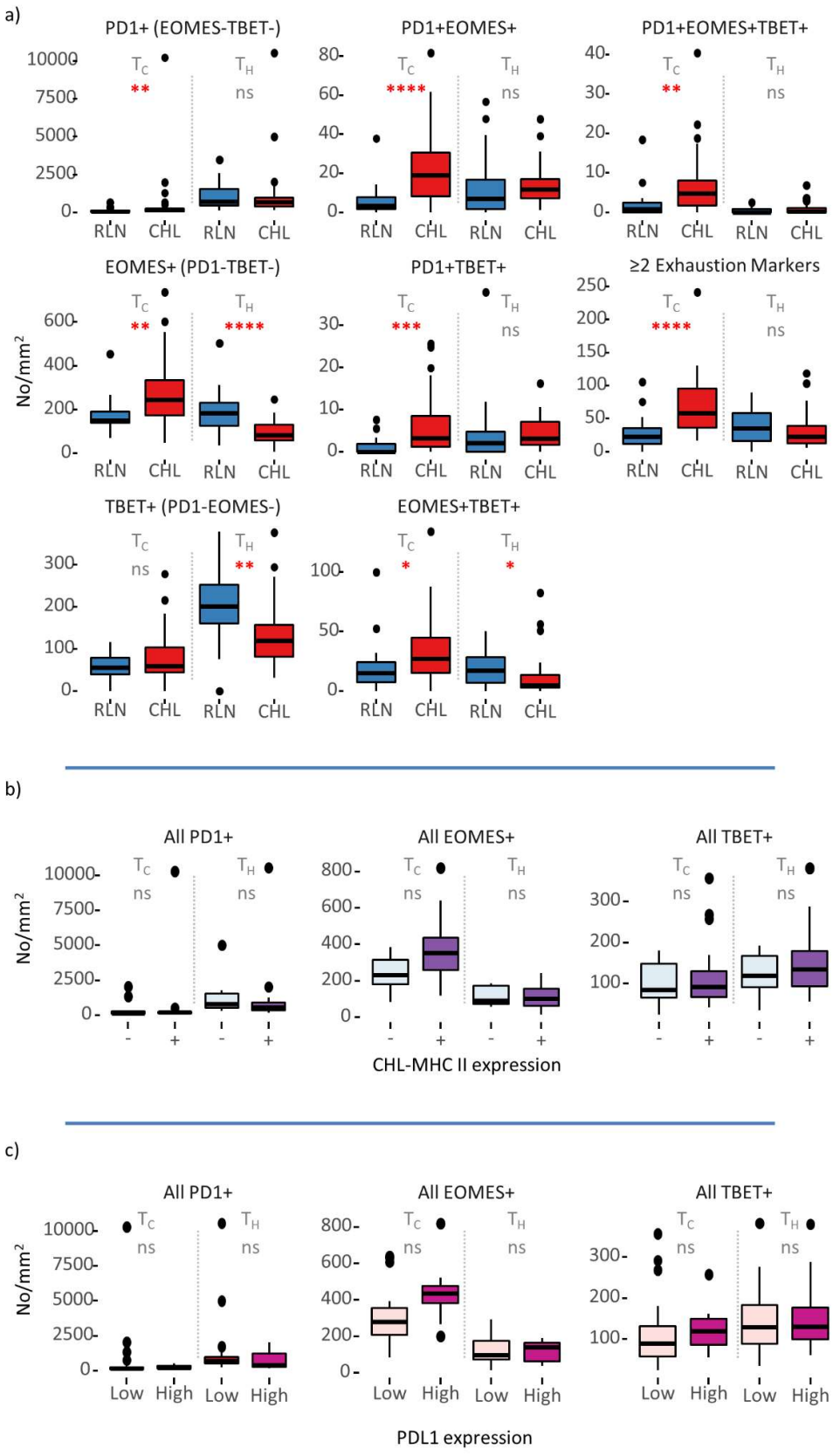

Figure 6.5: a) Comparison of TBET and EOMES co-expression in RLN and CHL by mIHC demonstrates similar numbers of infiltrating cells expressing exhaustion markers in CHL in the T_H group but an increase in the T_C group as compared to RLN tissues. c) Comparison of CHL cohort by CHL cell expression (a marker of response to PD1 inhibitors) of MHC II detects no relationship to individual markers or subsets. c) Comparison of CHL cohort by PDL1 expression (a second marker of response to PD1 inhibitors) detects no relationship to individual markers or subsets.

T_C = Cytotoxic T cell, T_H = T helper cell, T_C cells defined as CD8 positive. T_H cells defined as exhaustion marker positive but CD8 negative. CHL n = 50, RLN n = 28 on TMA. Statistics: Wilcoxon unpaired. p values corrected for multiple comparison by Holm-Bonferroni method

6.4.3: Functional studies

We sought to confirm our findings by functionally testing evidence of exhaustion. In light of recent literature suggesting a prominent role for T_H cells and hypothesising T_H exhaustion we designed assays to quantify two aspects of T_H function that are reported to be compromised in exhaustion: proliferative and cytokine production capacity.[133,159,216]

6.4.3.1: Proliferative capacity

Loss of proliferative capacity is a recognised feature of T_H exhaustion.[379] Proliferation to CD3/28 stimulation was assessed by CSFE assay. 14 CHL were compared to 5 RLN over three independent experiments with RLN samples evenly distributed across batches. Cell viability at defrost varied significantly across experimental runs ($p = 0.008$) with improved viability in later batches. In four cases, all from the CHL group, a single vial of cells was available, likely reflecting the condition or size of the starting biopsy. Case where only one vial was available were closely associated with poor viability at defrost ($p = 0.004$). CHL samples were selected to represent differing histology types and EBV viral status. Biopsies from all CHL single cell suspension (SCS) samples were represented on the TMAs used for IHC studies, enabling comparison to the rest of the cohort to ensure samples were representative. Expression of PDL1, CD68 (macrophages), TBET (T_H1), GATA3 (T_H2), RORγT (T_H17) and PD1 were similar

between samples used for functional studies and the wider cohort (p = ns). Higher expression of FOXP3 (T_{Reg}) was seen in the flow SCS group was compared to the wider cohort (p = 0.04). This finding was not explained by the high representation of EBV^+ cases.

No difference in proliferative capacity of live $CD3^+$ T cells (p = 0.8) or live $CD3^+CD4^+$ T_H was observed between CHL and RLN (p = 0.89). Subgroup analysis was performed within the CHL samples, although this was limited by sample size. No significant difference in T or T_H proliferation was seen by histological subtype (NS-CHL n = 10, MC-CHL n = 4, p = 0.2 and 0.9 respectively). When stratified by EBV status significantly more proliferation was seen in T cells from EBV^+ biopsies and a trend to higher proliferation was seen in the T_H cells (EBV^+CHL n = 7, EBV negative CHL n = 8, p = 0.017 and 0.13 respectively). No significant difference in proliferative capacity was observed by batch (p = 0.52) but reduced proliferation was seen in samples where only one vial was available (p = 0.049). Samples where one vial was available were universally EBV^-, of NS-CHL subtype and were associated with lower TBET and CD68 infiltration (p = 0.004 and 0.002 respectively) but were similar in regard to other markers. The significance of this is unclear.

Table 6.6: Correlation of proliferative capacity in CHL SCS to IHC infiltration of T cell markers

	T		T_H	
	R	***P***	***R***	***P***
TBET	0.5	0.067	ns	ns
GATA3	ns	ns	ns	ns
RORGT	ns	ns	ns	ns
FOXP3	ns	ns	ns	ns
PD1	ns	ns	-0.49	0.078
CD68	**0.6**	**0.025**	0.53	0.054
PDL1	0.5	0.069	0.5	0.069

T = proliferation of all T cells, T_H = proliferation of $CD3^+CD4^+$ T cells

Correlations between overall T and T_H proliferative capacity in SCS and marker quantification in paired diagnostic biopsies by IHC were performed in the CHL patients. A moderate positive correlation and trend to fair positive correlation was observed between CD68 positivity and T or T_H proliferation respectively (Table 6.6). Similarly trends to fair positive correlations were

seen with PDL1 expression and TBET infiltration. A trend to fair negative correlation was seen between T_H proliferation and PD1 infiltration.

In a subset of 10 CHL and 3 RLN SCS the addition of pembrolizumab or isotype control was assessed. Overall, no significant change in proliferative capacity was noted with the addition of pembrolizumab or, between pembrolizumab and isotype irrespective CHL or RLN origin.

In summary, no significant difference in proliferation or trend to difference was observed between proliferative capacity of T cells overall, or of T_H cells from CHL-derived or RLN-derived SCS. Comparison of CHL SCS samples to markers in paired biopsies quantified by IHC showed a positive association between proliferation and CD68 or PDL1 expression but a negative association between proliferation and PD1 expression.

Figure 6.6: Proliferative capacity of CHL and RLN SCS

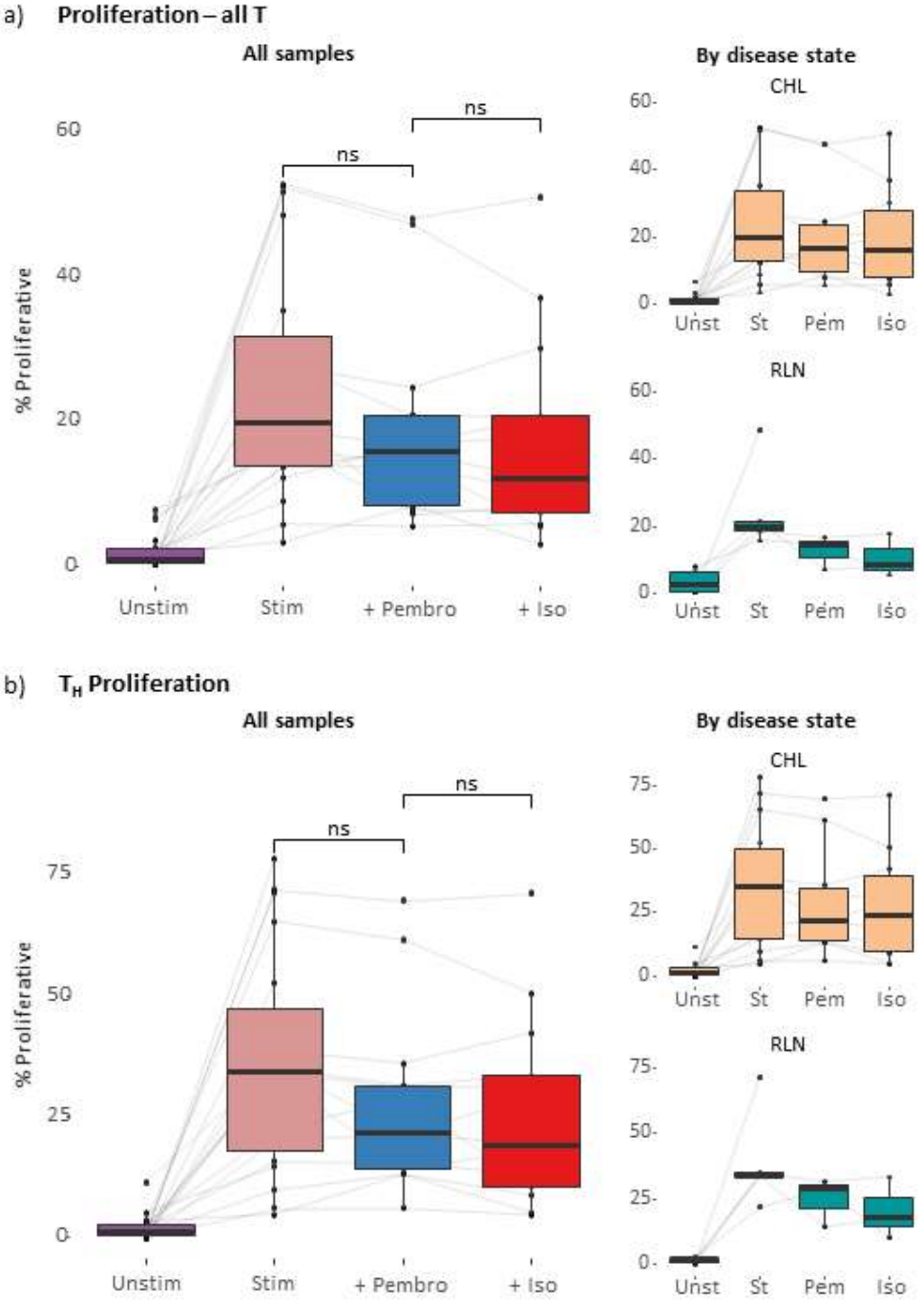

Figure 6.6: Higher proliferation seen in T cells and T_H cells with CD3/28 stimulation. CHL (n = 15) or RLN (n = 5) lymph node single cell suspensions by flow cytometry. No significant difference in proliferation was seen with the addition of Pembrolizumab or isotype control (paired Wilcoxon rank). Results were similar when stratified by disease state. Unstim/Unst = unstimulated, Stim/St = CD3/28 stimulated, + Pembro/Pem = CD3/28 plus pembrolizumab, + Iso = CD3/28 plus isotype.

6.4.3.2: Cytokine production capacity

Cytokine production capacity to PMA/ionomycin stimulation was assessed. Ki67 and PD1 expression was recorded in pre-stimulation samples. PD1 expression in the absence of proliferation as measured by Ki67 expression was used as a surrogate for exhaustion. $Ki67^{-}PD1^{+}$ T_C cells were present at similar levels in CHL and RLN samples, whereas $Ki67^{-}PD1^{+}$ T_H were significantly reduced ($p = 0.019$). Conversely, a significantly higher proportion of proliferative $Ki67^{+}$ T_H was seen in CHL, as was a trend towards higher $Ki67^{+}$ T_C ($p = 0.011$ and 0.098 respectively). In stimulated samples the capacity to produce IL2 and/or IFNγ was assessed. Non-cytokine productive $Ki67^{-}PD1^{+}$ T_C and non-cytokine productive $Ki67^{-}PD1^{+}$ T_H made up a significantly smaller fraction of CHL samples as compared to RLN. ($p = 0.025$ and 0.015 respectively). No significant difference in overall cytokine responsiveness of T_C or T_H was observed.

Correlations were assessed between cytokine assay metrics. Significant positive correlations were seen between T_C and T_H cytokine production capacity and T_C and T_H Ki67 expression ($p<0.001$ and $p<0.0001$ respectively). Additionally, positive correlations were observed between T_C and T_H PD1 expression ($p<0.01$). Less anticipated was a positive correlation between T_C PD1 expression and T_C cytokine production capacity ($p<0.01$). This relationship was not observed in the T_H compartment. Negative associations were observed between $Ki67^{-}PD1^{+}$ non-cytokine productive cells in both T_C and T_H compartments and overall cytokine productivity ($p<0.001$ respectively).

No correlation was seen between proliferative capacity and any of the metrics assessed in the cytokine assays. Correlations between cytokine assay metrics and cellular infiltration of paired diagnostic biopsies measured by IHC demonstrated a moderate positive correlation between PDL1 expression and both T_H and T_C Ki67 expression (rho 0.55, 0.57, $p = 0.048$, 0.035 respectively) but no other significant associations were detected.

Figure 6.7: Cytokine production capacity of CHL and RLN SCS

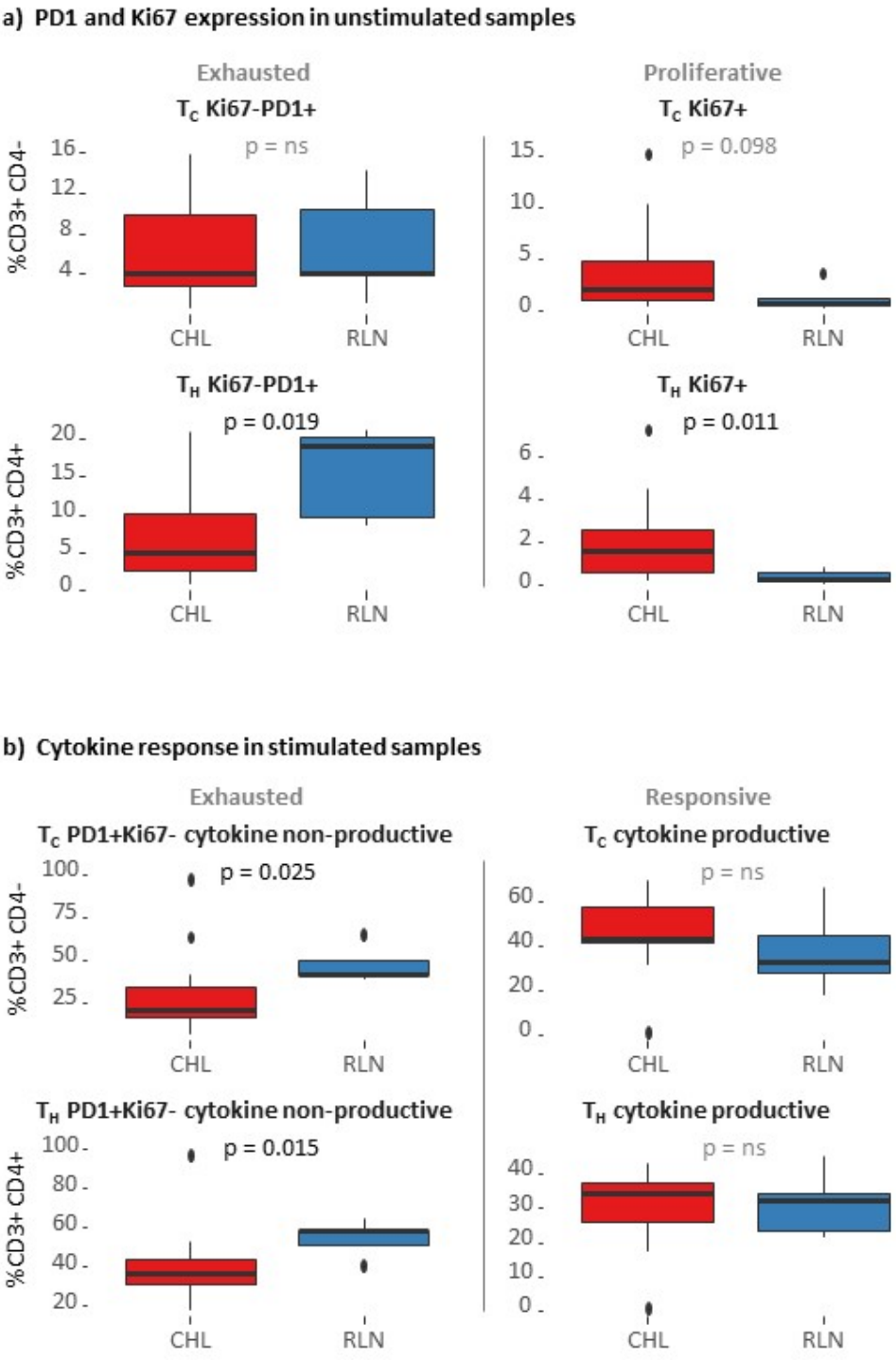

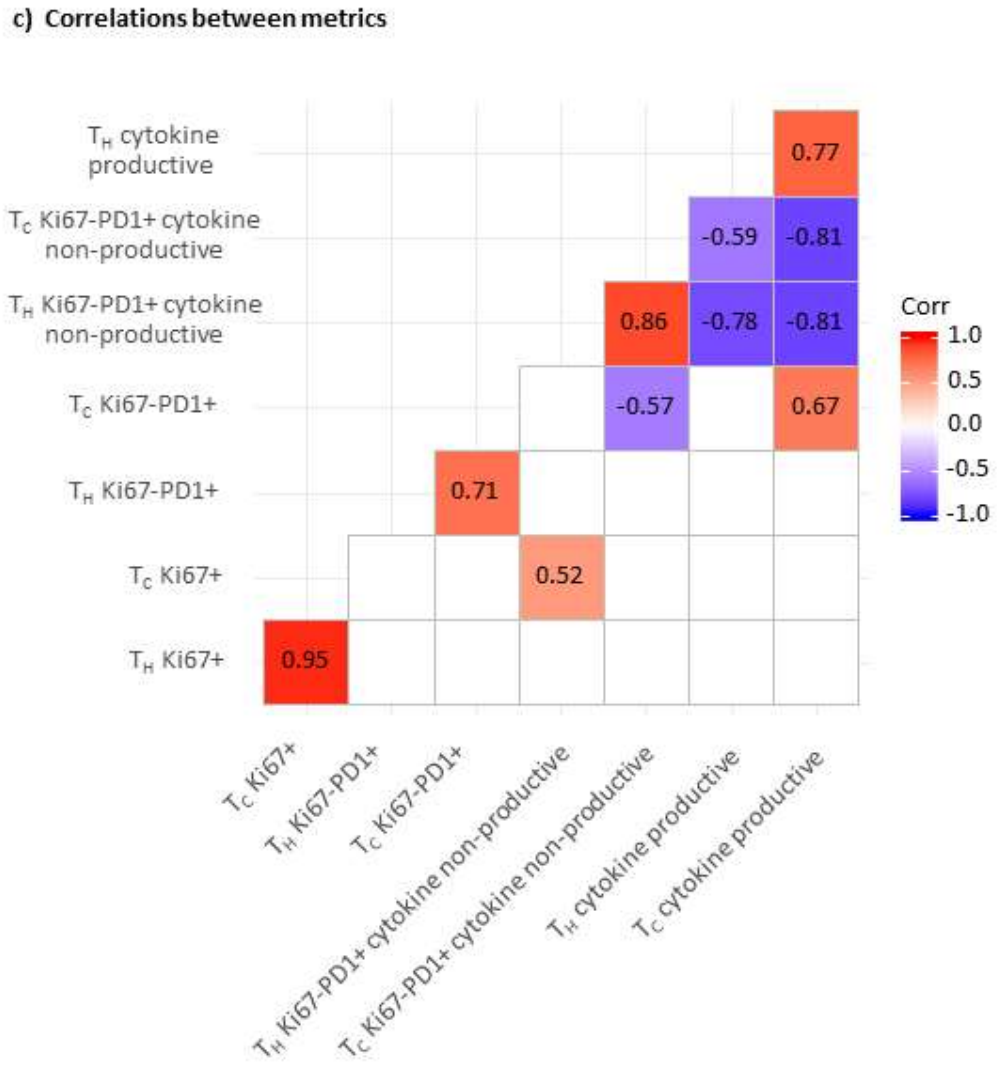

Figure 6.7: a) Ki67 and PD1 expression in T_H ($CD3^+CD4^+$) and T_C ($CD3^+CD4^-$) in unstimulated CHL (n = 15) or RLN (n = 5) lymph node single cell suspensions by flow cytometry. Comparisons of non-proliferative $PD1^+Ki67^-$ "exhausted" phenotype T_C and T_H and proliferative $Ki67^+$ T_C and T_H expressed as a proportion of all T_C or T_H. b) IL2 and/or IFNγ responsiveness after PMA/Ionomycin stimulation of CHL or RLN lymph node single cell suspensions. . Comparisons of non-proliferative non cytokine producing $PD1^+Ki67^-$cytokine$^-$ "exhausted" T_C and T_H and of IL2 and/or IFNγ responsive T_C and T_H expressed as a proportion of all T_C or T_H. c) Correlation matrix between subsets measured during cytokine response assay within the CHL samples. Correlations are displayed at a significance level of $p < 0.05$. T_H cells defined as live $CD3^+CD4^+$. T_C cells defined as live $CD3^+CD4^-$. Cytokine productive defined as expressing either IL2 or IFNγ on PMA/Ionomycin stimulation. Correlations by Spearman's rank

6.5: Discussion

6.5.1: IHC and multiplex IHC

By IHC, quantification of PD1 expressing cells revealed low levels of PD1 expression despite prominent infiltration of T cells and marked expression of PDL1. Comparison to expression in RLN revealed significantly lower expression in CHL tissue, even after the exclusion of germinal centres (containing $PD1^+$ T_{FH}) and stratifying to $PD1^{weak}$ expression, a phenotype that is reported to be associated with greater responsiveness to PD1 inhibition in the context of exhaustion in mice.[191] No enrichment of PD1 was seen in paired cases at relapse or over serial relapses excluding the possibility that responses in heavily pre-treated cases was due to accumulation of $PD1^+$ cells in relapse. Additionally, an inverse correlation was seen between PDL1 expression and PD1 and an inverse relationship was seen between CHL-MHC II expression and PD1.

Deeper phenotyping by multiplex IHC demonstrated low levels of TIM3 and LAG3 both independently and co-expressed with PD1, significantly lower or similar to levels seen in RLN. This effect was consistent in T_C and T_H subsets. Comparison was made to PDL1 and CHL MHC II expression as these are reported to be predictive of PD1 inhibitor response. No relationship was seen between any combination of these exhaustion markers and either PDL1 or CHL MHC II. In a second panel co-expression with TBET and EOMES was assessed. Cells multiply expressing PD1, EOMES and or TBET were not significantly different between CHL and RLN in the T_H subset. In the T_C subgroup increased numbers of cells co-expressing PD1 and one or more of these markers was detected in the CHL group. Again, no relationship was seen between these exhaustion markers and either PDL1 or CHL MHC II. The TIM3 and LAG3 data is not consistent with a prominent exhausted population in CHL in either the T_H or T_C lineage. The TBET and EOMES data is less clear, possibly suggesting exhaustion in the T_C group alone. It is unclear how to resolve these apparently conflicting data. However, it should be noted that whilst both TBET and EOMES are associated with T cell exhaustion they play broad and important roles in the T cell compartment and their expression cannot necessarily be equated to exhaustion, even in the context of PD1 expression.[379–381]

6.5.2: Functional testing

The correlations performed between proliferation in SCS and marker expression by IHC were limited by sample size (n = 14) and most identified associations approached but did not reach statistical significance so should not be over interpreted. However, it is notable that as might be anticipated, proliferation to CD3/28 stimulation decreased with increasing PD1 expression as might be expected if PD1 expression represented exhaustion. It is also notable that whilst an inverse relationship was identified with PD1 expression the opposite association was seen with PDL1 and CD68 expression.

No increase in proliferation was seen with the addition of pembrolizumab. Pembrolizumab obstructs the binding of anti-PD1 antibody clones leading to loss of PD1 detection by flow cytometry and the reappearance of detectable PD1 expression on therapy has been associated with loss of clinical response.[382,383] Loss of detection of PD1 was seen in pembrolizumab-treated samples, consistent with effective binding of pembrolizumab to PD1-expressing T cells. Despite this, no consistent increase in proliferation was detected at day 5 with the addition of pembrolizumab either in CHL or RLN SCS. Anti-PD1 effect is more frequently measured *in vitro* by IL2 production assay.[384] The paper by Yamamoto *et al.* measured IL2 production and added PD1 inhibitors bulk stimulated CHL SCS.[268] They observed a significant increase in one patient, a modest effect in a second and no effect in a single patient with DLBCL. They did not have sufficient biological replicates to apply any statistical test to these results. Because of the methodological difference it is not possible to make direct comparison to our assay. An effect on proliferation would be expected given that this is a recognised feature of T cell exhaustion if a significant exhausted population were present, however, the role of APC in this context is not clear. Yamamoto *et al.* added PD1 inhibitors to bulk SCS in the absence of any other stimulation.[268] The addition of CD3/28 stimulation in our system directly tests the ability of T cells to proliferate in response to strong T cell receptor (TCR) stimulus and co-stimulation but bypasses the role of APC which present PDL1.[385] It is therefore unclear if blocking PD1 in the context of non-physiologic strong TCR stimulation without the requirement for an APC accurately reflects the biology.[190]

6.5.3: Implications for PD1 inhibitor activity

The question of whether PD1 inhibitors act through reversal of exhaustion in CHL raises two related but independent questions. Firstly, whether exhaustion detectable in the CHL microenvironment, and secondly whether PD1 inhibitors acting via reversal of exhaustion.

Focussing on the first question, our data finds little evidence of a prominent exhausted population in CHL above that seen in reactive tissues by IHC, multiplex IHC or flow. The only contradictory evidence identified was an increased number of $PD1^+$ $TBET^+$ and/or $EOMES^+$ T_C cells in CHL, albeit at low levels. An important question when interpreting these data is how well PD1 expression alone as identified by IHC or flow represents exhaustion. If exhaustion-related PD1 was expressed below detection levels in IHC or other populations expressing PD1 in a different context such as T_{FH} were prominent this might obscure the signal of a true exhausted population. To address this, we have excluded germinal centre regions from all analyses. The inverse relationship (which approached significance) seen between PD1 expression by IHC and proliferation to CD3/28) is reassuring in this respect, as is the data identifying lower levels of $PD1^+Ki67^-$ cytokine non-productive T_H and T_C post stimulation as this links functional evidence to PD1 expression. Taken together our data points to levels of exhaustion below that seen in reactive tissues and exhausted cells comprising a very low percentage of T cells infiltrating the CHL microenvironment. These data run contrary to common opinion but are in fact consistent with the majority of IHC-based studies that quantified PD1 in CHL, which record PD1 expression at low levels. [22,201–210] They might be resolved with data that identifying higher mean PD1 levels within T_H1 cells, as this may simply reflect higher basal PD1 expression in this subset.[216] Finally, they are consistent with the functional data provided by Greaves *et al.* and whilst they conflict with data from Yamamoto *et al*. their analysis was limited to two patients.[22,268]

A criticism of these data is that we do not have a robust positive control for exhaustion and have not conclusively demonstrated the presence of an exhausted population in any sample. This raises the possibility that there is an exhausted population present that has not been detected by our approach. It is also acknowledged that we do not assess TCR clonality, hence cannot exclude the possibility of rare but important exhausted tumour-specific clones. The quantification of exhaustion by IHC in primary human tissue challenging as it is not possible to confirm the exhausted phenotype with functional testing, although deeper phenotyping goes some way to address this. This problem was considered during study design, but selection of a true positive control is difficult. Most studies have quantified exhausted cells by flow in the peripheral blood. Given that this is a different compartment the phenotype and expected cell frequencies may differ and this cannot be used as a method of validating IHC data. Additionally, the tumour environment is where effector cell activity takes place so it is here

that detection is most important. The malignancy where exhaustion is best defined is melanoma, and might therefore be the best positive control but melanoma occurs in a different tissue and comparison of expected cell frequencies and PD1 expression across tissue type is problematic.[195] Definitive evidence of exhaustion is scarce in studies of the lymphoma microenvironment, although two studies in follicular lymphoma are suggestive and together provide the best example of a positive control of an exhausted phenotype characterised in lymph node. One study identifies exhaustion defined by $PD1^{weak}TIM3^{+}$ cells, noting that $CD4^{+}PD1^{weak}TIM3^{+}$ cells are less IFNγ and IL2 productive than the $TIM3^{+}$ subset and show reduced STAT1 phosphorylation to IFNγ and STAT3 phosphorylation to IL6.[386] It is unclear if this is an exhausted subset. The reduced cytokine expression is suggestive but may be due to differentiation/effector subtype differences between the two groups. The significance of reduced phosphorylation to STATs in response to cytokine treatment is unclear as this is not a commonly accepted test of exhaustion. Trials in follicular lymphoma have shown a modest response to PD1 inhibitors.[387] If the $CD4^{+}PD1^{weak}TIM3^{+}$ subset does represent exhaustion it is notable that this phenotype was seen at significantly lower levels in CHL than RLN in our study. A second study by the same group identified a $CD4^{+}PD1^{+}LAG3^{+}$ subset as representing exhaustion.[388] The authors noted that overall $PD1^{+}$ cells were more cytokine responsive (this could be artefact of activation-induced upregulation, although the short stimulation period makes this less likely), but that the $PD1^{+}LAG3^{+}$ population was enriched for TIM3, not cytokine responsive and restored with combined PD1 and LAG3 blockade. In our study we found no significant difference in frequency of the $CD4^{+}PD1^{+}LAG3^{+}$ population in CHL compared to RLN and a significantly reduced frequency of the $CD4^{+}PD1^{+}LAG3^{+}TIM3^{+}$ population.

An equally important question is whether PD1 inhibitor activity is related to exhaustion, irrespective of its presence. To address this, we evaluated the link between known predictors of response to PD1 inhibition in CHL (PDL1 and CHL MHC II expression). We found an inverse correlation between PD1 expression and PDL1 in CHL. Two smaller studies found no correlation.[201,208] When comparing CHL MHC II expression to PD1 frequency we found an inverse relationship, the opposite to that seen between CHL MHC II and PD1 inhibitor response. Additionally, no relationship was detected when subgroups expressing multiple exhaustion markers were assessed. Further to this, a trend to negative relationship was observed between PD1 expression and proliferative capacity was observed (consistent with exhaustion) alongside a trend to positive relationship between PDL1 and proliferative capacity. Taken together these data find no evidence of a link between PD1 expression and either PDL1 or CHL-MHC II.

In conclusion we find no evidence of an exhausted population above that seen in reactive tissue and no evidence that the infiltration of putatively exhausted $PD1^+$ cells is related to the expression of established predictors of PD1 response including the PD1's ligand, PDL1. This represents the most thorough assessment of exhaustion with the largest cohort published to date in CHL. Data is concordant across two modalities (IHC and flow cytometry) and IHC data was replicated with two antibody clones.

Low PD1 expression is counterintuitive given the responsiveness of CHL to PD1 inhibition and these data point to a disconnect between the expression of PD1 and PDL1. This result is less surprising in light of the diverse roles played by PDL1 including its mediation of activation and tolerance during the normal immune response without necessarily inducing exhaustion.[389] There is significant evidence that PDL1 maintains exhaustion and blockade can rescue exhausted T cells.[379] It is less clear that PDL1 actually induces exhaustion. PD1 is upregulated in T cells on activation and chronic antigen stimulation induces an exhausted phenotype without the presence of PDL1. Knockout of PD1 or PDL1 ameliorates the expansion of exhausted T cells in chronic viral infection but this effect could also be explained by PDL1 signals maintaining exhaustion.[390] High PDL1 expression on the tumour does not therefore necessarily imply exhaustion and this is borne out by our findings. An elegant study in solid tumours similarly highlighted that the assumption that PD1 inhibitors work purely by reversal of T cell exhaustion is not necessarily borne out by patient data.[391] By compared TCR repertoires in tumour and blood before and after anti-PD1 therapy they identified that tumour-specific TIL within the microenvironment before therapy were unlikely to display an activated phenotype post therapy and that TCR sequences of tumour-specific TIL post therapy were not detected in the tumour pre therapy implying that they are newly recruited to the microenvironment.[392] This pattern is more in keeping with PD1 inhibitors modulating activation and differentiation.

Given these data we explored the connection between T cell dynamics and PDL1 in the tumour microenvironment. We focus on the role of T_H cells in light of the identified role for CHL expression of MHC II, which implies antigen presenting capacity and direct interaction with T_H.

6.5.4: Future work

Elements of this study have data outstanding which might strengthen the findings presented above. Supernatants were harvested during the bulk stimulation of CHL cells and RLN with plans to run using a flow-based multiplex cytokine assay to give a broader picture of cytokine

responsiveness. Additionally, data was collected to examine the spatial relationships between CHL cells, $PD1^{+}$/$TBET^{+}$/$EOMES^{+}$ cells and PDL1 expression which requires analysis.

This study has been limited to global T cell exhaustion phenotypes but does not address the possibility that reversal of exhaustion in antigen-specific clones are mediating the effect. A next step would therefore be to address antigen specificity. Novel technologies are making this more feasible and a study design incorporating antibodies classifying by TCRvβ family into an IMC panel would be informative. Additionally, a recent study paired TCR sequencing data with single cell RNA sequencing, demonstrating an elegant method to assess specificity of exhausted cells which could be adapted to this question. By analysing tumour and peripheral blood pre and on treatment they demonstrate that activated tumour specific cells post PD1 therapy in basal cell carcinoma carry new TCR sequences not detectable in the tumour prior to therapy, supporting a model of recruitment of new T cell clones over reinvigoration of exhaustion.[391,392]

Chapter 7: Skewing of T cell differentiation and its relationship to PDL1 and CHL-MHC II expression

7.1: Introduction

The data in the preceding chapters supports the presence of an $PDL1^+$ myeloid microenvironment which is actively recruited and induced by the CHL cell. However, despite the narrative in the literature, it does not support the presence of a significant exhausted T cell population (T_C or T_H) or a relationship between markers of T cell exhaustion and the expression of PDL1. It also finds no relationship between markers of T cell exhaustion and CHL MHC II expression, a second factor known to predict PD1 inhibitor response.

7.1.1: Beyond exhaustion: alternative roles for the PD1-PDL1 axis

Whilst many studies in cancer have focussed PD1 as an exhaustion marker, extensive data exists highlighting that the axis regulates multiple facets of immune homeostasis. PD1 regulates every stage of T cell development including within the thymus, limiting naïve T activation, influencing differentiation, affecting effector function and mediating exhaustion.[393] T-Ex are identifiable by sustained high PD1 expression, whereas most T cells appear $PD1^-$. The fact that most cells do not express observable PD1 expression levels does not imply that they are not PDL1 responsive. PD1 is barely detectable on resting T cells but its engagement is a potent inhibitor of the earliest activation events.[393–395] PD1 is rapidly upregulated on T cell activation suggesting an important role in early T cell fate and low levels of PD1 are sufficient for potent inhibition of activation.[394,396] PD1 ligation during activation modulates the strength of TCR signal.[193,194] This in turn affects the antigen recognition threshold, determining whether a T cell is activated, resulting in an antigen-specific modulation of activation.[194]

PD1 influences not just whether a T cell is activated but also its fate once activated, modulating effector differentiation, inducing anergy and duration of activation. The modulation of TCR signal strength by PD1 in turn impacts effector functions by altering differentiation.[190] TCR signal strength is directly implicated in the fate of T_H cells as they differentiate, with very low signal strengths resulting in anergy, low leading to tumour-protective T_H2 and T_{Reg} and higher leading to anti-tumour T_H1 and T_H17.[272,397,398] Data suggests that the absence of PD1 inhibits the generation of T_{Reg} and that low affinity TCRs similarly

support T_{Reg} function.[399,400] Interestingly, ITK deficiency (one of the primary immunodeficiencies predisposing to CHL) also dampens the TCR signalling pathway skewing from T_H17 to T_{Reg}.[401]

The axis is also central to regulating anergy. In tertiary lymphoid structures PD1-PDL1 interactions are required for the induction of T cell anergy post activation and early blockade of the axis can prevent anergy.[402] Similarly in NKT cells, blockade of the PD1-PDL1 axis prevents the induction of anergy during activation but cannot reverse an established anergic state.[196] These data point to an important role for the axis within tertiary lymphoid structures that may be particularly relevant in the context of lymphoid tumours. More generally, the PD1-PDL1 axis regulates tolerance, protecting against tissue damage from autoreactive cells (without the requirement for exhaustion).[403]

After activation further evidence suggests a role for the axis as an effector molecule of $FOXP3^+$ T_{Reg}.[404] Data are mixed regarding this mechanism, with initial reports identifying a small suppressive effect if any.[194,403,405] However, with the advent of PD1 inhibitor therapy this mechanism has garnered more attention due to the emergence of Hyper-progressive disease.[406] $PD1^{hi}T_{Reg}$ have been identified in the context of Hyper-progressive disease on PD1 inhibitor therapy. A recent report links $PD1^{hi}T_{Reg}$ to an increased risk of Hyper-progressive disease in gastric cancer, reporting an increase in $PD1^{hi}T_{Reg}$ suppressive function with PD1 inhibition.[407] Consistent with this, the FOXP3+ T cell compartment is larger in PD1 deficient mice, although this may reflect activation rather than true T_{Reg}.[194] Notably in gastric cancer infiltration of T_{Reg} is associated with adverse prognosis whereas in CHL it is associated with good prognosis.[176,408] Further data suggests whilst an early expansion in T_{Reg} is seen with PD1 blockade this precedes a subsequent collapse in T_{Reg} numbers due to a requirement for PD1 signalling to maintain the T_{Reg} population and a shift in T_{Reg} phenotype.[409] Taken together these data highlight marked effects on T_{Reg} function and homeostasis with PD1 blockade. Some of these effects promote depletion and phenotypic shift whereas others may increase suppressive potential - a double edged sword.

Further roles are likely. T cell distribution and trafficking are influenced by PDL1, although it is unclear if this is a direct effect or if PDL1 expression is identifying areas of immune privilege.[410] PDL1 is also expressed on T cells and the function in this context is poorly defined although may connect to PD1 as a T_{Reg} effector molecule. Additional roles in regulation of the antibody response, likely due to high PD1 expression on naïve B cells and on T_{FH}.[411,412]

These data demonstrate that the physiological effects of elevated PDL1 expression extend far beyond the maintenance of exhaustion. Data associating CHL-MHC II expression with response to PD1 inhibitors is suggestive of a role for T_H cells. We therefore assessed dynamics of T_H cell differentiation and distribution in CHL and their relationship to PDL1 expression.

7.2: Aims and Objectives

7.2.1: Aims

To test the relationship between PDL1 and CHL antigen presenting function and T_H differentiation in the CHL microenvironment.

7.2.2: Objectives

1. To assess frequencies of T_H subtypes in the CHL microenvironment and their relationship to each other and to PDL1 and CHL-MHC II expression.
2. To model the influence of PDL1 and CHL-MHC II expression on subset distribution
3. To functionally assess the skewing of T_H differentiation by CHL cells and the immunosuppressive microenvironment

7.3: Materials and Methods

7.3.1: Single marker IHC

T_H cells were quantified using markers for master transcription factors: TBET (T_H1), GATA3 (T_H2), RORγT (T_H17) and FOXP3 (T_{Reg}) on the entire patient cohort. See section 2.2.

7.3.2: Virtual multiplex IHC

Multiplex IHC (mIHC) was performed on 47 patients arrayed on a single TMA and compared to RLN controls. CD8 was placed last in the stripping panel due to failure to strip completely during validation experiments. Concurrent tonsil fresh and stripping controls and were run to assess for signal loss. See 2.3.

Table 7.1: mIHC stripping panels

	DAY 1	DAY 2	DAY 3	DAY 4	DAY 5	DAY 6	DAY 7
PANEL	CD4	TBET	RORγT	FOXP3	CD8		

7.3.3: Analysis and Clustering

Analysis and clustering was performed in R using the ggplot2 and pheatmap packages.[307,325]

7.3.4: Dual progressive IHC and spatial modelling

Serial sections of 10 CHL cases selected for strong CD30 signal were stained. The central section was stained for CD3 (identifying T cells) with DAB and CD30 (identifying CHL) with VIP chromogen. The CD30 was then stripped and restained for PDL1 (identifying CHL and microenvironmental PDL1). Serial sections on either side of the first were stained for FOXP3/CD8, RORγT/CD8, GATA3/CD8 and TBET/CD8. Images were then virtually aligned with Visiopharm software. Cell locations were mapped and exported to R for spatial analysis. CD8 was selected over CD4 due to cleaner cell identification with stronger signal and less background due to lack of macrophage CD4 signal. Dual staining approach allows identification of dual positivity to distinguish transcription factor positive CD8. Transcription factor staining in the absence of CD8 was classified as T_H.

In nearest neighbour analyses a comparison group of overall T_H distribution was inferred using the following function:

```
InfCD4 <- function(spatialpattern, neighbour){
 Tnn = nncross(spatialpattern$CD8, neighbour, what = "dist")
 ssize = if_else(spatialpattern$CD3$n/2 < spatialpattern$CD8$n, round(spatialpattern
$CD3$n/2), spatialpattern $CD8$n/1)
 Tnns = sample(Tnn, size = ssize)
 range = nncross(spatialpattern $CD3, neighbour, what = "dist")
 for (i in Tnns){
  id = which(abs(range-i)==min(abs(range-i)))
  range <- range[-id[1]]}
 return(range)}
```

This calculates the distance from every $CD8^+$ cell to e.g. CHL cell and every $CD3^+$ cell to CHL cell. Next, for every CD8 nearest neighbour distance the most similar CD3 nearest neighbour distance is subtracted from the CD3 distribution. The CD3 distribution that remains after this process is an estimate of CD4 distribution (a safe assumption given that double negative $CD3^+$ are rare). Counts of individual markers, especially membrane markers, are never entirely accurate due to difficulties in segmentation and signal strength. Therefore, direct comparison of membrane counts between different markers is difficult. Counts are however distributionally proportional so comparison by this method remains valid. Because of count discrepancies occasionally the CD8 count will exceed the CD3 count in absolute number. This is likely an artefact of the counting process and does not imply that no CD4 T cells are present. To account for this issue in the function if CD8 count exceeds 50% of the CD3 count a random sample of the CD8 count is used.

Figure 7.1: Spatial modelling IHC study design

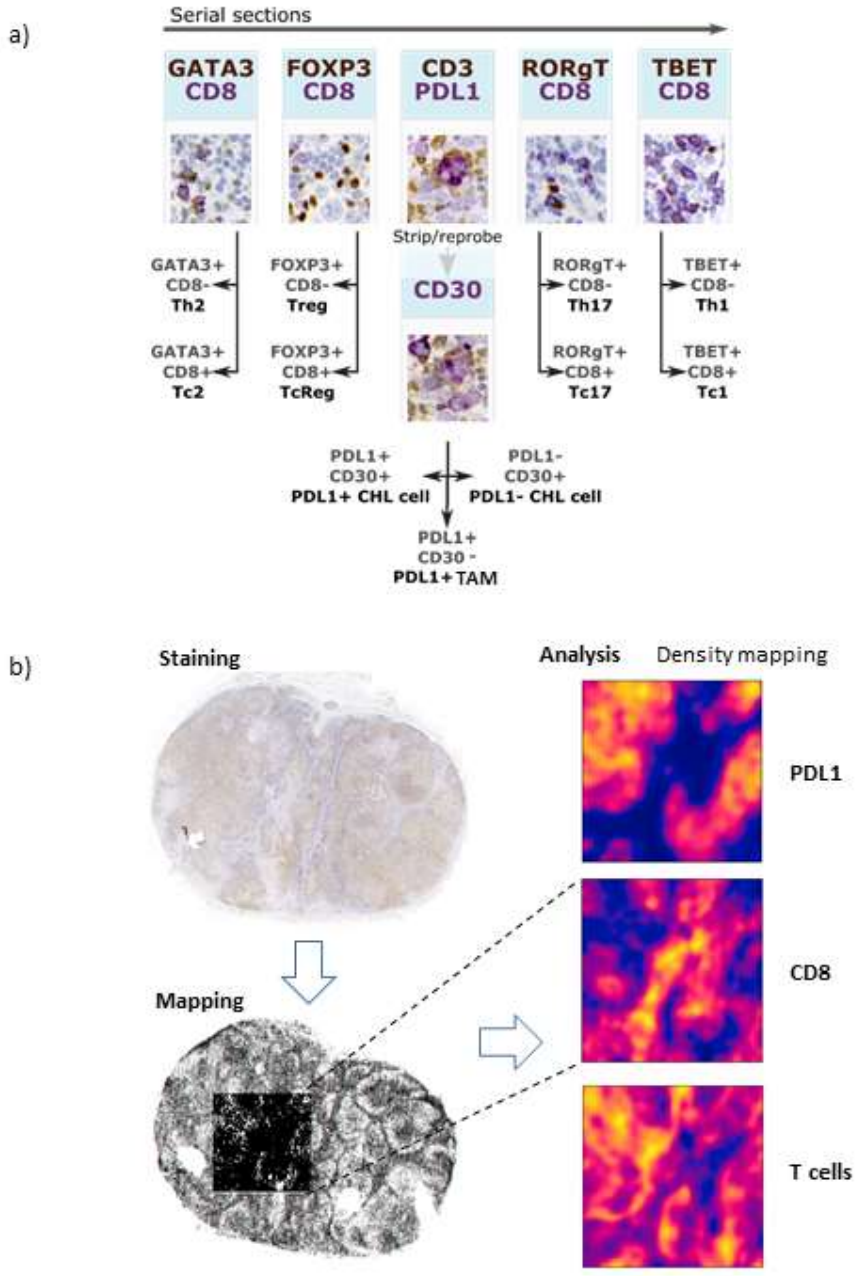

Figure 7.1: a) Dual staining of CD8 with master transcription factors for T_H2 (GATA3), T_{Reg} (FOXP3), T_H17 (RORγT) and T_H1 (TBET) on serial sections was used to identify T cell subtypes and classify as T_C or T_H. CD3 staining of the central section was used to permit comparison to the distribution of all T cells. A central section was stained with PDL1 and stripped and reprobed with CD30 enabling classification of cells into $CD30^+$ CHL cells by PDL1 status and mapping of PDL1 staining in the microenvironment. b) Slides were virtually aligned and cell locations mapped for analysis

7.3.5: *In vitro* modelling

Four *in vitro* models were developed during this PhD. The first modelled the effect of CHL secreted factors on T_H differentiation and involved an 8-day stimulation of negatively selected naïve $CD4^+$ T cells form healthy donors *in vitro* with CD3/CD28 stimulation and the addition on day 1 of 50% CHL KMH2 cell line conditioned media. For further details, see 2.3.8. The Naïve T/Lymphoma direct priming model was performed in the allogenic setting. A donor matched to L428 MHC II was sourced validation and these experiments are planned. L428 cell line has lost MHC I expression and one MHC II allele making HLA matching feasible.

Analysis of the Naïve T stimulation and macrophage-T cell priming models were performed by flow cytometry using a chemokine receptor panel to define T_H subsets (CD3, CD4, CD25, CD127, CXCR3, CCR4, CCR6, CCR10, DAPI). Analysis of the Naïve T/Lymphoma direct priming model was performed by flow cytometry using an intracellular panel for more robust T_{Reg} identification (CD3, CD4, CD25, CD127, FOXP3, TBET, Live/Dead efl780). The primed T cell cytotoxicity model remains under optimisation.

Figure 7.2: In vitro models

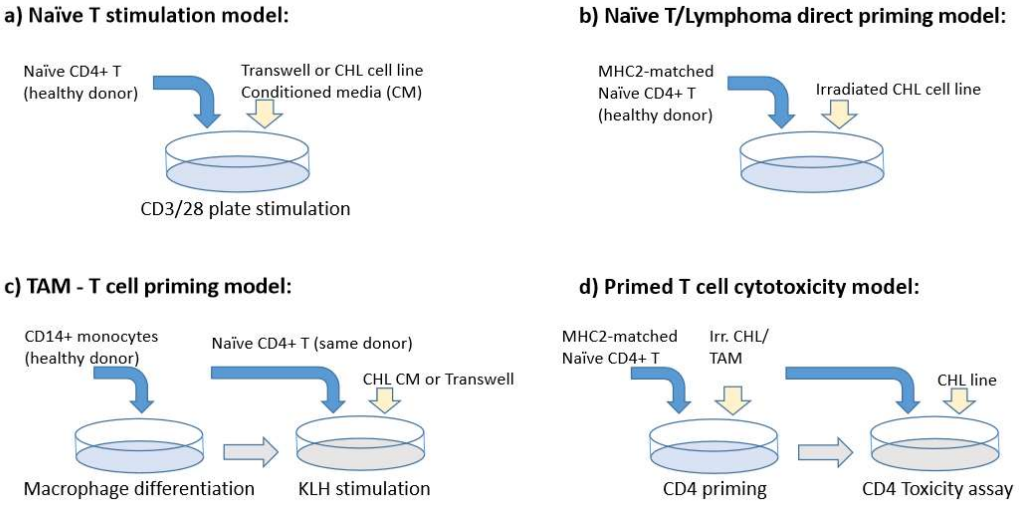

Figure 7.2: a) Naïve T cell stimulation model comparing the effect of CHL cell line conditioned media on the differentiation of T_H cells differentiating in response to CD3/CD28 stimulation. b) Direct priming model where naïve T_H are cocultured with irradiated CHL cell lines. This model is limited by the allo-effect. c) Tumour associated macrophage – T priming model (see chapter 4). Monocyte-derived macrophages are cultured from healthy donor PBMCs before priming with CHL cell line conditioned media. The media is then removed and autologous naïve T_H are added to test the functional effects of priming. d) Primed cytotoxicity model (under optimisation). Naïve T_H are co-cultured with irradiated cell lines (which die within 2-3 days). T_H differentiate over 8-day period before re-challenge with the cell line to test cytotoxicity against the cell line as a target. Effects of PD1 inhibition are then modelled within the system.

7.4: Results

7.4.1: Assessing T_H subsets by single marker IHC

7.4.1.1: Quantification of T cell subsets

Infiltration and skewing of T_H subset was assessed by quantification of master transcription factors for T_H lineages and calculated as a ratio to CD3 to account for variations in T cell infiltration. A significant enrichment of T_H1 and T_{Reg} was detected in CHL compared to RLN. No difference was detected in T_H2 infiltration and a significant paucity of T_H17 was detected. T_{Reg} and T_H2 are thought to play a tumour-supportive role whereas T_H1 and T_H17 play a putative anti-tumour role. The enrichment of T_{Reg} in the CHL microenvironment might therefore be predicted, as would enrichment of T_H2 although that was not detected in our study. The enrichment of T_H1 has previously been documented and is counterintuitive. This may represent an ineffective immune response or alternatively T_H1 might not be playing an anti-tumour role. The paucity of T_H17 is a novel finding and might suggest suppression of an anti-tumour population by the CHL cell.

Figure 7.3: Quantification of T cell subsets

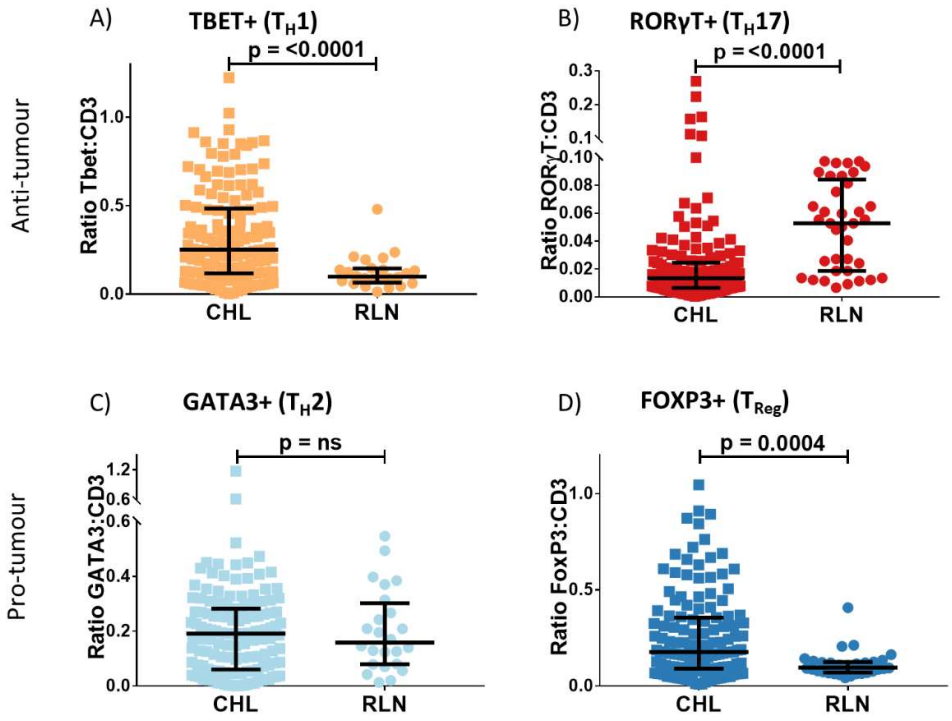

Figure 7.3: Comparison of T_H transcription factor expression in CHL compared to Reactive Lymph Node by conventional IHC on TMA. T_H subsets quantified by single marker IHC of master transcription factors TBET, RORγT, GATA3 and FOXP3 (T_H1, T_H17, T_H2, T_{Reg} respectively) and expressed as ration to CD3. T_H1 and T_H17 have putatively anti-tumour roles and T_H2 and T_{Reg} pro-tumour. Comparisons by Mann-Whitney.

7.4.1.2: T_H cell subsets and viral status

In light of the fact that HIV is disproportionately associated with CHL, that incidence relates to CD4 count but viral suppression status and that T_H are specifically depleted by the HIV virus we hypothesised that the pattern of T_H depletion in HIV-associated CHL might highlight important T_H interactions to CHL as a whole. Of note, T_H17 cells are reported to be disproportionally depleted in HIV and are slow to recover on anti-retroviral therapy.[413] We identified a cohort of 18 patients treated for HIV-associated CHL suitable for arraying. CHL incidence peaked with CD4 counts from 100-400 irrespective of HIV treatment status in line with published data. RORγT staining by IHC was reduced in HIV-RLN compared to RLN (Mann Whitney p=<0.0001) and expression in both CHL and HIV associated CHL tissue was lower than HIV-RLN (one-way

ANOVA p=0.0026). Percentage CD4 positive was lower in HIV associated CHL than CHL in HIV negative patients ($p<0.0001$), however no correlation was seen between intra-tumoral CD4 count and peripheral blood CD4. Data were analysed as ratio to CD4 to account for the differences in parent T_H populations. RORγT:CD4 was reduced in HIV^+ RLN compared to HIV negative, although this did not reach statistical significance. RORγT:CD4 was reduced in CHL irrespective of viral status relative to both HIV^+ and HIV^- RLN. In contrast a significantly elevated TBET:CD4 and FOXP3:CD4 ratio was seen in HIV^+ relative to HIV^- RLN. Both TBET:CD4 and FOXP3:CD4 ratio were significantly increased in CHL tissue irrespective of viral status relative to HIV^- RLN but no significant difference was seen in comparison to HIV^+ RLN. In summary HIV^+ RLN (a condition predisposing to CHL) was characterised by reduced RORγT:CD4 and elevated TBET:CD4 and FOXP3:CD4 ratio, closely mirroring the pattern seen in CHL. However, no significant differences were detected between CHL subtypes by CHL status. From this we conclude firstly that the T_H disturbances seen in HIV may create an environment conducive to CHL survival and secondly that the pattern of T_H differentiation seen in CHL is specific to the CHL microenvironment rather than simply a reflection of host immune status. This finding also provides a validation cohort confirming novel observation of reduced T_H17 frequency (as measured by RORγT) in CHL.

Figure 7.4: T_H cell subsets and viral status

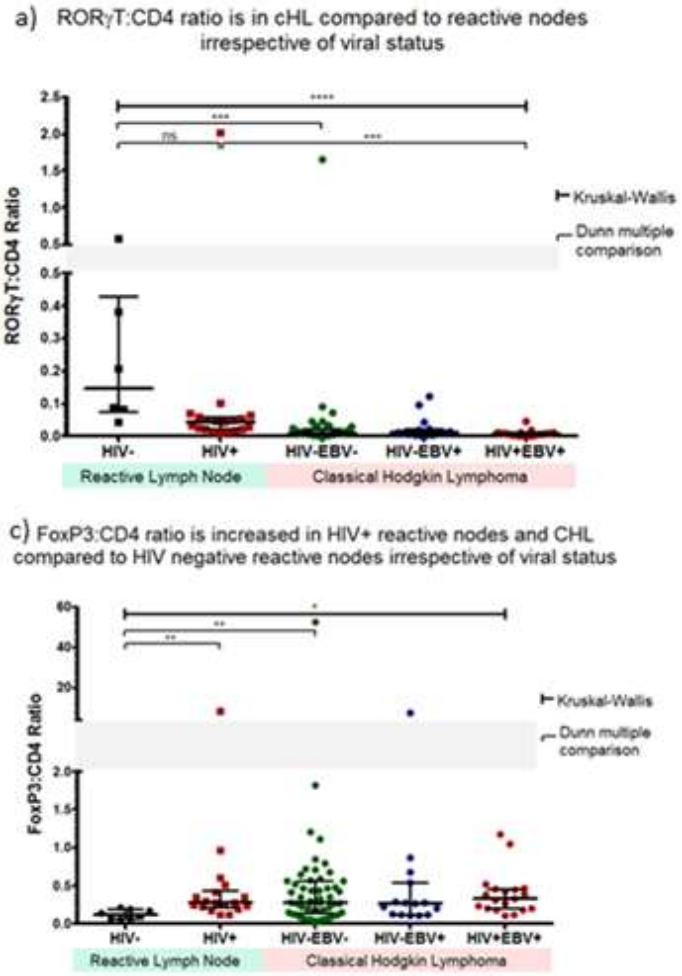

Figure 7.4: a) RORγT:CD4 ratio by conventional IHC on TMA. CHL and RLN stratified by HIV and EBV viral status. Across-group comparison by Kruskal-Wallis ($p<0.0001$). Pairwise by Dunn post-test. b) FOXP3:CD4 ratio comparison demonstrated a significant difference on Kruskal-Wallis ($p<0.05$). Dunn post-test comparison detected an increase in FOXP3 expression in HIV-RLN and CHL compared to HIV negative but no significant difference between HIV-RLN and HIV-associated CHL.

7.4.1.3: Relationships between T cell subsets and the PDL1 axis

In light of our finding of skewed T_H differentiation we assessed connections between T_H differentiation and PDL1 expression. Ratios of T_H transcription factors to CD3 infiltration were correlated against each other, against CD68 (to estimate macrophage infiltration) and PDL1. PDL1 correlated positively with GATA3:CD3 ratio (T_H2) and to TBET:CD3 ratio (T_H1) and negatively with RORγT:CD3 ratio (T_H17). No relationship was detected between T_{Reg} and PDL1 by correlation. Again, of note, no relationship was detected between PD1:CD3 ratio and PDL1 by correlation. Taken together this is suggestive of the CHL microenvironment being enriched for T_H1 and T_{Reg}, being both T_H17 and PD1 deplete. This is combined with a positive relationship between T_H1, T_H2 and both macrophages and PDL1, and a negative relationship between T_H17

and PDL1. Finally, a positive relationship was seen between T_H2 and T_{Reg} and a negative relationship between PD1 and T_{Reg}.

Figure 7.5: Correlation matrix between T cell subsets and the PDL1 axis

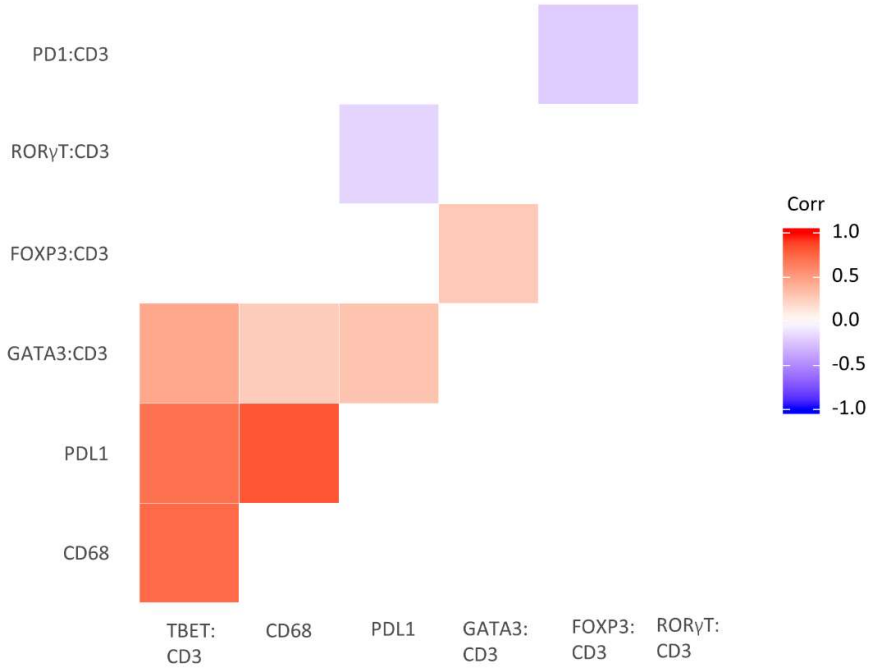

Figure 7.5: Correlation matrix between T_H master transcription factors as a ratio to CD3 and PDL1 demonstrates a negative correlation between RORγT:CD3 (T_H17) and a positive correlation between PDL1 and GATA3:CD3 (T_H2) on TMA. and TBET:CD3 (T_H1). Red indicates positive correlation, blue indicates negative. Colours are only displayed in cases reaching statistical significance. Data quantified by single marker IHC

7.4.1.4: Relationships between T cell subsets and CHL cell MHC II expression

We next assess the relationship between T_H subsets and CHL-MHC II expression. A positive association was noted between FOXP3:CD3 ratio (T_{Reg}) and CHL-MHC II expression ($p = 0.021$). with statistically insignificant trends towards a positive association seen in GATA3:CD3 (T_H2) which was statistically significant in the MC-CHL subgroup ($p = 0.07$ and $p = 0.006$ respectively). No relationship was seen between TBET:CD3 (T_H1) and RORγT:CD3 (T_H17) and CHL-MHC II expression and a negative relationship was observed between PD1:CD3 ratio and

CHL-MHC II (p = 0.037). These statistical relationships were unchanged when analysed as single IHC markers as opposed to CD3 ratio.

In summary, these data extend our findings of T_H1/T_{Reg} enrichment with T_H17 /PD1 paucity and correlations between T_H1 (positive), T_H2 (positive) and T_H17 (negative) and PDL1, demonstrating a positive relationship between both T_{Reg} and PDL1 expression and a negative relationship between PD1 and PDL1.

Figure 7.6: T_H cell subsets by CHL MHC II expression

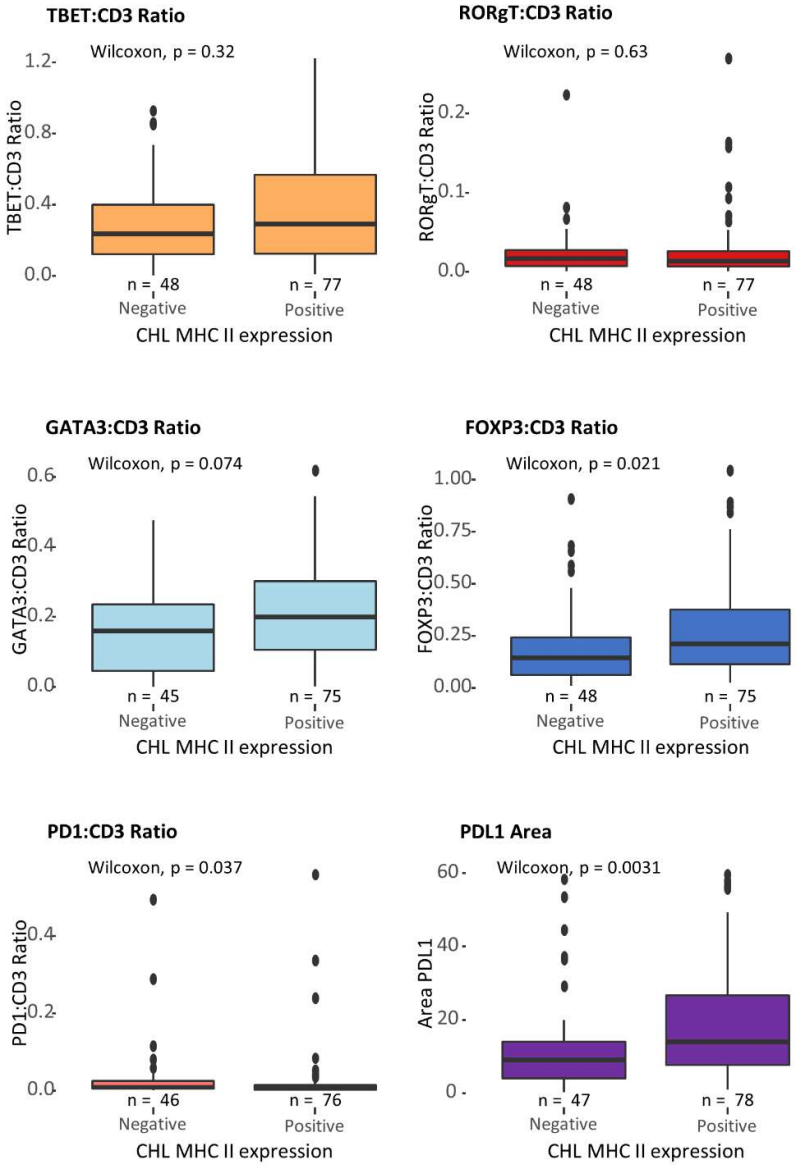

Figure 7.6: Comparison of T_H subsets in CHL by CHL-cell MHC II expression status. Quantified by single marker IHC of TBET, RORγT, GATA3 and FOXP3 (T_H1, T_H17, T_H2, T_{Reg} respectively) and PD1 expressed as ratio to CD3 on TMA. T_H1 and T_H17 have putatively anti-tumour roles and T_H2 and T_{Reg} pro-tumour. Comparisons by Wilcoxon unpaired rank-sum (Mann-Whitney)

7.4.1.5: Unsupervised hierarchical clustering

We next sought to assess the broader relationship between these metric. To do this we performed unsupervised hierarchical clustering of single marker IHC data across all CHL cases including markers of the major T_H subsets, PD1 as a marker of exhaustion, PDL1 and CD68. Overall, clustering of data demonstrated that the dominant signature related to tumour EBV status. However, when stratified by EBV status clusters with high PDL1 expression and CD68 positivity associated with T_H infiltration and subset skewing as did retention of CHL-MHC II expression. This effect was most pronounced in the EBV^+ group. The EBV^+ group also contained the majority of MC-CHL cases however, these were distributed across clusters. Notably, PD1 expression did not associate with PDL1, CD68 or CHL-MHC II in either subtype.

Figure 7.7: Unsupervised hierarchical clustering

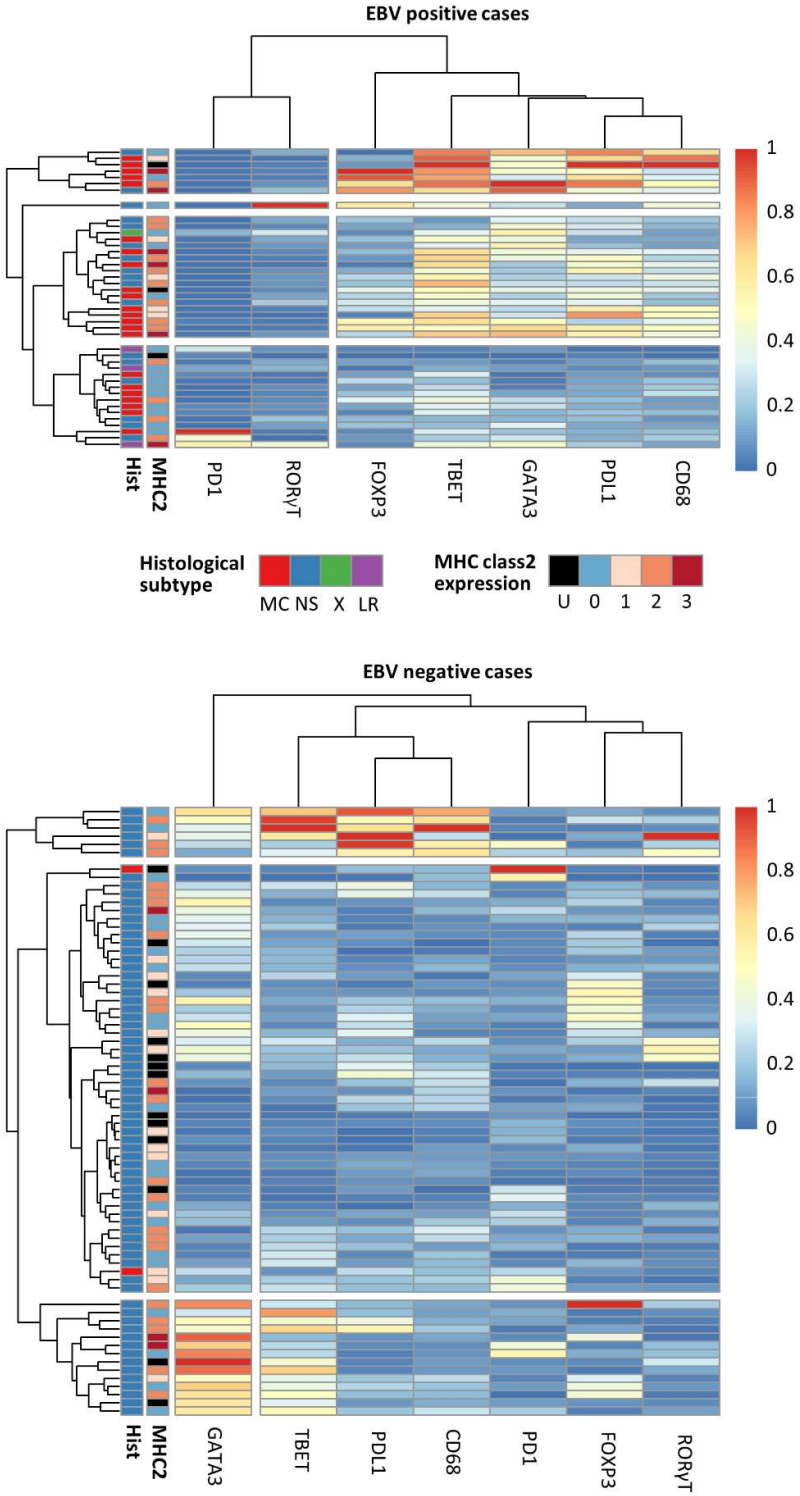

Figure 7.7: Unsupervised hierarchical clustering of cases by T_H cell master transcription factor expression (TBET = T_H1, GATA3 = T_H2, RORγT = T_H17, FOXP3 = T_{Reg}), PD1, PDL1 and CD68 (TAM) stratified by EBV status. Clusters marked by CHL-MHC II status (U = unclassified, 0 = negative, 1 = low/non-membranous, 2 = positive, 3 = strong positive) and histological subtype (MC = mixed cellularity, NS = nodular sclerosing, X = unclassifiable, LR = lymphocyte rich). Colour scaling is relative to all CHL cases within the heatmap. Therefore, FOXP3 "low" represents low relative to CHL cases as opposed to levels in reactive issue. Data represents CHL samples by IHC on TMA.

7.4.2: Summary of single marker IHC quantification data

There are limitations to single marker IHC. FOXP3 and to a lesser extent RORγT and TBET show a high level of T cell restriction, whereas GATA3 expression is also reported in B cells. All markers to varying degrees are expressed in both T_C and T_H. Therefore, single marker phenotyping, even expressed as ratios to CD3, is only indicative of T_H subset skewing. With these caveats, the data demonstrated an over-representation of T_H1 and T_{Reg} and under-representation of T_H17 and $PD1^+$ cells relative to RLN. We did not detect T_H2 enrichment by this method. T_H1 and T_H2 correlated positively with PDL1 whereas a negative correlation was seen to T_H17. A positive association was between T_{Reg} and CHL-MHC II whereas a negative association was seen between PD1 and CHL-MHC II. Within the myeloid compartment, PDL1 was positively associated with macrophages and with CHL-MHC II. Finally, unsupervised hierarchical clustering identified clusters associated with CHL-MHC II positivity and PDL1 expression that also associated with T_H1, T_H2 and T_{Reg} enrichment but not with PD1 expression. These clusters were most evident in EBV^+CHL. These data provide evidence of a connection between T_H subset differentiation and PDL1 and CHL MHC II expression (markers of PD1 inhibitor activity). Consistent with the findings in the previous chapter no relationship was detected to PD1 expression.

7.4.3: T_H phenotyping

To validate our single marker IHC data and investigate skewing of T_H differentiation we performed deeper phenotyping using multiplex IHC in a sub-cohort of 47 CHL cases and 31 RLN. This enables the robust identification of T_H cells and also permits assessment of dual-expression of transcription factors. Over-representation of $CD4^+TBET^+$ T_H1 and

CD4+TBET^{+}FOXP3^{+} T_H1 regulatory (T_H1_{Reg}) was detected in CHL cases whilst under-representation of CD4^{+}RORγT^{+}TBET^{+} $T_H1/17$, CD4^{+}RORγT^{+}T_H17, CD4^{+}RORγT^{+}FOXP3^{+} T_H17_{Reg} and CD4^{+}FOXP3^{+} T_{Reg} was seen.

Figure 7.8: T_H phenotyping and the relationship to CHL-MHCII and PDL1 expression

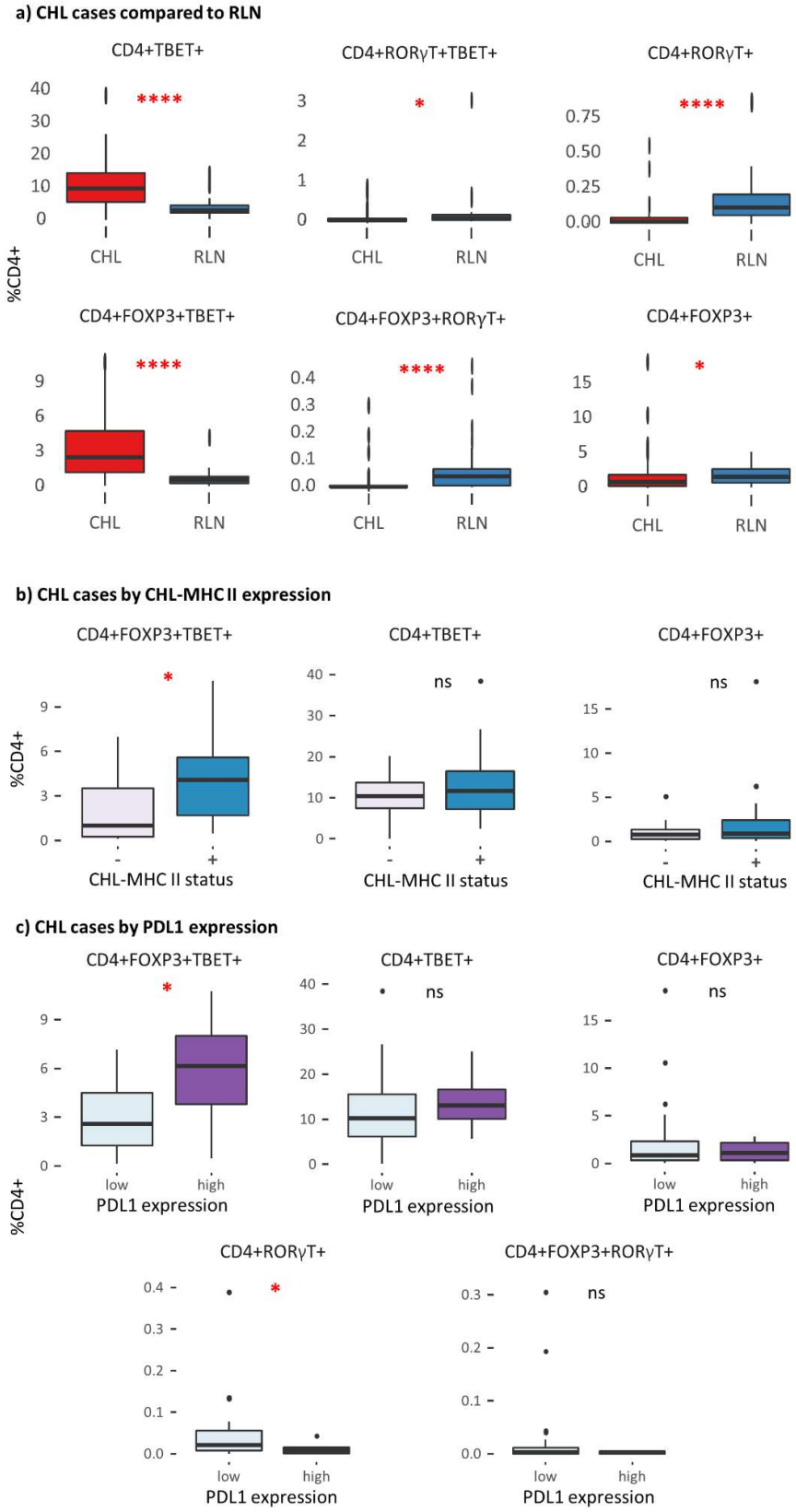

Figure 7.8: Analysis of CD4, CD8, RORγT, TBET and FOXP3 co-expression by multiplex IHC in CHL and reactive lymph node on TMA. a) Significant enrichment of $CD4^+TBET^+$ T_H1 ($FOXP3^-$ $ROR\gamma T^-$) and $CD4+TBET^+FOXP3^+$ T_H1_{Reg} was detected in CHL cases whilst significant under-representation of $CD4^+ROR\gamma T^+TBET^+$ $T_H1/17$, $CD4^+ROR\gamma T^+T_H17$, $CD4^+ROR\gamma T^+FOXP3^+$ T_H17_{Reg} and $CD4^+FOXP3^+$ T_{Reg} was seen. CHL n = 47, RLN n = 31. b) On comparison between MHC II negative vs. MHC II positive CHL cases, $CD4+TBET^+FOXP3^+$ T_H1_{Reg} enrichment was seen in CHL-MHC II positive cases but no enrichment of $CD4^+TBET^+$ T_H1 or $CD4^+FOXP3^+$ T_{Reg} was detected. CHL-MHC II negative n = 10, CHL-MHC II positive n = 23. CHL-MHC II status was scored manually. Scoring was blinded to results. c) On comparison between PDL1 high vs. PDL1 low CHL cases, $CD4+TBET^+FOXP3^+$ T_H1_{Reg} enrichment and $CD4+ROR\gamma T^+$ T_H17 under-representation was seen in PDL1 high cases whilst no difference in $CD4^+TBET^+$ T_H1, $CD4^+FOXP3^+ROR\gamma T^+$ T_H17_{Reg} or $CD4^+FOXP3^+$ T_{Reg} infiltration was detected. PDL1 low n = 31, PDL1 high n = 8. Cut at midpoint of the range of expression, blinded to results. Statistical comparisons were performed by unpaired Wilcoxon rank.

The levels of T_H1_{Reg} and T_H17_{Reg} expression between CHL and RLN mirrored that of T_H1 and T_H17 (Figure 7.4.3, panel a). There was no significant difference in ratios of T_H17 to T_H17_{Reg} between CHL and RLN. Ratios of T_H1 to T_H1_{Reg} showed a trend to over-representation of T_H1_{Reg} in CHL ($p = 0.09$). (data not shown). Notably, $CD4^+$ ($ROR\gamma T^-TBET^-$) $FOXP3^+$ T_{Reg} were significantly under-represented in CHL suggesting that the enrichment of T_{Reg} in CHL is specifically due to enrichment of T_H1_{Reg}. On comparison between MHC II negative vs. MHC II positive CHL cases, $CD4+TBET^+FOXP3^+$ T_H1_{Reg} enrichment was seen in CHL-MHC II positive cases but no enrichment of $CD4^+TBET^+$ T_H1 or $CD4^+FOXP3^+$ T_{Reg} was detected. This is notable as it fits with a hypothesis of CHL-MHC II expression conferring an ability to enrich for T_H1_{Reg} over and above enrichment for T_H1, potentially limiting the anti-tumour T_H1 response. On comparison between PDL1 high and PDL1 low CHL cases the same pattern of specific T_H1_{Reg} but not T_H1 or $TBET^-ROR\gamma T^-$ T_{Reg} enrichment was seen. Additionally, under-representation of $CD4+ROR\gamma T^+$ T_H17 but not of $CD4^+FOXP3^+ROR\gamma T^+$ T_H17_{Reg} was seen. These data are consistent with our hypothesis that PDL1 expression and CHL MHC II confer an ability to promote tumour-protective T_{Reg} differentiation and supress anti-tumour T_H17. Furthermore, they extend this to suggest that this may be mediated by control of anti-tumour T_H1 by preferential induction of T_H1_{Reg}. On subgroup analysis the above findings were seen across both NS-CHL and MC-CHL subtypes and were

seen irrespective of EBV or HIV viral status. These data are consistent and extend our observations by single marker IHC.

The above data is suggestive of marked T_H recruitment and T_H subset skewing in CHL when compared to reactive tissues and a link between skewing and both CHL-MHC II expression and PDL1. Specifically, an over-representation T_H cells with enrichment for T_H1 and T_{Reg}, specifically T_H1_{Reg}, and a paucity of T_H17. These correlative data describe T_H subtypes with the microenvironment but it is difficult to determine which types are directly induced by the tumour and which represent an appropriate immune response.

CHL cell infiltration is highly variable and it is likely that only cells in proximity to the tumour cells are directly interacting with the tumour. Cells at a greater distance may reflect the background signature of the node or being immune responders that are attracted to but are physically or chemically restrained from penetrating the tumour body. Crude cell counts will capture all of these cell types. Understanding the spatial relationship between cells and the tumour is therefore important. We sought to characterise the spatial relationships between CHL cells and T_H subsets.

7.4.4: Spatial modelling

We performed in depth spatial analysis on 10 CHL cases to assess T_H skewing by CHL cells and its relationship to PDL1 and CHL MHC II.

The optimal test of enrichment and the best method to evaluate true CHL-T_C contact would be a permutation test of random labelling. However, because only CD3 and CD8 locations were recorded this analysis approach was not possible. T_H spatial distribution was therefore inferred by comparison of T_C distribution to T cell distribution as a whole. T_H spatial enrichment relative to the T_C population was observed in 6/10 cases. This suggests that T_H provide a barrier around CHL cells limiting the ability for anti-tumour T_C to come into physical contact with the tumour cell (which is required for their effector functions).

Figure 7.9: T_H spatial skewing analysis

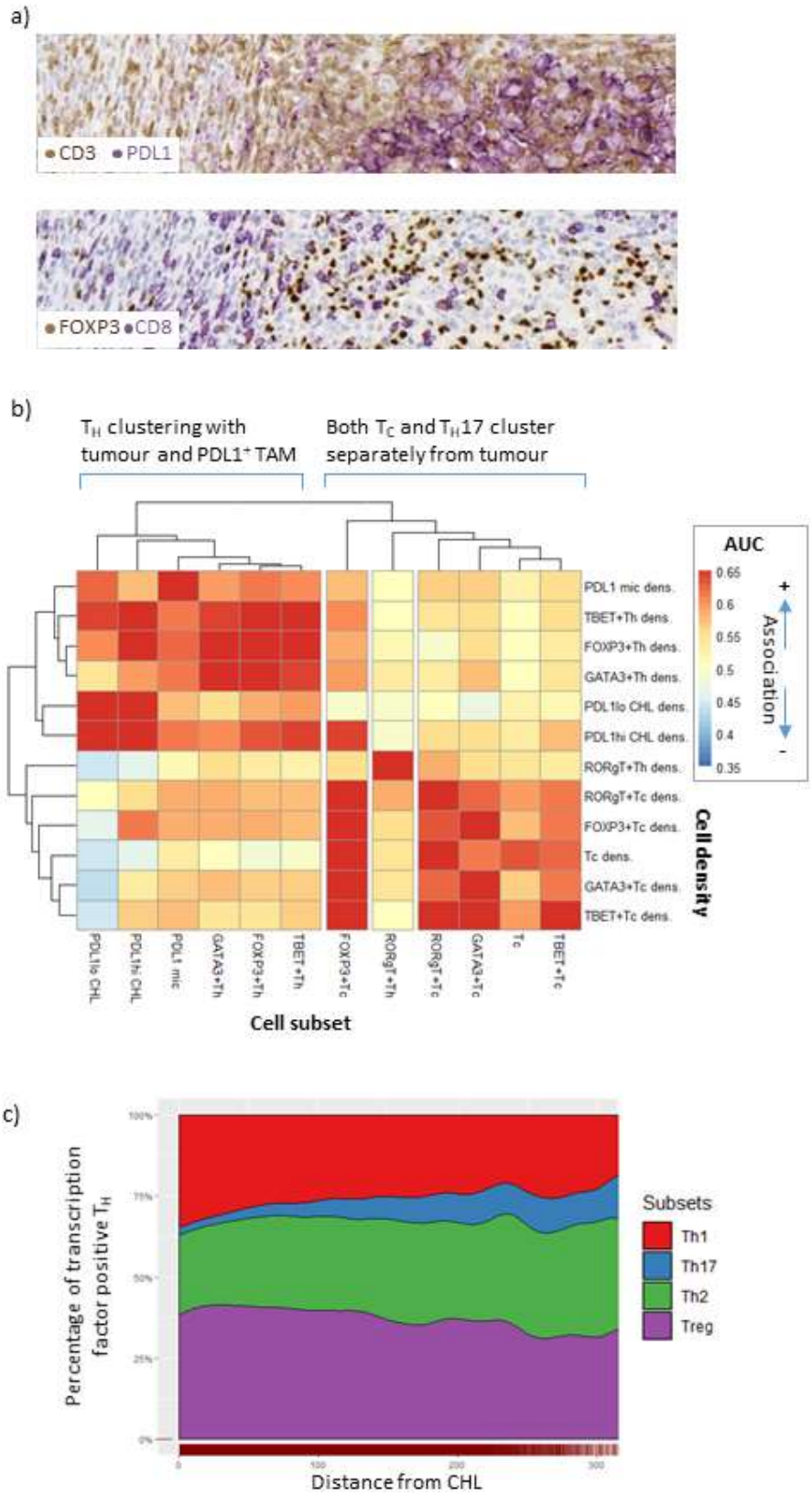

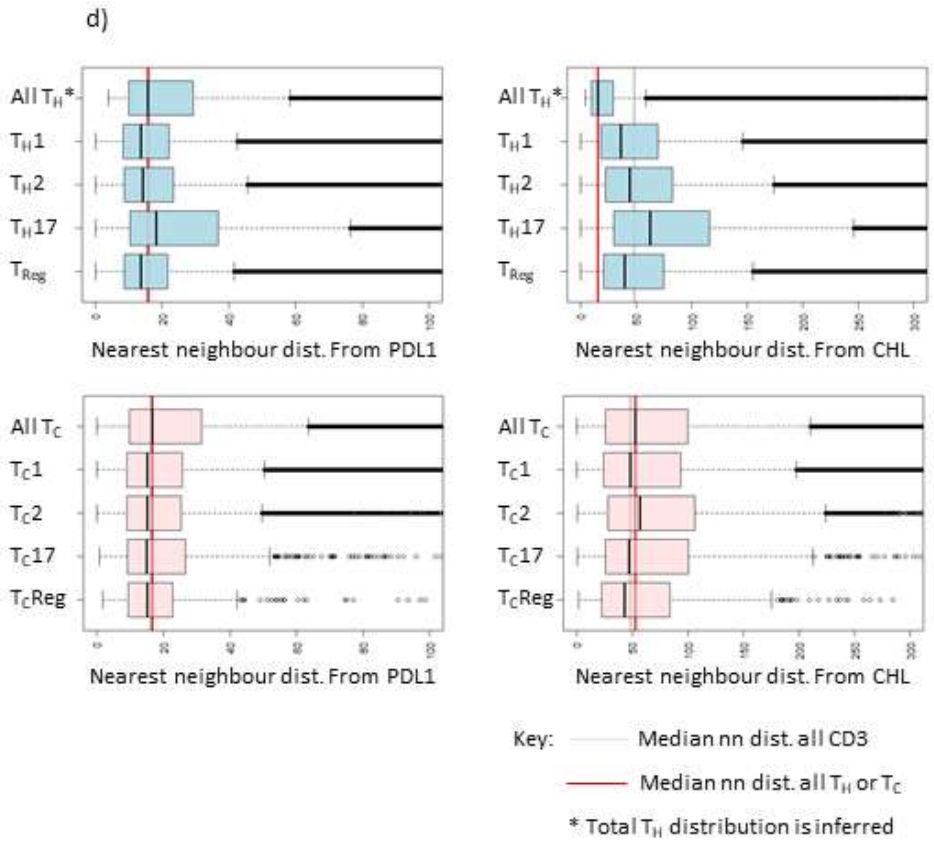

Figure 7.9: Spatial analysis of a single case. A central section was stained with CD3 and PDL1 before stripping of PDL1 and restaining with CD30. Serial sections were stained with FOXP3 plus CD8, RORγT plus CD8, TBET plus CD8 and GATA3 plus CD8. Images were virtually aligned. a) Top: Dual staining of CD3 (brown) surrounding and within the CHL tumour region. PDL1 (purple) marking CHL cells and myeloid microenvironment. Bottom: CD8 negative FOXP3 cells within the tumour. b) Spatial interdependency analysis (a novel analysis) – heatmap and clustering of AUC values (area under a receiver operator curve) quantifying the ability of the density of a cell type B (y axis) to predict the distribution of cell type A (x axis). See methods. Analysis demonstrates that T_H1, T_H2, T_{Reg}, CHL and PDL1$^+$ microenvironmental cells positively predict the locations of each other and cluster together. In contrast the majority of T_C phenotypes cluster together. Notably T_H17 cluster with T_C and not with other T_H cells. c) Relative distribution plot of transcription factor positive T_H subsets with increasing nearest neighbour distance from CHL cells. d) Nearest neighbour distances from PDL1 (left) or CHL cells (right) of T_H (blue) and T_C (red) subsets. Distribution of T_H overall is inferred by subtraction of the mapped T_C distribution from the mapped T cell distribution. Red line represents the median nearest neighbour distance for all T_C or T_H. Grey line represents the median nearest neighbour distance for all T cells.

In all cases CHL and PDL1^{+} macrophages were clustered together. In 7/10 cases T_H clustered with PDL1^{+} macrophages and CHL and separately from T_C. Notably in 5 of the 7 cases T_H17 separated from the other T_H subsets clustering with T_C. In 8/9 cases the location of PDL1^{+} cells and CHL cells was positively associated with areas of high T_H1 density and in 8/9 by areas of high T_{Reg} density. Conversely in 7/10 cases the location of T_H1 and T_{Reg} was positively associated with areas of high CHL and PDL1 density. Of note due to the experimental design dual expression of FOXP3 and TBET could not be assessed. The phenotyping data discussed in 7.4.3 suggests a significant proportion of cells classified as T_H1 in this experiment will in fact be T_H1_{Reg}. No relationship was detected between the pattern of spatial skewing and PDL1 expression or CHL MHC II, however assessment was limited by study size.

7.4.5: *in vitro* modelling

Direct effects of CHL cells on T_H differentiation were modelled *in vitro*. Naïve T_H cells from healthy donors were collected by negative selection before treatment with CD3/28 stimulation in the presence of CHL cell line supernatant to model secreted effects or in the presence of the cell line to model contact-dependent effects.

At day 8 with three donors using plate stimulation with or without the addition of KMH2 CHL cell line a significant but modest increase in CD25^{hi}CD127^{lo} T_{Reg} was observed. This was observed with the addition of CD3/28 stimulation and not seen when cells were cultured with conditioned media alone, consistent with a relationship to T_H activation and differentiation. In one of three donors the addition of conditioned media in the presence of CD3/28 stimulation also resulted in a significant reduction in T_H17 numbers. This was consistent across three technical replicates per condition and across three conditions testing whether the addition of LPS or T_H17-differentiating cytokines TGFβ, IL6, IL1β and IL23 (many of which are present in the CHL microenvironment) could abrogate the effect. This reduction in T_H17 was not observed with the other two donors in a second experiment, although it is notable that for the second experiment a different batch of conditioned media was used.

At day 8 co-culture with CHL cell lines led to marked differentiation towards CD25^{hi}CD127^{lo}FOXP3^{+} T_{Reg}. This effect was much greater than that observed with CD3/28 stimulation in the presence of conditioned media. Of note these cells exhibited high expression of PD1 and expressed TBET consistent with a T_H1_{Reg} phenotype. Interpretation of attempts to model the effects of PD1 inhibition on this interaction were limited by difficulties establishing

control conditions. The addition of a humanised IgG4 isotype control gave rise to biological signal with a reduction in T_{Reg} numbers in a dose dependant manner. This was replicated with two cell lines and multiple donors over two experiments. The addition of Pembrolizumab produced a downregulation but not abrogation of PD1 signal consistent with anti-PD1 binding and a more modest reduction in T_{Reg} numbers. However, the signal observed in the isotype control made it impossible to be confident that this was a PD1-specific effect. A similar effect was seen with the addition of a mouse isotype.

Figure 7.10: Naïve CD4 and CHL cell line co-culture gated to CD3+CD4+

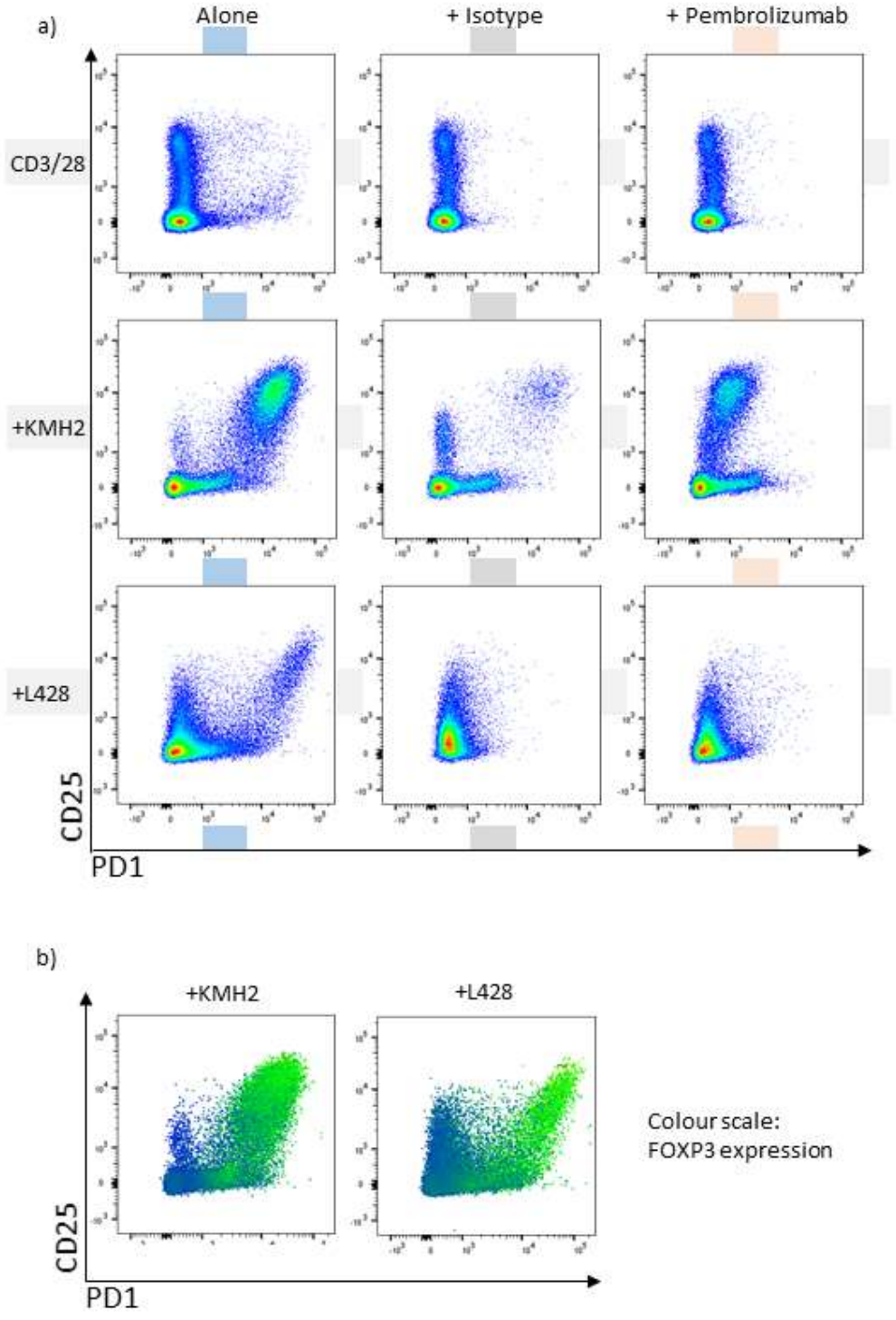

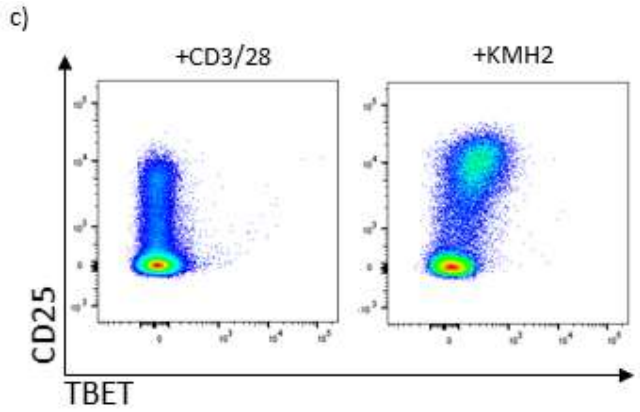

Figure 7.10: a) Naïve $CD4^+$ T cells negatively selected from healthy donor single cell suspensions were stimulated for 8 days with CD3/28 antibodies (top) or either KMH2 (middle) or L428 (bottom) CHL cell lines. In all cases a significant population of $CD25^{hi}$ $CD127^{lo}FOXP3^+$ T_{Reg} was observed, however on coculture with CHL cell lines, particularly in the case of KMH2, the population was more prominent and highly expressed PD1 (left column). On addition of Pembrolizumab (right column) the $PD1^{hi}$ T_{Reg} population was lost on in the case of L428 coculture and slightly reduced in size and PD1 expression (consistent with PD1 occupancy) in the case of KMH2. However, unexpectedly, on addition of humanised isotype control (middle) a greater loss of the T_{Reg} populations was observed, raising concern that the observed effect was not PD1-specific. b) Addition of a colour map of FOXP3 expression supports a T_{Reg} identity for the $CD25^{hi}PD1^{hi}$ population. c) Plotting TBET expression against CD25 demonstrated elevated TBET expression in CHL-induced T_{Reg} not observed with CD3/28 stimulation.

7.5: Discussion

Our data identifies a series of novel findings and validates others. We validate the disproportionate enrichment of T_H1 and T_{Reg} and strengthen this data by demonstrating their spatial enrichment. We document the marked enrichment of T_H over T_C and physical exclusion of T_C from $PDL1^{hi}$ regions. Our novel findings include the suppression of T_H17, the enrichment and induction of T_H1_{Reg} and the connection between PDL1 and CHL MHC II expression and these effects. These data, combined with the low levels of exhaustion and lack of relationship between exhaustion markers and PDL1 or CHL MHC II documented in the last chapter highlight a potential alternative mechanism for the action of PD1 inhibitors in CHL.

The elevation of FOXP3^{+}T_{Reg} is well documented in CHL and functional testing has demonstrated their suppressive function.[22,176,414] The induction of T_{Reg} differentiation by CHL cell lines is also documented.[221] High levels of T_H1 have similarly been noted.[22] We identify for that a large proportion of these T_H1 are in fact T_H1_{Reg}, validating deep phenotyping data from a small mass cytometry cohort.[216] We further identify a connection between T_H1_{Reg} induction and both PDL1 and CHL MHC II expression and suggestive of disproportionate induction of T_H1_{Reg} over T_H1. Due to the association between high FOXP3 expression and good prognosis has been suggested that T_{Reg} are in fact supressing CHL cell growth. The fact that some CHL cells survive without MHC II expression and the link we identify between MHC II and T_{Reg} induction makes this appear less likely. If the consequence of MHC II expression was to induce a cell type limiting tumour growth and loss of MHC II would not restrict growth, then this adaptation would quickly be selected for. We put forward an alternative hypothesis whereby MHC II helps the CHL cell establish a T_{Reg} rich microenvironment but that when treatment is introduced the balance of the microenvironment shifts from regulatory to activated. At this point the retained MHC II expression becomes a vulnerability as it is a means of identification and killing by cytotoxic T_H cells.

The importance of cytotoxic T_H cells is increasingly recognised in immunobiology, although the lack of specific markers makes them hard to detect and study.[220,415] Their presence is not well established in CHL. However, they are known to play important roles in controlling EBV infected B cells and their differentiation is observed in response to CHL cell lines, although it is unclear if the alloreaction contributes to this.[96,221] The differentiation of both T_{Reg} and cytotoxic T_H in response to CHL cell lines has been taken as evidence that the cell types cooperate to supress CHL growth.[221,416] However, it is equally possible that one balances the other. The fact that MHC I loss is prevalent in CHL makes it unlikely that T_C can be playing a significant role in immune surveillance even during PD1 blockade.[133] This is compounded by the low infiltration of T_C into PDL1^{hi} regions, which may relate to trafficking or T_C specific apoptosis.[417] NK cells may play a role but, unlike T_H, they are scarce in CHL tumours (data not shown). Cytotoxic T_H are therefore a likely candidate as a key immune effector.

The finding of elevated PD1 expression in T_{Reg} induced *in vitro* is unexpected and difficult to interpret. We have not performed phenotyping to determine whether T_{Reg} in primary tissue are PD1^{+} but the distribution patterns and lack of correlation makes this appear unlikely and if the case only a small minority. The finding may be an artefact of the alloreaction or other *in vitro* effect. PD1 has been linked to T_{Reg} effector function although evidence is mixed. Some studies suggest PD1 improves T suppressive capacity and resistance to apoptosis.[418–420] Furthermore, PD1 blockade allows responders to overcome suppression of proliferation.[384]

Conversely, a recent and concerning phenomenon that has been noted with the advent of checkpoint blockade is hyperprogressive disease, which has been associated with the pathological expansion of $PD1^+T_{Reg}$ and amplification of T_{Reg} function.[407,409] Hyperprogressive disease has been noted in CHL although it is unclear if this was connected to $PD1^+T_{Reg}$ amplification and T_{Reg} reduction has been seen with PD1 blockade in glioblastoma.[421] The implications and relevance of this phenomenon in CHL are therefore still to be determined.

A novel observation within our data relates to the role of T_H17 cells. Multiple factors within the CHL microenvironment appear conducive to the development of T_H17 including the secretion of TGFβ, IL6 and IL21 by the CHL cell, the presence of IL23p19 in macrophages (although our data suggests not IL12p40 the other subunit required to form IL23) and the presence of IL1β in the microenviroment.[422,423] This combination of cytokines are classically used for T_H17 polarisation *in vitro*. Similarly, other factors such as soluble CD30 and prostaglandin E2 promote T_H17.[164,424] In spite of this we observe low levels of T_H17 relative to reactive tissue and elevation of other factors such as PDL1 and IL27p28 (a subunit of IL27). With both of these factors we observe an inverse relationship to T_H17 numbers (as measured by RORγT). Of note, our data can be reconciled with a previous paper which identified elevated IL27p28 in EBV^- CHL and suggested that T_H17 were elevated by quantifying $STAT3^+$ cells.[139] RORγT has much higher specificity to T_H17 than STAT3 which is also associated with T regulatory 1 (T_R1), a cell type recently reported as frequent in CHL.[264,344,371] Similarly the use of IL17 as a marker for T_H17 is reportedly unreliable due to its production by other cells including neutrophils.[258,425] T_H17 are infrequent cells but are increasingly recognised to have unusual properties such as stem potential and to take a central role in autoimmunity. Their role in cancer remains controversial with some studies suggesting anti- and some pro-tumour roles.[425,426] It is currently unclear whether the suppression of T_H17 in CHL represents the active control of an anti-tumour phenotype or a by-product of CHL cells hijacking mechanisms to skew the T_H population towards T_H1_{Reg} or T_H1.

7.5.1: Future work:

These data could be consolidated by expanding the spatial analysis cohort, adapting the experimental design to enable assessment of dual expression of transcription factors.

Interpretation of the *in vitro* data was limited by signal from the isotype control. Further validation is required to understand and control for this. Further evidence is required to prove that the differentiation of T_H1_{Reg} is mediated by PDL1 and MHC II. If the isotype issue cannot be

bypassed a CRISPR based approach to over and under-express PDL1 might be required. We have generated a CRISPR knockdown of CIITA (the master transactivator of MHC II) of the L428 cell line to demonstrate that MHC II is required to drive T_H1_{Reg} differentiation. Additionally, it is unclear how much the alloreaction contributes to the observed effect. To assess this, we have sourced an HLA-matched donor to the L428 cell line.

We hypothesise that retaining MHC II expression assists CHL cells in the promotion of a T_H1_{Reg} rich microenvironment, but that PD1 inhibition shifts differentiation towards an anti-tumour microenvironment. At this point retained MHC II expression becomes a vulnerability due to the action of cytotoxic T_H. Cytotoxic T_H are known to be induced alongside T_{Reg} on co-culture with CHL cell lines. A further test of our hypothesis is therefore to test whether inhibition of the PD1-PDL1 axis can shift the balance from regulatory to cytotoxic T_H. We are optimising an *in vitro* model to evaluate this.

Chapter 8: Discussion

8.1: High PDL1 expression in the absence of exhaustion

8.1.1 A PDL1^{hi} myeloid environment

PDL1 expression in CHL is present on both CHL cells and within the myeloid microenvironment. PDL1 expression is important given the fact that it is predictive of PD1 inhibitor response, however it is unclear whether this is attributable to PDL1 expression on CHL, in the microenvironment or both. It is also unclear if PDL1 plays the same role in each setting and there is little data to support the assumption that the roles are aligned.

We confirm that macrophages are enriched around CHL and that these macrophages express PDL1. We demonstrate that PDL1 intensity is inversely proportional to distance suggesting induction by a secreted factor and confirm *in vitro* that CHL cell line supernatant leads to upregulation of PDL1 on monocyte-derived macrophages. However, whilst multiple immunoregulatory molecules were upregulated in macrophages in CHL relative to reactive lymph nodes, we were unable to detect a consistent immune tolerant macrophage "signature" and immunosuppressive markers did not cluster into distinct patterns although in a minority of cases M2 markers such as CD163, IDO1 and less consistently Gal1 appeared to coincide. Surprisingly, cases of high PDL1 expression on macrophages correlated with high expression of IL23p19 and CD40, thought to be a pro-inflammatory M1 markers, and not with M2 markers such as IDO1 and CD163. Overall cases did not cluster into clear immunosuppressive or inflammatory groups and PDL1 could not be directly linked to immunosuppression with a correlative approach. Preliminary data performing deeper phenotyping and modelling within a single CHL case demonstrated variably PDL1^{+} macrophages and classical monocytes localising to tumour but the expression of CD163 (an M2 marker) localising not to macrophages but to intermediate monocytes which localised away from the tumour in the perivascular area. This is interesting given that CD163 is prognostic in CHL on meta-analysis and is put forward as evidence of an M2 microenvironment, whilst an IHC study has previously commented that CD68 positivity and CD163 positivity does not appear to inhabit the same regions of the tumour.[145,148] These data again confirm the relationship between myeloid PDL1 expression and CHL, but highlight the absence of M2 marker co-expression in this case. Finally, preliminary functional data assessing the effect on T cell differentiation of CHL priming of macrophages again failed to demonstrate the promotion of tolerant T cell phenotypes, and even revealed a trend to the opposite. Conversely, as discussed in Chapter 7, a PDL1^{hi} environment associated

with CHL MHC II expression and increased FOXP3 numbers, although it is unclear if the effects of PDL1 in this context are due to CHL or microenvironmental expression. Additionally, this model is reductionist in that it assessed the effects of priming as an isolated event before removing the conditioned media. This is necessary to separate the effects of priming from the direct effects of conditioned media on T cells, however *in vivo* cells are exposed to ongoing cytokine secretion which provides important priming signals in addition to the effects of CHL direct antigen presentation and CHL-secreted soluble PDL1.[427]

In summary these data strongly suggest that myeloid PDL1 expression is directly CHL induced. However, they highlight complexities within the myeloid environment and whilst they do not exclude the possibility that myeloid PDL1 expression implies a suppressive phenotype they suggest this may be oversimplification. Further functional and deep phenotyping data is required to consolidate these findings.

The possibility that the $PDL1^+$ myeloid environment is not straight-forwardly immunosuppressive is surprising on the face of it given evidence that the phenotype is CHL recruited and induced. If these cells represented an anti-tumour population then CHL cells would be expected to downregulate mechanisms recruiting them. However, given that macrophages are non-malignant and form an important part of the immune response, it is too simplistic to attempt to characterise them purely as “pro” or “anti” tumour. For the CHL cell to gain from the $PDL1^+$ microenvironment they need to provide net benefit rather than be purely “pro-tumour”, either through mixed T cell mediated effects or other mechanisms. The possibility that they are not entirely anti-inflammatory may also align with other unexpected features of the CHL microenvironment such as the unexpected local enrichment of T_H1 cells.

8.1.2 The role of EBI3 and IL27 in the myeloid microenvironment

We validated studies reporting monomeric EBI3 secretion by CHL cells and the induction of IL27p28 in the microenvironment, the component parts of the immunomodulatory cytokine IL27. Multiple technical issues meant we could not demonstrate formed IL27 in tissue or demonstrate a link to PDL1 upregulation beyond correlation. We are unable to conclude that IL27 is a major mechanism underlying PDL1 upregulation in CHL, although cannot exclude it. We do however identify a series of observations that are suggestive of the influence of IL27 within the CHL microenvironment including characteristic shifts within the T cell compartment such as T_H17 suppression, T_H1 and T_H1_{Reg} induction. Recent data also suggests the presence of T

regulatory 1 (T_R1).[344] These are suggestive of a role for IL27. For these reasons the hypothesis remains attractive and may be worth limited further exploration as discussed in section 5.6.

8.1.3 Exhaustion and PD1 inhibitor activity

Reversal of T cell exhaustion is widely accepted as the mechanism of action of PD1 inhibitors and significant evidence supports this in solid tumours such as melanoma. However, multiple other roles for PD1-PDL1 interactions have been identified in recent years and we now understand this axis to be central to immune cell activation and peripheral tolerance. The efficacy of PD1 inhibitors in CHL is frequently taken as evidence that T cell exhaustion is prominent in the microenvironment. However, our data finds lower expression of PD1 in CHL relative to reactive lymph node, and lower expression of lymphocytes co-expressing PD1 and other exhaustion markers. Furthermore, we find no difference in proliferative or cytokine production capacity between CHL and reactive lymph nodes and a significant enrichment of $Ki67^+$ T_H and paucity of $PD1^+Ki67^-T_H$ in CHL. Finally, we assessed connections between PD1 expression and PDL1 and CHL MHC II, increased expression of which predict response to PD1 inhibition. Instead we observe a negative association between PD1 and PDL1 expression and between PD1 and CHL MHC II expression. Finally, we observe a trend to positive correlation between proliferative capacity and PDL1 and a trend to negative correlation between proliferative capacity and PD1. This represents the most comprehensive assessment of exhaustion in CHL to date.

Whilst initially counter-intuitive and challenging to the accepted narrative, these findings are in line with published data. There is little direct published evidence of T cell exhaustion in CHL, with IHC-based studies reporting low expression.[22] The identification of MHC II expression rather than MHC I has led to speculation that T_H exhaustion rather than T_C exhaustion plays a central role, but we find little data to support this.[133,159,216] Furthermore, PD1 inhibitor trials which have found frequencies of $PD1^+$ cells not to be predictive of response, and in some cases associated with lesser response.

There are marked differences between cancers originating from immune cells within and immune microenvironment and those occurring in other tissues, including the roles of the PD1-PDL1 axis in the parent tissue. The assumption that PD1 inhibitors act by reversal of exhaustion is drawn from data in solid tumours and T_C biology. Whilst it remains possible that exhaustion is relevant within immune subpopulations, the absence of a significant exhaustion signature and the lack of correlation between markers of exhaustion and known predictors of

PD1 inhibitor response is sufficient grounds to consider other mechanisms of PD1 inhibitor action.

8.1.4 The role of MHC II and PDL1-induced T_H skewing in PD1 inhibitor activity

Quantification and phenotyping revealed that the CHL microenvironment is characterised by enrichment of T_H cells and local exclusion of T_C. We documented an overrepresentation of T_{Reg} and T_H1 as has previously been observed and made the novel observation that T_H17 were underrepresented.[22] These patterns were mirrored in the reactive nodes of patients with HIV but the T_H phenotypes between HIV associated CHL and HIV negative CHL were similar suggesting this pattern is specific to the CHL microenvironment rather than a reflection of prior host immune status. Correlations to total PDL1 revealed a positive association with macrophage, T_H1 and T_H2 frequency and a negative association with T_H17, a pattern also seen by unsupervised clustering particularly in EBV^+ cases. Evaluation against CHL MHC II expression demonstrated higher T_{Reg} numbers in the MHC II positive group.

Deeper phenotyping revealed the overrepresentation of T_H1 and paucity of T_H17 but also identified that the elevation in T_{Reg} numbers was restricted to $T_H1_{Reg,}$, a finding supported by a recent mass cytometry study performing deep phenotyping in a set of 8 CHL patients.[216] Furthermore, comparison of these data to both total PDL1 and CHL MHC II expression revealed a significant increase in T_H1_{Reg} in the positive/high expression groups but not T_H1. T_H17 were also significantly reduced in the total $PDL1^{hi}$ group whereas T_H17_{Reg} were not. Ratios of T_H1:T_H1_{Reg} showed a trend to overrepresentation of T_H1_{Reg} but this did not reach statistical significance so cannot be stated with confidence.

Spatial modelling demonstrated a skewing effect with clustering of T_H1, T_H2 and T_{Reg} in the peritumoural $PDL1^+$ regions but separate clustering of T_C together with T_H17 suggesting their exclusion from the tumour area. Study design prevented us from distinguishing which cells were T_H1 vs T_H1_{Reg} and skewing effect did not significantly correlate with overall PDL1 expression or CHL MHC II but the analysis was limited to 10 cases of varying histological subtype.

These finding were supported by *in vitro* data demonstrating that the presence of CHL cell line conditioned media during stimulation of naïve T_H increases T_{Reg} differentiation, and this effect is amplified in direct co-culture where there is a strong differentiation drive towards a

$PD1^{+}T_H1_{Reg}$ phenotype. The significance of the strong PD1 expression on T_H1_{Reg} induced *in vitro* is currently unclear and requires further evaluation.

Taken together these data suggest a pattern of T_H1_{Reg} and T_H1 enrichment and T_H17 suppression. Furthermore, CHL MHC II expression appears to assist CHL cells in the induction of T_H1_{Reg}, thought to preferentially suppress a T_H1 response. PDL1 was similarly associated with induction of T_H1 but preferentially of T_H1_{Reg} and with the suppression of T_H17.

8.1.5 Synthesis: MHCII expression: A double edged sword

In summary we validate the enrichment of $PDL1^{+}$ macrophage in the CHL microenvironment, provide evidence that this is directly induced by the CHL cell and that $PDL1^{hi}$ cases are more frequently CHL MHC II expressing. Despite this, we are unable to find evidence of T cell exhaustion above levels seen in reactive lymph node and no relationship between exhaustion markers and either PDL1 or CHL MHC II expression (predictors of PD1 inhibitor response in CHL). In contrast we find evidence of an association between T_H1_{Reg} and T_H1 induction, and T_H17 suppression and both PDL1 and CHL MHC II. Further, our data supports CHL MHC II preferentially inducing T_H1_{Reg} over T_H1, perhaps limiting the immune response and tilting the balance in favour of tumour growth. It appears that maintenance of antigen presenting function by retained expression of MHC II therefore assists CHL to establish cell-extrinsic immune defences by establishing a T_{Reg}-rich microenvironment.

The fact that CHL MHC II expression is associated with good response to PD1 inhibitors suggests that this strategy is a double-edged sword. Even in the absence of exhaustion PD1 inhibitors result in a reinvigoration of the T cell microenvironment, allowing the recruitment of new clones.[391] We hypothesise that this reinvigoration shifts the balance from suppressive to anti-tumour phenotypes. If the balance shifts then MHC II expression turns from an asset to a vulnerability, allowing cytotoxic T_H (known to be induced by CHL cell lines) to identify and kill.

Figure 8.1: MHC II expression: A double edged sword

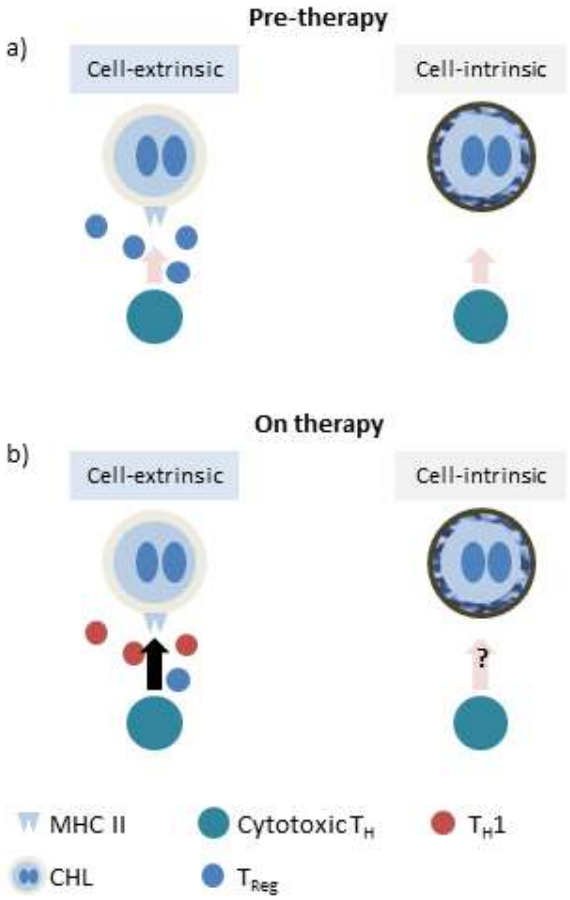

Figure 8.1: a) Before therapy CHL tumours expressing MHC II induce a protective T_{Reg} environment preventing their elimination by immune effector cells (a cell extrinsic defence). CHL cells that lose MHC II avoid detection by hiding from the immune system (a cell intrinsic defence).

b) Immunotherapy shifts and activates the immune microenvironment but does not affect the malignant cell directly. Cells relying on extrinsic defences become vulnerable. MHC II now becomes a vulnerability because it is a mechanism of identification for cytotoxic T_H. However, tumours adopting cell-intrinsic defences remain undetected.

8.2: A complementary immune evasion cluster hypothesis

Cancer survival is a dynamic balance between the ability of the tumour to evade or outgrow immune surveillance and that of the immune system to clear it. In cancer somatic mutations generate unique tumour antigen but tumours reduce their exposure by stochastically acquiring adaptations which are selected for by evolutionary pressure exerted by the immune response.[428,429] In most scenarios the immune surveillance actors (e.g. T_C, T_H, NK, Natural Killer T (NKT), macrophages etc.) within each patient remain unchanged. However, the evolutionary pressure exerted by the immune response is dynamic because every acquired evasion mutation shifts exposure, reducing pressure from one actor and in turn increasing pressure

from another. For example, MHC I loss reduces selective pressure from T_C cells but increases pressure from NK cells and in turn the selection of complementary mechanisms reducing NK exposure. Conversely, in the absence of MHC I loss there is be less pressure selecting for mechanisms of NK evasion. This predicts that complementary evasion mechanisms should be co-selected and cluster together. Data exists to support this hypothesis.[73] T_C are major actors of immune surveillance who identify and kill via MHC I, but loss of MHC I is a trigger for NK killing via missing self.[73] Co-selection of *B2M* (leading to MHC I loss) and *CD58* mutations (reducing NK exposure) is seen in DLBCL and in CHL where MHC I loss is associated with increased expression of HLA-G.[72,430]

This hypothesis suggests that the chance acquisition of different early mutations or variations in innate susceptibility may promote divergent evolution towards tumours with stable but different evasion clusters. An analogy would be predator evasion on the savannah. Rhinoceros and zebra have a recent common ancestor and exist in the same environment.[431] Rhinoceros adopt a complementary cluster of mechanisms including large size, armoured skin, weaponry and strength to evade predation. Zebra adopt a cluster of speed, agility and camouflage. Both face the same predators (big cats, hyena etc.). Individual elements within each cluster are not readily exchangeable leading to specialisation in one approach. Both evasion clusters are effective in the steady state but have different inherent vulnerabilities. In CHL the EBV infection status may provide an example of variation in innate susceptibility leading to different complementary evasion clusters. HLA I polymorphisms associated with EBV^+ CHL appear to confer some protection against T_C identification.[127] This reduces selective pressure from T_C and therefore more selective pressure is experienced from actors such as T_H increasing the possibility of selection for MHC II loss, as is seen.[131] EBV^+ disease is also associated with a higher degree of T_C infiltration.[22] Rather than a "healthy" immune response this may reflect effective avoidance of recognition at a cell-cell level leading to less evolutionary pressure to evolve mechanisms to reduce it. Conversely in EBV negative disease is associated with HLA II polymorphisms suggesting altered T_H exposure and also a high frequency of MHC I loss, which in turn associates with selection for NK evasion.[112,131,430]

The presence of cancer demonstrates that the malignant cell has adopted a successful evasion strategy, however, the introduction of treatment changes the environment. At this point the nature of the evasion techniques become important in determining the success of an immunotherapy strategy. A broad range of evasion mechanisms have been documented and attempts to categorise these have been described, most recently in lymphoma into "Hide" (reduced identification of tumour cells or hiding behind a supportive microenvironment) or

"Defend" (increased resistance to killing, reducing effectiveness of immune effectors or inducing death in immune effectors).[432]

This categorisation informative but if the hypothesis outlined above held true it is not clear that evolutionary pressure would select for this "Hide" group over "Defend" as cell intrinsic hide mechanisms e.g. reduced costimulatory molecules, are likely to be complementary to cell intrinsic "defend" mechanisms e.g. resistance to apoptosis. Similarly, cell extrinsic "hide" mechanisms e.g. induction of a suppressive microenvironment via MHC II is likely to be complementary to a cell intrinsic "defend" mechanisms such as effector inhibition via MHC and PDL1.

Approached from an evolutionary perspective we propose an amended classification which would be more consistent with complementary clustering:

- Cell-intrinsic: Hide (most susceptible to cellular/engager therapy)
- Cell-intrinsic: Defend (most susceptible to conventional therapy)
- Cell extrinsic: Recruit (most susceptible to checkpoint therapy)

As discussed above, MHC II expression is an interesting example in that either retention or loss confers benefit depending upon whether a cell-intrinsic or extrinsic strategy is being adopted. Retention of MHC II appears to aid the CHL cell in recruiting an immunosuppressive microenvironment. This in turn would reduce selective pressure to acquire mechanisms to reduce cellular immunogenicity. Loss of an immunosuppressive environment would leave these cells exposed to immune surveillance. Conversely loss of MHC II reduces exposure to T_H cytotoxicity. Cells that adopt cell-intrinsic evasion mechanisms would remain unaffected by loss of their microenvironment.

Checkpoint inhibiting immunotherapy strategies reinvigorate the T cell response, improving function and killing capacity but do not improve the ability to identify cells that have lost MHC expression (a cell-intrinsic hide strategy). They may improve killing of cells relying on resistance to killing (a cell-intrinsic defend strategy) but will be most effective in killing cells adopting a cell-extrinsic strategy as these will have faced the least pressure to minimise immunogenicity. The predictive power of MHC II for PD1 inhibitor response in CHL is consistent with this.[133] MHC I loss is prevalent in CHL limiting the potential for T_C recognition even in the context of a reinvigorated immune response so it is likely that T_H and T_H cytotoxicity play a particularly important role in this disease. Conversely cellular therapies such as bispecific T cell engagers and chimeric antigen receptor T cells bypass the MHC complex and therefore would be suitable for tumours adopting a cell-intrinsic hide approach. However, they remain susceptible

to induction of exhaustion (a cell-intrinsic defend mechanism) and the effects of T_{Reg} (a cell-extrinsic defence).[433]

A complicating factor in testing this hypothesis lies in identifying a signature as different evasion mechanisms may lead to the same evasion tactic by multiple means. For example, MHC I functional loss can be achieved by multiple mechanisms including mutations of the MHC I pathway, transcriptional mechanisms, downregulation, shedding and more.[434] To demonstrate this effect by clustering of known evasion genes may therefore be unsuccessful unless a large an robust dataset was available. This is challenging in CHL as most available genetic data is form small cohorts with either flow sorting or microdissection of individual CHL cells. A number of predictions could however be made and tested:

1 High T_{Reg} numbers should predict PD1 inhibitor response.
2 An inverse relationship may be seen between tumour neoantigen load and T_{Reg} number.
3 Combinations between checkpoint and cellular or bispecific T cell engagers should have better combined efficacy than each alone (although may be limited by toxicity).

Alternatively, it may require testing in a different disease model.

8.3: New tools in spatial analysis for multiplex imaging

We introduce and adapt a toolkit of techniques for spatial analysis and apply them to multiplex imaging of cellular tissues. The modelling techniques and statistical packages used are the result of combined work of many individuals and represent a statistical discipline.[317] The novelty in this PhD lies only in their application to multiplex data to answer biological questions. However, we believe that their application in this manner has the potential to advance the range and type of questions we can ask of histological tissue. Furthermore, that recent advances in multiplex imaging technology, in situ sequencing and processing power means that whilst the techniques are not new their potential to shed light on these vast datasets is only just becoming evident. The fact that they are well described and validated then becomes a strength.

Chapter 9: Original Manuscripts and Abstracts

9.1: Abstracts

2019 Taylor JG, Clear A, Truelove E, Calaminici M, Gribben JG: *Beyond Exhaustion: The PD1-PDL1 Axis Shapes the Classical Hodgkin Lymphoma Microenvironment.* Oral presentation, American Hematology Society Annual Meeting, 7-10 December 2019, Orlando, USA

2018 Taylor JG, Clear A, Matthew J, Calaminici M, Gribben JG: *The T_{Reg} /T_H17 Axis Is Skewed in Classical Hodgkin Lymphoma by PDL1+Ve but Not PDL1-Ve Lymphoma Cells and by Lymphoma MHC Class 2 Expression.* Poster presentation, American Hematology Society Annual Meeting, 1-4 December 2018, San Diego, USA

2018 **Taylor JG, Clear A, Greaves P, Poynton M, Caporale M, Calaminici M, Gribben JG:** ***T_H17 cells in Classical Hodgkin Lymphoma are constrained by the PD1-PDL1 axis and may play an important role in the action of PD1 checkpoint inhibitors*****.** Oral presentation, European Hematology Society Annual Conference, 14-17 June 2018, Stockholm, Sweden

2018 **Taylor JG, Clear A, Greaves P, Poynton M, Caporale M, Calaminici M, Gribben JG:** ***Programmed Death Ligand 1 expression in the microenvironment of Classical Hodgkin Lymphoma is induced by lymphoma cells via an IL27-dependent mechanism*****.** Poster, European Hematology Society Annual Conference, 14-17 June 2018, Stockholm, Sweden

2017 **Taylor JG, Seddon T, Alizedeh K, Agrawal C, Kempster L, Gribben JG, Agrawal S,** ***Single centre experience of Zarzio biosimilar granulocyte-colony stimulating factor (GCSF) for healthy donor mobilization; Good leukapheresis yields and safety profile at 24 month median follow-up.*** Poster, European Society for Blood and Marrow Transplantation, 26-29 March 2017, Marseille, France

2016 **Navarro-Bailon A*, Taylor JG*, Matthews J, Montoto S, Gribben JG,** ***The role of Watch and Wait in Nodular Lymphocyte Predominant Hodgkin Lymphoma: Single Centre Data from the Modern Era*** *****contributed equally**.** Poster, International

Symposium on Hodgkin Lymphoma, 22-25 October 2016, Cologne, Germany

9.2: Original Articles

2019 Taylor JG, Clear A, Calaminici M, Gribben JG. Programmed cell death protein-1 (PD1) expression in the microenvironment of classical Hodgkin lymphoma is similar between favorable and adverse outcome and does not enrich over serial relapses with conventional chemotherapy Haematologica. 2019 Jan;104(1):e42-e44. PMID: 30598496

2019 Taylor JG, Gribben JG, Chapter: The Biological Basis for Targeting Immunoregulatory Functions Novel Targeted Drugs for the Treatment of Lymphoma, The Biological Basis for Innovative Drug Discovery and Development. Editors: O'Connor OA, Amengual JE, Gerecitano J. Springer ISBN 978-1-59745-286-1 (in press, due 10.06.2021)

Chapter 10: References

1. Townsend, W. & Linch, D. Hodgkin's lymphoma in adults. *The Lancet* **380**, 836–847 (2012).
2. Vallansot, R. o. *et al.* 20-year follow-up of Hodgkin lymphoma: Predictors of survival and secondary malignancies. *Hematol. Oncol.* **35**, 306–307 (2017).
3. Ng, A. K. & van Leeuwen, F. E. Hodgkin lymphoma: Late effects of treatment and guidelines for surveillance. *Semin. Hematol.* **53**, 209–215 (2016).
4. Huang, X. *et al.* Epidemiology of Classical Hodgkin Lymphoma and Its Association with Epstein Barr Virus in Northern China. *PLOS ONE* **6**, e21152 (2011).
5. von Tresckow, B. & Moskowitz, C. H. Treatment of relapsed and refractory Hodgkin Lymphoma. *Semin. Hematol.* **53**, 180–185 (2016).
6. Ansell, S. M. *et al.* PD-1 blockade with nivolumab in relapsed or refractory Hodgkin's lymphoma. *N. Engl. J. Med.* **372**, 311–319 (2015).
7. Armand, P. *et al.* Programmed Death-1 Blockade With Pembrolizumab in Patients With Classical Hodgkin Lymphoma After Brentuximab Vedotin Failure. *J. Clin. Oncol. Off. J. Am. Soc. Clin. Oncol.* (2016) doi:10.1200/JCO.2016.67.3467.
8. Follows, G. A. *et al.* Guidelines for the first line management of classical Hodgkin lymphoma. *Br. J. Haematol.* **166**, 34–49 (2014).
9. Shindiapina, P. & Alinari, L. Pembrolizumab and its role in relapsed/refractory classical Hodgkin's lymphoma: evidence to date and clinical utility. *Ther. Adv. Hematol.* **9**, 89–105 (2018).
10. Eichenauer, D. A. *et al.* Hodgkin lymphoma: ESMO Clinical Practice Guidelines for diagnosis, treatment and follow-up. *Ann. Oncol. Off. J. Eur. Soc. Med. Oncol.* **29**, iv19–iv29 (2018).
11. Collins, G. P. *et al.* Guideline on the management of primary resistant and relapsed classical Hodgkin lymphoma. *Br. J. Haematol.* **164**, 39–52 (2014).

12. Herrera, A. F. *et al.* Interim results of brentuximab vedotin in combination with nivolumab in patients with relapsed or refractory Hodgkin lymphoma. *Blood* **131**, 1183–1194 (2018).
13. Ramchandren, R. *et al.* Nivolumab for Newly Diagnosed Advanced-Stage Classic Hodgkin Lymphoma: Safety and Efficacy in the Phase II CheckMate 205 Study. *J. Clin. Oncol. Off. J. Am. Soc. Clin. Oncol.* JCO1900315 (2019) doi:10.1200/JCO.19.00315.
14. Connors, J. M. *et al.* Brentuximab Vedotin with Chemotherapy for Stage III or IV Hodgkin's Lymphoma. *N. Engl. J. Med.* **378**, 331–344 (2018).
15. Ansell, S. M. *et al.* Nivolumab for Relapsed/Refractory Diffuse Large B-Cell Lymphoma in Patients Ineligible for or Having Failed Autologous Transplantation: A Single-Arm, Phase II Study. *J. Clin. Oncol. Off. J. Am. Soc. Clin. Oncol.* **37**, 481–489 (2019).
16. Goldkuhle, M. *et al.* Nivolumab for adults with Hodgkin's lymphoma (a rapid review using the software RobotReviewer). *Cochrane Database Syst. Rev.* **7**, CD012556 (2018).
17. Armand, P. *et al.* Nivolumab for Relapsed/Refractory Classic Hodgkin Lymphoma After Failure of Autologous Hematopoietic Cell Transplantation: Extended Follow-Up of the Multicohort Single-Arm Phase II CheckMate 205 Trial. *J. Clin. Oncol. Off. J. Am. Soc. Clin. Oncol.* **36**, 1428–1439 (2018).
18. Spina, V. *et al.* Circulating tumor DNA reveals genetics, clonal evolution and residual disease in classical Hodgkin lymphoma. *Blood* (2018) doi:10.1182/blood-2017-11-812073.
19. Latchman, Y. *et al.* PD-L2 is a second ligand for PD-1 and inhibits T cell activation. *Nat. Immunol.* **2**, 261–268 (2001).
20. Green, M. R. *et al.* Integrative analysis reveals selective 9p24.1 amplification, increased PD-1 ligand expression, and further induction via JAK2 in nodular sclerosing Hodgkin lymphoma and primary mediastinal large B-cell lymphoma. *Blood* **116**, 3268–3277 (2010).
21. Chen, R. *et al.* Blockade of the Pd-1 Checkpoint with Anti–Pd-L1 Antibody Avelumab Is Sufficient for Clinical Activity in Relapsed/Refractory Classical Hodgkin Lymphoma (chl). *Hematol. Oncol.* **35**, 67–67 (2017).

22. Greaves, P. *et al.* Defining characteristics of classical Hodgkin lymphoma microenvironment T-helper cells. *Blood* **122**, 2856–2863 (2013).
23. Harris, N. L. *et al.* A revised European-American classification of lymphoid neoplasms: a proposal from the International Lymphoma Study Group. *Blood* **84**, 1361–1392 (1994).
24. Eichenauer, D. A. *et al.* Hodgkin's lymphoma: ESMO Clinical Practice Guidelines for diagnosis, treatment and follow-up. *Ann. Oncol. Off. J. Eur. Soc. Med. Oncol.* **25 Suppl 3**, iii70-75 (2014).
25. Mack, T. M. *et al.* Concordance for Hodgkin's Disease in Identical Twins Suggesting Genetic Susceptibility to the Young-Adult Form of the Disease. *N. Engl. J. Med.* **332**, 413–419 (1995).
26. Kristinsson, S. Y. *et al.* Hodgkin lymphoma risk following infectious and chronic inflammatory diseases: a large population-based case–control study from Sweden. *Int. J. Hematol.* **101**, 563–568 (2015).
27. Thomsen, H. *et al.* Heritability estimates on Hodgkin's lymphoma: a genomic- versus population-based approach. *Eur. J. Hum. Genet.* **23**, 824–830 (2015).
28. Jones, K. *et al.* The impact of HLA class I and EBV latency-II antigen-specific CD8+ T cells on the pathogenesis of EBV+ Hodgkin lymphoma. *Clin. Exp. Immunol.* **183**, 206–220 (2016).
29. Jarrett, R. F. Risk factors for Hodgkin's lymphoma by EBV status and significance of detection of EBV genomes in serum of patients with EBV-associated Hodgkin's lymphoma. *Leuk. Lymphoma* **44 Suppl 3**, S27-32 (2003).
30. Hjalgrim, H. *et al.* Infectious mononucleosis, childhood social environment, and risk of Hodgkin lymphoma. *Cancer Res.* **67**, 2382–2388 (2007).
31. Campos, A. H. J. F. M. *et al.* Frequency of EBV associated classical Hodgkin lymphoma decreases over a 54-year period in a Brazilian population. *Sci. Rep.* **8**, 1–8 (2018).
32. De Matteo, E., García Lombardi, M., Preciado, M. V. & Chabay, P. Changes in EBV Association Pattern in Pediatric Classic Hodgkin Lymphoma From a Single Institution in Argentina. *Front. Oncol.* **9**, (2019).

33. Mueller, N. Epidemiologic studies assessing the role of the Epstein-Barr virus in Hodgkin's disease. *Yale J. Biol. Med.* **60**, 321–332 (1987).

34. Hjalgrim, H., Søegaard, S. H., Hjalgrim, L. L. & Rostgaard, K. Childhood use of antimicrobials and risk of Hodgkin lymphoma: a Danish register-based cohort study. *Blood Adv.* **3**, 1489–1492 (2019).

35. Bell, A. J. *et al.* Germ-line transmitted, chromosomally integrated HHV-6 and classical Hodgkin lymphoma. *PloS One* **9**, e112642 (2014).

36. Siddon, A., Lozovatsky, L., Mohamed, A. & Hudnall, S. D. Human herpesvirus 6 positive Reed-Sternberg cells in nodular sclerosis Hodgkin lymphoma. *Br. J. Haematol.* **158**, 635–643 (2012).

37. Lacroix, A. *et al.* Involvement of human herpesvirus-6 variant B in classic Hodgkin's lymphoma via DR7 oncoprotein. *Clin. Cancer Res. Off. J. Am. Assoc. Cancer Res.* **16**, 4711–4721 (2010).

38. Glaser, S. L. *et al.* Exposure to childhood infections and risk of Epstein-Barr virus--defined Hodgkin's lymphoma in women. *Int. J. Cancer* **115**, 599–605 (2005).

39. Wick, G. & Grubeck-Loebenstein, B. Primary and secondary alterations of immune reactivity in the elderly: impact of dietary factors and disease. *Immunol. Rev.* **160**, 171–184 (1997).

40. Schüler, F., Hirt, C. & Dölken, G. Chromosomal translocation t(14;18) in healthy individuals. *Semin. Cancer Biol.* **13**, 203–209 (2003).

41. Ismail, S. I., Naffa, R. G., Yousef, A.-M. F. & Ghanim, M. T. Incidence of bcr-abl fusion transcripts in healthy individuals. *Mol. Med. Rep.* **9**, 1271–1276 (2014).

42. Karube, K., Scarfò, L., Campo, E. & Ghia, P. Monoclonal B cell lymphocytosis and 'in situ' lymphoma. *Semin. Cancer Biol.* **24**, 3–14 (2014).

43. Roulland, S. *et al.* Long-term clonal persistence and evolution of t(14;18)-bearing B cells in healthy individuals. *Leukemia* **20**, 158–162 (2006).

44. Stein, H. & Hummel, M. Cellular origin and clonality of classic Hodgkin's lymphoma: immunophenotypic and molecular studies. *Semin. Hematol.* **36**, 233–241 (1999).
45. Willenbrock, K. *et al.* T-Cell Variant of Classical Hodgkin's Lymphoma with Nodal and Cutaneous Manifestations Demonstrated by Single-Cell Polymerase Chain Reaction. *Lab. Invest.* **82**, 1103–1109 (2002).
46. Kanzler, H., Küppers, R., Hansmann, M. L. & Rajewsky, K. Hodgkin and Reed-Sternberg cells in Hodgkin's disease represent the outgrowth of a dominant tumor clone derived from (crippled) germinal center B cells. *J. Exp. Med.* **184**, 1495–1505 (1996).
47. Greiner, A. *et al.* Differential expression of activation-induced cytidine deaminase (AID) in nodular lymphocyte-predominant and classical Hodgkin lymphoma. *J. Pathol.* **205**, 541–547 (2005).
48. Braeuninger, A. *et al.* Hodgkin and Reed–Sternberg cells in lymphocyte predominant Hodgkin disease represent clonal populations of germinal center-derived tumor B cells. *Proc. Natl. Acad. Sci.* **94**, 9337–9342 (1997).
49. Seitz, V., Hummel, M., Walter, J. & Stein, H. Evolution of classic Hodgkin lymphoma in correlation to changes in the lymphoid organ structure of vertebrates. *Dev. Comp. Immunol.* **27**, 43–53 (2003).
50. Marafioti, T. *et al.* Hodgkin and reed-sternberg cells represent an expansion of a single clone originating from a germinal center B-cell with functional immunoglobulin gene rearrangements but defective immunoglobulin transcription. *Blood* **95**, 1443–1450 (2000).
51. Buettner, M., Greiner, A., Avramidou, A., Jäck, H.-M. & Niedobitek, G. Evidence of abortive plasma cell differentiation in Hodgkin and Reed-Sternberg cells of classical Hodgkin lymphoma. *Hematol. Oncol.* **23**, 127–132 (2005).
52. Tiacci, E. *et al.* Analyzing primary Hodgkin and Reed-Sternberg cells to capture the molecular and cellular pathogenesis of classical Hodgkin lymphoma. *Blood* **120**, 4609–4620 (2012).

53. Spender, L. C. & Inman, G. J. Inhibition of Germinal Centre Apoptotic Programmes by Epstein-Barr Virus. *Adv. Hematol.* **2011**, (2011).

54. Zafar, H., Riaz, S. & Badar, F. Clinical Impact of Immunophenotype-CD15/CD30 on Outcome of Hodgkin Lympoma. *Blood* **124**, 2952–2952 (2014).

55. Weniger, M. A. & Küppers, R. NF-κB deregulation in Hodgkin lymphoma. *Semin. Cancer Biol.* **39**, 32–39 (2016).

56. Watanabe, M. *et al.* AP-1 Mediated Relief of Repressive Activity of the CD30 Promoter Microsatellite in Hodgkin and Reed-Sternberg Cells. *Am. J. Pathol.* **163**, 633–641 (2003).

57. Weniger, M. A. *et al.* Human CD30+ B cells represent a unique subset related to Hodgkin lymphoma cells. *J. Clin. Invest.* (2018) doi:10.1172/JCI95993.

58. Davies, D. R., Padlan, E. A. & Sheriff, S. Antibody-antigen complexes. *Annu. Rev. Biochem.* **59**, 439–473 (1990).

59. Victora, G. D. & Nussenzweig, M. C. Germinal centers. *Annu. Rev. Immunol.* **30**, 429–457 (2012).

60. Chan, T. D. & Brink, R. Affinity-based selection and the germinal center response. *Immunol. Rev.* **247**, 11–23 (2012).

61. Shlomchik, M. J. & Weisel, F. Germinal center selection and the development of memory B and plasma cells. *Immunol. Rev.* **247**, 52–63 (2012).

62. Pham, P., Bransteitter, R., Petruska, J. & Goodman, M. F. Processive AID-catalysed cytosine deamination on single-stranded DNA simulates somatic hypermutation. *Nature* **424**, 103–107 (2003).

63. Di Noia, J. M. & Neuberger, M. S. Molecular mechanisms of antibody somatic hypermutation. *Annu. Rev. Biochem.* **76**, 1–22 (2007).

64. Lieber, M. R. Mechanisms of Human Lymphoid Chromosomal Translocations. *Nat. Rev. Cancer* **16**, 387–398 (2016).

65. Frieder, D. *et al.* Antibody diversification: mutational mechanisms and oncogenesis. *Immunol. Res.* **35**, 75–88 (2006).

66. Tsai, A. G. *et al.* Human chromosomal translocations at CpG sites and a theoretical basis for their lineage and stage specificity. *Cell* **135**, 1130–1142 (2008).

67. Dunn, G. P., Old, L. J. & Schreiber, R. D. The three Es of cancer immunoediting. *Annu. Rev. Immunol.* **22**, 329–360 (2004).

68. Cavanna, L., Pagani, R., Seghini, P., Zangrandi, A. & Paties, C. High grade B-cell gastric lymphoma with complete pathologic remission after eradication of Helicobacter pylori infection: report of a case and review of the literature. *World J. Surg. Oncol.* **6**, 35 (2008).

69. Cattelan, A. M. *et al.* Long-term clinical outcome of AIDS-related Kaposi's sarcoma during highly active antiretroviral therapy. *Int. J. Oncol.* **27**, 779–785 (2005).

70. Carbone, A. & Gloghini, A. Relationships between lymphomas linked to hepatitis C virus infection and their microenvironment. *World J. Gastroenterol.* **19**, 7874–7879 (2013).

71. Lipinski, K. A. *et al.* Cancer Evolution and the Limits of Predictability in Precision Cancer Medicine. *Trends Cancer* **2**, 49–63 (2016).

72. Challa-Malladi, M. *et al.* Combined Genetic Inactivation of Beta2-Microglobulin and CD58 Reveals Frequent Escape from Immune Recognition in Diffuse Large B-cell Lymphoma. *Cancer Cell* **20**, 728–740 (2011).

73. Raulet, D. H. Missing self recognition and self tolerance of natural killer (NK) cells. *Semin. Immunol.* **18**, 145–150 (2006).

74. Goldie, J. H. & Coldman, A. J. A mathematic model for relating the drug sensitivity of tumors to their spontaneous mutation rate. *Cancer Treat. Rep.* **63**, 1727–1733 (1979).

75. Juskevicius, D., Dirnhofer, S. & Tzankov, A. Genetic background and evolution of relapses in aggressive B-cell lymphomas. *Haematologica* **102**, 1139–1149 (2017).

76. Obermann, E. C. *et al.* Clonal Relationship of Classical Hodgkin Lymphoma and Its Recurrences. *Clin. Cancer Res.* **17**, 5268–5274 (2011).

77. Tran, H. *et al.* Immunodeficiency-associated lymphomas. *Blood Rev.* **22**, 261–281 (2008).

78. Palendira, U. & Rickinson, A. B. Primary immunodeficiencies and the control of Epstein–Barr virus infection. *Ann. N. Y. Acad. Sci.* **1356**, 22–44 (2015).

79. Shabani, M., Nichols, K. E. & Rezaei, N. Primary immunodeficiencies associated with EBV-Induced lymphoproliferative disorders. *Crit. Rev. Oncol. Hematol.* **108**, 109–127 (2016).

80. Biggar, R. J. *et al.* Hodgkin lymphoma and immunodeficiency in persons with HIV/AIDS. *Blood* **108**, 3786–3791 (2006).

81. Engels, E. A. Non-AIDS-defining malignancies in HIV-infected persons: etiologic puzzles, epidemiologic perils, prevention opportunities. *AIDS Lond. Engl.* **23**, 875–885 (2009).

82. Izawa, K. *et al.* Inherited CD70 deficiency in humans reveals a critical role for the CD70–CD27 pathway in immunity to Epstein-Barr virus infection. *J. Exp. Med.* **214**, 73–89 (2017).

83. Abolhassani, H. *et al.* Combined immunodeficiency and Epstein-Barr virus–induced B cell malignancy in humans with inherited CD70 deficiency. *J. Exp. Med.* **214**, 91–106 (2017).

84. Martis, N. & Mounier, N. Hodgkin lymphoma in patients with HIV infection: a review. *Curr. Hematol. Malig. Rep.* **7**, 228–234 (2012).

85. Huck, K. *et al.* Girls homozygous for an IL-2–inducible T cell kinase mutation that leads to protein deficiency develop fatal EBV-associated lymphoproliferation. *J. Clin. Invest.* **119**, 1350–1358 (2009).

86. Niedobitek, G. *et al.* Immunohistochemical detection of the Epstein-Barr virus-encoded latent membrane protein 2A in Hodgkin's disease and infectious mononucleosis. *Blood* **90**, 1664–1672 (1997).

87. Minamitani, T. *et al.* Mouse model of Epstein–Barr virus LMP1- and LMP2A-driven germinal center B-cell lymphoproliferative disease. *Proc. Natl. Acad. Sci.* 201701836 (2017) doi:10.1073/pnas.1701836114.

88. Baumforth, K. R. N. *et al.* Expression of the Epstein-Barr Virus-Encoded Epstein-Barr Virus Nuclear Antigen 1 in Hodgkin's Lymphoma Cells Mediates Up-Regulation of CCL20 and the Migration of Regulatory T Cells. *Am. J. Pathol.* **173**, 195–204 (2008).

89. Kang, M.-S. & Kieff, E. Epstein–Barr virus latent genes. *Exp. Mol. Med.* **47**, e131 (2015).

90. Dolcetti, R., Dal Col, J., Martorelli, D., Carbone, A. & Klein, E. Interplay among viral antigens, cellular pathways and tumor microenvironment in the pathogenesis of EBV-driven lymphomas. *Semin. Cancer Biol.* **23**, 441–456 (2013).

91. Kilger, E., Kieser, A., Baumann, M. & Hammerschmidt, W. Epstein-Barr virus-mediated B-cell proliferation is dependent upon latent membrane protein 1, which simulates an activated CD40 receptor. *EMBO J.* **17**, 1700–1709 (1998).

92. Schmitz, R. *et al.* TNFAIP3 (A20) is a tumor suppressor gene in Hodgkin lymphoma and primary mediastinal B cell lymphoma. *J. Exp. Med.* **206**, 981–989 (2009).

93. van Eijk, M., Medema, J. P. & de Groot, C. Cutting edge: cellular Fas-associated death domain-like IL-1-converting enzyme-inhibitory protein protects germinal center B cells from apoptosis during germinal center reactions. *J. Immunol. Baltim. Md 1950* **166**, 6473–6476 (2001).

94. Micheau, O., Lens, S., Gaide, O., Alevizopoulos, K. & Tschopp, J. NF-κB Signals Induce the Expression of c-FLIP. *Mol. Cell. Biol.* **21**, 5299–5305 (2001).

95. Straus, S. E. *et al.* The development of lymphomas in families with autoimmune lymphoproliferative syndrome with germline Fas mutations and defective lymphocyte apoptosis. *Blood* **98**, 194–200 (2001).

96. Juno, J. A. *et al.* Cytotoxic CD4 T Cells—Friend or Foe during Viral Infection? *Front. Immunol.* **8**, (2017).

97. Aldinucci, D., Gloghini, A., Pinto, A., Colombatti, A. & Carbone, A. The role of CD40/CD40L and interferon regulatory factor 4 in Hodgkin lymphoma microenvironment. *Leuk. Lymphoma* **53**, 195–201 (2012).

98. Mancao, C., Altmann, M., Jungnickel, B. & Hammerschmidt, W. Rescue of "crippled" germinal center B cells from apoptosis by Epstein-Barr virus. *Blood* **106**, 4339–4344 (2005).

99. Li, H. *et al.* Epstein-Barr virus lytic reactivation regulation and its pathogenic role in carcinogenesis. *Int. J. Biol. Sci.* **12**, 1309–1318 (2016).

100. Bohlius, J. *et al.* HIV-1-related Hodgkin lymphoma in the era of combination antiretroviral therapy: incidence and evolution of $CD4^+$ T-cell lymphocytes. *Blood* **117**, 6100–6108 (2011).

101. Gloghini, A. & Carbone, A. Why would the incidence of HIV-associated Hodgkin lymphoma increase in the setting of improved immunity? *Int. J. Cancer* **120**, 2753–2754 (2007).

102. Gopal, S. *et al.* Lymphoma immune reconstitution inflammatory syndrome in the center for AIDS research network of integrated clinical systems cohort. *Clin. Infect. Dis. Off. Publ. Infect. Dis. Soc. Am.* **59**, 279–286 (2014).

103. Sayad, A., Akbari, M. T., Mehdizadeh, M., Movafagh, A. & Hajifathali, A. The Association of HLA-Class I and Class II with Hodgkin's Lymphoma in Iranian Patients. *BioMed Research International* https://www.hindawi.com/journals/bmri/2014/231236/ (2014) doi:10.1155/2014/231236.

104. Berberich, F. R., Berberich, M. S., King, M. C., Engleman, E. G. & Grumet, F. C. Hodgkin's disease susceptibility: linkage to the HLA locus demonstrated by a new concordance method. *Hum. Immunol.* **6**, 207–217 (1983).

105. Law, P. J. *et al.* Genome-wide association analysis of chronic lymphocytic leukaemia, Hodgkin lymphoma and multiple myeloma identifies pleiotropic risk loci. *Sci. Rep.* **7**, 41071 (2017).

106. Cozen, W. *et al.* A meta-analysis of Hodgkin lymphoma reveals 19p13.3 TCF3 as a novel susceptibility locus. *Nat. Commun.* **5**, 3856 (2014).

107. Enciso-Mora, V. *et al.* A genome-wide association study of Hodgkin's lymphoma identifies new susceptibility loci at 2p16.1 (REL), 8q24.21 and 10p14 (GATA3). *Nat. Genet.* **42**, 1126–1130 (2010).

108. Moutsianas, L. *et al.* Multiple Hodgkin lymphoma-associated loci within the HLA region at chromosome 6p21.3. *Blood* **118**, 670–674 (2011).

109. Cozen, W. *et al.* A genome-wide meta-analysis of nodular sclerosing Hodgkin lymphoma identifies risk loci at 6p21.32. *Blood* **119**, 469–475 (2012).

110. Sud, A. *et al.* Genome-wide association study implicates immune dysfunction in the development of Hodgkin lymphoma. *Blood* blood-2018-06-855296 (2018) doi:10.1182/blood-2018-06-855296.

111. Hors, J. & Dausset, J. HLA and susceptibility to Hodgkin's disease. *Immunol. Rev.* **70**, 167–192 (1983).

112. Diepstra, A. *et al.* Association with HLA class I in Epstein-Barr-virus-positive and with HLA class III in Epstein-Barr-virus-negative Hodgkin's lymphoma. *Lancet Lond. Engl.* **365**, 2216–2224 (2005).

113. Johnson, P. C. D. *et al.* Modeling HLA associations with EBV-positive and -negative Hodgkin lymphoma suggests distinct mechanisms in disease pathogenesis. *Int. J. Cancer* **137**, 1066–1075 (2015).

114. Urayama, K. Y. *et al.* Genome-Wide Association Study of Classical Hodgkin Lymphoma and Epstein–Barr Virus Status–Defined Subgroups. *JNCI J. Natl. Cancer Inst.* **104**, 240–253 (2012).

115. Kushekhar, K. *et al.* Genetic Associations in Classical Hodgkin Lymphoma: A Systematic Review and Insights into Susceptibility Mechanisms. *Cancer Epidemiol. Prev. Biomark.* **23**, 2737–2747 (2014).

116. Delahaye-Sourdeix, M. *et al.* A Novel Risk Locus at 6p21.3 for Epstein-Barr Virus-Positive Hodgkin Lymphoma. *Cancer Epidemiol. Biomark. Prev. Publ. Am. Assoc. Cancer Res. Cosponsored Am. Soc. Prev. Oncol.* **24**, 1838–1843 (2015).

117. Khan, G. *et al.* Phenotype and frequency of Epstein-Barr virus-infected cells in pretreatment blood samples from patients with Hodgkin lymphoma. *Br. J. Haematol.* **129**, 511–519 (2005).

118. Gallagher, A. *et al.* Detection of Epstein-Barr virus (EBV) genomes in the serum of patients with EBV-associated Hodgkin's disease. *Int. J. Cancer* **84**, 442–448 (1999).

119. Smatti, M. K. *et al.* Epstein–Barr Virus Epidemiology, Serology, and Genetic Variability of LMP-1 Oncogene Among Healthy Population: An Update. *Front. Oncol.* **8**, (2018).

120. Hjalgrim, H. *et al.* HLA-A alleles and infectious mononucleosis suggest a critical role for cytotoxic T-cell response in EBV-related Hodgkin lymphoma. *Proc. Natl. Acad. Sci. U. S. A.* **107**, 6400–6405 (2010).

121. Niens, M. *et al.* HLA-A*02 is associated with a reduced risk and HLA-A*01 with an increased risk of developing EBV+ Hodgkin lymphoma. *Blood* **110**, 3310–3315 (2007).

122. Alexander, F. E. *et al.* Epstein-Barr Virus and HLA-DPB1-*0301 in young adult Hodgkin's disease: evidence for inherited susceptibility to Epstein-Barr Virus in cases that are EBV(+ve). *Cancer Epidemiol. Biomark. Prev. Publ. Am. Assoc. Cancer Res. Cosponsored Am. Soc. Prev. Oncol.* **10**, 705–709 (2001).

123. Alexander, F. E. *et al.* Risk factors for Hodgkin's disease by Epstein-Barr virus (EBV) status: prior infection by EBV and other agents. *Br. J. Cancer* **82**, 1117–1121 (2000).

124. Alexander, F. E. *et al.* An epidemiologic study of index and family infectious mononucleosis and adult Hodgkin's disease (HD): evidence for a specific association with EBV+ve HD in young adults. *Int. J. Cancer* **107**, 298–302 (2003).

125. Hjalgrim, H. *et al.* Characteristics of Hodgkin's lymphoma after infectious mononucleosis. *N. Engl. J. Med.* **349**, 1324–1332 (2003).

126. Hjalgrim, H. *et al.* Risk of Hodgkin's disease and other cancers after infectious mononucleosis. *J. Natl. Cancer Inst.* **92**, 1522–1528 (2000).

127. Brennan, R. M. & Burrows, S. R. A mechanism for the HLA-A*01-associated risk for EBV+ Hodgkin lymphoma and infectious mononucleosis. *Blood* **112**, 2589–2590 (2008).

128. Forrest, C., Hislop, A. D., Rickinson, A. B. & Zuo, J. Proteome-wide analysis of CD8+ T cell responses to EBV reveals differences between primary and persistent infection. *PLOS Pathog.* **14**, e1007110 (2018).

129. Su, W.-H., Hildesheim, A. & Chang, Y.-S. Human Leukocyte Antigens and Epstein–Barr Virus-Associated Nasopharyngeal Carcinoma: Old Associations Offer New Clues into the Role of Immunity in Infection-Associated Cancers. *Front. Oncol.* **3**, (2013).

130. Bosshart, H. & Jarrett, R. F. Deficient major histocompatibility complex class II antigen presentation in a subset of Hodgkin's disease tumor cells. *Blood* **92**, 2252–2259 (1998).

131. Nijland, M. *et al.* HLA dependent immune escape mechanisms in B-cell lymphomas: Implications for immune checkpoint inhibitor therapy? *Oncoimmunology* **6**, e1295202 (2017).

132. Roemer, M. G. M. *et al.* Classical Hodgkin Lymphoma with Reduced β2M/MHC Class I Expression Is Associated with Inferior Outcome Independent of 9p24.1 Status. *Cancer Immunol. Res.* **4**, 910–916 (2016).

133. Roemer, M. G. M. *et al.* Expression of Major Histocompatibility Complex (MHC) Class II, but Not MHC Class I, Predicts Outcome in Patients with Classical Hodgkin Lymphoma (cHL) Treated with Nivolumab (Programmed Death-1 [PD-1] Blockade). *Blood* **130**, 1450–1450 (2017).

134. Diepstra, A. *et al.* HLA Class II Expression by Hodgkin Reed-Sternberg Cells Is an Independent Prognostic Factor in Classical Hodgkin's Lymphoma. *J. Clin. Oncol.* **25**, 3101–3108 (2007).

135. Lee, S. P. *et al.* Antigen Presenting Phenotype of Hodgkin Reed-Sternberg Cells: Analysis of the HLA Class I Processing Pathway and the Effects of Interleukin-10 on Epstein-Barr Virus-Specific Cytotoxic T-Cell Recognition. *Blood* **92**, 1020–1030 (1998).

136. Murray, P. G., Constandinou, C. M., Crocker, J., Young, L. S. & Ambinder, R. F. Analysis of major histocompatibility complex class I, TAP expression, and LMP2 epitope sequence in Epstein-Barr virus-positive Hodgkin's disease. *Blood* **92**, 2477–2483 (1998).

137. Huang, X. *et al.* Expression of HLA class I and HLA class II by tumor cells in Chinese classical Hodgkin lymphoma patients. *PloS One* **5**, e10865 (2010).

138. Fletcher, L. B. *et al.* HLA expression and HLA type associations in relation to EBV status in Hispanic Hodgkin lymphoma patients. *PloS One* **12**, e0174457 (2017).

139. Duffield, A. S. *et al.* Th17 immune microenvironment in Epstein-Barr virus-negative Hodgkin lymphoma: implications for immunotherapy. *Blood Adv.* **1**, 1324–1334 (2017).

140. Steidl, C. *et al.* MHC class II transactivator CIITA is a recurrent gene fusion partner in lymphoid cancers. *Nature* **471**, 377–381 (2011).

141. Burger, J. A., Ghia, P., Rosenwald, A. & Caligaris-Cappio, F. The microenvironment in mature B-cell malignancies: a target for new treatment strategies. *Blood* **114**, 3367–3375 (2009).

142. Scott, D. W. & Gascoyne, R. D. The tumour microenvironment in B cell lymphomas. *Nat. Rev. Cancer* **14**, 517–534 (2014).

143. Gascoyne, R. D. & Steidl, C. *VII. The role of the microenvironment in lymphoid cancers*.

144. Steidl, C. *et al.* Tumor-Associated Macrophages and Survival in Classic Hodgkin's Lymphoma. *N. Engl. J. Med.* **362**, 875–885 (2010).

145. Guo, B., Cen, H., Tan, X. & Ke, Q. Meta-analysis of the prognostic and clinical value of tumor-associated macrophages in adult classical Hodgkin lymphoma. *BMC Med.* **14**, (2016).

146. Tan, K. L. *et al.* Tumor-associated macrophages predict inferior outcomes in classic Hodgkin lymphoma: a correlative study from the E2496 Intergroup trial. *Blood* **120**, 3280–3287 (2012).

147. Kamper, P. *et al.* Tumor-infiltrating macrophages correlate with adverse prognosis and Epstein-Barr virus status in classical Hodgkin's lymphoma. *Haematologica* **96**, 269–276 (2011).

148. Harris, J. A. *et al.* CD163 versus CD68 in tumor associated macrophages of classical hodgkin lymphoma. *Diagn. Pathol.* **7**, 12 (2012).

149. Tudor, C. S. *et al.* Macrophages and Dendritic Cells as Actors in the Immune Reaction of Classical Hodgkin Lymphoma. *PLoS ONE* **9**, (2014).

150. Crane, G. M. *et al.* Tumor-Infiltrating Macrophages in Post-Transplant, Relapsed Classical Hodgkin Lymphoma Are Donor-Derived. *PLoS ONE* **11**, (2016).

151. Li, F. *et al.* Tumor-Associated Macrophages Can Contribute to Antitumor Activity through FcγR-Mediated Processing of Antibody-Drug Conjugates. *Mol. Cancer Ther.* **16**, 1347–1354 (2017).

152. Niens, M. *et al.* Serum chemokine levels in Hodgkin lymphoma patients: highly increased levels of CCL17 and CCL22. *Br. J. Haematol.* **140**, 527–536 (2008).

153. Vari, F. *et al.* Immune evasion via PD-1/PD-L1 on NK-cells and monocyte/macrophages is more prominent in Hodgkin lymphoma than DLBCL. *Blood* blood-2017-07-796342 (2018) doi:10.1182/blood-2017-07-796342.

154. Koh, Y. W., Park, C., Yoon, D. H., Suh, C. & Huh, J. CSF-1R Expression in Tumor-Associated Macrophages Is Associated With Worse Prognosis in Classical Hodgkin Lymphoma. *Am. J. Clin. Pathol.* **141**, 573–583 (2014).

155. Mantovani, A., Allavena, P., Sica, A. & Balkwill, F. Cancer-related inflammation. *Nature* **454**, 436–444 (2008).

156. Jeannin, P., Paolini, L., Adam, C. & Delneste, Y. The roles of CSFs on the functional polarization of tumor-associated macrophages. *FEBS J.* **285**, 680–699 (2018).

157. Choe, J.-Y. *et al.* Indoleamine 2,3-dioxygenase (IDO) is frequently expressed in stromal cells of Hodgkin lymphoma and is associated with adverse clinical features: a retrospective cohort study. *BMC Cancer* **14**, 335 (2014).

158. Ruella, M. *et al.* Overcoming the Immunosuppressive Tumor Microenvironment of Hodgkin Lymphoma Using Chimeric Antigen Receptor T Cells. *Cancer Discov.* **7**, 1154–1167 (2017).

159. Carey, C. D. *et al.* Topological analysis reveals a PD-L1-associated microenvironmental niche for Reed-Sternberg cells in Hodgkin lymphoma. *Blood* **130**, 2420–2430 (2017).

160. Karakhanova, S., Bedke, T., Enk, A. H. & Mahnke, K. IL-27 renders DC immunosuppressive by induction of B7-H1. *J. Leukoc. Biol.* **89**, 837–845 (2011).

161. Zhang, Y. *et al.* The role of the PD-1/PD-L1 axis in macrophage differentiation and function during pregnancy. *Hum. Reprod.* **34**, 25–36 (2019).

162. Dhupkar, P., Gordon, N., Stewart, J. & Kleinerman, E. S. Anti-PD-1 therapy redirects macrophages from an M2 to an M1 phenotype inducing regression of OS lung metastases. *Cancer Med.* **7**, 2654–2664 (2018).

163. Xiong, H. *et al.* Anti-PD-L1 treatment results in functional remodeling of the macrophage compartment. *Cancer Res.* canres.3208.2018 (2019) doi:10.1158/0008-5472.CAN-18-3208.

164. Passwell, J., Levanon, M., Davidsohn, J. & Ramot, B. Monocyte PGE2 secretion in Hodgkin's disease and its relation to decreased cellular immunity. *Clin. Exp. Immunol.* **51**, 61–68 (1983).

165. Greaves, P. The function and origin of the CD4+ T cell in the classical Hodgkin lymphoma microenvironment. (2012).

166. Juszczynski, P. *et al.* The AP1-dependent secretion of galectin-1 by Reed–Sternberg cells fosters immune privilege in classical Hodgkin lymphoma. *Proc. Natl. Acad. Sci. U. S. A.* **104**, 13134–13139 (2007).

167. Fozza, C. & Longinotti, M. T-Cell Traffic Jam in Hodgkin's Lymphoma: Pathogenetic and Therapeutic Implications. *Adv. Hematol.* **2011**, 501659 (2011).

168. Carbone, A. *et al.* Expression of functional CD40 antigen on Reed-Sternberg cells and Hodgkin's disease cell lines. *Blood* **85**, 780–789 (1995).

169. Trümper, L. *et al.* Assessment of clonality of rosetting T lymphocytes in Hodgkin's disease by single-cell polymerase chain reaction: detection of clonality in a polyclonal background in a case of lymphocyte predominance Hodgkin's disease. *Ann. Hematol.* **80**, 653–661 (2001).

170. Roers, A., Montesinos-Rongen, M., Hansmann, M. L., Rajewsky, K. & Küppers, R. Amplification of TCRbeta gene rearrangements from micromanipulated single cells: T cells

rosetting around Hodgkin and Reed-Sternberg cells in Hodgkin's disease are polyclonal. *Eur. J. Immunol.* **28**, 2424–2431 (1998).

171. Ishida, Y., Agata, Y., Shibahara, K. & Honjo, T. Induced expression of PD-1, a novel member of the immunoglobulin gene superfamily, upon programmed cell death. *EMBO J.* **11**, 3887–3895 (1992).

172. Leach, D. R., Krummel, M. F. & Allison, J. P. Enhancement of antitumor immunity by CTLA-4 blockade. *Science* **271**, 1734–1736 (1996).

173. Daud, A. I. *et al.* Tumor immune profiling predicts response to anti–PD-1 therapy in human melanoma. *J. Clin. Invest.* **126**, 3447–3452 (2016).

174. Machado, L. *et al.* Expression and function of T cell homing molecules in Hodgkin's lymphoma. *Cancer Immunol. Immunother.* **58**, 85–94 (2009).

175. Shang, B., Liu, Y., Jiang, S. & Liu, Y. Prognostic value of tumor-infiltrating FoxP3+ regulatory T cells in cancers: a systematic review and meta-analysis. *Sci. Rep.* **5**, (2015).

176. Greaves, P. *et al.* Expression of FOXP3, CD68, and CD20 at Diagnosis in the Microenvironment of Classical Hodgkin Lymphoma Is Predictive of Outcome. *J. Clin. Oncol.* **31**, 256–262 (2013).

177. Kataoka, K. *et al.* Aberrant PD-L1 expression through 3'-UTR disruption in multiple cancers. *Nature* **534**, 402–406 (2016).

178. Gibney, G. T., Weiner, L. M. & Atkins, M. B. Predictive biomarkers for checkpoint inhibitor-based immunotherapy. *Lancet Oncol.* **17**, e542–e551 (2016).

179. Taube, J. M. *et al.* Association of PD-1, PD-1 ligands, and other features of the tumor immune microenvironment with response to anti-PD-1 therapy. *Clin. Cancer Res. Off. J. Am. Assoc. Cancer Res.* **20**, 5064–5074 (2014).

180. Steidl, C. The ecosystem of classical Hodgkin lymphoma. *Blood* **130**, 2360–2361 (2017).

181. Crespo, J., Sun, H., Welling, T. H., Tian, Z. & Zou, W. T cell anergy, exhaustion, senescence, and stemness in the tumor microenvironment. *Curr. Opin. Immunol.* **25**, 214–221 (2013).

182. Schietinger, A. & Greenberg, P. D. Tolerance and Exhaustion: Defining Mechanisms of T cell Dysfunction. *Trends Immunol.* **35**, 51–60 (2014).

183. Wherry, E. J. T cell exhaustion. *Nat. Immunol.* **12**, 492–499 (2011).

184. Barber, D. L. *et al.* Restoring function in exhausted CD8 T cells during chronic viral infection. *Nature* **439**, 682–687 (2006).

185. Baitsch, L., Fuertes-Marraco, S. A., Legat, A., Meyer, C. & Speiser, D. E. The three main stumbling blocks for anticancer T cells. *Trends Immunol.* **33**, 364–372 (2012).

186. Nurieva, R., Wang, J. & Sahoo, A. T-cell tolerance in cancer. *Immunotherapy* **5**, 513–531 (2013).

187. Wherry, E. J. *et al.* Molecular signature of CD8+ T cell exhaustion during chronic viral infection. *Immunity* **27**, 670–684 (2007).

188. Wherry, E. J., Blattman, J. N., Murali-Krishna, K., van der Most, R. & Ahmed, R. Viral persistence alters CD8 T-cell immunodominance and tissue distribution and results in distinct stages of functional impairment. *J. Virol.* **77**, 4911–4927 (2003).

189. Riches, J. C. *et al.* T cells from CLL patients exhibit features of T-cell exhaustion but retain capacity for cytokine production. *Blood* **121**, 1612–1621 (2013).

190. Wei, F. *et al.* Strength of PD-1 signaling differentially affects T-cell effector functions. *Proc. Natl. Acad. Sci. U. S. A.* **110**, E2480-2489 (2013).

191. Blackburn, S. D., Shin, H., Freeman, G. J. & Wherry, E. J. Selective expansion of a subset of exhausted CD8 T cells by alphaPD-L1 blockade. *Proc. Natl. Acad. Sci. U. S. A.* **105**, 15016–15021 (2008).

192. Porichis, F. *et al.* Responsiveness of HIV-specific CD4 T cells to PD-1 blockade. *Blood* **118**, 965–974 (2011).

193. Mizuno, R. *et al.* PD-1 Primarily Targets TCR Signal in the Inhibition of Functional T Cell Activation. *Front. Immunol.* **10**, (2019).

194. Okazaki, T., Chikuma, S., Iwai, Y., Fagarasan, S. & Honjo, T. A rheostat for immune responses: the unique properties of PD-1 and their advantages for clinical application. *Nat. Immunol.* **14**, 1212–1218 (2013).

195. Blackburn, S. D. *et al.* Tissue-specific differences in PD-1 and PD-L1 expression during chronic viral infection: implications for CD8 T-cell exhaustion. *J. Virol.* **84**, 2078–2089 (2010).

196. Parekh, V. V. *et al.* PD-1:PD-L blockade prevents anergy induction and enhances the anti-tumor activities of glycolipid-activated iNKT cells. *J. Immunol. Baltim. Md 1950* **182**, 2816–2826 (2009).

197. Chikuma, S. *et al.* PD-1-mediated suppression of IL-2 production induces CD8+ T cell anergy in vivo. *J. Immunol. Baltim. Md 1950* **182**, 6682–6689 (2009).

198. Türeci, O., Schmitt, H., Fadle, N., Pfreundschuh, M. & Sahin, U. Molecular definition of a novel human galectin which is immunogenic in patients with Hodgkin's disease. *J. Biol. Chem.* **272**, 6416–6422 (1997).

199. Scheeren, F. A. *et al.* IL-21 is expressed in Hodgkin lymphoma and activates STAT5: evidence that activated STAT5 is required for Hodgkin lymphomagenesis. *Blood* **111**, 4706–4715 (2008).

200. Bennett, F. *et al.* Program death-1 engagement upon TCR activation has distinct effects on costimulation and cytokine-driven proliferation: attenuation of ICOS, IL-4, and IL-21, but not CD28, IL-7, and IL-15 responses. *J. Immunol. Baltim. Md 1950* **170**, 711–718 (2003).

201. Muenst, S., Hoeller, S., Dirnhofer, S. & Tzankov, A. Increased programmed death-1+ tumor-infiltrating lymphocytes in classical Hodgkin lymphoma substantiate reduced overall survival. *Hum. Pathol.* **40**, 1715–1722 (2009).

202. Koh, Y. W., Jeon, Y. K., Yoon, D. H., Suh, C. & Huh, J. Programmed death 1 expression in the peritumoral microenvironment is associated with a poorer prognosis in classical Hodgkin lymphoma. *Tumour Biol. J. Int. Soc. Oncodevelopmental Biol. Med.* **37**, 7507–7514 (2016).

203. Hollander, P. *et al.* High proportions of PD-1+ and PD-L1+ leukocytes in classical Hodgkin lymphoma microenvironment are associated with inferior outcome. *Blood Adv.* **1**, 1427–1439 (2017).

204. Xia, B. *et al.* [Expressions and prognostic significance of PTEN and PD-1 protein in patients with classical Hodgkin's lymphoma]. *Zhonghua Xue Ye Xue Za Zhi Zhonghua Xueyexue Zazhi* **39**, 839–844 (2018).

205. Wang, T. T. *et al.* [Expression and prognostic significance of microenvironment related prognostic factors in patients with classical Hodgkin's lymphoma]. *Zhonghua Yi Xue Za Zhi* **97**, 1400–1405 (2017).

206. Chetaille, B. *et al.* Molecular profiling of classical Hodgkin lymphoma tissues uncovers variations in the tumor microenvironment and correlations with EBV infection and outcome. *Blood* **113**, 2765–3775 (2009).

207. Nguyen, T. *et al.* Expression of TIA1 and PAX5 in Classical Hodgkin Lymphoma at Initial Diagnosis May Predict Clinical Outcome. *Appl. Immunohistochem. Mol. Morphol.* **24**, 383–391 (2016).

208. Menter, T., Bodmer-Haecki, A., Dirnhofer, S. & Tzankov, A. Evaluation of the diagnostic and prognostic value of PDL1 expression in Hodgkin and B-cell lymphomas. *Hum. Pathol.* **54**, 17–24 (2016).

209. Dorfman, D. M., Brown, J. A., Shahsafaei, A. & Freeman, G. J. Programmed death-1 (PD-1) is a marker of germinal center-associated T cells and angioimmunoblastic T-cell lymphoma. *Am. J. Surg. Pathol.* **30**, 802–810 (2006).

210. Nam-Cha, S. H. *et al.* PD-1, a follicular T-cell marker useful for recognizing nodular lymphocyte-predominant Hodgkin lymphoma. *Am. J. Surg. Pathol.* **32**, 1252–1257 (2008).

211. Paydas, S., Bağır, E., Seydaoglu, G., Ercolak, V. & Ergin, M. Programmed death-1 (PD-1), programmed death-ligand 1 (PD-L1), and EBV-encoded RNA (EBER) expression in Hodgkin lymphoma. *Ann. Hematol.* **94**, 1545–1552 (2015).

212. Péricart, S. *et al.* Profiling Immune Escape in Hodgkin's and Diffuse large B-Cell Lymphomas Using the Transcriptome and Immunostaining. *Cancers* **10**, (2018).

213. Sasse, S. *et al.* Programmed cell death protein-1 (PD-1)-expression in the microenvironment of classical Hodgkin lymphoma at relapse during anti-PD-1-treatment. *Haematologica* (2018) doi:10.3324/haematol.2018.196279.

214. Taylor, J. G., Clear, A., Calaminici, M. & Gribben, J. G. Programmed cell death protein-1 (PD1) expression in the microenvironment of classical Hodgkin lymphoma is similar between favorable and adverse outcome and does not enrich over serial relapses with conventional chemotherapy. *Haematologica* **104**, e42–e44 (2019).

215. Jenkins, R. W., Barbie, D. A. & Flaherty, K. T. Mechanisms of resistance to immune checkpoint inhibitors. *Br. J. Cancer* **118**, 9–16 (2018).

216. Cader, F. Z. *et al.* Mass cytometry of Hodgkin lymphoma reveals a CD4+ regulatory T-cell-rich and exhausted T-effector microenvironment. *Blood* **132**, 825–836 (2018).

217. Tian, Y. *et al.* Unique phenotypes and clonal expansions of human CD4 effector memory T cells re-expressing CD45RA. *Nat. Commun.* **8**, 1473 (2017).

218. Larbi, A. & Fulop, T. From "truly naïve" to "exhausted senescent" T cells: When markers predict functionality. *Cytometry A* **85**, 25–35 (2014).

219. Crawford, A. *et al.* Molecular and transcriptional basis of CD4+ T cell dysfunction during chronic infection. *Immunity* **40**, 289–302 (2014).

220. Tian, Y., Sette, A. & Weiskopf, D. Cytotoxic CD4 T Cells: Differentiation, Function, and Application to Dengue Virus Infection. *Front. Immunol.* **7**, (2016).

221. Tanijiri, T. *et al.* Hodgkin's Reed-Sternberg cell line (KM-H2) promotes a bidirectional differentiation of CD4+CD25+Foxp3+ T cells and CD4+ cytotoxic T lymphocytes from CD4+ naive T cells. *J. Leukoc. Biol.* **82**, 576–584 (2007).

222. Kunicki, M. A., Amaya Hernandez, L. C., Davis, K. L., Bacchetta, R. & Roncarolo, M.-G. Identity and Diversity of Human Peripheral Th and T Regulatory Cells Defined by Single-Cell Mass Cytometry. *J. Immunol. Baltim. Md 1950* (2017) doi:10.4049/jimmunol.1701025.

223. Geginat, J. *et al.* Plasticity of Human CD4 T Cell Subsets. *Front. Immunol.* **5**, (2014).

224. Sawant, D. V. & Vignali, D. A. A. Once a Treg, always a Treg? *Immunol. Rev.* **259**, 173–191 (2014).

225. Kleinewietfeld, M. & Hafler, D. A. The plasticity of human Treg and Th17 cells and its role in autoimmunity. *Semin. Immunol.* **25**, 305–312 (2013).

226. Ma, Y. *et al.* The CD4+CD26|[minus]| T-cell population in classical Hodgkin's lymphoma displays a distinctive regulatory T-cell profile. *Lab. Invest.* **88**, 482–490 (2008).

227. Poppema, S. Immunology of Hodgkin's disease. *Baillieres Clin. Haematol.* **9**, 447–457 (1996).

228. Salgado, F. J. *et al.* CD26: a negative selection marker for human Treg cells. *Cytom. Part J. Int. Soc. Anal. Cytol.* **81**, 843–855 (2012).

229. Wu, R. *et al.* The microenvironment of classical Hodgkin lymphoma: heterogeneity by Epstein–Barr virus presence and location within the tumor. *Blood Cancer J.* **6**, e417 (2016).

230. Chemnitz, J. M. *et al.* RNA fingerprints provide direct evidence for the inhibitory role of TGFβ and PD-1 on CD4+ T cells in Hodgkin lymphoma. *Blood* **110**, 3226–3233 (2007).

231. Poppema, S. The nature of the lymphocytes surrounding Reed-Sternberg cells in nodular lymphocyte predominance and in other types of Hodgkin's disease. *Am. J. Pathol.* **135**, 351–357 (1989).

232. Wein, F. *et al.* Complex immune evasion strategies in classical Hodgkin lymphoma. *Cancer Immunol. Res.* (2017) doi:10.1158/2326-6066.CIR-17-0325.

233. Ishida, T. *et al.* Specific Recruitment of CC Chemokine Receptor 4–Positive Regulatory T Cells in Hodgkin Lymphoma Fosters Immune Privilege. *Cancer Res.* **66**, 5716–5722 (2006).

234. Kapp, U. *et al.* Interleukin 13 Is Secreted by and Stimulates the Growth of Hodgkin and Reed-Sternberg Cells. *J. Exp. Med.* **189**, 1939–1946 (1999).

235. deLeeuw, R. J., Kost, S. E., Kakal, J. A. & Nelson, B. H. The Prognostic Value of FoxP3+ Tumor-Infiltrating Lymphocytes in Cancer: A Critical Review of the Literature. *Clin. Cancer Res.* **18**, 3022–3029 (2012).

236. Gaetano, R. D. *et al.* Flow cytometry CD4+CD26−CD38+ lymphocyte subset in the microenvironment of Hodgkin lymphoma-affected lymph nodes. *Ann. Hematol.* **93**, 1319–1326 (2014).

237. Marshall, N. A., Vickers, M. A. & Barker, R. N. Regulatory T Cells Secreting IL-10 Dominate the Immune Response to EBV Latent Membrane Protein 1. *J. Immunol.* **170**, 6183–6189 (2003).

238. Cedeno-Laurent, F., Opperman, M., Barthel, S. R., Kuchroo, V. K. & Dimitroff, C. J. Galectin-1 triggers an immunoregulatory signature in T helper cells functionally defined by IL-10 expression. *J. Immunol. Baltim. Md 1950* **188**, 3127–3137 (2012).

239. Jundt, F. *et al.* Hodgkin/Reed-Sternberg Cells Induce Fibroblasts to Secrete Eotaxin, a Potent Chemoattractant for T Cells and Eosinophils. *Blood* **94**, 2065–2071 (1999).

240. Iikuni, N., Lourenço, E. V., Hahn, B. H. & La Cava, A. Cutting Edge: Regulatory T Cells Directly Suppress B Cells in Systemic Lupus Erythematosus. *J. Immunol. Baltim. Md 1950* **183**, 1518–1522 (2009).

241. Wein, F. & Küppers, R. The role of T cells in the microenvironment of Hodgkin lymphoma. *J. Leukoc. Biol.* **99**, 45–50 (2016).

242. Carbone, A., Gloghini, A., Gruss, H. J. & Pinto, A. CD40 ligand is constitutively expressed in a subset of T cell lymphomas and on the microenvironmental reactive T cells of follicular lymphomas and Hodgkin's disease. *Am. J. Pathol.* **147**, 912–922 (1995).

243. Kim, L.-H., Eow, G.-I., Peh, S. C. & Poppema, S. The role of CD30, CD40 and CD95 in the regulation of proliferation and apoptosis in classical Hodgkin's lymphoma. *Pathology (Phila.)* **35**, 428–435 (2003).

244. Gruss, H. J. *et al.* Expression and function of CD40 on Hodgkin and Reed-Sternberg cells and the possible relevance for Hodgkin's disease. *Blood* **84**, 2305–2314 (1994).

245. Gruss, H. J., Ulrich, D., Braddy, S., Armitage, R. J. & Dower, S. K. Recombinant CD30 ligand and CD40 ligand share common biological activities on Hodgkin and Reed-Sternberg cells. *Eur. J. Immunol.* **25**, 2083–2089 (1995).

246. Delabie, J. *et al.* The B7/BB1 antigen is expressed by Reed-Sternberg cells of Hodgkin's disease and contributes to the stimulating capacity of Hodgkin's disease-derived cell lines. *Blood* **82**, 2845–2852 (1993).

247. Van Gool, S. W. *et al.* Expression of B7-2 (CD86) molecules by Reed-Sternberg cells of Hodgkin's disease. *Leukemia* **11**, 846–851 (1997).

248. Nozawa, Y., Wakasa, H. & Abe, M. Costimulatory molecules (CD80 and CD86) on Reed-Sternberg cells are associated with the proliferation of background T cells in Hodgkin's disease. *Pathol. Int.* **48**, 10–14 (1998).

249. Coler, R. N. *et al.* Vaccination produces CD4 T cells with a novel CD154-CD40 dependent cytolytic mechanism. *J. Immunol. Baltim. Md 1950* **195**, 3190–3197 (2015).

250. Roeser, J. C., Leach, S. D. & McAllister, F. Emerging strategies for cancer immunoprevention. *Oncogene* **34**, 6029–6039 (2015).

251. Aldinucci, D. *et al.* Expression of CCR5 receptors on Reed–Sternberg cells and Hodgkin lymphoma cell lines: Involvement of CCL5/Rantes in tumor cell growth and microenvironmental interactions. *Int. J. Cancer* **122**, 769–776 (2008).

252. Liu, F., Zhang, Y., Wu, Z.-Q. & Zhao, T. Analysis of CCL5 expression in classical Hodgkin's lymphoma L428 cell line. *Mol. Med. Rep.* **4**, 837–841 (2011).

253. Fischer, M. *et al.* Expression of CCL5/RANTES by Hodgkin and Reed-Sternberg cells and its possible role in the recruitment of mast cells into lymphomatous tissue. *Int. J. Cancer* **107**, 197–201 (2003).

254. Islam, S. A. & Luster, A. D. T cell homing to epithelial barriers in allergic disease. *Nat. Med.* **18**, 705–715 (2012).

255. Teichmann, M., Meyer, B., Beck, A. & Niedobitek, G. Expression of the interferon-inducible chemokine IP-10 (CXCL10), a chemokine with proposed anti-neoplastic functions, in Hodgkin lymphoma and nasopharyngeal carcinoma. *J. Pathol.* **206**, 68–75 (2005).

256. Ohshima, K. *et al.* Infiltration of Th1 and Th2 lymphocytes around Hodgkin and Reed-Sternberg (H&RS) cells in Hodgkin disease: Relation with expression of CXC and CC chemokines on H&RS cells. *Int. J. Cancer* **98**, 567–572 (2002).

257. Theurich, S. *et al.* Brentuximab vedotin combined with donor lymphocyte infusions for early relapse of Hodgkin lymphoma after allogeneic stem-cell transplantation induces tumor-specific immunity and sustained clinical remission. *J. Clin. Oncol. Off. J. Am. Soc. Clin. Oncol.* **31**, e59-63 (2013).

258. Ferrarini, I., Rigo, A., Zamò, A. & Vinante, F. Classical Hodgkin lymphoma cells may promote an IL-17-enriched microenvironment. *Leuk. Lymphoma* 1–11 (2019) doi:10.1080/10428194.2019.1636983.

259. Lu, T. *et al.* Aberrant Circulating Th17 Cells in Patients with B-Cell Non-Hodgkin's Lymphoma. *PLoS ONE* **11**, (2016).

260. Yoshida, N. *et al.* A High RORγT/CD3 Ratio is a Strong Prognostic Factor for Postoperative Survival in Advanced Colorectal Cancer: Analysis of Helper T Cell Lymphocytes (Th1, Th2, Th17 and Regulatory T Cells). *Ann. Surg. Oncol.* **23**, 919–927 (2016).

261. Du, J., Huang, C., Zhou, B. & Ziegler, S. F. Isoform-Specific Inhibition of RORα-Mediated Transcriptional Activation by Human FOXP3. *J. Immunol.* **180**, 4785–4792 (2008).

262. Solt, L. A. & Burris, T. P. Action of RORs and Their Ligands in (Patho)physiology. *Trends Endocrinol. Metab. TEM* **23**, 619–627 (2012).

263. Solt, L. A. *et al.* Suppression of TH17 differentiation and autoimmunity by a synthetic ROR ligand. *Nature* **472**, 491–494 (2011).

264. Jetten, A. M. Retinoid-related orphan receptors (RORs): critical roles in development, immunity, circadian rhythm, and cellular metabolism. *Nucl. Recept. Signal.* **7**, (2009).

265. Chemnitz, J. M. *et al.* Prostaglandin E2 Impairs CD4+ T Cell Activation by Inhibition of lck: Implications in Hodgkin's Lymphoma. *Cancer Res.* **66**, 1114–1122 (2006).

266. Boniface, K. *et al.* Prostaglandin E2 regulates Th17 cell differentiation and function through cyclic AMP and EP2/EP4 receptor signaling. *J. Exp. Med.* **206**, 535–548 (2009).

267. Gandhi, M. K. *et al.* Galectin-1 mediated suppression of Epstein-Barr virus–specific T-cell immunity in classic Hodgkin lymphoma. *Blood* **110**, 1326–1329 (2007).

268. Yamamoto, R. *et al.* PD-1–PD-1 ligand interaction contributes to immunosuppressive microenvironment of Hodgkin lymphoma. *Blood* **111**, 3220–3224 (2008).

269. Roemer, M. G. M. *et al.* PD-L1 and PD-L2 Genetic Alterations Define Classical Hodgkin Lymphoma and Predict Outcome. *J. Clin. Oncol. Off. J. Am. Soc. Clin. Oncol.* **34**, 2690–2697 (2016).

270. Niedobitek, G., Päzolt, D., Teichmann, M. & Devergne, O. Frequent expression of the Epstein-Barr virus (EBV)-induced gene, EBI3, an IL-12 p40-related cytokine, in Hodgkin and Reed-Sternberg cells. *J. Pathol.* **198**, 310–316 (2002).

271. Baban, B. *et al.* IDO activates regulatory T cells and blocks their conversion into Th17-like T cells. *J. Immunol. Baltim. Md 1950* **183**, 2475–2483 (2009).

272. Zhang, Y. *et al.* PD-L1 up-regulation restrains Th17 cell differentiation in *STAT3* loss- and *STAT1* gain-of-function patients. *J. Exp. Med.* jem.20161427 (2017) doi:10.1084/jem.20161427.

273. Toscano, M. A. *et al.* Nuclear factor (NF)-κB controls expression of the immunoregulatory glycan-binding protein galectin-1. *Mol. Immunol.* **48**, 1940–1949 (2011).

274. Satoh, T., Wada, R., Yajima, N., Imaizumi, T. & Yagihashi, S. Tumor microenvironment and RIG-I signaling molecules in Epstein Barr virus-positive and -negative classical Hodgkin lymphoma of the elderly. *J. Clin. Exp. Hematop. JCEH* **54**, 75–84 (2014).

275. Samanta, M., Iwakiri, D., Kanda, T., Imaizumi, T. & Takada, K. EB virus-encoded RNAs are recognized by RIG-I and activate signaling to induce type I IFN. *EMBO J.* **25**, 4207–4214 (2006).

276. Samanta, M., Iwakiri, D. & Takada, K. Epstein-Barr virus-encoded small RNA induces IL-10 through RIG-I-mediated IRF-3 signaling. *Oncogene* **27**, 4150–4160 (2008).

277. Martin, P. *et al.* Association of DDX58 177 C > T polymorphism with decreased risk of Epstein-Barr virus-related nodular sclerosis classical Hodgkin lymphoma. *Leuk. Lymphoma* **58**, 438–444 (2017).

278. Jenabian, M.-A. *et al.* Distinct Tryptophan Catabolism and Th17/Treg Balance in HIV Progressors and Elite Controllers. *PLOS ONE* **8**, e78146 (2013).

279. Planès, R. *et al.* HIV-1 Tat protein induces PD-L1 (B7-H1) expression on dendritic cells through tumor necrosis factor alpha- and toll-like receptor 4-mediated mechanisms. *J. Virol.* **88**, 6672–6689 (2014).

280. Green, M. R. *et al.* Constitutive AP-1 Activity and EBV Infection Induce PD-L1 in Hodgkin Lymphomas and Post-transplant Lymphoproliferative Disorders: Implications for Targeted Therapy. *Clin. Cancer Res.* **18**, 1611–1618 (2012).

281. Egelhofer, T. A. *et al.* An assessment of histone-modification antibody quality. *Nat. Struct. Mol. Biol.* **18**, 91–93 (2011).

282. Michel, M. C., Wieland, T. & Tsujimoto, G. How reliable are G-protein-coupled receptor antibodies? *Naunyn. Schmiedebergs Arch. Pharmacol.* **379**, 385–388 (2009).

283. Berglund, L. *et al.* A genecentric Human Protein Atlas for expression profiles based on antibodies. *Mol. Cell. Proteomics MCP* **7**, 2019–2027 (2008).

284. Baker, M. Reproducibility crisis: Blame it on the antibodies. *Nat. News* **521**, 274 (2015).

285. Hughes, M. & Health, J. B. S. of P. The Principles of Humane Experimental Technique. *Johns Hopkins Bloomberg School of Public Health* http://altweb.jhsph.edu/pubs/books/humane_exp/het-toc.

286. Uhlen, M. *et al.* A proposal for validation of antibodies. *Nat. Methods* **13**, 823–827 (2016).

287. Tjalsma, H. *et al.* Profiling the humoral immune response in colon cancer patients: diagnostic antigens from Streptococcus bovis. *Int. J. Cancer* **119**, 2127–2135 (2006).

288. Hewitt, S. M., Baskin, D. G., Frevert, C. W., Stahl, W. L. & Rosa-Molinar, E. Controls for Immunohistochemistry: The Histochemical Society's Standards of Practice for Validation of Immunohistochemical Assays. *J. Histochem. Cytochem.* **62**, 693–697 (2014).

289. Holmseth, S. *et al.* Specificity controls for immunocytochemistry: the antigen preadsorption test can lead to inaccurate assessment of antibody specificity. *J. Histochem. Cytochem. Off. J. Histochem. Soc.* **60**, 174–187 (2012).

290. Mirlacher, M. *et al.* Influence of slide aging on results of translational research studies using immunohistochemistry. *Mod. Pathol. Off. J. U. S. Can. Acad. Pathol. Inc* **17**, 1414–1420 (2004).

291. Fedchenko, N. & Reifenrath, J. Different approaches for interpretation and reporting of immunohistochemistry analysis results in the bone tissue – a review. *Diagn. Pathol.* **9**, (2014).

292. Alkushi, A. Validation of tissue microarray biomarker expression of breast carcinomas in Saudi women. *Hematol. Oncol. Stem Cell Ther.* **2**, 394–398 (2009).

293. Van den Brink, G. R. *et al.* H pylori colocalises with MUC5AC in the human stomach. *Gut* **46**, 601–607 (2000).

294. van der Loos, C. M. Multiple Immunoenzyme Staining: Methods and Visualizations for the Observation With Spectral Imaging. *J. Histochem. Cytochem.* **56**, 313–328 (2008).

295. Tsujikawa, T. *et al.* Quantitative multiplex immunohistochemistry reveals myeloid-inflamed tumor-immune complexity associated with poor prognosis. *Cell Rep.* **19**, 203–217 (2017).

296. Glass, G., Papin, J. A. & Mandell, J. W. SIMPLE: a sequential immunoperoxidase labeling and erasing method. *J. Histochem. Cytochem. Off. J. Histochem. Soc.* **57**, 899–905 (2009).

297. Lan, H. Y., Mu, W., Nikolic-Paterson, D. J. & Atkins, R. C. A novel, simple, reliable, and sensitive method for multiple immunoenzyme staining: use of microwave oven heating to block antibody crossreactivity and retrieve antigens. *J. Histochem. Cytochem. Off. J. Histochem. Soc.* **43**, 97–102 (1995).

298. Han, L. *et al.* Phenotypical analysis of ectoenzymes CD39/CD73 and adenosine receptor 2A in CD4+ CD25high Foxp3+ regulatory T-cells in psoriasis. *Australas. J. Dermatol.* **59**, e31–e38 (2018).

299. de Jong, D. *et al.* Immunohistochemical Prognostic Markers in Diffuse Large B-Cell Lymphoma: Validation of Tissue Microarray As a Prerequisite for Broad Clinical Applications—A Study From the Lunenburg Lymphoma Biomarker Consortium. *J. Clin. Oncol.* **25**, 805–812 (2007).

300. Koulis, A., Trivedi, P., Ibrahim, H., Bower, M. & Naresh, K. N. The role of the microenvironment in human immunodeficiency virus-associated classical Hodgkin lymphoma. *Histopathology* **65**, 749–756 (2014).

301. Liebers, J., Wurzel, P., Reisinger, K. B. & Hansmann, M.-L. 3D image analysis reveals differences of CD30 positive cells and network formation in reactive and malignant human lymphoid tissue (classical Hodgkin Lymphoma). *PloS One* **14**, e0224156 (2019).

302. Rinker, T. W. & Kurkiewicz, D. pacman: Package Management for R. version 0.5.0. Buffalo, New York. (2017).

303. Müller, K. here: A Simpler Way to Find Your Files. R package version 0.1. (2017).

304. Wickham, H. conflicted: An Alternative Conflict Resolution Strategy. R package version 1.0.4. (2019).

305. Wickham, H., Hester, J. & Chang, W. devtools: Tools to Make Developing R Packages Easier. R package version 2.1.0. (2019).

306. Morgan, M. BiocManager: Access the Bioconductor Project Package Repository. R package version 1.30.4. (2018).

307. Wickham, H. tidyverse: Easily Install and Load the 'Tidyverse'. R package version 1.2.1. (2017).

308. Temple Lang, D. XML: Tools for Parsing and Generating XML Within R and S-Plus. R package version 3.98-1.16. (2018).

309. Wickham, H. Reshaping Data with the reshape Package. Journal of Statistical Software, 21(12), 1-20. (2007).

310. Wickham, H. scales: Scale Functions for Visualization. R package version 1.0.0. (2018).

311. Chen, H. Rphenograph: R implementation of the phenograph algorithm. R package version 0.99.1.9001. (2015).

312. Van Gassen, S., Callebaut, B. & Saeys, Y. FlowSOM: Using self-organizing maps for visualization and interpretation of cytometry data. (2019).

313. Ellis, B. *et al.* flowCore: Basic structures for flow cytometry data. R package version 1.50.0. (2019).

314. Krijthe, J. H. Rtsne: T-Distributed Stochastic Neighbor Embedding using a Barnes-Hut Implementation. (2015).

315. Chen, H., Lau, M., Wong, M., Newell, E. & Poidinger, M. Cytofkit: A Bioconductor Package for an Integrated Mass Cytometry Data Analysis Pipeline. (2016).

316. Elberg, A. B. largeVis: High-Quality Visualizations of Large, High-Dimensional Datasets. R package version 0.2.2. (2019).

317. Baddeley, A., Rubak, E. & Turner, R. *Spatial Point Patterns: Methodology and Applications with R*. (Chapman and Hall/CRC Press, 2015).

318. Pebesma, E. J., Bivand, R. S. & Gomez-Rubio, V. sp: Classes and methods for spatial data in R. and Applied spatial data analysis with R. (2005).

319. Arnold, J. B. ggthemes: Extra Themes, Scales and Geoms for 'ggplot2'. R package version 4.2.0. (2019).

320. Kassambara, A. ggpubr: 'ggplot2' Based Publication Ready Plots. R package version 0.2.2. (2019).

321. Schloerke, B. *et al.* GGally: Extension to 'ggplot2'. R package version 1.4.0. (2018).

322. Wilke, C. O. cowplot: Streamlined Plot Theme and Plot Annotations for 'ggplot2'. R package version 1.0.0. (2019).

323. Slowikowski, K. ggrepel: Automatically Position Non-Overlapping Text Labels with 'ggplot2'. R package version 0.8.1. (2019).

324. Neuwirth, E. RColorBrewer: ColorBrewer Palettes. R package version 1.1-2. (2014).

325. Kolde, R. pheatmap: Pretty Heatmaps. R package version 1.0.12. (2019).

326. Schapiro, D. *et al.* miCAT: A toolbox for analysis of cell phenotypes and interactions in multiplex image cytometry data. *Nat. Methods* **14**, 873–876 (2017).

327. Li, F. & Zhang, L. Comparison of point pattern analysis methods for classifying the spatial distributions of spruce-fir stands in the north-east USA. *For. Int. J. For. Res.* **80**, 337–349 (2007).

328. Colombo, A. *et al.* Abstract 1189: Revisiting immune exhaustion in Hodgkin's lymphoma. (2019) doi:1189-1189. 10.1158/1538-7445.SABCS18-1189.

329. Clark, P. J. & Evans, F. C. Distance to Nearest Neighbor as a Measure of Spatial Relationships in Populations. *Ecology* **35**, 445–453 (1954).

330. Dixon, P. M. Nearest Neighbor Methods. 28.

331. Taylor, J., Clear, A., Matthews, J., Calaminici, M. & Gribben, J. The Treg/Th17 Axis Is Skewed in Classical Hodgkin Lymphoma By PDL1+Ve but Not PDL1-Ve Lymphoma Cells and By Lymphoma MHC Class 2 Expression.. *Blood* (2018) doi:132. 4124-4124. 10.1182/blood-2018-99-119126.

332. Amarnath, S. *et al.* The PDL1-PD1 Axis Converts Human Th1 Cells Into Regulatory T Cells. *Sci. Transl. Med.* **3**, 111ra120 (2011).

333. Guo, X. *et al.* High Serum Level of Soluble Programmed Death Ligand 1 is Associated With a Poor Prognosis in Hodgkin Lymphoma. *Transl. Oncol.* **11**, 779–785 (2018).

334. Barros, M. H. M., Segges, P., Vera-Lozada, G., Hassan, R. & Niedobitek, G. Macrophage Polarization Reflects T Cell Composition of Tumor Microenvironment in Pediatric Classical Hodgkin Lymphoma and Has Impact on Survival. *PLoS ONE* **10**, (2015).

335. Suarez, G. V. *et al.* PD-1/PD-L1 Pathway Modulates Macrophage Susceptibility to Mycobacterium tuberculosis Specific CD8 + T cell Induced Death. *Sci. Rep.* **9**, 1–14 (2019).

336. Lu, D. *et al.* Beyond T Cells: Understanding the Role of PD-1/PD-L1 in Tumor-Associated Macrophages. *Journal of Immunology Research* https://www.hindawi.com/journals/jir/2019/1919082/ (2019) doi:10.1155/2019/1919082.

337. Chang, W. extrafont: Tools for using fonts. R package version 0.17. (2014).

338. Wenseleers, T. & Vanderaa, C. *export: Streamlined Export of Graphs and Data Tables.* (2018).

339. Wang, X.-F. *et al.* The role of indoleamine 2,3-dioxygenase (IDO) in immune tolerance: focus on macrophage polarization of THP-1 cells. *Cell. Immunol.* **289**, 42–48 (2014).

340. Abebayehu, D. *et al.* Galectin-1 Promotes an M2 Macrophage Response to Polydioxanone Scaffolds. *J. Biomed. Mater. Res. A* **105**, 2562–2571 (2017).

341. Moon, K. R. *et al.* Visualizing Structure and Transitions for Biological Data Exploration. *bioRxiv* 120378 (2019) doi:10.1101/120378.

342. Italiani, P. & Boraschi, D. From Monocytes to M1/M2 Macrophages: Phenotypical vs. Functional Differentiation. *Front. Immunol.* **5**, (2014).

343. Arnold, C. E., Gordon, P., Barker, R. N. & Wilson, H. M. The activation status of human macrophages presenting antigen determines the efficiency of Th17 responses. *Immunobiology* **220**, 10–19 (2015).

344. Aoki, T. Single Cell Transcriptome Analysis Reveals Disease-Defining T Cell Subsets in the Tumor Microenvironment of Classic Hodgkin Lymphoma. in (ASH, 2019).

345. Oyler-Yaniv, A. *et al.* A tunable diffusion-consumption mechanism of cytokine propagation enables plasticity in cell-to-cell communication in the immune system. *Immunity* **46**, 609–620 (2017).

346. Huse, M., Lillemeier, B. F., Kuhns, M. S., Chen, D. S. & Davis, M. M. T cells use two directionally distinct pathways for cytokine secretion. *Nat. Immunol.* **7**, 247–255 (2006).

347. Larousserie, F. *et al.* Analysis of Interleukin-27 (EBI3/p28) Expression in Epstein-Barr Virus- and Human T-Cell Leukemia Virus Type 1-Associated Lymphomas. *Am. J. Pathol.* **166**, 1217–1228 (2005).

348. Jones, L. L. & Vignali, D. A. A. Molecular interactions within the IL-6/IL-12 cytokine/receptor superfamily. *Immunol. Res.* **51**, 5–14 (2011).

349. Gately, M. K. *et al.* The interleukin-12/interleukin-12-receptor system: role in normal and pathologic immune responses. *Annu. Rev. Immunol.* **16**, 495–521 (1998).

350. Horlad, H. *et al.* An IL-27/Stat3 axis induces expression of programmed cell death 1 ligands (PD-L1/2) on infiltrating macrophages in lymphoma. *Cancer Sci.* **107**, 1696–1704 (2016).

351. Hirahara, K. *et al.* Interleukin-27 priming of T cells controls IL-17 production in trans via induction of the ligand PD-L1. *Immunity* **36**, 1017–1030 (2012).

352. Yang, J. *et al.* Epstein-Barr virus-induced gene 3 negatively regulates IL-17, IL-22 and RORgamma t. *Eur. J. Immunol.* **38**, 1204–1214 (2008).

353. Liang, Y. *et al.* Epstein-Barr Virus-Induced Gene 3 (EBI3) Blocking Leads to Induce Antitumor Cytotoxic T Lymphocyte Response and Suppress Tumor Growth in Colorectal Cancer by Bidirectional Reciprocal-Regulation STAT3 Signaling Pathway. *Mediators of Inflammation* https://www.hindawi.com/journals/mi/2016/3214105/ (2016) doi:10.1155/2016/3214105.

354. Wang, X. *et al.* A novel IL-23p19/Ebi3 (IL-39) cytokine mediates inflammation in Lupus-like mice. *Eur. J. Immunol.* **46**, 1343–1350 (2016).

355. Bridgewood, C. *et al.* The IL-23p19/EBI3 heterodimeric cytokine termed IL-39 remains a theoretical cytokine in man. *Inflamm. Res.* **68**, 423–426 (2019).

356. Flores, R. R. *et al.* IL-Y, a Synthetic Member of the IL-12 Cytokine Family, Suppresses the Development of Type 1 Diabetes in NOD Mice. *Eur. J. Immunol.* **45**, 3114–3125 (2015).

357. Chehboun, S. *et al.* Epstein-Barr virus-induced gene 3 (EBI3) can mediate IL-6 trans-signaling. *J. Biol. Chem.* jbc.M116.762021 (2017) doi:10.1074/jbc.M116.762021.

358. Hasegawa, H. *et al.* Expanding Diversity in Molecular Structures and Functions of the IL-6/IL-12 Heterodimeric Cytokine Family. *Front. Immunol.* **7**, (2016).

359. Devergne, O., Birkenbach, M. & Kieff, E. Epstein–Barr virus-induced gene 3 and the p35 subunit of interleukin 12 form a novel heterodimeric hematopoietin. *Proc. Natl. Acad. Sci. U. S. A.* **94**, 12041–12046 (1997).

360. Bargou, R. C. *et al.* High-level nuclear NF-kappa B and Oct-2 is a common feature of cultured Hodgkin/Reed-Sternberg cells. *Blood* **87**, 4340–4347 (1996).

361. Steidl, C. *et al.* Gene expression profiling of microdissected Hodgkin Reed-Sternberg cells correlates with treatment outcome in classical Hodgkin lymphoma. *Blood* **120**, 3530–3540 (2012).

362. Zhang, S.-A. *et al.* Effect of EBI3 on radiation-induced immunosuppression of cervical cancer HeLa cells by regulating Treg cells through PD-1/PD-L1 pathway. *Tumour Biol. J. Int. Soc. Oncodevelopmental Biol. Med.* **39**, 1010428317692237 (2017).

363. Devergne, O. *et al.* A novel interleukin-12 p40-related protein induced by latent Epstein-Barr virus infection in B lymphocytes. *J. Virol.* **70**, 1143–1153 (1996).

364. Pflanz, S. *et al.* IL-27, a Heterodimeric Cytokine Composed of EBI3 and p28 Protein, Induces Proliferation of Naive CD4+ T Cells. *Immunity* **16**, 779–790 (2002).

365. Abdi, K. *et al.* Free IL-12p40 Monomer is a Polyfunctional Adapter for Generating Novel IL-12-Like Heterodimers Extracellularly. *J. Immunol. Baltim. Md 1950* **192**, 6028–6036 (2014).

366. Sorrentino, C. *et al.* Interleukin-30/IL-27p28 shapes prostate cancer stem-like cell behavior and is critical for tumor onset and metastasization. *Cancer Res.* (2018) doi:10.1158/0008-5472.CAN-17-3117.

367. Müller, S. I. *et al.* A folding switch regulates interleukin 27 biogenesis and secretion of its α-subunit as a cytokine. *Proc. Natl. Acad. Sci.* **116**, 1585–1590 (2019).

368. Dietrich, C., Candon, S., Ruemmele, F. M. & Devergne, O. A Soluble Form of IL-27Rα Is a Natural IL-27 Antagonist. *J. Immunol.* **192**, 5382–5389 (2014).

369. Hsi, E. D. *et al.* Serum levels of TARC, MDC, IL10 and soluble CD163 in Hodgkin lymphoma: a SWOG S0816 correlative study. *Blood* (2019) doi:10.1182/blood-2018-08-870915.

370. Hohaus, S. *et al.* Clinical significance of interleukin-10 gene polymorphisms and plasma levels in Hodgkin lymphoma. *Leuk. Res.* **33**, 1352–1356 (2009).

371. Wang, H. *et al.* IL-27 induces the differentiation of Tr1-like cells from human naive CD4+ T cells via the phosphorylation of STAT1 and STAT3. *Immunol. Lett.* **136**, 21–28 (2011).

372. Hall, A. O. *et al.* The cytokines interleukin 27 and interferon-γ promote distinct Treg cell populations required to limit infection-induced pathology. *Immunity* **37**, 511–523 (2012).

373. Nishino, R. *et al.* Identification of Epstein-Barr virus-induced gene 3 as a novel serum and tissue biomarker and a therapeutic target for lung cancer. *Clin. Cancer Res. Off. J. Am. Assoc. Cancer Res.* **17**, 6272–6286 (2011).

374. Greaves, P. *et al.* The PD1/PD-L1 Axis in the Classical Hodgkin Lymphoma Microenvironment: PD-1 Is Rarely Expressed but Identifies Patients with High-Risk Disease. *Blood* **118**, 1560–1560 (2011).

375. Selby, M. J. *et al.* Preclinical Development of Ipilimumab and Nivolumab Combination Immunotherapy: Mouse Tumor Models, In Vitro Functional Studies, and Cynomolgus Macaque Toxicology. *PLOS ONE* **11**, e0161779 (2016).

376. European Medicines Authority Assessment Report: Keytruda. (2015).

377. Lober, B. & Obst, R. Mechanisms of CD4+ T Cell Exhaustion by persisting antigen (LYM3P.737). *J. Immunol.* **192**, 64.11-64.11 (2014).

378. Shimabukuro-Vornhagen, A. *et al.* Lymphocyte-rich classical Hodgkin's lymphoma: clinical presentation and treatment outcome in 100 patients treated within German Hodgkin's Study Group trials. *J. Clin. Oncol. Off. J. Am. Soc. Clin. Oncol.* **23**, 5739–5745 (2005).

379. Wherry, E. J. & Kurachi, M. Molecular and cellular insights into T cell exhaustion. *Nat. Rev. Immunol.* **15**, 486–499 (2015).

380. McLane, L. M. *et al.* Differential localization of T-bet and Eomes in CD8 T cell memory populations. *J. Immunol. Baltim. Md 1950* **190**, 3207–3215 (2013).

381. Paley, M. A. *et al.* Progenitor and terminal subsets of CD8+ T cells cooperate to contain chronic viral infection. *Science* **338**, 1220–1225 (2012).

382. Ogasawara, R. *et al.* Loss of nivolumab binding to T cell PD-1 predicts relapse of Hodgkin lymphoma. *Int. J. Hematol.* (2019) doi:10.1007/s12185-019-02737-4.

383. Zelba, H. *et al.* Accurate quantification of T-cells expressing PD-1 in patients on anti-PD-1 immunotherapy. *Cancer Immunol. Immunother. CII* **67**, 1845–1851 (2018).

384. Wang, C. *et al.* In Vitro Characterization of the Anti-PD-1 Antibody Nivolumab, BMS-936558, and In Vivo Toxicology in Non-Human Primates. *Cancer Immunol. Res.* **2**, 846–856 (2014).

385. Zhao, Y. *et al.* Antigen-Presenting Cell-Intrinsic PD-1 Neutralizes PD-L1 in cis to Attenuate PD-1 Signaling in T Cells. *Cell Rep.* **24**, 379-390.e6 (2018).

386. Yang, Z.-Z. *et al.* PD-1 expression defines two distinct T-cell sub-populations in follicular lymphoma that differentially impact patient survival. *Blood Cancer J.* **5**, e281 (2015).

387. Lesokhin, A. M. *et al.* Nivolumab in Patients With Relapsed or Refractory Hematologic Malignancy: Preliminary Results of a Phase Ib Study. *J. Clin. Oncol. Off. J. Am. Soc. Clin. Oncol.* **34**, 2698–2704 (2016).

388. Yang, Z.-Z. *et al.* Expression of LAG-3 defines exhaustion of intratumoral PD-1+ T cells and correlates with poor outcome in follicular lymphoma. *Oncotarget* **8**, 61425–61439 (2017).

389. Sharpe, A. H., Wherry, E. J., Ahmed, R. & Freeman, G. J. The function of programmed cell death 1 and its ligands in regulating autoimmunity and infection. *Nat. Immunol.* **8**, 239–245 (2007).

390. David, P. *et al.* The PD-1/PD-L1 Pathway Affects the Expansion and Function of Cytotoxic CD8+ T Cells During an Acute Retroviral Infection. *Front. Immunol.* **10**, (2019).

391. Callahan, M. K. & Wolchok, J. D. Recruit or Reboot? How Does Anti-PD-1 Therapy Change Tumor-Infiltrating Lymphocytes? *Cancer Cell* **36**, 215–217 (2019).

392. Yost, K. E. *et al.* Clonal replacement of tumor-specific T cells following PD-1 blockade. *Nat. Med.* **25**, 1251–1259 (2019).

393. Riley, J. L. PD-1 signaling in primary T cells. *Immunol. Rev.* **229**, 114–125 (2009).

394. Chemnitz, J. M., Parry, R. V., Nichols, K. E., June, C. H. & Riley, J. L. SHP-1 and SHP-2 associate with immunoreceptor tyrosine-based switch motif of programmed death 1 upon primary human T cell stimulation, but only receptor ligation prevents T cell activation. *J. Immunol. Baltim. Md 1950* **173**, 945–954 (2004).

395. Parry, R. V. *et al.* CTLA-4 and PD-1 receptors inhibit T-cell activation by distinct mechanisms. *Mol. Cell. Biol.* **25**, 9543–9553 (2005).

396. Greenwald, R. J., Freeman, G. J. & Sharpe, A. H. The B7 Family Revisited. *Annu. Rev. Immunol.* **23**, 515–548 (2005).

397. van Panhuys, N. TCR Signal Strength Alters T–DC Activation and Interaction Times and Directs the Outcome of Differentiation. *Front. Immunol.* **7**, (2016).

398. Snook, J. P., Kim, C. & Williams, M. A. TCR signal strength controls the differentiation of CD4+ effector and memory T cells. *Sci. Immunol.* **3**, (2018).

399. Qiao, G. *et al.* Program death-1 regulates peripheral T cell tolerance via an anergy-independent mechanism. *Clin. Immunol. Orlando Fla* **143**, 128–133 (2012).

400. Sprouse, M. L. *et al.* Cutting Edge: Low-Affinity TCRs Support Regulatory T Cell Function in Autoimmunity. *J. Immunol. Baltim. Md 1950* (2017) doi:10.4049/jimmunol.1700156.

401. Gomez-Rodriguez, J. *et al.* Itk-mediated integration of T cell receptor and cytokine signaling regulates the balance between Th17 and regulatory T cells. *J. Exp. Med.* **211**, 529–543 (2014).

402. Tsushima, F. *et al.* Interaction between B7-H1 and PD-1 determines initiation and reversal of T-cell anergy. *Blood* **110**, 180–185 (2007).

403. Yoshida, T., Jiang, F., Honjo, T. & Okazaki, T. PD-1 deficiency reveals various tissue-specific autoimmunity by H-2b and dose-dependent requirement of H-2g7 for diabetes in NOD mice. *Proc. Natl. Acad. Sci. U. S. A.* **105**, 3533–3538 (2008).

404. Machicote, A., Belén, S., Baz, P., Billordo, L. A. & Fainboim, L. Human CD8+HLA-DR+ Regulatory T Cells, Similarly to Classical CD4+Foxp3+ Cells, Suppress Immune Responses via PD-1/PD-L1 Axis. *Front. Immunol.* **9**, 2788 (2018).

405. Fife, B. T. *et al.* Insulin-induced remission in new-onset NOD mice is maintained by the PD-1-PD-L1 pathway. *J. Exp. Med.* **203**, 2737–2747 (2006).

406. Champiat, S. *et al.* Hyperprogressive Disease Is a New Pattern of Progression in Cancer Patients Treated by Anti-PD-1/PD-L1. *Clin. Cancer Res.* **23**, 1920–1928 (2017).

407. Kamada, T. *et al.* PD-1+ regulatory T cells amplified by PD-1 blockade promote hyperprogression of cancer. *Proc. Natl. Acad. Sci.* 201822001 (2019) doi:10.1073/pnas.1822001116.

408. Perrone, G. *et al.* Intratumoural FOXP3-positive regulatory T cells are associated with adverse prognosis in radically resected gastric cancer. *Eur. J. Cancer Oxf. Engl. 1990* **44**, 1875–1882 (2008).

409. Asano, T. *et al.* PD-1 modulates regulatory T-cell homeostasis during low-dose interleukin-2 therapy. *Blood* **129**, 2186–2197 (2017).

410. Brunner-Weinzierl, M. C. & Rudd, C. E. CTLA-4 and PD-1 Control of T-Cell Motility and Migration: Implications for Tumor Immunotherapy. *Front. Immunol.* **9**, (2018).

411. Thibult, M.-L. *et al.* PD-1 is a novel regulator of human B-cell activation. *Int. Immunol.* **25**, 129–137 (2013).

412. Good-Jacobson, K. L. *et al.* PD-1 regulates germinal center B cell survival and the formation and affinity of long-lived plasma cells. *Nat. Immunol.* **11**, 535–542 (2010).

413. DaFonseca, S. *et al.* Impaired Th17 polarization of phenotypically naive CD4+ T-cells during chronic HIV-1 infection and potential restoration with early ART. *Retrovirology* **12**, (2015).

414. Marshall, N. A. *et al.* Immunosuppressive regulatory T cells are abundant in the reactive lymphocytes of Hodgkin lymphoma. *Blood* **103**, 1755–1762 (2004).

415. Takeuchi, A. *et al.* CRTAM determines the CD4+ cytotoxic T lymphocyte lineage. *J. Exp. Med.* **213**, 123–138 (2016).

416. Quesada, A. E. *et al.* Expression of Sirt1 and FoxP3 in classical Hodgkin lymphoma and tumor infiltrating lymphocytes: Implications for immune dysregulation, prognosis and potential therapeutic targeting. *Int. J. Clin. Exp. Pathol.* **8**, 13241–13248 (2015).

417. Shi, F. *et al.* PD-1 and PD-L1 upregulation promotes CD8(+) T-cell apoptosis and postoperative recurrence in hepatocellular carcinoma patients. *Int. J. Cancer* **128**, 887–896 (2011).

418. Park, H. J. *et al.* PD-1 upregulated on regulatory T cells during chronic virus infection enhances the suppression of CD8+ T cell immune response via the interaction with PD-L1 expressed on CD8+ T cells. *J. Immunol. Baltim. Md 1950* **194**, 5801–5811 (2015).

419. Wong, M., La Cava, A. & Hahn, B. H. Blockade of programmed death-1 in young (New Zealand Black x New Zealand White)F1 mice promotes the suppressive capacity of CD4+ regulatory T cells protecting from lupus-like disease. *J. Immunol. Baltim. Md 1950* **190**, 5402–5410 (2013).

420. Francisco, L. M. *et al.* PD-L1 regulates the development, maintenance, and function of induced regulatory T cells. *J. Exp. Med.* **206**, 3015–3029 (2009).

421. DiDomenico, J. *et al.* The immune checkpoint protein PD-L1 induces and maintains regulatory T cells in glioblastoma. *Oncoimmunology* **7**, e1448329 (2018).

422. Oelmann, E., Stein, H., Berdel, W. E. & Herbst, H. Expression of Interleukin-1 and Interleukin-1 Receptors Type 1 and Type 2 in Hodgkin Lymphoma. *PloS One* **10**, e0138747 (2015).

423. Acosta-Rodriguez, E. V., Napolitani, G., Lanzavecchia, A. & Sallusto, F. Interleukins 1β and 6 but not transforming growth factor-β are essential for the differentiation of interleukin 17–producing human T helper cells. *Nat. Immunol.* **8**, 942–949 (2007).

424. Plattel, W. J. *et al.* Biomarkers for evaluation of treatment response in classical Hodgkin lymphoma: comparison of sGalectin-1, sCD163 and sCD30 with TARC. *Br. J. Haematol.* **175**, 868–875 (2016).

425. Young, M. R. I. Th17 Cells in Protection from Tumor or Promotion of Tumor Progression. *J. Clin. Cell. Immunol.* **7**, (2016).

426. Asadzadeh, Z. *et al.* The paradox of Th17 cell functions in tumor immunity. *Cell. Immunol.* (2017) doi:10.1016/j.cellimm.2017.10.015.

427. Mahoney, K. M. *et al.* A secreted PD-L1 splice variant that covalently dimerizes and mediates immunosuppression. *Cancer Immunol. Immunother. CII* (2018) doi:10.1007/s00262-018-2282-1.

428. Gilboa, E. The risk of autoimmunity associated with tumor immunotherapy. *Nat. Immunol.* **2**, 789–792 (2001).

429. Vesely, M. D., Kershaw, M. H., Schreiber, R. D. & Smyth, M. J. Natural innate and adaptive immunity to cancer. *Annu. Rev. Immunol.* **29**, 235–271 (2011).

430. Diepstra, A. *et al.* HLA-G protein expression as a potential immune escape mechanism in classical Hodgkin's lymphoma. *Tissue Antigens* **71**, 219–226 (2008).

431. Rose, K. D. *et al.* Early Eocene fossils suggest that the mammalian order Perissodactyla originated in India. *Nat. Commun.* **5**, 1–9 (2014).

432. de Charette, M. & Houot, R. Hide or defend, the two strategies of lymphoma immune evasion: potential implications for immunotherapy. *Haematologica* (2018) doi:10.3324/haematol.2017.184192.

433. Li, X. & Chen, W. Mechanisms of failure of chimeric antigen receptor T-cell therapy. *Curr. Opin. Hematol.* **26**, 427–433 (2019).

434. Hewitt, E. W. The MHC class I antigen presentation pathway: strategies for viral immune evasion. *Immunology* **110**, 163–169 (2003).